UNIVERSITY OF SOUTHAMPTON

FACULTY OF ENGINEERING AND THE ENVIRONMENT

Civil, Maritime and Environmental Engineering and Science

A NUMERICAL STUDY OF RESISTANCE COMPONENTS OF HIGH-SPEED CATAMARANS AND THE SCALE EFFECTS ON FORM FACTOR

by

SARAWUTH SRINAKAEW

Thesis for the degree of Doctor of Philosophy

October 2017

UNIVERSITY OF SOUTHAMPTON

ABSTRACT

FACULTY OF ENGINEERING AND THE ENVIRONMENT

Civil, Maritime and Environmental Engineering and Science

Thesis for the degree of Doctor of Philosophy

A NUMERICAL STUDY OF RESISTANCE COMPONENTS OF HIGH-SPEED CATAMARANS AND THE SCALE EFFECTS ON FORM FACTOR

By Sarawuth Srinakaew

Resistance and powering of ships is one of the most important aspects for Naval Architects and it still heavily relies on scale model testing. The catamaran is a particular case that is treated slightly different from the monohull due to the interference effects between demihulls. There are various works from previous researches dealing with this challenge. Since catamarans have been introduced, resistance components and form factor have been evaluated by focusing on the influence of many aspects such as hull form, speed, and hull separation. The methods by which the resistance is evaluated, either experimentally or numerically are mostly driven by the size of physical test facilities or computational power available. This thesis investigates the resistance components of high-speed catamarans and the effect of scale on form factor using a commercial CFD code.

The numerical investigation into resistance components and form factor of the high-speed catamarans focuses on the hull geometry, separation to length ratio (S/L) and scale. The hull geometries include the Wigley III and NPL round bilge 5b catamarans. The CFD results are compared against Insel's experimental series. The investigation into the effect of scale on form factor (1+k) are made for the Wigley III and NPL 5b catamarans S/L = 0.3. Three different models of those hull configurations are created, which are 1L, 2L for both hulls, 4L for Wigley III catamaran and 10L for NPL 5b catamaran respectively. The numerical domain to ship dimension ratios are constant for the Wigley III catamarans. The influence of domain size, recreating two towing tanks and the unbounded condition, are investigated. Wave elevations, resistance components and form factors are evaluated and compared.

The CFD results show good agreement with the original experimental results, and allow deeper understanding into the resistance components, form factor and free surface wave elevations. The CFD simulation domain size has an important influence on the resistance. To some extent the ITTC recommended blockage corrections can correct for this, but the wave system is significantly different and cannot be corrected. The CFD investigation into the influence of scale on form factor shows that form factor is both speed and model length dependent. So, it is noted that a larger model produces more accurate predictions of form factor and that the form factor should be evaluated at the design speed rather than determined by either low speed or high-speed runs.

TABLE OF CONTENTS

List of Tables

List of Figures

DECLARATION OF AUTHORSHIP

I, Sarawuth SRINAKAEW, declare that this thesis entitled *A Numerical Study of Resistance Components of High-Speed Catamarans and Scale Effects on Form Factor* and the work presented in it are my own and has been generated by me as the result of my own original research.

I confirm that:

1. This work was done wholly or mainly while in candidature for a research degree at this University;
2. Where any part of this thesis has previously been submitted for a degree or any other qualification at this University or any other institution, this has been clearly stated;
3. Where I have consulted the published work of others, this is always clearly attributed;
4. Where I have quoted from the work of others, the source is always given. With the exception of such quotations, this thesis is entirely my own work;
5. I have acknowledged all main sources of help;
6. Where the thesis is based on work done by myself jointly with others, I have made clear exactly what was done by others and what I have contributed myself;
7. Parts of this work have been published as: (Srinakaew et al., 2016), and the accepted paper waiting for the publication for the Journal of Maritime and Naval Technology titled "*Numerical Study of Resistance and Form Factor of High-Speed Catamarans*".

Signed: ....

Date: ....

Acknowledgements

First of all, I am most grateful to my Ph.D. supervisors, Dr Dominic J. Taunton and Prof Dominic A. Hudson, for their guidance, support, encouragement and patience throughout the time of my research career. Without their supports, I could not find the right way I should follow to complete my research.

This research could not be done without the great reliability and opportunity from Royal Thai Navy. I am grateful to Royal Thai Navy for their financial support throughout the project.

I also would like to thank my friends: Prin, Arun and Pisessud (Jaew) who have been supporting me for the numerical, simulations and data acquisitions.

I am also grateful to the CD-adapco supporting team "*Steve Portal*" for their helps and advices on CFD code, STAR CCM+.

Moreover, my parents and family watched me from a distance while I have been working towards my degree. The completion of this thesis will mean a lot to them so I dedicate this project to my loving parents, without whose love, this project would not be completed.

Finally, and most importantly, I would like to thank Thanaporn for her support, encouragement, understanding and quiet patience.

Nomenclatures and Abbreviations

Nomenclatures

Symbol	Description
B	Hull breadth *(m)*
C_B	Block coefficient (-)
C_F	Frictional resistance coefficient *(-)*
C_R	Residuary resistance coefficient *(-)*
C_T	Total resistance coefficient *(-)*
C_V	Viscous resistance coefficient *(-)*
C_W	Wave resistance coefficient *(-)*
E	Energy $(kg(m/s)^2)$
Fn	Froude number *(-)*
g	Acceleration due to gravity (m/s^2)
k	Turbulent dissipation rate (m^2/s^3)
L	Hull length *(m)*
Re	Reynolds' number *(-)*
S	Separation distance between the centrelines of demihulls
T	Hull draught *(m)*
$\boldsymbol{U}$	Velocity vector *(m/s)*
U_∞	Free stream velocity *(m/s)*
y_1	First layer thickness *(m)*
y_+	Dimensionless wall distance *(-)*
$(1+k)$	Form factor *(-)*
α_i	Volume fraction *(-)*
β	Viscous resistance interference factor *(-)*
ε	Specific dissipation rate / WaveFrequency(*rad/s*)
ζ	Wave Elevation (*m*)
λ	Model scale *(-)*
μ	Dynamic viscosity (Ns/m^2)
ν	Kinematic viscosity (m^2/s)
ρ	Density of water (kg/m^3)
τ	Wave resistance interference factor *(-)*
ω	Turbulent kinetic energy $(kg(m/s)^2)$
σ	Frictional resistance interference factor *(-)*
Ω	Residuary resistance interference factor *(-)*
Φ	Form resistance interference factor *(-)*
∇	Displacement volume (m^3)

Abbreviations

Acronym	Description
CFD	Computational fluid dynamics
EFD	Experimental fluid dynamics
FVM	Finite volume method
GUI	Graphical user interface
ITTC	International Towing Tank Conference
RANS	Reynolds averaged Navier-Stokes
SST	Shear stress transport
VOF	Volume of fluid

Chapter 1: Introduction

1.1 Background

Catamaran vessels have been developed over the past decades especially for the commercial and military purposes. Commercial catamarans are of particular interest due to high speed and large deck area. Most of the commercial catamarans can operate in the high-speed regime. The initiation of a catamaran seems to be the need of the people to travel between small islands in Norway where road transportation is restricted. Nowadays, under these requirements catamaran are operated worldwide mainly for island regions, water channels and rivers. For the military purposes, amphibious warfare is the most common use. Due to the larger deck area and higher speed, they can carry a larger amount of troops to the frontline much quicker compared to the old workhorses, e.g. landing ship tank (LST) and landing craft personal vehicle (LCVP). Rather than just send the men to the shore, they also can supply ordnances, fuel, parts and food much faster.

Catamaran development seems to focus on various aspects such as weight, structure, stability and speed. The majority of the modern catamaran are particularly designed in the size range from 45 to 170 feet (about 15 to 50m) because it provides advantages over other vessels in term of speed, dimensions, shallower draught, fuel efficiency and stability. Passenger and car ferry, for example, are the most dominant catamaran applications, which can be seen across the globe. Moreover, its shallower draught allows the ferry to go further close to the shore, which means that no deep-water port and infrastructures are required.

Smaller and faster catamarans are mostly popular in leisure activities and sports. These can be seen in high-speed boat competitions and sailing boats. Catamaran hull has been used because it can help in reducing resistance in a high-speed regime, $Fn > 0.7$ (Insel, 1990). Beyond the speed competition, wealthy and seagoing people are interested in catamaran yachts because their higher speed provides a better experience and consumes less fuel, which results in lower operating cost and maintenance. Another catamaran application, which is now significantly under investigation and investment by Jupp et al. (2014), is high-speed small catamarans operating in wind farms. They have been operated as crew boat to send engineers and technicians to wind farms to carry out the maintenance operations and replacement services.

1.2 Research Challenge

As mentioned in the previous section, the speed is one of the most domination aspects, which raise the attention to the catamaran. To design the catamaran to operate at the high-speed regime, most of the hulls are designed with the high body slenderness. To select the most suitable and effective propulsion system, it is important to estimate the resistance of the catamaran precisely. Many ship resistance prediction approaches have been proposed such as experiment, numerical and empirical methods which are discussed in chapter 2. Normally these approaches are used to estimate the resistance of the model scale while the prediction of resistance of the ship strongly relies on the extrapolation of the form factor (1+k). Hence, it is important to calculate the form factor correctly.

In the recent years, most of the resistance and form factor investigations mainly focus on the model-ship resistance of both the monohull and catamaran. However, the investigations into the scale effects on resistance prediction and form factor of the catamarans still need to be fulfilled.

The investigation of resistance and scale effects on form factor can be broken down into three main aspects: approaches, hull characteristics and dynamic conditions. The approaches refer to the methods used in estimating resistance, form factors and scale effects. The hull characteristics refer to hull form, dimensions and particulars. The dynamic conditions consist of sinkage and trim conditions.

1.2.1 Approaches

- The experiment is the most common and reliable method for determining resistance, form factor, and scale effects on form factor. Although this method has prominent advantages over other methods in term of accuracy and reliability, cost seems to be the main drawback. Another disadvantage of this method is that the sizes of the model are determined by the limitations of the towing tank dimensions and facilities.

- Theoretical and numerical approaches based on the potential flow theory have been used to investigate the flow field around the hull by mostly focusing on wave interference effects, seakeeping and influence of the viscosity on wave making capability (Doctors (2003) and Chandraprabha (2003)).

- An empirical method based on the statistical data of the existing models and ships to derive the empirical formulae to determine resistance components and form factor. This method is normally used in the early stage design (Molland et al., 2011).

- Increases in computational power available to naval architects and marine engineers, together with more efficient codes, have made CFD one of the effective tools for early stage ship design and investigations (Voxakis, 2012). CFD tools with viscous flow computations are being used to provide detailed predictions of resistance components, the flow around the hull, the wake field, occurrence of flow separation, for appendage alignment (Reven et al., 2008).

1.2.2 Hull Characteristics

There are various physical characteristics, which are usually investigated including hull form and variants, length to displacement ratio ($L/\nabla^{1/3}$), length to breadth ratio (L/B), breadth to draught ratio (B/T), block coefficient (C_B), prismatic coefficient (C_P), separation to length ratio (S/L) and scale (λ). Many hull forms have been investigated such as KCS, KVLCC, Wigley hull, Delft series, NPL series and DTMB series.

Each hull form has different hull particulars, which suit different applications. For example, KCS and KVLCC series are suitable for low speed (Fn) study which can be seen in Tokyo and Gothenburg workshops (2000, 2005 and 2010 respectively). Wigley hull series is mostly used as a starting point for various studies because there is no transom stern causing flow separation and complexity to the problems. For the high-speed regime Wigley, NPL, Delft and DTMB series seem to be more attractive due to the high slenderness of the hull.

An investigation into length to displacement ratio ($L/\nabla^{1/3}$), length to breadth ratio (L/B), breadth to draught ratio (B/T), block coefficient (C_B) and prismatic coefficient (C_P) is usually made in the early design stage. The process is to find to optimum model for a certain application. For example, in 1992, Journée investigated the added resistance in waves for four Wigley hull variants in the series including I, II, III and IV. The variants of the Wigley hull series have different hull characteristics; model I and II have a higher C_B compared with model III and IV. The differences between model I and II, and III and IV are the L/B. Moreover, the empirical method is normally used to deal with these hull characteristics in the early design stage (Bertram and Schneekluth (1998) and Molland et al. (2011)).

Hull separation to length ratio (S/L) is widely investigated because it influences the flow characteristics, resistance, form factor and interference effects between demihulls. Normally, a range of separation to length ratio between 0.1 and 0.5 is investigated. Higher range is out of interest due to less influence of the flow interference (Moraes et al., 2004).

Another physical characteristic is the scale, which plays an importance role in influencing form factor (Reynolds' number dependence). The range of scales is varied depending on the availability of towing tank dimensions and limitations of the facilities, validating data for the numerical investigation and computational power available.

1.2.3 Dynamic conditions

The dynamic conditions in this study refer to dynamic sinkage and trim. In reality, when catamarans running through the water at the steady state, sinkage and trim will also reach the steady point. The catamaran resistance components of the fixed and free conditions are quite different. Not only the r`esistance but also the fluid flow characteristics around the catamaran are different between fixed and free conditions. Most of the catamaran investigations into form factor using CFD focus on the fixed trim and sinkage retrieved from the experiments, especially for the Geosim series (Kouh et al. 2009 and Broglia et al., 2011). The main advantage of the fixed sinkage and trim is that the cost of the simulation time can be reduced.

1.2.4 Research Question

Many aspects of catamaran resistance have been investigating since past decades by focusing on many factors discussed in section 1.2.1 to 1.2.3. However, the studies of scale effect on form factor using CFD of Wigley hull and NPL series by applying Geosim series are still limited. The range of Froude numbers used in Geosim methods is also limited (1 or 2 Froude numbers) with the low speed. Moreover, the investigation into how the form factor of the catamaran is influenced by the increasing model size for the whole range of the operating Froude numbers, especially for the high-speed regime is still limited.

Although the experimental fluid dynamics (EFD) is the most reliable approach for investigating resistance and form factor, the limitations seem to be found for the big model due to the tank dimensions, carriage speed and safety. To overcome these limitations, CFD code one of the valuable tools has been used to investigate the flow around hulls, resistance components, form factor and scale. Capabilities of CFD are now covering the investigation of the flow field, motions and forces. Moreover, CFD is one of the preferable tools in investigating inviscid and viscous effects on the hydrodynamic performance of multihull vessels.

Although CFD could model monohull and catamarans at full-scale, this is still computationally expensive that it is still usual to conduct model tests and use a scaling procedure. However, the expensive cost of EFD seems to push this approach to a dilemma. Since the EFD shows that model size is limited by towing tank dimensions and safety, to investigate into the larger model seems to be unachievable. Despite the fact that CFD code could investigate any larger size compared with the EFD approach, the optimum scale and absolute size are still questioned.

Unlike experimental fluid dynamics, by using the CFD code, the model size is not determined by the dimensions of the towing tank because the computational domain could be extended to avoid reflection of the wall. Normally, numerical domain is determined by the model length. This means that larger numerical domain the larger number of cells, which results in high computational cost. Hence, the investigation into the numerical domain dimensions for ship resistance, form factor and scale is still needed. Hence, three main questions are needed to be addressed and answered; what scale and absolute model size should be used, what numerical domain dimensions should be used and how these two conditions affect the accuracy of the scaling processes.

1.3 Aims and Objectives

1.3.1 Aims

This research project aims to investigate the scale effects on resistance prediction, form factor and the resistance of high-speed catamarans in calm water using commercial CFD code, by focusing on determining the scale, model size and numerical domain dimensions. The study focuses on displacement catamarans with different variables including speed, scale, separation to length ratio (S/L) and numerical domain dimensions.

In order to simulate the ship travelling through the water with a constant speed, flow phenomena need to be determined and evaluated correctly. These phenomena comprise of wave elevation along the hull, flow separation behind transom stern, transverse and divergent wave system, and flow interference between demihulls. To achieve the aims of this project, the objectives are broken down into small steps, which relate to the realistic flow phenomenon, resistance prediction method and geosim series method. These steps consist of numerical wave tank, grid dependency and turbulence models for resistances, the double-model method, scale effects and numerical domain dimensions.

1.3.2 Objectives

- To verify and validate CFD wave elevation at different positions such as along the hull, behind transom stern and far field area, the numerical wave tank study provides more understanding and confidence in basic principle for using commercial CFD code and how to create waves. Two important stages for the numerical wave tank are grid dependency verification and simulation validation. These processes focus on how the number of cells per wave height affects the accuracy of the results and validation process will carry on comparing CFD results with the experimental results done by other researchers and theoretical results.

- To find the suitable grid and turbulence model to determine resistance components. Grid dependence for resistance prediction is investigated in the same way a numerical wave tank by focusing on how mesh qualities affect the results and find the optimum number of cells to determine resistance components. Turbulence models are also justified simultaneously to minimise the computational cost to find the most effective model to determine resistance components.
- To evaluate the double-model method to determine viscous resistance (C_V). The simulations are run with the single-phase flow. The process is introduced to gain more understanding and confidence in determining the acceptable viscous resistance, which is then used to calculate form factor.
- To investigate model scales to find the optimum model size for determining resistance components and form factor of displacement monohull and catamarans using commercial CFD code.
- To investigate the tank and numerical domain dimensions to minimise effects due to reflection off the wall.
- To show the model size and numerical domain dimensions affect the accuracy of the scaling process.

1.4 Novel Contributions

Regarding the aims and objectives stated in section 1.3, the novel contributions from this thesis consist of the followings:

The first novel contribution of this thesis is the extension of the numerical validation of the Wigley III over the range of the Froude numbers following Insel's experiments. The resistance components and form factor (1+k) for four Wigley III hull configurations including monohull, catamaran S/L = 0.2, 0.3 and 0.4 are investigated using CFD code. Although the Wigley hull series have been used for the resistance and form factor studies over the past decades, only some certain hull separations and Froude numbers were focused in a single piece of work. The average form factor and the variation of form factor over the range of Froude numbers are presented in this thesis. The resistance components and form factor are also investigated over the range of Froude numbers for two NPL 5b hull configurations including a monohull and a catamaran S/L = 0.3. The viscous resistance interference factor (β) and wave resistance interference factor (τ) are presented for both Wigley III and NPL 5b. The CFD results presented in this thesis show the reasonable accuracy compared with Insel's experiments.

The investigation into the scale effects on resistance and form factor for the Wigley III catamaran using Geosim series are presented. Three different model scales of the Wigley III catamaran S/L = 0.3, which include 1L, 2L and 4L are created and calculated resistance components and form factor. The validation of the CFD results is made against Insel's experiment, the Froude and Hughes approaches discussed in section 5.1.

The scale effects on the form factor for the NPL 5b catamaran S/L = 0.3 are also investigated. Three models are created, two smaller models are similar to the Wigley III while the biggest model is 10L. The models are run in three different numerical domain sizes. The smallest model, 1L, duplicates the experimental study by Insel in Southampton Solent towing tank. The 2L model is calculated in the numerical domain size equivalent to University of Southampton Boldrewood towing tank. The biggest model is treated as the unbounded condition as running in open water. Resistance components and form factor are calculated using CFD and the validations are made the same way as the Wigley III. Not only the resistance components and form factor but also the wave elevations at different positions are measured and presented for the NPL 5b scale effect study. Wave elevations are measured at four positions including along the hull on both sides, at the centreline of the catamaran, behind transom stern throughout the numerical domain and at y/L = 0.5. The results could be taken into the consideration in conducting the experiment in the towing tank.

1.5 Thesis Structure

This thesis is divided into 9 chapters including introduction, literature review, the use of CFD techniques, resistance and form factor of Wigley III, scale effects on form factor for Wigley III catamarans, resistance and form factor for the hull with a transom stern, blockage effects and scale effects on form factor of NPL 5b, overall discussions and conclusions and recommendations.

Chapter 1 represents the overall introduction to the project by starting from a general background, research challenges, aims and objectives and novel contributions of this thesis.

Chapter 2 presents literature review and the principle behind the CFD approach which is used as a tool to determine resistance components and form factor. This chapter provides more detail on how the resistance components and form factor are predicted using different approaches. The CFD principle is implemented and the equations behind the code are explained. The main methods discussed here are the RANS and VOF methods, which are mostly used to model the flow. Turbulence models and boundary conditions are also crucial because different models are suitable for different flow types. Moreover, grid generation is discussed since this process affects the accuracy of the results.

The use of the CFD techniques in calculating resistance components and form factor are shown in chapter 3. This chapter starts by focusing on the numerical towing tank, which provides more understanding on how to select to a suitable number of cells to capture wave elevations. The grid dependency for the resistance study is the process to determine the most suitable mesh quality to be used in the simulations. Turbulence model justification is performed to figure out which model provides the most accurate results. The double-model method is introduced to estimate the viscous resistance coefficient, which is then used to calculate wave resistance.

The CFD results for Wigley III for both monohull and catamarans are presented in chapter 4. The results consist of resistance components, form factor, viscous resistance interference factor (β), wave resistance interference factor (τ) and wave cut along the hull. The scale effects on resistance components and form factor of the

Wigley III are presented in chapter 5. The CFD results of the hull with transom stern, for the NPL 5b hull form, and the scale effects on form factor are presented in chapter 6 and 7 respectively. Chapter 8 presents the overall discussions of the CFD results shown in the previous chapters. The last chapter states the conclusions of the current works and the recommendations for the future works.

Chapter 2: Literature Review and Involved Theories

2.1 Literature Review

The resistance of a catamaran is one of the challenging problems in Naval Architecture, Marine, Offshore and Ocean Engineering. There are various works from many researchers dealing with this challenge. Since catamarans have been introduced, their resistance components have been evaluated by focusing on many aspects such as hull form, speed and hull separation to length ratio (S/L). Many methods for estimating the resistance were also proposed such as a direct measurement from a model and a full-scale catamaran, empirical and numerical approaches. However, the resistance prediction of catamarans requires more details to estimate all resistance characteristics to achieve the most suitable design. Due to the complex phenomenon of catamaran travelling through water, the interference effects between demihulls need to be considered carefully in addition to the resistance of a single hull. These can be broken down into resistance components as seen in Hughes's form factor approach (1954). Interference effects can cause the high water spray in the tank and between demihulls which restrict the practical use of the model test, mostly depend on speed, hull separation (S/L), sinkage and trim due to the safety condition (Insel (1990) and Chandraprapha (2003)).

The most significant use of the experimental model test of catamarans was introduced by Insel and Molland (1992). They carried out a series of experiments of monohull and catamarans of Wigley and NPL hulls, comparing the results with thin ship theory method, and produced a series of catamaran resistance components. Their results have been used as the reference experimental data for many research since the publication. Following this work, many series of resistance experiments were conducted at the University of Southampton by Molland et al. (1996) and Wellicome et al. (1999). Molland et al. conducted a series of the experiment on a systematic series of high-speed displacement monohull and catamarans in a shallow water and NPL hull series was again used in this study. They focus on a range of length to displacement ratios ($L/\nabla^{1/3}$), separation to length ratios (S/L), a range of Froude Numbers of Fn= 0.25-1.2 and Froude Numbers based on water depth, Fn_H. Their results showed a better understanding of wave resistance of high speed displacement ship in shallow water. These results consist of a set of resistance components, trim and sinkage. To this point, it can be seen that various factors which can affect the resistance of a catamaran including speed (Fn), separation to length ratio (S/L), trim and sinkage.

Nowadays, as computer performance has developed, a numerical approach is mature enough to use as a tool to predict resistance components. CFD is now widely used in determining resistance components. There are many works investigating resistance by applying this technique as a tool. Utama (1999) used CFX^{TM} code with Reynold-Averaged Navier-Stokes Equations (RANS) to calculate resistance components and form factor for the ellipsoid and NPL catamarans and the results showed a good agreement with the experiment. In 2004, Moraes et al. used SHIPFLOW code with slender body theory to calculate resistance components of the catamaran and they found that results validated against the experiments showed that separation to length ratio (S/L) higher than 0.6 did not affect wave resistance. Pranzitelli (2011) used Fluent CFD code with RANS equations to calculate free surface around Wigley hull and predict resistance components. He investigated the flow at Froude number 0.267 by focusing on steady state simulation with Volume of Fluid Method (VOF). He concluded that it is possible to obtain a good estimation of flow field and total resistance coefficient using commercial CFD code.

Free surface flow investigation using CFD code was also made by Larsson et al. (2010) and Wackers et al. (2011) also summarised in Gothenburg Workshop 2010 on Numerical Ship Hydrodynamics. Aktar et al. (2013) computed wave resistance around Wigley hull in calm water using the Fluent code with RANS equations. The results comparison was made against the Boundary Element Method (BEM) and experiments. They found that Fluent can produce good agreement with the experimental results. Zha et al. (2014) studied the resistance of high-speed catamarans in calm water at different speed. The models were fixed with initial trim and sinkage with three different Froude numbers (Fn = 0.194, 0.388 and 0.776). The results were compared with model tests and agree very well with measured data. Samuel et al. (2015) investigate resistance components of converted traditional monohull fishing vessel into catamaran by using commercial CFD code with Slender Body Methods. The frictional resistance is calculated from ITTC 1957 correlation line, wave resistance is obtained from Slender

Body Methods and viscous resistance is determined by using form factor (1+k). The results show a good agreement with empirical formulas.

Most of the works discussed here mainly focus on how accurate that commercial CFD code can produce in estimating resistance components. Incompressible RANS equations and continuity equations with volume of fluid (VOF) method are the most favourable choice in dealing with the flow around a ship hull. Some papers present resistance of the ship for the whole range of Froude number whilst some focus on certain Froude numbers (i.e. Zha et al, 2014). Separation to length ratio was also investigated; i.e. Morarez (2004). The results obtained mainly presented resistance components against Froude or Reynolds' numbers, wave elevation along the hull, far filed wave cut, trim, sinkage and form factor.

Since resistance prediction mainly uses a form factor approach, it is important to investigate the resistance of the model correctly. This approach was introduced by Hughes (1954) in which form effect is taken into account in the extrapolation process. The example of this approach is the experimental method suggested by ITTC 1957. The form factor is firstly obtained from model tests hence the resistance of a full-scale ship. This approach relies on the independence of form factor on the Reynolds' number (Re). ITTC 1996 suggested that Reynolds' number plays an important role in varying form factor. Garofallidis (1996) and Bruzzone et al. (1997) conducted a series of experiment to investigate the scale effect on form factor; however, their results showed undesirable values. They concluded that the results were affected by turbulence due to tank interference rather than Reynolds' number.

Rather than the experimental study, the CFD approach is also capable to investigate the scale effect on form factor. In 1998, Kasahara and Masuda investigated the flow around ship using CFD at different model scales and found that form factor increases with Reynolds' number for the large model. The investigations of scale effect between a model and a full-scale ship of KVLCC were presented at Gothenburg Workshop 2000 (Larsson et al., 2002) and the results showed that form factor (k) of a full-scale ship is approximately 50 percent higher than model scale. ITTC 2002 also suggested that the scale effect on form factor might be affected by friction correlation line. Tokyo Workshop was summarised by Hino (2005) that form factor of KVLCC2 increases with Reynolds' number and comparatively agree with experiments.

Kouh et al. (2009) used a CFD code to investigate scale effect on form factor by focusing on doubling model size. They pointed out that total resistance coefficient tends to decrease relative to increasing Reynolds' number. When doubling the model size, form factor showed a nearly linear increase, which reflected a realistic Reynolds' number dependence. Raven et al. (2008) investigated scale effects on resistance of a model and a full-scale KVLCC2 using PARNASSOS CFD code. They focused on the scale effects by looking at the viscous and wave resistance. Form factor of scaling up model is significantly high compared with model scale, which could result in the increase of viscous resistance for the scaling up model. The scaling up model affected the wave resistance prediction and showed that wave resistance coefficient for a full-scale ship is 20% higher than model scale. They concluded that these differences could be from stern wave system and seemed to be reduced by viscous effects.

To widen understanding how to estimate resistance and form factor discussed above, the following sections describe the principle behind these works.

2.1.1 Resistance components of catamarans

Generally, the resistance of the ship is broken down into small components depending on the forces acting on the hull. The details of resistance components and other contributing components such as wave breaking and transom drag can be seen in figure 2.1.

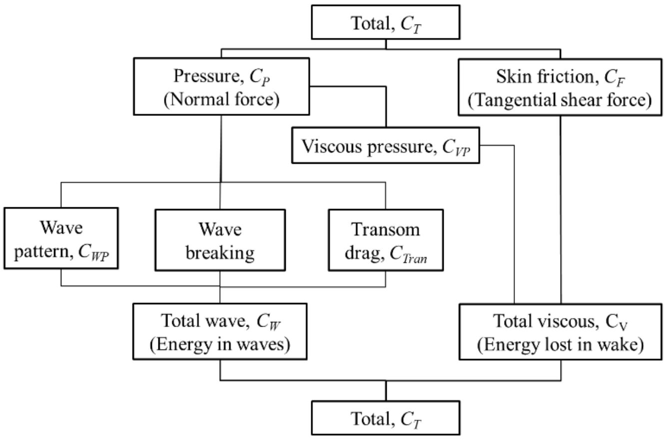

Figure 2.1 Resistance components (Molland et al., 2011)

From figure 2.1, applying traditional Froude Approach (1870), total resistance components can be expressed as:

$$C_T = C_F + C_R \qquad 2.1$$

Where, C_F is skin friction resistance which is equivalent to flat plate with the same length using ITTC 1957, $C_F = \frac{0.075}{(logRe-2)^2}$, C_R is residual resistance and derived from the model test by using equation 2.1 and become:

$$C_{TM} = C_{FM} + C_{RM} \qquad 2.2$$

Where, $C_{RS} = C_{RM}$, hence, we get:

$$C_{TS} = C_{TM} - (C_{FM} - C_{FS}) \qquad 2.3$$

By applying Hughes approach seen in figure 2.1 from bottom to top.

$$C_T = C_V + C_W \qquad 2.4$$

Where C_V is a viscous resistance coefficient involving skin friction and viscous pressure resistance.

$$C_T = C_F + C_{F0} + C_W \qquad 2.5$$

Where, $C_{F0} = kC_F$, hence it can be written as:

$$C_T = (1+k)C_F + C_W \qquad 2.6$$

By applying Froude's law as $C_{WS} = C_{WM}$, equation 2.3 becomes:

$$C_{TS} = C_{TM} - (1+k)(C_{FM} - C_{FS}) \qquad 2.7$$

2.1.2 Form factor approaches

Standard ITTC practice purpose is to break down total resistance into viscous resistance and wave resistance dependent on Reynolds' number (Re) and Froude number (Fn) respectively.

$$C_T(Fn, Re) = C_V(Re) + C_W(Fn) = (1+k)C_F(Re) + C_W(Fn) \qquad 2.8$$

Resistance components of catamarans are also broken down in the same way. However, the total resistance of catamaran is different from monohull due to the interference from flow pattern between demihulls. Normally, there are two types of interference including viscous resistance interference and wave resistance interference

(Inel, 1990 and Utama, 1999). To make the breakdown of catamaran resistance components more straightforward and easy to follow, Insel (1990) summarised the resistance components using equation 2.1 as:

- ITTC 1957 approach

$$\begin{aligned} C_{Tcat} &= C_{Fcat} + C_{Rcat} \\ &= \sigma C_F + \Omega C_R \end{aligned} \qquad 2.9$$

Where σ is frictional resistance interference factor and Ω is residuary resistance interference factor.

- Insel (1990) approach

$$\begin{aligned} C_{Tcat} &= (1+k_{cat})C_{Fcat} + C_{Wcat} \\ &= (1+\phi k)\ \sigma C_F + \tau C_W \end{aligned} \qquad 2.10$$

Where ϕ is a form resistance interference factor, and τ is a wave resistance interference factor. In this approach, ϕ is taken into account due to the effects of pressure field change around demihulls caused by flow interference. ϕ and σ can be combined together and written as $(1+\phi k)\sigma = (1+\beta k)$. It can be seen here (1+k) is called the form factor and β is viscous resistance interference factor which can be determined by applying various techniques such as towing tank experiment, wind tunnel without the presence of wave resistance and CFD approach.

2.1.2.1 Model Experiments

Molland et al. (2011) summarised techniques exploiting the experiment to determine the form factor. They pointed out that (1+k) normally depends on hull form and can be estimated directly and indirectly from the model experiment. The experimental technique used to derive form factor can be divided into three main techniques including:

- Running the model test at very low Froude number where total resistance coefficient runs parallel to the skin friction resistance coefficient line (wave resistance tends to zero) and form factor can be found as:

$$(1+k) = C_T/C_F \qquad 2.11$$

- Extrapolation of C_W at low speed. This technique is similar to the first one but the range of Froude number is relatively low (i.e. 0.1~0.2). However, they suggested that it was difficult to measure resistance correctly at low speed. ITTC Recommendation Procedure for Resistance (2008) pointed out that Prohaska (1996) adopted the same technique but used more data points at a low-speed range and showed that the form factor was calculated as:

$$C_T/C_F = (1+k) + AFn^4/C_F \qquad 2.12$$

Where A is the gradient. After that ITTC reconsidered and proposed the modification of Prohaska formula was (Molland et al., 2011):

$$C_T/C_F = (1+k) + AFn^n/C_F \qquad 2.13$$

- Measurement of resistance components directly. This technique can measure two main components: viscous resistance, C_V and wave pattern resistance, C_{WP}. From equation 2.4 and 2.5 we can see that form factor can be derived as:

$$(1+k) = C_V/C_F \qquad 2.14$$

$$\text{and} \quad (1+k) = (C_T - C_{WP})/C_F \qquad 2.15$$

The viscous resistance can be measured by using wake traverse analysis technique and then the form factor can be derived as shown in equation 2.14. This technique was used by Shearer and Cross (1965), Towsin (1968, 1971), and Insel and Molland (1992). Insel and Molland (1992) applied the technique to determine form factor of Wigley and NPL series catamarans. They measured C_V using Melville Jones (1929) formulas to evaluate the viscous drag. Only three Froude numbers, (Fn = 0.35, 0.5 and 0.7) that were investigated and they found that the results were very satisfactory for the high Froude number (Fn = 0.7). Another work adopted Melville Jones formula was investigated by Utama (1999). He applied the method to the wind tunnel experiments. He suggested that although this technique was satisfactory, the time required was impractical for this method.

C_{WP} was another parameter used to derive form factor for their work. Insel and Molland (1992) used experimental wave pattern resistance and wake analysis to derive form factors over the whole speed range using equation 2.15. Wave cuts were made at different positions in y-direction and measured downstream. They concluded that wave breaking was not included resulted in overestimate viscous resistance which may lead to overestimation of the form factor. The good point of this method was that the wave pattern resistance can be measured in a routine manner.

2.1.2.2 Geosim Series

In 1927, Telfer gave the definition to the geosim series or geosims for a series of models. This technique investigates models at different scales (Reynolds' number dependence) at the corresponding Froude numbers. However, this method needs to be made carefully because they are made at different geometrical scales. Hence, to overcome this issue Garcia-Gomez (2000) suggested that hydrodynamic qualities have to be evaluated. He also added that Iso-Froude line allows choosing the models which have the similar hydrodynamic behaviour. The geosim method has been investigated using different techniques such as experiment and CFD.

There are previous works dealing with scale effect on form factor using geosim method. van Lammeren et al. (1955) studied the scale effects on form factors for model scales of 18, 23, 40, and 60. This work was later reinvestigated by 16th ITTC (1981) to ensure the scale effects on form factor and they found that form factor increases with Reynolds' numbers. In the same year, Lackenby (1955) also investigated the scale effects of a small model with the scale factors of 6.35, 7.938, 11.906 and 15.875. The Report of OTI (1986) showed the experimental results of the geosim of Ore Carrier with model scales of 25, 34.4, 45 and 60. The results showed that model scale of 45 had the highest C_T at the same Iso-Froude line. Later on, the the Report of the 20th ITTC (1993) pointed out that this work mainly focused on the appendage drag and the scale effects on form factor were also considered. Lopez-Acevedo (1995) also conducted a series of experiments of the models with the scales of 32, 40, 60 and 80 and indicated that the results agree with the previous works. All the results discussed above showed that scale effect on form factor is Reynolds' number dependence.

As computers have developed both in term of processing capability and software, computational fluid dynamics (CFD) software is also mature enough to solve the hydrodynamic problems. There are some examples of previous works studied the scale effects on form factor using CFD approach. Tzabiras (1992) investigated the scale effects of two models with four different Reynolds' numbers varying from 10^6-10^9. For the low Reynolds' number, all CFD setups were as modelled as the experiment conducted by Patal et al. (1973). Due to the absence of free surface in this study, the form factor was calculated using equation 2.11. They found that the form factor increased with Reynolds' number and the smallest models of two bodies provided the overestimate of overall resistance by 7.2% and 10.5% respectively.

Kouh et al. (2009) used the CFD numerical approach to investigate the scale effects on form factor. They chose 6 different hull geometries without appendages consisting of Wigley hull, KVLCC2, DTMB 5415, Fishing vessel, DTRC 4621 and Torpedo as their main models. The range of Reynolds' number was between 10^7 and 10^9. Form factors were calculated using equation 2.14. A double-model assumption was adopted to obtain C_V. To use this method, it is assumed that there is no free surface flow by using a single-phase simulation in which wave resistance can be neglected and only viscous pressure can be measured. The results were presented in term of a form factor against Re, a ratio of viscous pressure component to a friction component (r*), a ratio of viscous pressure component to a friction component of a flat plate (r_P), and a ratio of friction component to a flat plate (r_F). They concluded that form factor presented a nearly linear relationship and increased with Re, and the dependence of r_P on Re influenced the scale effects on form factor.

Broglia et al (2011) investigated flow characteristics of the Delft 372 high-speed catamaran using geosim method. The CFD code was used as a supporting tool in the investigation. The main objective of the work was to investigate the flow interference phenomena between demihulls by focusing at the dependence of Re. Geosim method was used to simulate the flow at Re between 10^6 and 10^8 for two Froude numbers (0.3 and 0.45). Model scales were 2, 4, 8 and 13.33 of both monohulls and catamarans. Trim and sinkage were fixed as retrieved from experiments by Van't Veer (1998). The results showed a good agreement with experiment for high Fn whilst not satisfactory for lower Fn.

2.1.2.3 Empirical methods

The empirical method is mainly used by the ship designers in the early design stage. The amount of the experimental or numerical data of ship resistance are gathered and analysed to obtain the optimal hull forms and suitable form factor. The use of this method is described in Muhammad et al. (2014). NPL 4b was used as parent hull. By varying block coefficient (C_B) from -10% to +10%, other hull particulars are also changed i.e. B, L/B, Ws, and B/T. The results showed that form factor reduces when the separation to length ratio increases which showed a good agreement with experimental and numerical results. Samuel et al. (2015) extended the work of Muhammad by applying the empirical formula to use a fishing boat converted into a catamaran. In that study, form factors obtained from the empirical formula is used to calculate wave resistance.

2.2 CFD Implementation

2.2.1 Background

Computational fluid dynamics is a branch of fluid mechanics that uses numerical methods and algorithms to solve and analyse problems involving fluid flows. To understand the calculations made in the background of the CFD software, it is important to understand the theory behind the software. For the problems concerning the hydrodynamics, global pressures and fluid velocity components must be calculated in a 3-dimensional space surrounding the vessel in the fluid domain. It is possible to calculate the forces and moments acting on the vessel, whether steady or unsteady. A commercial CFD code allows the user to make further assumptions in flow behaviours depending on the nature of the problems.

Recently, there are a lot of CFD software which can deal with the problem discussed above i.e. OpenFaom, ANSYS (Fluent and CFX), and STAR-CD. This software has different advantages and disadvantages which can influence the user's requirements. For example, OpenFOAM has an extensive range of features to solve anything from complex fluid flows involving chemical reactions, turbulence and heat transfer, to solid dynamics and electromagnetics. The main disadvantage of this software is that users need to be an expert in C language. ANSYS software package is a commercial CFD software, which combines the relevant software together such as Workbench, a worksheet for the whole process, ICEM mesh tool and solvers (Fluent and CFX). This kind of package is favourable in term of graphical user interface (GUI). However, the complexity in combining these packages is the main disadvantage .

2.2.2 Equations and Methods for Marine CFD

Mainly, CFD software concerns hydrodynamic problems which majority of the problems will deal with global pressure and fluid velocity components in a 3-dimensional space around the submerged part of the marine vehicle or any other platforms that are investigated. Furthermore, it is possible to calculate forces and momentums acting on the interesting objects in both steady and unsteady state. Hence, to start with CFD software, it is better to understand definitions of the general fluid equations of motions. Mostly, commercial CFD software applications have been designed to solve all kinds of the problem associated with fluid flow i.e. in case of compressible, incompressible, viscous and turbulence flow and heat transfer which is applied to boundary conditions. Equations of motion of fluid will be discussed in the following sections.

2.2.2.1 General Equations

Normally, equations of fluid flow are initiated from the conservation laws of physics under the following assumptions:

- Fluid mass is conserved
- Rate of change of momentum equals the sum of forces acting on the fluid structure (Newton 2nd Law)
- Rate of change of energy equals the sum of the rate of heat addition to and the rate of work done on particle or Law of energy conservation.

It should be noted that in this case, we can ignore the rate of change of heat transfer, so only momentum equations are considered. The governing equations for unsteady, three dimensional, compressible viscous flow can be written as:

- Continuity equation:

$$\frac{\partial \rho}{\partial t} + \nabla \cdot (\rho U) = 0 \qquad 2.16$$

- Momentum Equations:

x component

$$\frac{\partial (\rho u)}{\partial t} + \nabla \cdot (\rho u U) = -\frac{\partial p}{\partial x} + \frac{\partial \tau_{xx}}{\partial x} + \frac{\partial \tau_{yx}}{\partial y} + \frac{\partial \tau_{zx}}{\partial z} + \rho f_x \qquad 2.17$$

y component

$$\frac{\partial(\rho v)}{\partial t} + \nabla \cdot (\rho v U) = -\frac{\partial p}{\partial y} + \frac{\partial \tau_{xy}}{\partial x} + \frac{\partial \tau_{yy}}{\partial y} + \frac{\partial \tau_{zy}}{\partial z} + \rho f_y \qquad 2.18$$

z component

$$\frac{\partial(\rho w)}{\partial t} + \nabla \cdot (\rho w U) = -\frac{\partial p}{\partial w} + \frac{\partial \tau_{xz}}{\partial x} + \frac{\partial \tau_{yz}}{\partial y} + \frac{\partial \tau_{zz}}{\partial z} + \rho f_z \qquad 2.19$$

Where: ρ is fluid density

$U = (u, v, w)$ is the fluid velocity

p is pressure

$f = (f_x, f_y, f_z)$ is a body force e.g. weight due to gravity and magnetic force

τ_{nn} is viscous stress

These equations are known as the Navier-Stokes equations named after the Frenchman Claude Navier and the English man George Stokes. As this project needs to deal mainly with the incompressible flow, which fluid viscosity is constant throughout the flow so the continuity equation can be rewritten as:

$$\nabla \cdot U = 0 \qquad 2.20$$

The momentum equations are as follow:

x component

$$\rho \frac{Du}{\partial t} = -\frac{\partial p}{\partial x} + \mu \nabla^2 u + \rho f_x \qquad 2.21$$

y component

$$\rho \frac{Dv}{\partial t} = -\frac{\partial p}{\partial y} + \mu \nabla^2 v + \rho f_y \qquad 2.22$$

z component

$$\rho \frac{Dw}{\partial t} = -\frac{\partial p}{\partial z} + \mu \nabla^2 w + \rho f_z \qquad 2.23$$

Where D/Dt is the substantial derivative given by:

$$\frac{D}{Dt} = \frac{\partial}{\partial t} + u \frac{\partial}{\partial x} + v \frac{\partial}{\partial y} + w \frac{\partial}{\partial z} \qquad 2.24$$

It can be seen that continuity and momentum equations are decoupled from the energy equation and sufficient to solve the velocity and pressure fields in incompressible flows.

2.2.2.2 Turbulent Models

Although the equations derived previously are sufficient to describe the incompressible, laminar and continuous flow, in reality, there are non-linear flows happening which can cause unsteady flow. Hence, it is not possible to solve the flow problem numerically. To overcome this issue, turbulence models are introduced by applying numerical methods. These methods allow the flows to be solved numerically. To make it more simply, it is assumed that the components of the flow velocity and pressure consist of mean value with superimposed fluctuations. This means that the fluctuations vary within the spectrum of the values in term of frequency and amplitude. Hence this allows the spectrum of the turbulent kinetic energy to be analysed by using statistical tools. Reynolds-averaged Navier-Stokes Equations (RANSE) is the most recognised model which applies a turbulent model to the equations of motion. It can be seen that on the time average, x-component momentum equation becomes:

$$\begin{aligned}&\rho\left[\frac{\partial(u^2)}{\partial x}+\frac{\partial(uv)}{\partial y}+\frac{\partial(uw)}{\partial z}\right]\\&=-\frac{dP}{dx}+\frac{\partial}{\partial x}\left[\mu\frac{\partial u}{\partial x}-\rho\overline{u'^2}\right]+\frac{\partial}{\partial y}\left[\mu\frac{\partial u}{\partial y}-\rho\overline{u'v'}\right]+\frac{\partial}{\partial z}\left[\mu\frac{\partial u}{\partial z}-\rho\overline{u'w'}\right]\end{aligned}\tag{2.25}$$

y-component momentum equation becomes:

$$\begin{aligned}&\rho\left[\frac{\partial(v^2)}{\partial y}+\frac{\partial(uv)}{\partial x}+\frac{\partial(vw)}{\partial z}\right]\\&=-\frac{dP}{dy}+\frac{\partial}{\partial y}\left[\mu\frac{\partial v}{\partial y}-\rho\overline{v'^2}\right]+\frac{\partial}{\partial x}\left[\mu\frac{\partial v}{\partial x}-\rho\overline{u'v'}\right]+\frac{\partial}{\partial z}\left[\mu\frac{\partial v}{\partial z}-\rho\overline{v'w'}\right]\end{aligned}\tag{2.26}$$

z-component momentum equation becomes:

$$\begin{aligned}&\rho\left[\frac{\partial(w^2)}{\partial z}+\frac{\partial(uw)}{\partial x}+\frac{\partial(vw)}{\partial y}\right]\\&=-\frac{dP}{dz}+\frac{\partial}{\partial z}\left[\mu\frac{\partial w}{\partial z}-\rho\overline{w'^2}\right]+\frac{\partial}{\partial x}\left[\mu\frac{\partial w}{\partial x}-\rho\overline{u'w'}\right]+\frac{\partial}{\partial y}\left[\mu\frac{\partial w}{\partial y}-\rho\overline{v'w'}\right]\end{aligned}\tag{2.27}$$

As can be seen, Reynolds' stress ($\rho\overline{u'v'},\rho\overline{u'w'}, and\ \rho\overline{v'w'}$) are treated as extra stress which initiated from the nature of the flow. There are many methods to evaluate these stresses and most of them rely to a greater or lesser extent on further assumptions and simplifications. Consequently, the results are subjected to fluctuation or turbulence which leads to complexity in fulfilling theory. To deal with this complex problem, one of the simplest assumptions has been proposed by assuming that the combined effect of Reynolds stresses is as an additional viscosity acting to produce fluid stress. These can simplify the production of the eddy viscosity (v_e) and the local velocity gradient. The most common method to evaluate these values is the use of the k-ε model or the two-equation model which can be seen as:

$$v_e = C_\mu k^2/\varepsilon \qquad 2.28$$

Where, $C_\mu$is a constant with normal value of 0.09

k is the turbulent kinetic energy per unit mass and

ε is the rate of dissipation of turbulent kinetic energy per unit mass

There are several improvements and variants from this principle such as RNG k-ε, k-ω, and Realisable k-ε (Wilcox (1998) and Menter and Kuntz (2002)). However, the way to choose the suitable turbulent model is the most important point of view, which mostly depends on flow types. In realistic flow, the most likely to occur for the flow around the ship especially for a high-speed vessel is the turbulence flow. The turbulent flow behaviour varies almost all over the vessel surface lying under the water. According to this kind of flow, turbulence models should be applied correctly to the problem to achieve the most appropriate and accurate results.

2.2.3 Boundary Conditions

To simulate the flow correctly, there are other aspects which need to be considered and dealt with carefully. One of those is boundary condition due to the fact the flow will be simulated in three-dimensional space. The following in this section will discuss the importance of boundary conditions which could influence the simulation accuracy. There are generally two types of boundary condition which can be applied to the problem including:

- Dirichlet boundary condition, this describes where a fixed or prescribed value is defined for the variable of interest at known points on the boundary.
- Neumann condition, this explains where the gradient, which is commonly normal to the boundary, of the variable is known.

The first boundary condition is used to calculate the flow around a moving ship at a constant forward speed with an axis system also moving with the ship. The fluid is assumed to enter the domain at an upstream boundary or inlet which can be described as the ship is fixed while water and air flow through it. Normally, in this case, velocity at inlet boundary is set as the ship speed but in opposite direction. In addition to that pressure and forces acting on the ship can be measured by set velocity component around the hull as zero or known as non-slip wall boundary condition.

The second boundary condition is initiated under the time-consuming reduction concept. This results in symmetry boundary condition, normally known as symmetry plane. The symmetry plane normally is applied along the hull centreline which can reduce the size of the computational domain and number of cells. Moreover, the scalar pressure and velocity components are tangential to this boundary which means that the gradient normal to this boundary is zero.

Outlet boundary for both types of boundary conditions is mostly set as pressure outlet for marine application to get better results. However, inlet boundary can be applied on other planes such as side, top and bottom depending on the type of solution method used. For example, STAR-CCM+ mostly recommends inlet on all planes except symmetry plane and outlet when k-ε and k-ω turbulent models are used (STAR CCM+ version 8.04 tutorial).

2.2.4 Volume of Fluid Method (VOF)

The VOF method is based on a concept of a fractional volume of fluid. It is assumed that the fraction of fluid in each cell is represented by a function, F, and its value is unity in a cell full of water and zero value represents no water. Hence, a cell which has a value between 0 and 1 must contain a free surface. The free surface field can be expressed by the transport equation in conservative form as follow:

$$\frac{\partial F}{\partial t}+\frac{\partial uF}{\partial x}+\frac{\partial vF}{\partial y}+\frac{\partial wF}{\partial z}=0 \qquad 2.29$$

Where t is the physical time

u, v and w are Cartesian components of velocity

The VOF model description assumes that all immiscible fluid phases presented in a control volume share velocity, pressure and temperature fields. Hence, the same set of basic governing equations describing momentum, mass and energy transport in a single-phase flow is solved. The equations are solved for an equivalent fluid whose physical properties are calculated as functions of the physical properties of its constituent phases and their volume fractions.

2.2.5 Discretization

This is the process by which the governing equations of fluid mechanics are replaced by equivalent expressions: at discrete points in the case of a partial differential equation, known as *finite difference method*, and for discrete volumes in the case of an integral equation, known as *finite volume method*. In this case, only the finite difference method will be discussed briefly since both methods are very similar but finite difference method is easier to understand. The example of the finite difference grids can be seen in figure 2.2. The principle behind this method is to replace the original differential equation with algebraic expressions evaluated at the discrete points only and this will influence the neighbouring points.

- ***Finite difference method***

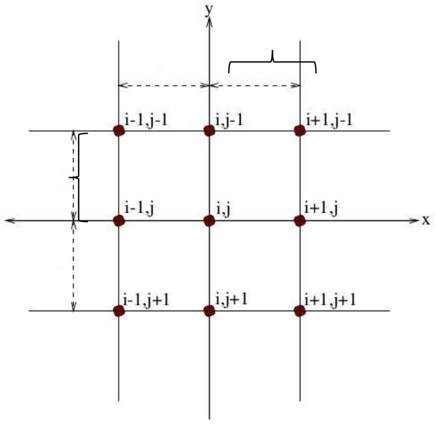

Figure 2.2 Finite difference grids (Anderson, 1995)

To apply this principle effectively, it is important to apply Taylor's series expansion. From figure 2.2, considering the right-hand point of i, it is said that $u_{i,j}$ donates the x-component of velocity at point (i, j) so the velocity $u_{i+1,j}$ at point $(i +$

$1, j)$ can be expressed in term of Taylor's series expansion about the point (i, j) as seen in equation 2.30.

$$u_{i+1,j} = u_{i,j} + \left(\frac{\partial u}{\partial x}\right)_{i,j} \Delta x + \left(\frac{\partial^2 u}{\partial x^2}\right)_{i,j} \frac{(\Delta x)^2}{2} + \left(\frac{\partial^3 u}{\partial x^3}\right)_{i,j} \frac{(\Delta x)^3}{6} + \cdots \qquad 2.30$$

or

$$\left(\frac{\partial u}{\partial x}\right)_{i,j} = \frac{u_{i+1,j} - u_{i,j}}{\Delta x} - \left(\frac{\partial^2 u}{\partial x^2}\right)_{i,j} \frac{(\Delta x)^2}{2} - \left(\frac{\partial^3 u}{\partial x^3}\right)_{i,j} \frac{(\Delta x)^3}{6} + \cdots \qquad 2.31$$

As if the partial derivative is approximated with the finite difference expression:

$$\left(\frac{\partial u}{\partial x}\right)_{i,j} = \frac{u_{i+1,j} - u_{i,j}}{\Delta x} + O(\Delta x) \qquad 2.32$$

As can be seen, the remaining on the right-hand side are neglected and the sum of these terms is called the truncation error. This expression is known as the first-order accuracy which is the lowest order. Where $O(\Delta x)$ represents *term of order* Δx. Likewise, considering the left side; the expression obtained is called first-order backward difference as seen in equation 2.33.

$$\left(\frac{\partial u}{\partial x}\right)_{i,j} = \frac{u_{i,j} - u_{i-1,j}}{\Delta x^2} + O(\Delta x) \qquad 2.33$$

In order to get more accurate results, the higher orders are needed. For the second-order central difference, this can be obtained by subtracting equation 2.32 from equation 2.33 and rearrange:

$$\left(\frac{\partial^2 u}{\partial x^2}\right)_{i,j} = \frac{u_{i+1,j} - 2u_{i,j} + u_{i-1,j}}{(\Delta x)^2} + O(\Delta x)^2 \qquad 2.34$$

In the same way, considering $u_{i,j}$ respect to y we will get the second-order central difference as:

$$\left(\frac{\partial^2 u}{\partial x \partial y}\right)_{i,j} = \frac{u_{i+1,j+1} - u_{i+1,j-1} - u_{i-1,j+1} + u_{i-1,j-1}}{4\Delta x \Delta y} + O[(\Delta x)^2(\Delta y)^2] \qquad 2.35$$

The second-order accuracy in space is the most common general-purpose for CFD code due to the fact that there are some disadvantages of higher orders. Higher-order accuracy requires more grid points resulting in more computational time for each time or spatial step. However, the desired accuracy level for various CFD cannot be justified; hence to avoid complexity and high time consuming, second-order accuracy is said to be adequate for the majority of CFD applications.

- ***Finite volume method***

In the finite volume method, the integral form of the conservation equations is applied to the control volume defined by a cell to get the discrete equations for the cell. For steady, incompressible flow, the continuity equation can be reduced to:

$$\int_S \overrightarrow{V} \cdot \hat{n} dS = 0 \qquad 2.36$$

Where this is the integration over the surface S of the control volume and $\hat{n}$ is the outward normal at the surface. This can be clearly seen in figure 2.3.

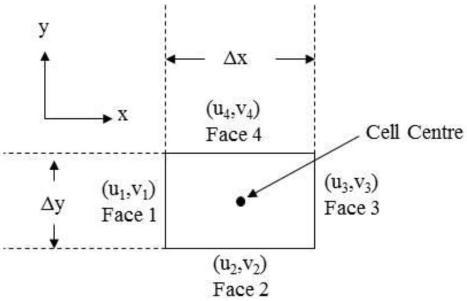

Figure 2.3 Finite volume cells (Anderson, 1995)

From figure 2.3, the velocity at face i is taken to be $\overrightarrow{V_i} = u_i\hat{\imath} + v_i\hat{\jmath}$. To this point, mass conservation equation (Eqn. 2.36) is applied to the control volume, which can be defined by the cell as:

$$-u_1\Delta y - v_2\Delta x + u_3\Delta y + v_4\Delta x = 0 \qquad 2.37$$

Equation 2.37 is called the discrete form of the continuity equation for the cell. This equals the sum of the net mass flow into the control volume and set it to zero.

2.2.6 First Layer Thickness

The first layer thickness can be defined as a wall distance which is the first distance from the centroid of the first cell adjacent to the hull. Normally, this value is defined as a dimensionless distance known as y^+.

$$y^+ = \frac{\rho u_* y_1}{\mu} \qquad 2.38$$

Where, y_1 is the first layer thickness (m)
ρ is fluid density (kg/m^3)
μ is fluid dynamic viscosity (Ns/m^2)
u_* is frictional velocity

The mesh should be arranged in the suitable range for geometry and flow problem. The values of y^+ at the wall adjacent cells directly influence the prediction of friction and drag. In this case, first layer thickness should be dealt with carefully to achieve the most suitable wall distance hence friction and drag.

2.2.7 Grid Generation

Regarding the STAR CCM+ version 8.04 meshing tool, a mesh is the discretized representation of the computational domain, which the physic solvers use to calculate a numerical solution. There are two main mesh types which are normally used: unstructured and structured meshes.

Unstructured meshes are widely used with the complex geometry where a structured mesh is difficult to generate due to geometry and domain limitations. Basically, tetrahedral and polyhedral cells are generated in this mesh type. The polyhedral mesh is relatively easy and efficient to build and requires no more surface preparation compared with a tetrahedral mesh and it contains approximately five times fewer cells compared with a tetrahedral mesh as can be seen in figure 2.4. The tetrahedral mesher provides an efficient and simple solution for complex-mesh generation problems. Out of the two provided meshes, the tetrahedral is the fastest and uses the least amount of memory for a given number of cells. Multi-part or multi-region meshes with a conformal mesh interface are allowed.

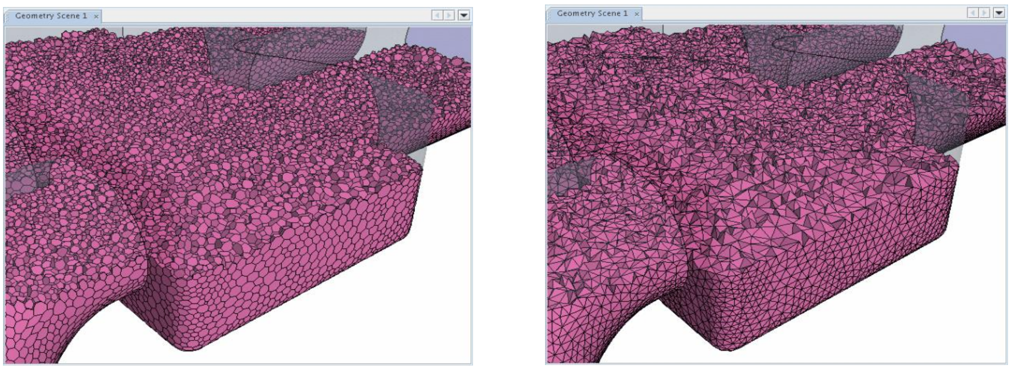

a) Polyhedral b) Tetrahedral

Figure 2.4 Unstructured mesh (STAR CCM+ v8.04)

Another mesh types are structured meshes, normally appropriate for simple geometries and domains. It mainly contains hexahedral cells. There are three main structured mesh configurations including C, H and O grid. C type is suitable for a simple geometry and rounded with the rectangular domain where the mesh can be extruded in the straight direction as shown in figure 2.5. H-grid is mainly used with the rectangular domain where the mesh can be extruded in all directions, see figure 2.6. For rounded and oval geometry and domains, the O-grid mesh is the most suitable application and this can be seen in figure 2.7.

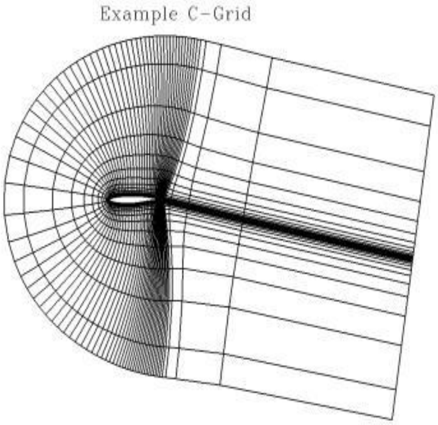

Figure 2.5 C-grid mesh (STAR CCM+ v8.04)

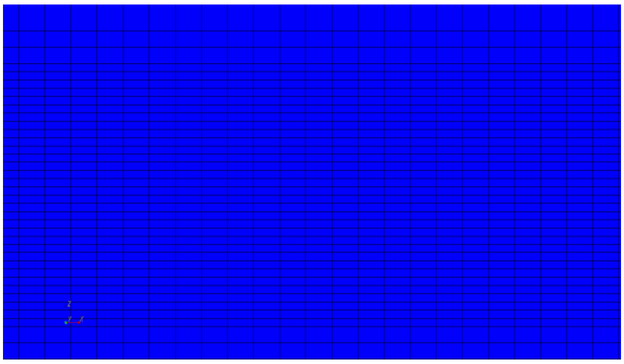

Figure 2.6 H-grid mesh

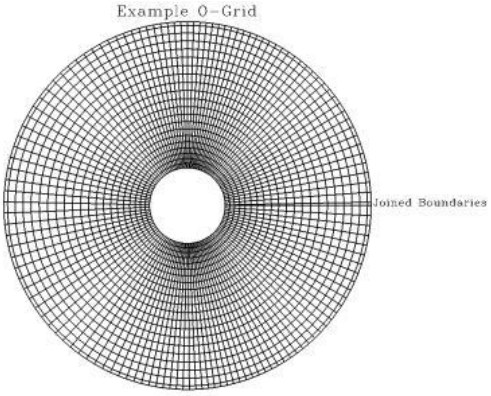

Figure 2.7 O-grid mesh (STAR CCM+ v8.04)

STAR-CCM+ provides meshers and tools, which can be used to generate a quality mesh for various geometries and applications (STAR CCM+ v. 8.04 tutorial). There are many mesh strategies, which are suitable for different applications. For this stage, a surface remesher and a trimmed mesher with prism layer are used. The surface remesher is a tool to recreate and improve an existing surface and optimize it for a volume mesh. This tool is very important because if the geometry surface is created roughly during the mesh process, surface will be recreated or repaired to get better results. The trimmed cell mesher provides a robust and efficient method of producing a high-quality grid for both simple and complex mesh generation problems. It combines a number of desirable meshing attributes in a single meshing scheme including:

- predominantly hexahedral mesh with minimal cell skewness
- refinements that are based upon surface mesh size and other user-defined refinement controls
- surface quality independence
- alignment with a user-specified coordinate system

Chapter 3: The Use of CFD Techniques

3.1 Introduction to the Methodology

Since this research project focuses on how to estimate resistance components and form factor of the high-speed catamaran using commercial CFD code, it is important to understand how to use the CFD code correctly. The use of CFD techniques in determining those parameters is demonstrated in this chapter.

To create the flow around hull travelling with advance speed through the water, it is important to understand how the flow phenomena appear in reality. To this point, this study divides characteristic of the flow into two main components including flow characteristic near the hull geometry, and divergent and transverse wave at far field area. The flow close to the hull is mainly determined by evaluating wave elevation along the hull, which is measured from experiments and numerical studies. For example, at the far field region, wave elevation also needs to be considered carefully because it can be used in estimating viscous pressure and wave pattern resistance.

Numerical wave tank study focuses on how to create a mesh to capture the waves correctly. This can be done by concentrating on grid generation: how the number of cells per wavelength and wave height affects the accuracy of the results. Total grid for resistance shows the importance of cells to solve the flow equations to obtain the precise results. Mostly, the grid dependence is investigated by generating different types of the grid from coarsest to finest and then the results will be validated against the experiment. Turbulence models are also compared to select to most effective model for estimating resistance simultaneously. The flow pattern in the wake area is concerned by focusing on how the grid generation affects the accuracy of the results and is validated by measuring wave cuts at certain position with the experiment.

3.2 Numerical Wave Tank

Wave simulation is the first step for this research. This small step is one of the most important processes because in reality when the ship travelling through the water wave system will appear around the hull. The wave system is sometimes used as the tool to assess the degree of accuracy, i.e. the wave elevation along the hull and wave cut at far field area. These wave systems have different amplitudes and lengths; thus, to capture the accurate flow field, it needs to determine how to create a grid of the appropriate quality.

3.2.1 Grid Dependency

Before simulating the cases, it is important to optimize the mesh quality, which will be used in the full running cases. Mainly, the cells per wavelength and wave height are the most important. According to STAR CCM+ v 8.04 tutorials, at least 20 cells per wave height and higher for short waves are recommended. Windén (2012) also suggested that cell per wave height should be between 30 and 40. The number of cells per wavelength can also affect the accuracy of the simulation thus STAR CCM+ (v 7.0 and 8.04) tutorials suggest that 80-100 cells per wavelength could provide desirable results. To minimize the cases, which can be the time consumption, only cells per wave height will be investigated while cells per wavelength will be kept as the recommendation by STAR CCM+ tutorial. The wave used in the grid dependency verification is shown in table 3.1. Grid dependency verification for numerical wave tank focuses on W1 in table 3.1.

Table 3.1 Waves used for validation

Wave	H (m)	λ (m)	T (s)
W1	0.0425	1.210	0.88
W2	0.0395	1.560	1.00
W3	0.0560	3.510	1.50
W4	0.0755	6.000	2.00

Cells per wave height will be varied from 10 to 40 by increasing 10 interval cells in each case, except in between 20 and 30 the interval is 5 cells. The coarsest grid is about 0.252 million cells while the finest grid is about 0.942 million cells. A mesh refinement is also used in this step to reduce the number of cells. The refinement used in these simulations applies the progressive technique, which doubles cell size for each refined region from the free surface through the water column. Five different grids are created to optimize the suitable number of cells per wave height as shown in table 3.2.

Table 3.2 Grid generations

Mesh Type	Cells		Total cells (x10^6)
	Cells/λ	Cells/H	
G1	100	10	0.252
G2	100	20	0.512
G3	100	25	0.631
G4	100	30	0.755
G5	100	40	0.942

To avoid the effect from the outlet boundary, the damping region is deployed at the outlet, which at least equals the wavelength. Moreover, the number of cells in y-direction is also kept as the minimum, 2 global cells on faces. This technique is applied to reduce the simulation from full 3D to 2.5D. The physical time for these simulations is set to be 20s to allow the waves to develop fully. In these cases, the CFL number is set to be between 0.5 and 1.0. A symmetry plane is used to reduce cells and time consumption. The 1st order Stokes wave is selected to analyze grid dependency. During the simulation, both CFD and theoretical results will be plotted simultaneously to compare the results. Wave profiles are measured at the middle of the tank from the inlet boundary. The position, where the probe is, is considered as the fact that the distance is long enough for waves to propagate fully and far from the outlet to avoid reflection effect, see figure 3.1.

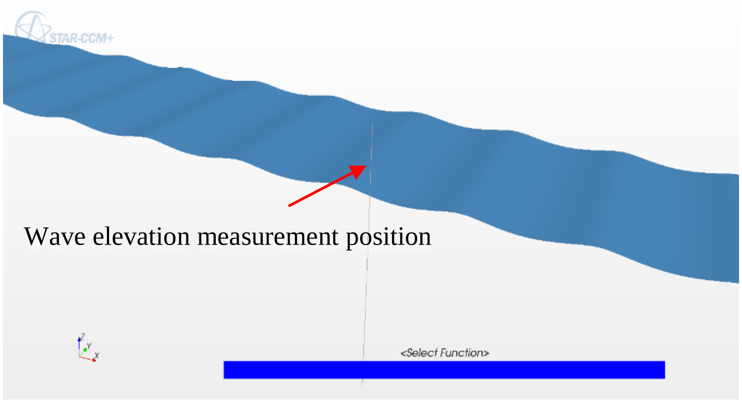

Figure 3.1 Wave free surface

The verification results show root mean square error (RMSE) for the grids. As can be seen in figures 3.2 and 3.3, the number of cells increases the better the results. As found from the literature, 20 cells per wave height can yield an acceptable result. Regarding the STAR CCM+ tutorials and recommendations for the short wave as appearing in the wave system around ship hull, number of cells per wave height between 30 and 40 provide quite similar results, hence it could be concluded that the optimum point would be within this region.

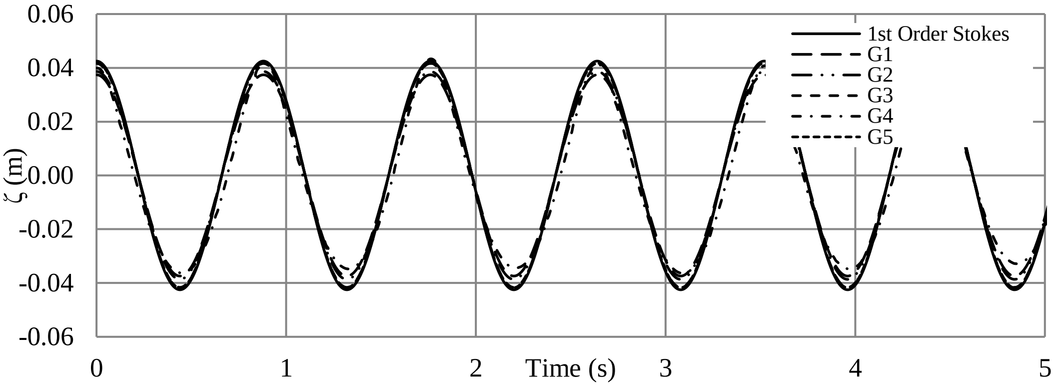

Figure 3.2 Wave W1 results

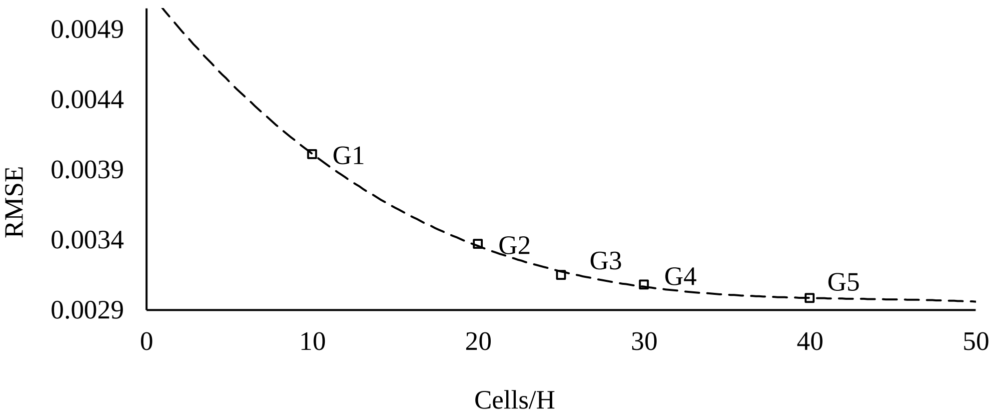

Figure 3.3 Wave results RMSE

3.2.2 Validations

In order to validate the CFD simulation, the 1^{sh} order Stokes waves are used in this step due to the availability of validation data. Case settings are almost the same with the grid dependency study except the domain size replicates the Southampton Solent towing tank. Towing tank dimensions are 60m in length, 3.7m in width and

1.86m in depth. Measurement and plot are taken using the same technique with the grid dependency study. The CFD results are validated against the 1st order Stokes, experiment on regular waves produced by Denchfield (2010) and CFD results from Wood (2013). The validation shows quite good agreement with theory and other's results, which can be seen from figures 3.4 to 3.6.

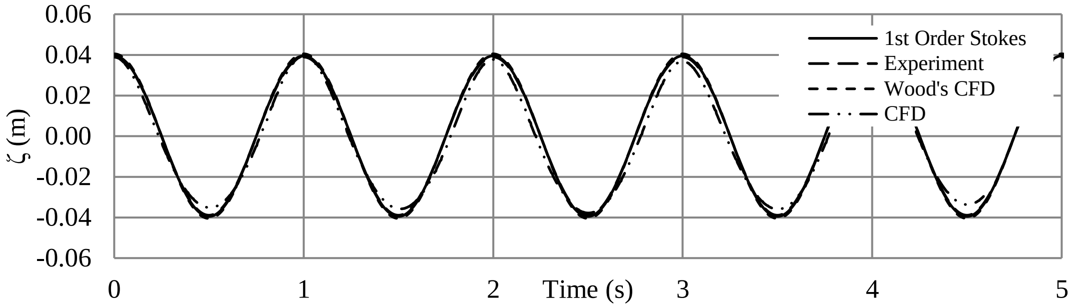

Figure 3.4 Wave W2 validation

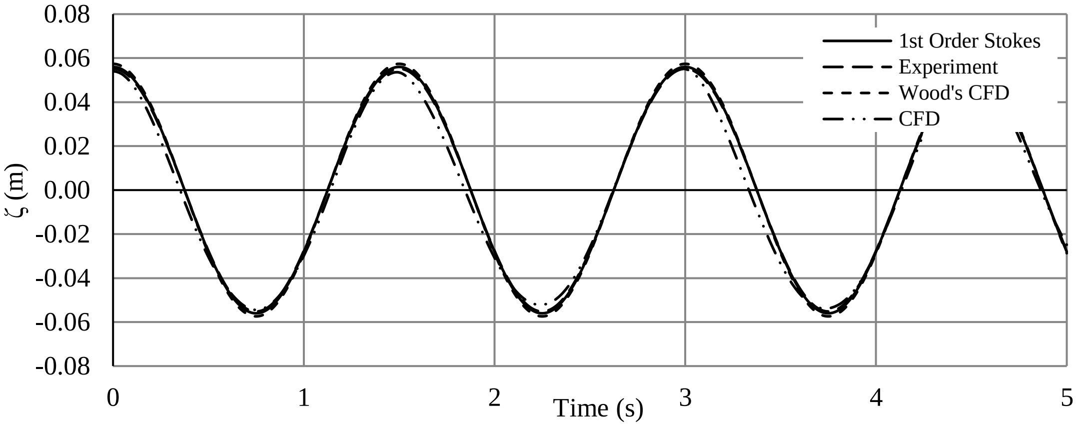

Figure 3.5 Wave W3 validation

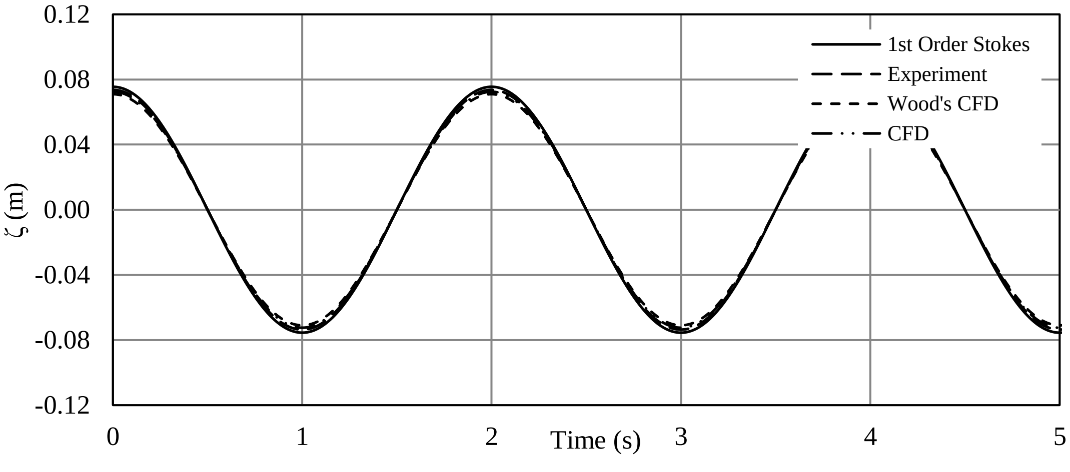

Figure 3.6 Wave W4 validation

3.3 Grid Dependence on Hull Resistance

3.3.1 Hull Geometry

There are numbers of hull geometries for high-speed vessels which can be investigated such as NPL, Delft 372, NOR and Wigley, however, to avoid the complexities in evaluating the accuracy of the simulation due to the flow separation behind transom stern, Wigley hull is the most suitable choice for this step. There are four variant models of the Wigley and each model is generated from the mathematical formulation. The model I and II have very high C_M, which can result in high C_B and this means that these models are not suitable for being used in the high-speed vessel research. The model III and IV have the same C_M but higher slenderness than model I and II, but the length to breadth ratio of model IV is halved of model III (Journeé, 1992). It can be concluded that the slenderness of model III is higher than model IV. Therefore, model III is selected to investigate the resistance of high-speed vessel in this study. Wigley hull is originally created from the mathematical formulation, a right-handed coordinate system defined by O(ξ,η,ζ), which can be seen in equation 3.1.

Where O is original amidships in the water plane
ξ is longitudinal axis, positive forwards
η is lateral axis, positive to the port side
ζ is vertical axis, positive downward

$$\eta = (1-\zeta^2)(1-\xi^2)(1+a_2\xi^2+a_4\xi^4)+\alpha\zeta^2(1-\zeta^8)(1-\xi^2)^4 \qquad 3.1$$

Where $a_2 = 0.2$ for all models
$a_4 = 0.0$ for all models
$\alpha = 1.0$ for model I and II with Cm = 0.909
$\alpha = 0.0$ for model III and IV with Cm = 0.667

Let multiple ξ by 2/L, η by 2/B and ζ by 1/T

Where L = Length, B = Breadth and T = Draught of the ship

Substitute all values to equation 3.1 so new mathematical formulation of the Wigley III becomes:

$$\eta = \frac{B}{2}\left[1-\left(\frac{\zeta}{T}\right)^2\right]\left[1-\left(\frac{2\xi}{L}\right)^2\right]\left[1+a_2\left(\frac{2\xi}{L}\right)^2\right] \qquad 3.2$$

Wigley III hull particulars can be seen in table 3.3 and figure 3.7

Table 3.3 Wigley III hull particulars

Model	Wigley III
L, *m*	1.80
L/B	10.00
B/T	1.60
$L/\nabla^{1/3}$	7.116
C_B	0.444
C_P	0.667
C_W	0.667
WS, m^2	0.482

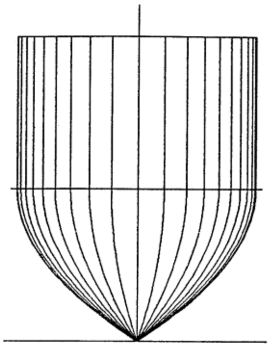

Figure 3.7 Wigley III (Insel, 1990)

3.3.2 Mesh Techniques

Grid dependency is also the first step for resistance simulation. The grids are the same with wave generation including coarse, medium and fine mesh respectively. Regarding the experimental results retrieved by Insel (1990), the experiment was done in the Southampton Solent towing tank, thus domain dimensions and other setups need to be the same with those conditions. Domain dimensions are presented in table 3.4. It should be noted that turbulence models used in this step are k-ε and SST k-ω with a higher degree (2nd order) of accuracy (STAR CCM+ tutorial v 7.0 and 8.04). From the literature, it is suggested that the total number of cells to estimate resistance components is at least 1 million cells. Hence, the range of cells is between 1.87 and 6.37 million cells, see table 3.5.

There are several factors, which need to be considered to create an appropriate grid for determining resistance components. The first factor is mesh density close to the hull. The density in this area must be denser when moving close to the hull to capture the boundary layer. Mesh density at the aft part of the hull must be fine enough to capture the viscous wake. The free surface is another area that needs special treatment due to the fact it is sensitive for the multiphase simulation so mesh density in the free surface must be fine enough to capture wave pattern correctly. The transition between these areas must be smooth. The last factor is the number of cells should be minimized to reduce calculation time.

Regarding those factors discussed in the previous paragraph, several refinement blocks are used. Three blocks are created around the hull including a small block close to the hull, a block near the hull and the biggest block at the surrounding area. In the wake area, the refinement-block shape is designed following the wave system occurs around the hull to minimize number of cells. Another two blocks are added to cover all free surface area which one block is doubling of another. These refinement blocks can be seen in figures 3.8, 3.9 and 3.10 respectively. Tables 3.4 and 3.5 show the numerical domain dimensions and setups. By applying all wall function (all wall y^+), wall y^+ is kept as lower than 1 or between 30 and 50 as recommended by STAR CCM+ tutorial.

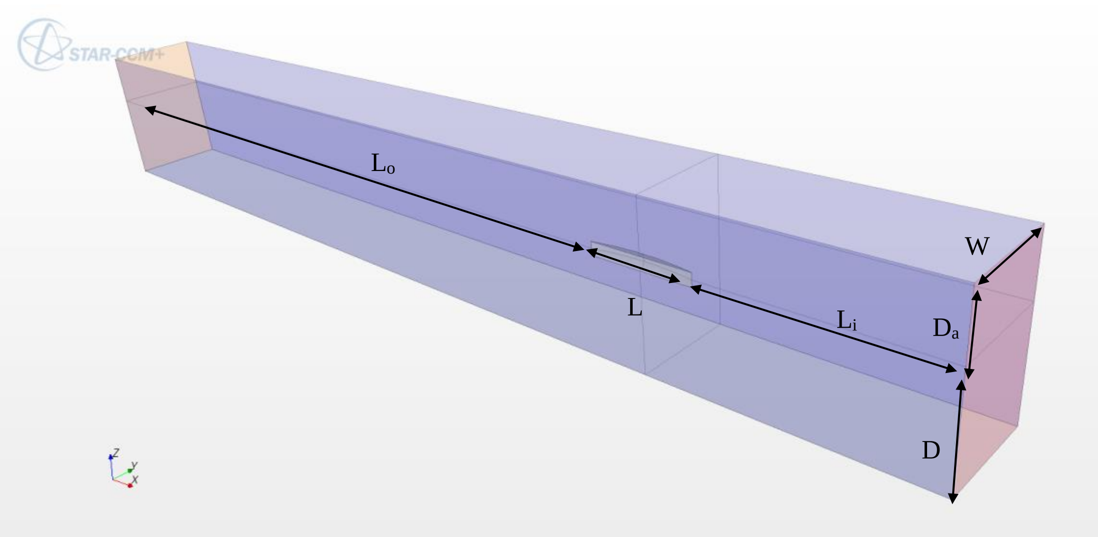

Figure 3.8 Numerical domain

Table 3.4 Numerical domain

Hull length, *m*	L	1.80
Tank width, *m*	W	1.85
Tank depth, *m*	D	1.80
Air, *m*	D_a	1.00
Inlet from bow	L_i	3L
Outlet from stern	L_o	9L

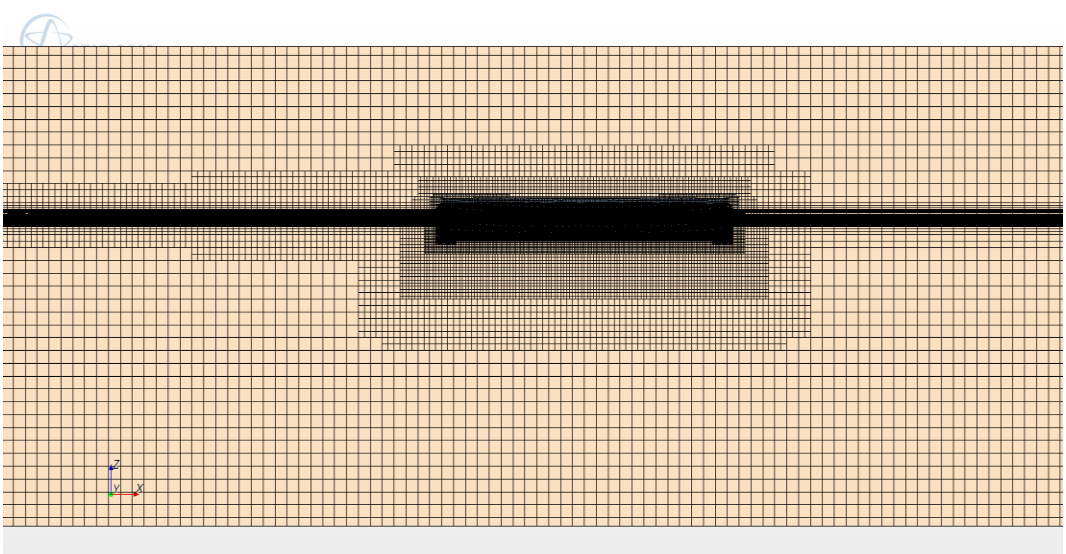

Figure 3.9 Mesh created around the hull and free surface

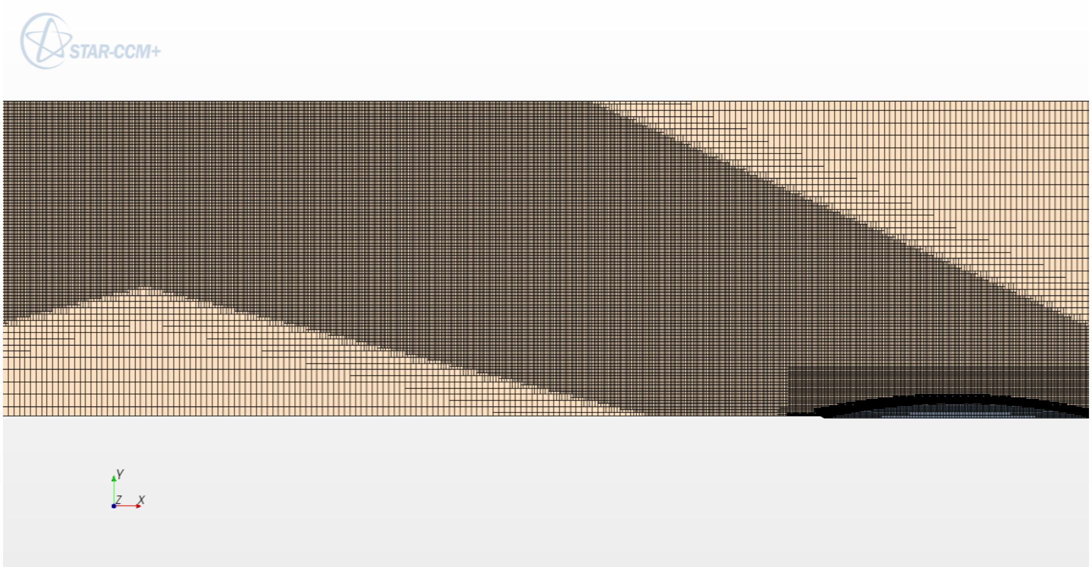

Figure 3.10 Mesh created to capture viscous wake and wave pattern

Table 3.5 Grid generation for resistance study

Mesh	G1	G2	G3	G4	G5
Domain:					
Length from inlet	3L	3L	3L	3L	3L
Length from outlet	9L	9L	9L	9L	9L
Beadth (*m*)	1.85	1.85	1.85	1.85	1.85
Draught (*m*)	1.8	1.8	1.8	1.8	1.8
Air (*m*)	1.0	1.0	1.0	1.0	1.0
Cells ($x\ 10^6$)	~1.87	~2.75	~3.78	~5.54	~6.37
Turbulence model	k-ε and SST k-ω				
Average wall y^+	$y^+ < 1$ or $30 < y^+ < 50$				
Boundary condition:					
Velocity Inlet	Inlet and Top				
Pressure Outlet	Outlet				
Non-slip Wall	Hull and Deck				
Slip wall	Side and Bottom				
Symmetry	Symmetry plane				

3.3.3 Simulation Results

Table 3.6 Result validations

Grid	Cells (M)	C_T (x 10^{-3})			
		k-ε	% Error	SST k-ω	%
Fn = 0.35					
Experiment		5.495			
G1	~ 1.87	5.124	-6.76	5.246	-4.53
G2	~ 2.75	5.346	-2.71	5.381	-2.07
G3	~ 3.78	5.413	-1.49	5.433	-1.12
G4	~ 5.54	5.447	-0.87	5.462	-0.60
G5	~ 6.37	5.448	-0.85	5.467	-0.51

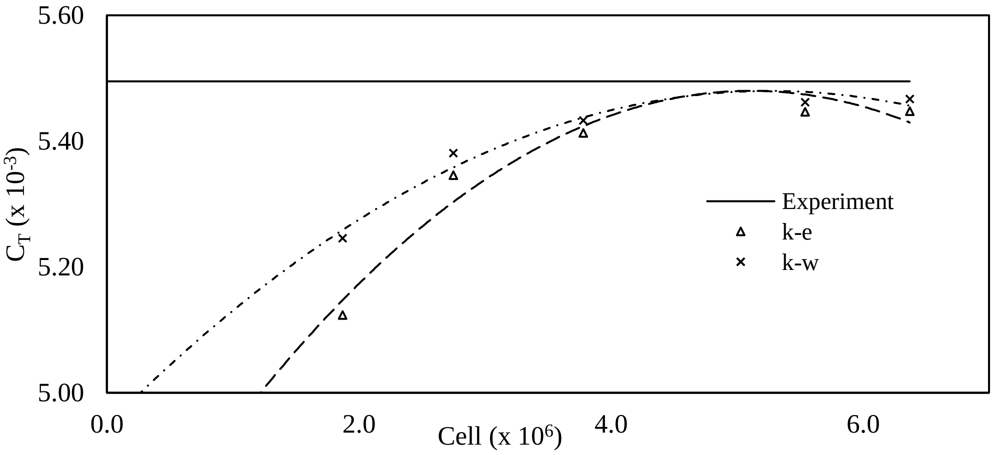

Figure 3.11 Result validations

From table 3.6 and figure 3.11, errors in resistance prediction reduce when the number of cells increase and the errors are slightly decreased between G4 and G5. Hence, it can be concluded that the number of cells should be between 5 and 6 million cells. Wave elevation along the hull is also measured to ensure that the flow field around the hull agrees with the experimental results, which can be seen in figure 3.12. It can be seen that the number of cells slightly affects the accuracy of wave elevation along the hull, which the results show a slight difference between grid types.

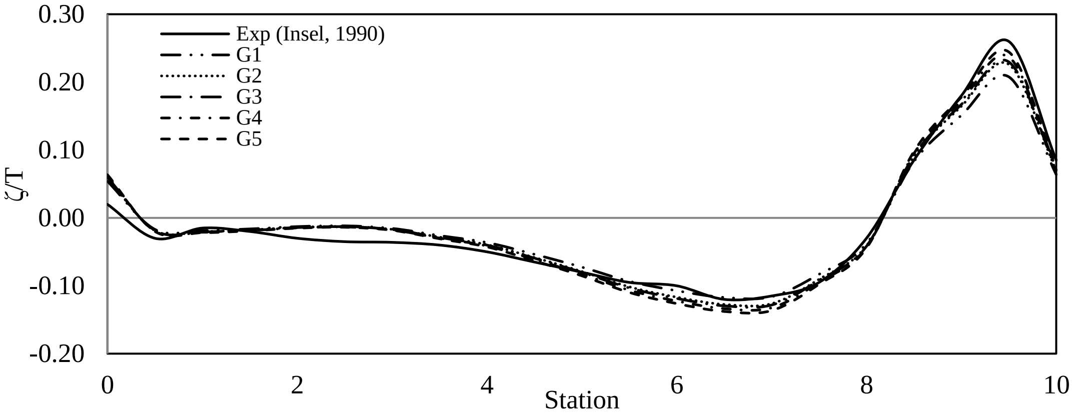

Figure 3.12 Wave elevation along at Fn = 0.35

Wave elevation measured at the far field area and validated against Insel's experimental data. Most of the wave pattern is captured correctly with an only minor error. Although mesh refinement resolution at the free surface area is created correctly, there are some large differences in some area especially at longer distances from the hull as can be seen in figure 3.13. Three grids show the dependence of mesh density on free surface wave elevation. The results agree with the literature that the finer mesh gives the better degree of accuracy.

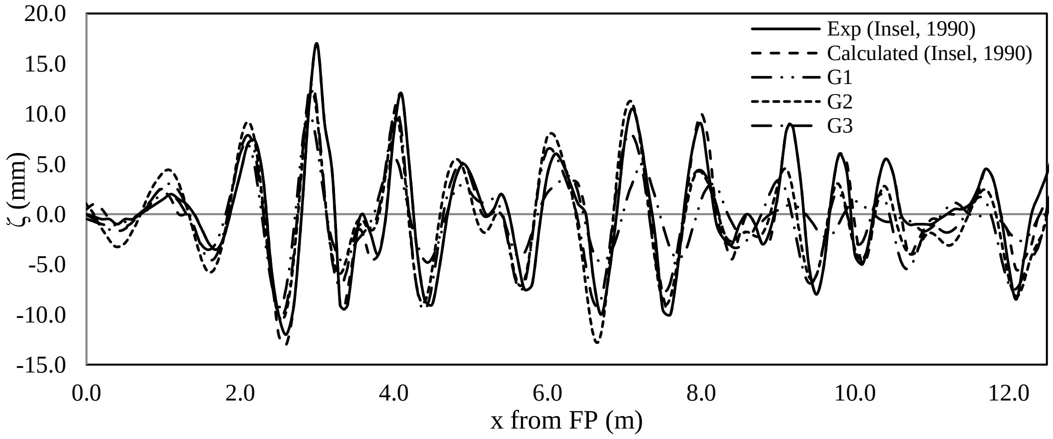

Figure 3.13 Wave cut at far field area

3.3.4 Numerical Uncertainties

To verify the results, CFD uncertainty is assessed by applying verification procedures expressed by Stern et al. (1999). To minimise the number of cases investigated, only SST k-ω turbulence model is verified for G3 to G5. These grids are selected because the results show a good monotonic convergence towards the finest grid, see table 3.6 and figure 3.11. The verification is determined by consideration to iterations and grid convergence study. The procedures are as follow:

$$\delta_{Simulation} = \delta_{iteration} + \delta_{grid\ dependence} \quad 3.3$$

$$U^2_{Simulation} = U^2_{iteration} + U^2_{grid\ dependence} \quad 3.4$$

Where, δ is error and U is uncertainty

Table 3.7 Result changes

Grid	G3	G4	G5	Exp
C_T ($x10^{-3}$)	5.433	5.462	5.467	5.495
Solution Change, ε ($x10^{-3}$)	-0.029	-0.005		

$$R_{Solution\ Change} = \varepsilon_{G4-G5}/\varepsilon_{G3-G4} = -0.005/-0.029 = 0.172$$

Three result convergence conditions are as follows:

a) Monotonic convergence: $0 < R_{Solution\ Change} < 1$
b) Oscillatory convergence: $-1 < R_{Solution\ Change} < 0$
c) Divergence: $R_{Solution\ Change} > 1$ or $R_{Solution\ Change} < -1$

In this case, as results shown in table 3.7, it can be seen that result ratio is fallen into a) which is between 0 and 1. Hence, it can be concluded that this simulation study shows a monotonic convergence. Figure 3.14 shows that the residuals drop between four and seven orders, from 0 to 10^{-4} and 10^{-7} respectively with the small fluctuations. As shown in figure 3.15, the variations in resistance components are very small in the 1000 iterations interval period. All three grids show the same results for iteration errors and uncertainties. Hence, it is assumed that iteration errors and uncertainties are neglected since they are relatively small compared with grid errors and uncertainties. Thus, equation 3.3 and 3.4 become as:

$$\delta_{Simulation} = \delta_{grid\ dependence} \qquad 3.5$$

$$U_{Simulation} = U_{grid\ dependence} \qquad 3.6$$

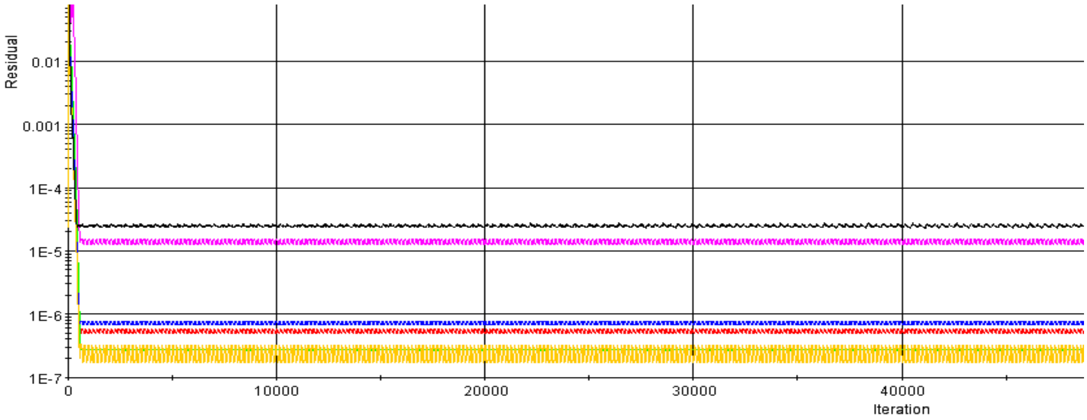

Figure 3.14 Result Residuals

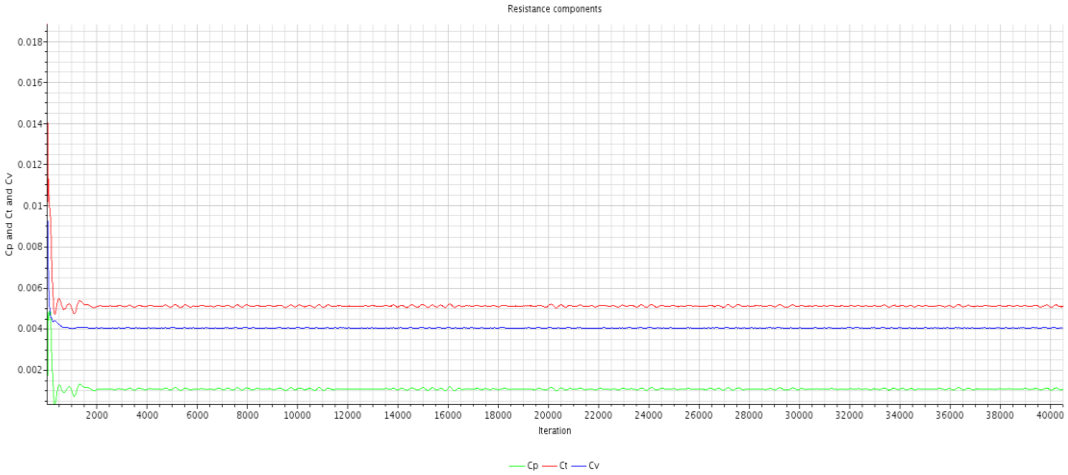

Figure 3.15 Resistance components history against iterations

Due to the result convergence shows a monotonic convergence hence generalised Richardson Extrapolation (RE) is used to estimate errors of the finest grid (G5), order of accuracy (P_G) and the correction factor (C_G), which is derived by Stern et al. (1999) as shown below:

$$P_G = \ln(\frac{\varepsilon_{G3-G4}}{\varepsilon_{G4-G5}})/\ln(R_G) = \ln(\frac{-0.029 * 10^{-3}}{-0.005 * 10^{-3}})/\ln(\sqrt{2} = 5.01) \qquad 3.7$$

$$\begin{aligned} \delta_{RE_{G5}} &= \varepsilon_{G4-G5}/(R_G^{P_G} - 1) = -0.005 * 10^{-3}/\sqrt{2}^{5.01} - 1 \\ &= -1.04 \times 10^{-6} \end{aligned} \qquad 3.8$$

$$C_G = (R_G^{P_G} - 1)/\left(R_G^{P_{G,est}} - 1\right) = (\sqrt{2}^{5.01} - 1)/\left(\sqrt{2}^{2} - 1\right) = 4.72 \qquad 3.9$$

Where R_G is grid refinement ratio. $P_{G,est}$ is equalled the order of accuracy.

For the monotonic convergence condition (Stern et al., 1999), the correction factor is checked and fallen into two condition: for C_G a value of 4.72 is considered sufficiently less or greater than 1 and equals to 1.

For the first condition 4.72 is less or greater than 1 which is considered as lacking confidence in results obtained, hence U_G is needed to be estimated rather than $\delta_G$using the following equation:

$$U_G = \left|C_G \delta_{RE_{G5}}\right| + \left|(1 + C_G)\delta_{RE_{G5}}\right| = 8.76\ x\ 10^{-6} \qquad 3.10$$

So U_G is about 1.6 x $10^{-3}\%S_{G5}$

For the second condition, C_G is considered close to 1, which implies that the result leads to the confidence. Hence, the grid error and grid uncertainty correction (δ_G and U_{GC}) are estimated by using the following equations:

$$\delta_{G5} = C_G \delta_{RE_{G5}} = -4.909\ x\ 10^{-6} \qquad 3.11$$

$$U_{GC} = \left|(1 - C_G)\delta_{RE_{G5}}\right| = 3.86\ x\ 10^{-6} \qquad 3.12$$

Hence the corrected solution for G5 is:

$$S_{C_{G5}} = S_{G5} - \delta_{G5} = 5.472\ x\ 10^{-3} \qquad 3.13$$

It can be seen that δ_{G5} is 8.98 x $10^{-4}\%S_{G5}$ and U_{GC} is 7.06 x $10^{-4}\%S_{G5}$, which are smaller than 1.6 x $10^{-3}\%S_{G5}$. The confidence in the grid uncertainty is acceptable.

3.4 Double-Model Method for Viscous Resistance

The CFD code has built-in functions for calculating resistance components of the free surface ship, three main components are calculated directly from the CFD code including total resistance (C_T), frictional resistance (C_F) and pressure (residual) resistance (C_P or C_R) coefficients. Other resistance coefficients that are focused in this study including viscous resistance (C_V) and wave resistance (C_W) coefficients need a specific approach to estimate.

There is a well-known method dealing with the viscous and wave resistance called a double-body method proposed by Dawson (1977) and widely used. The principle behind this method is that the free surface boundary condition is treated as the still water surface rather than the free surface with waves, which means that the free surface is undisturbed. This is done by reflecting the underwater part of the hull in the still water plane (symmetry plane), which produces a double body of the hull. The symmetry plane reflects the hull and numerical domain with the sources of equal strength. The velocity field is symmetric with respect to the still water surface and is considered as the double-body flow. The symmetry boundary condition for the scalar pressure, and velocity components tangential to these type of boundaries is that their gradients normal to these boundaries are zero.

To verify the use of this method two hull geometries are used, which include ellipsoid and a Wigley hull.

3.4.1 Ellipsoid

The ellipsoid catamaran with S/L = 0.37 is used to demonstrate the use of the double-model method. This model is chosen because of the CFD and experimentally validated data conducted by Utama in 1999. The ellipsoid particulars are shown in table 3.8. The experiment was conducted in the wind tunnel at the University of Southampton which has a 3.6m x 2.5m dimensions and maximum wind speed of 40 m/s.

Table 3.8 Ellipsoid particulars

L	1.20 m
B	0.20 m
WS	0.601 m^2
∇	0.025 m^3
C_B	0.521
C_M	0.785
C_P	0.664
$L/\nabla^{1/3}$	4.104

Numerical domain dimensions are as follows: 2L from the bow, 5L from the aft, width and depth match the wind tunnel dimensions. The single-phase ellipsoid simulation is carried out with two speeds including 20 and 30 m/s. Grid generation technique, which is used for the ellipsoid simulation, is the same as the Wigley hull, see figures 3.16 to 3.18. However, the aft part of the ellipsoid is treated differently from the Wigley hull because it is running in a different fluid. Due to a long turbulent flow region behind the aft part of the ellipsoid, another refinement block is added, which is shown in figures 3.17 and 3.18. The final mesh for the ellipsoid study is about 2.5 – 3 million cells. The SST k-ω turbulence model with low wall y^+ is used for the ellipsoid.

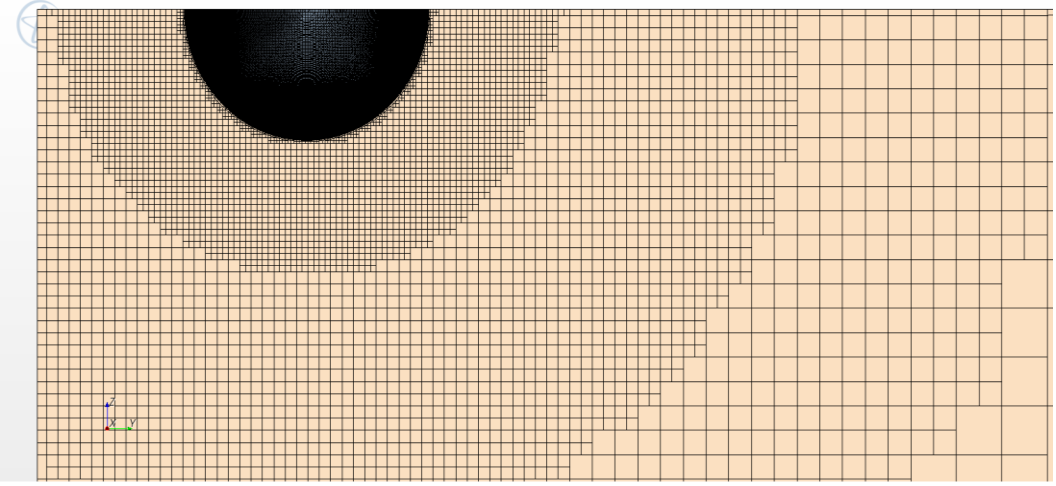

Figure 3.16 Mesh around the ellipsoid on y-z plane

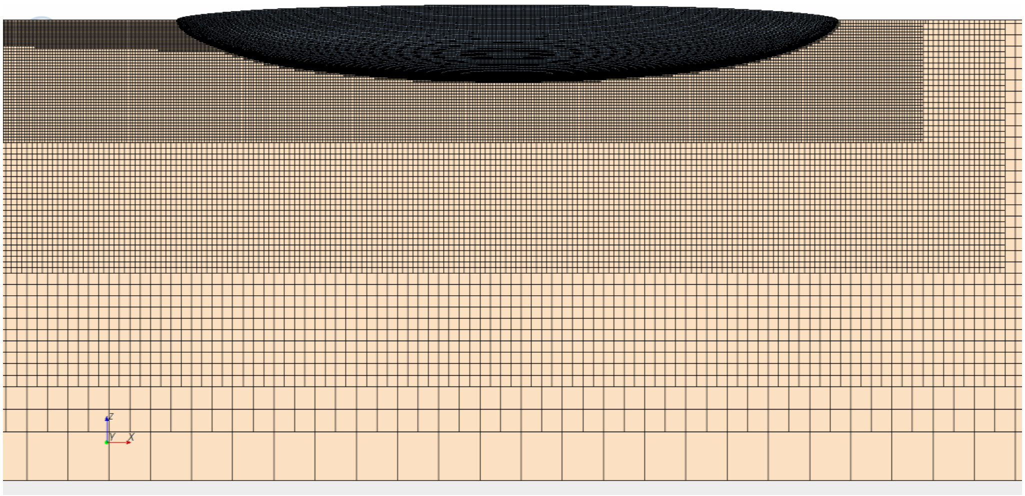

Figure 3.17 Mesh around the ellipsoid on x-z plane

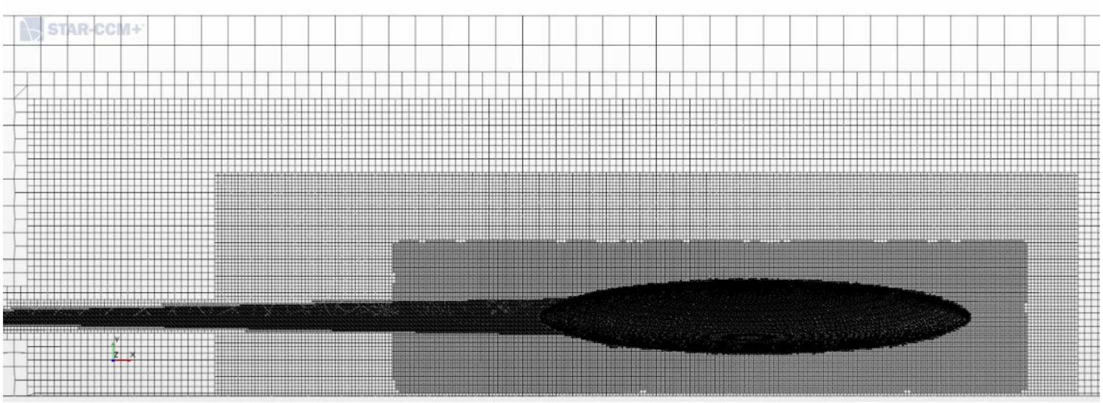

Figure 3.18 Mesh around the ellipsoid on x-y plane

The CFD results shown in table 3.9 include drag coefficient (C_D), skin friction coefficient (C_F) and form factor (1+k). The error percentage margin for the drag coefficient of CFD compared with the experimental results is less than 1.5 percent. The CFD C_F shows a good agreement with the experimental results with the percentage error between 1.342 and 4.169. The form factor is equated C_D/C_F. The CFD form factor is 1.09 for a speed U = 20 m/s compared with 1.12 for the experiment. For U = 30 m/s, the CFD form factor is 1.22 while the experimental form factor is 1.28. The present CFD investigation is also compared with Utama (1999) CFD results. It is found that the present CFD work shows a better form factor prediction using the double-model method as shown in table 3.9.

Table 3.9 The ellipsoid results

		U = 20.33m/s, Re = 1.58 x		U = 30.37m/s, Re = 2.37 x	
			% Error		% Error
C_D (x 10^{-3})	Experiment	3.907		4.096	
	Utama's	-		5.663	+ 38.257
	CFD	3.893	- 0.358	4.050	- 1.123
C_F (x 10^{-3})	Experiment	3.501		3.190	
	Utama's	-		4.074	+27.712
	CFD	3.548	+ 1.342	3.323	+ 4.169
1+k	Experiment	1.12		1.28	
	Utama's	-		1.39	+ 9.016
	CFD	1.09	- 2.678	1.22	- 4.687

3.4.2 Wigley hull

The double-model method is adopted for the Wigley monohull to estimate viscous and wave resistance coefficient. The numerical domain and mesh techniques are the same with the grid dependence for the total resistance. Froude number Fn = 0.35 is evaluated. The CFD C_V is 0.004156 comparing with 0.00426 for the experimental result. The percentage error is -2.462. The wave resistance coefficient is 0.001278 and 0.001311 for the experiment and CFD respectively. The Wigley monohull results are fully presented in chapter 4.

3.5 Investigation of Sinkage and Trim

Dynamic sinkage and trim normally occur when the ship travels through the water. To investigate the dynamic characteristics of the ship using CFD application, it is important to create the case carefully. There are some major differences between running steady and unsteady cases including 6 DOF rotation and translation, and the time step. Free motion of z translation and y rotation are monitored to measure dynamic sinkage and trim. The grid is generated using the same technique as the steady state. SST k-ω turbulence model is used. The average all y^+ is maintained as lower than 1 or between 30 and 50, which is the same for the steady simulations.

For free-surface applications, an important issue is to maintain a favourable convective Courant number, also known as the Courant-Friedrichs-Levy (CFL) number, in order for the high-resolution interface capturing (HRIC) scheme to track accurately the free surface position. The CFL number is defined as $CFL=U\cdot\Delta t/\Delta x$, where Δx is the associated grid spacing; in the case of free-surface flows the vertical mesh spacing is critical. By default, the HRIC method is optimized for free surfaces operating at CFL<0.5. The time-step size can be determined based on the mesh spacing. If the time-step size is too restrictive, the mesh can be coarsened but it can result in a loss of resolution.

This leads to final time step size for an unsteady Fn = 0.331 case is ***$5.45x10^{-4}s$***. The interval iteration for time step are 20 iterations. 60 hours on Irridis 4 with 16 processors can run 6 million cells case around 15000 iterations which the time is about

0.40875 second for the resutls. Hence, to run the physical time about 15-20s, it needs about ***2250 hours to 3000 hours or 93.5-125 days.*** Sinkage and trim measurements from CFD are shown in figures 3.19 and 3.20 respectively. It can be seen that the sinkage error between CFD and experiment is quite large (10.89 %) which the sinkage of CFD is 0.005404 m and the experiment is 0.0048735 m. The experimental results showed no trim for this speed while CFD results show a small change between negative and positive angles.

It can be seen that if the dynamic sinkage and trim are fully investigated it is seemingly not achievable in the period of the research. It was therefore decided to fix the model using the running dynamic sinkage and trim values measured by Insel (1990).

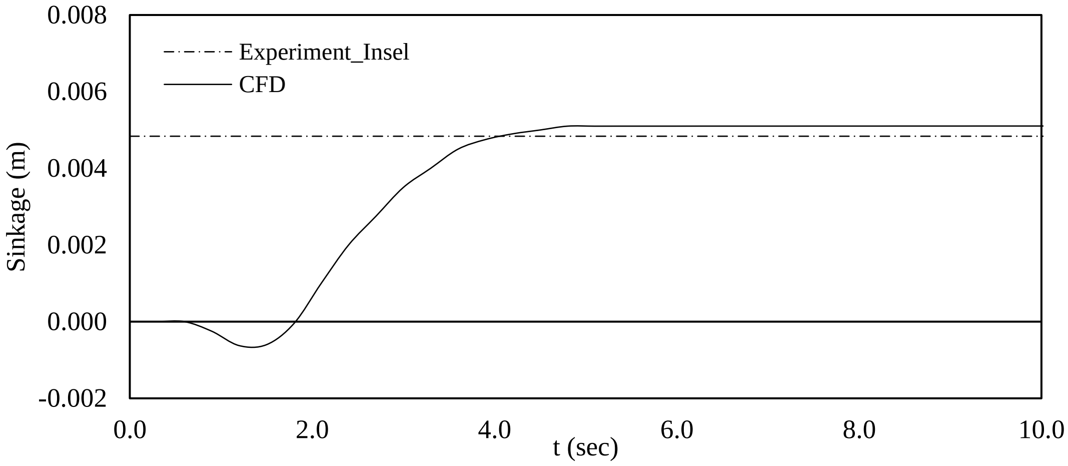

Figure 3.19 Sinkage measurement at Fn = 0.331

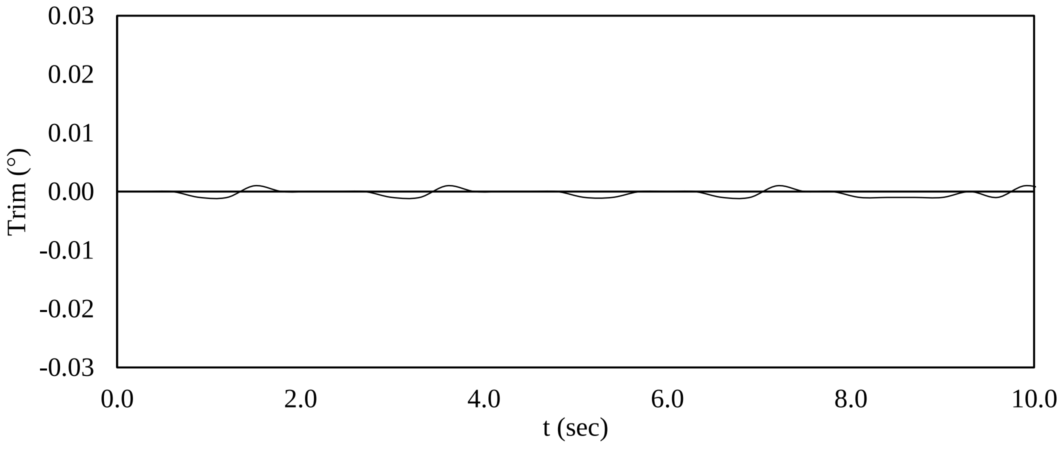

Figure 3.20 Trim measurement at Fn = 0.331 for CFD

3.6 Chapter Summary

This chapter covers two main simulations: numerical wave tank, resistance in calm water, sinkage and trim. For the numerical wave tank study, the key factor that influences the accuracy of the results is the number of cells per wave height. As the results show, the number of cells per wave height should be between 30 and 40 cells. The validations are also made by comparing the results with the 1st order Stokes wave, the experimental results from Denchfiled (2010) and CFD by Wood (2013). The results show quite good agreement.

Another simulation focuses on resistance in the calm water for Wigley III following Insel's experiment (1990). Three subtasks are investigated in this simulation including grid dependency, turbulence models and validations. From the grid study, the conclusion shows that the optimal number of cells should be between 5 and 6 million cells. Turbulence models are also investigated since there are two dominant models, $k-\varepsilon$ and SST $k-\omega$, that are recommended by other researchers. The final conclusion shows that SST $k-\omega$ provides better results than $k-\varepsilon$. Mesh procedure to capture the wave elevation in the wake area is also investigated by applying the number of cells from numerical wave tank study to find the most suitable total cells. The validation shows that the number of cells should be at least 6M cells with full refinement regarding the numerical results. The CFD uncertainty is also assessed and the result shows that the uncertainties of the CFD are acceptable and reliable.

The double-model method is implemented to demonstrate how the CFD code is used to calculate viscous and wave resistance coefficients.

The Wigley III monohull free to sinkage and trim investigation shows that it is difficult to achieve the desirable results due to the fact that simulation is very expensive in term of CPU and wall time limitations.

Chapter 4: Resistance and Form Factor of Wigley III

4.1 Numerical Domain and Mesh Techniques

4.1.1 Monohull

The numerical domain and mesh techniques used to calculate the resistance components of the monohull is the same as determined in the grid dependency study. However, there are some differences, which are described below. As resistance components are measured over the range of Froude numbers, the model is run at different speeds. Due to the use of SST k-ω turbulence model with wall function, the distance between the hull and centroid of the first cell changes for every speed to maintain y^+ as discussed in the previous chapter.

The flow field is another aspect that needs certain mesh refinement. According to the validated data obtained from Insel's experiment, wave elevation along the hull seems to rise with speed. To overcome this, the number of cells per wave height is set to be the same for all speed. The number of cells per wave height used in this simulation is between 30 and 40.

4.1.2 Catamarans

Generally, the numerical domain size for catamaran simulations is similar to that of the monohull. However, the mesh refinement for a catamaran is slightly different compared with the monohull. The space due to the separation between demihulls, where the complex flow phenomenon happens is treated with another refinement block. The mesh is very fine around this area and then coarsened towards the boundaries, as shown in figure 4.1.

To capture wave elevation along the hull on both sides of the demihulls, mesh resolution at the free surface between the demihulls is also set to be between 30 and 40 cells per wave height. Figure 4.2 presents the mesh refinement for the wave around the catamaran and far field area. For the free surface where the waves occur, the number of cells per wavelength and wave height are set to be the same as the separation area between demihulls. This technique results in an increase in the total number of cells by around 0.5 – 1.0 million cells. Hence, total cells for catamaran simulation is between 6 and 7 million cells.

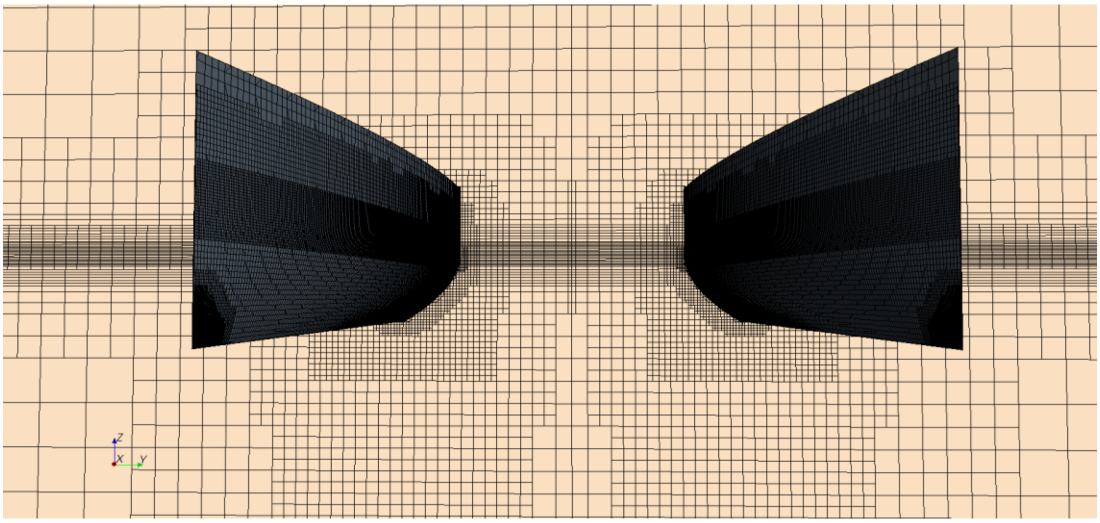

Figure 4.1 Grid generation between demihulls for Wigley III S/L = 0.3

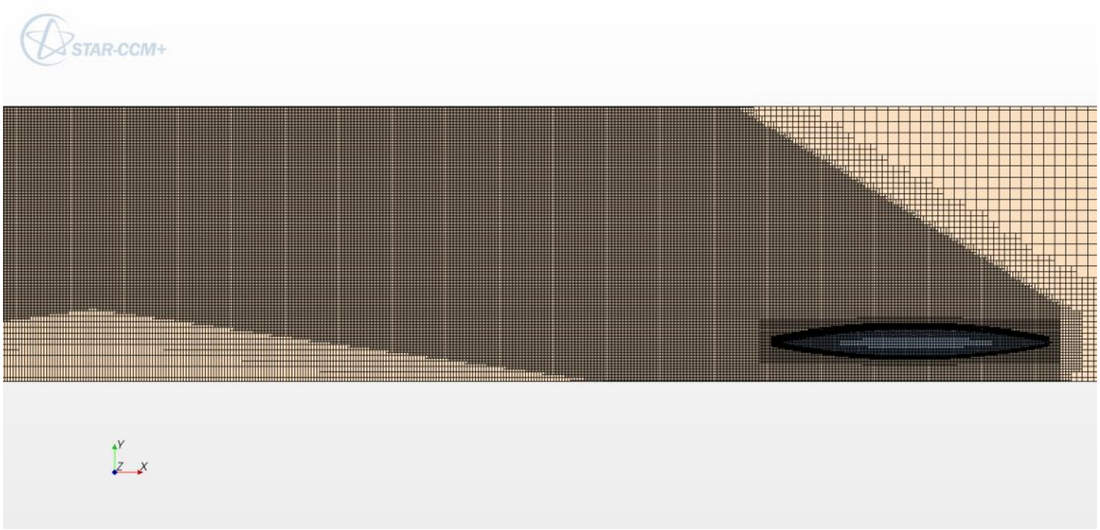

Figure 4.2 Grid generation for wake area for Wigley III S/L = 0.3

4.2 Resistance Components

4.2.1 Monohull

Resistance components of the monohull are presented in figures 4.3, 4.4 and 4.5, and tables 4.1 and 4.2. All resistance components show a good agreement with the experiment. However, CFD results show a lower magnitude of resistance components for C_T, C_V, C_R and C_W while C_F is over prediction.

Total resistance coefficient shows a good agreement with experiment over the Froude number range. Most of the CFD C_T are under predicted with a range of error between 0.510 and 1.327 percent. Frictional resistance coefficient (C_F) calculated using CFD, validated against ITTC correlation line shows a range of over prediction between 1.361 and 3.307 percent.

The comparison of frictional resistance coefficient of CFD results with the empirical formulae is shown in figure 4.3. Four frictional resistance formulae are compared including ITTC correlation line, Hughes (1954), Schoenherr (1932) and Grigson (1993). The CFD C_F agrees quite well with the ITTC correlation line and shows large over prediction compared with other empirical formulae. Because the validation data for this investigation are from Insel's experiment which he used the ITTC correlation line to calculate C_F and form factor (1+k), the validation for C_F in this study will be made against ITTC correlation line.

Viscous resistance coefficient shows a good agreement with experiment. The differences between CFD and experimental data reduces when speed increases. The under prediction of CFD C_V is very large for the $Fn < 0.50$, which exceeds 1.50 percent.

Figure 4.5 shows residual and wave resistance coefficients for the monohull. Residual resistance coefficient (C_R) shows the under prediction between CFD and experiment with a range of error between 3.553 and 29.633 percent. The CFD C_R shows a large under prediction for the low peed range as seen for $Fn < 0.35$.

Wave resistance coefficient (C_W) compared against experiment shows a good agreement over the range of Froude number with the range of under prediction between 0.614 and 3.682 and the over prediction between 0.576 and 2.796. The over prediction is very high at the lowest Froude number ($Fn = 0.20$) where the error of the wave resistance is 58.513 percent.

Table 4.1 Total, frictional and viscous resistance coefficients of Wigley III monohull

Fn	C_T (x 10^{-3})			C_F (x 10^{-3})			C_V (x 10^{-3})		
	Exp	CFD	Error (%)	ITTC	CFD	Error (%)	Exp	CFD	Error (%)
0.200	5.050	4.985	-1.289	4.425	4.545	2.715	4.779	4.633	-3.052
0.300	5.495	5.438	-1.038	4.069	4.172	2.526	4.395	4.251	-3.273
0.331	5.500	5.439	-1.110	3.990	4.072	2.074	4.309	4.208	-2.337
0.350	5.495	5.467	-0.510	3.945	4.023	1.969	4.261	4.156	-2.462
0.400	6.000	5.929	-1.188	3.842	3.895	1.369	4.150	4.087	-1.513
0.500	7.500	7.428	-0.966	3.679	3.773	2.549	3.974	3.922	-1.298
0.600	6.770	6.726	-0.648	3.553	3.671	3.307	3.838	3.799	-1.010
0.700	6.321	6.282	-0.621	3.452	3.515	1.815	3.728	3.711	-0.465
0.750	6.150	6.074	-1.236	3.408	3.473	1.902	3.681	3.645	-0.974
0.800	6.050	6.013	-0.612	3.368	3.433	1.935	3.637	3.627	-0.282
0.900	5.975	5.896	-1.327	3.296	3.352	1.709	3.560	3.554	-0.159

Table 4.2 Residual and wave resistance coefficients, and form factor of Wigley III monohull

Fn	C_R (x 10^{-3})			C_W (x 10^{-3})			1+k (CFD)	Re
	Exp	CFD	Error (%)	Exp	CFD	Error (%)		
0.200	0.625	0.440	-29.633	0.222	0.352	58.513	1.019	1.31E+06
0.300	1.426	1.266	-11.212	1.222	1.187	-2.869	1.019	1.96E+06
0.331	1.510	1.367	-9.522	1.278	1.231	-3.682	1.033	2.03E+06
0.350	1.550	1.444	-6.821	1.278	1.311	2.582	1.033	2.29E+06
0.400	2.158	2.034	-5.742	1.889	1.842	-2.504	1.049	2.62E+06
0.500	3.821	3.655	-4.351	3.611	3.506	-2.921	1.039	3.27E+06
0.600	3.217	3.055	-5.016	2.950	2.927	-0.774	1.035	3.93E+06
0.700	2.869	2.767	-3.553	2.556	2.571	0.576	1.056	4.58E+06
0.750	2.742	2.601	-5.136	2.444	2.429	-0.614	1.050	4.91E+06
0.800	2.682	2.580	-3.809	2.367	2.386	0.803	1.057	5.24E+06
0.900	2.679	2.543	-5.062	2.278	2.342	2.796	1.060	5.89E+06
							1.041	

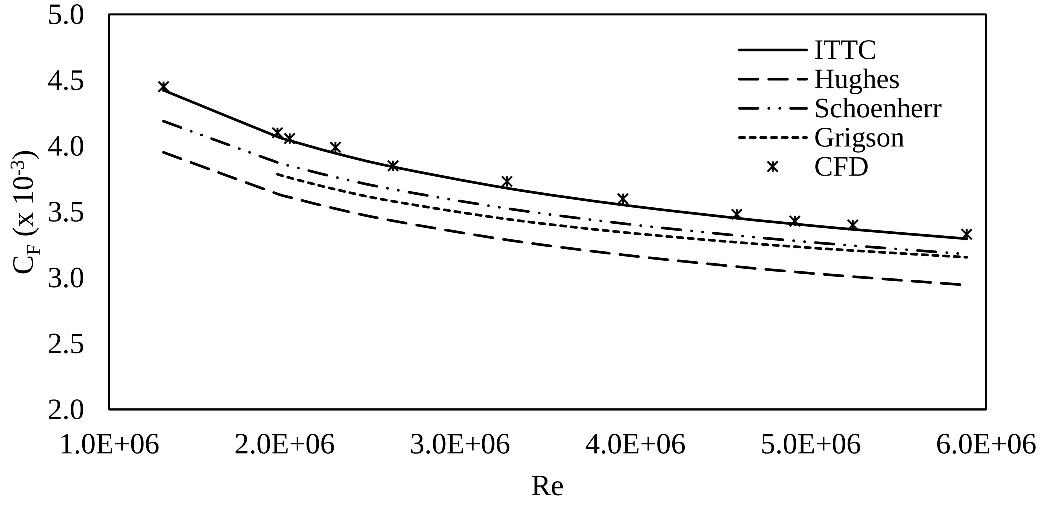

Figure 4.3 Comparison of frictional resistance coefficient with empirical formulae

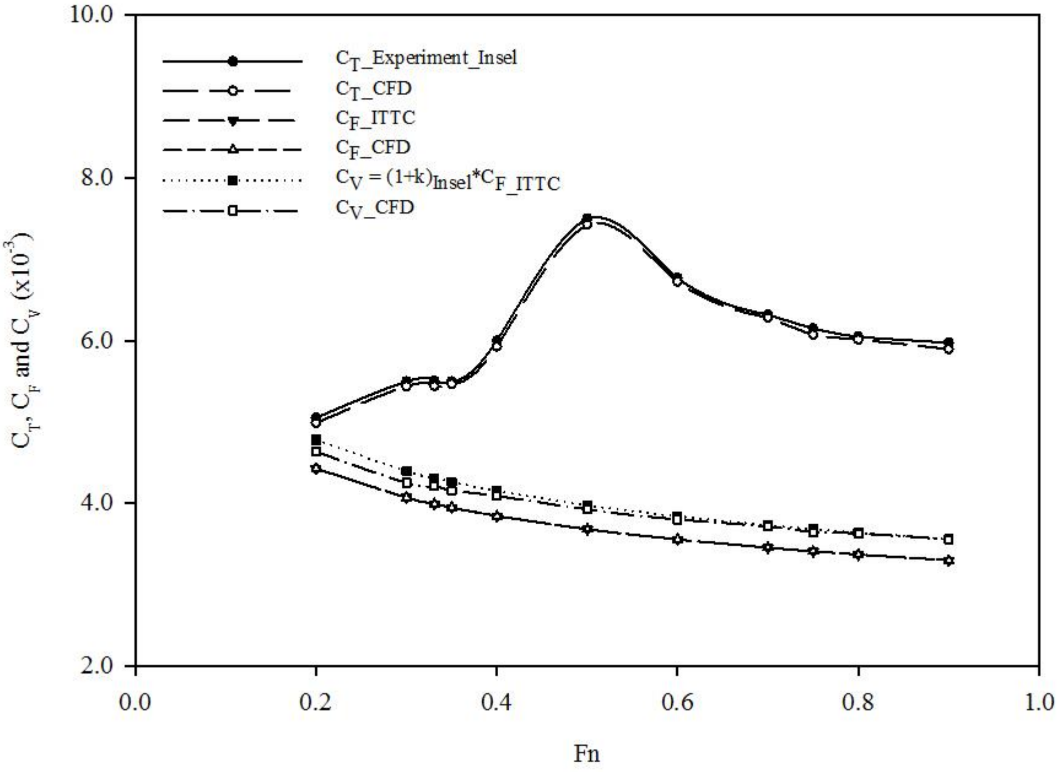

Figure 4.4 Total, frictional and viscous resistance coefficients of Wigley III monohull

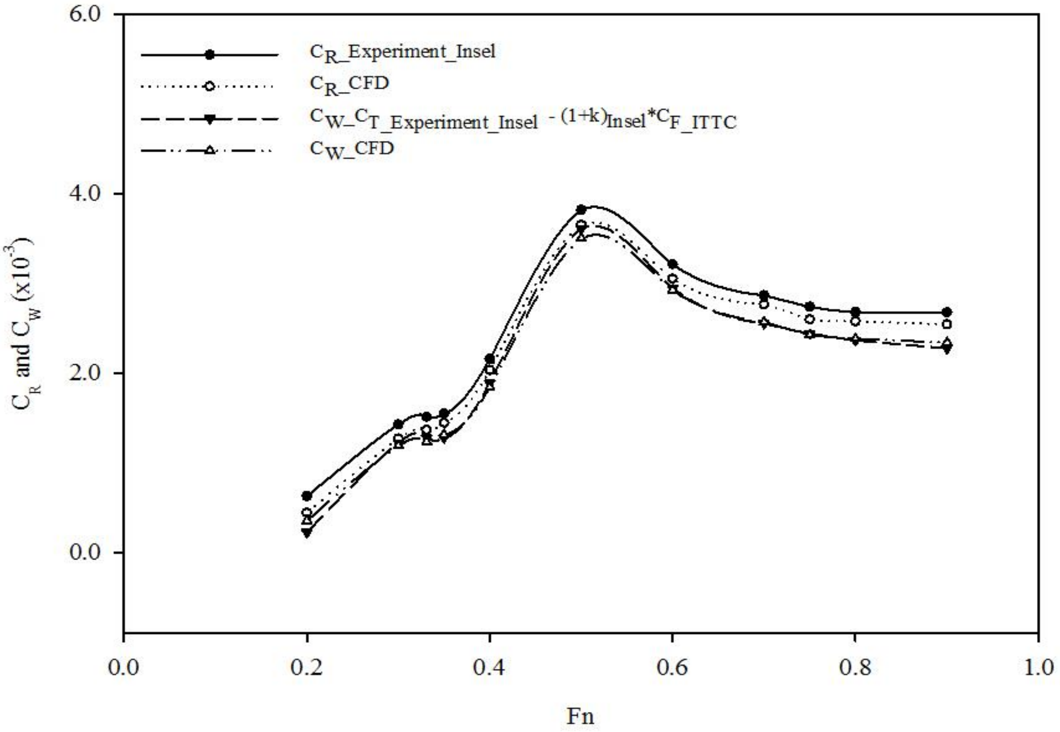

Figure 4.5 Residual and wave resistance coefficients of Wigley III monohull

4.2.2 Catamaran S/L = 0.3

The resistance results for S/L = 0.3 are presented in figures 4.6 and 4.7, and tables 4.3 and 4.4. All resistance coefficients show a good agreement with experiment. Total resistance coefficient (C_T) calculated using CFD shows quite good agreement with Insel's experiment. The range of under prediction is between 1.447 and 3.722%. The large differences between CFD and experimental results is found for the low Froude number, where Fn < 0.30.

Frictional resistance coefficient (C_F) also shows a good agreement with the ITTC correlation line. CFD results are over predicted compared with the ITTC correlation line over the range of Froude numbers. The range of error is between 1.792 and 3.617%. The prediction of viscous resistance coefficient shows a good agreement with experiment with a combination of under and over prediction. The under prediction is between 1.162 and 5.241 while the over prediction is between 0.691 and 2.670%. Residual and wave resistance obtained from CFD simulations are shown in figure 4.7 and table 4.4. The comparison of CFD and experimental C_R shows a range of under prediction between 5.072 and 30.387%. The range of error exceed 10.0% can be seen for Fn < 0.40. Wave resistance (C_W) shows a range of under prediction between 2.729 and 14.432%, and over prediction between 3.135 and 45.178%. The large differences between CFD and experimental results higher than 5.0%, can be seen at either ends of Froude numbers (Fn < 0.247 and Fn > 0.60) and for Fn = 0.35 and 0.367.

Table 4.3 Total, frictional and viscous resistance coefficients of Wigley III S/L = 0.3

Fn	C_T (x 10^{-3})			C_F (x 10^{-3})			C_V (x 10^{-3})		
	Exp	CFD	Error (%)	ITTC	CFD	Error (%)	Exp	CFD	Error (%)
0.200	5.330	5.150	-3.377	4.425	4.520	2.147	5.133	4.864	-5.241
0.247	5.667	5.465	-3.564	4.234	4.315	1.916	4.912	4.686	-4.595
0.272	5.440	5.238	-3.722	4.151	4.268	2.819	4.815	4.642	-3.610
0.300	6.500	6.312	-2.892	4.069	4.172	2.529	4.720	4.598	-2.599
0.310	6.670	6.574	-1.447	4.042	4.151	2.687	4.689	4.600	-1.909
0.350	5.380	5.200	-3.346	3.945	4.088	3.617	4.577	4.512	-1.400
0.367	5.310	5.153	-2.965	3.908	3.995	2.224	4.534	4.484	-1.087
0.400	6.890	6.728	-2.350	3.842	3.938	2.500	4.457	4.395	-1.386
0.500	8.900	8.724	-1.978	3.679	3.768	2.413	4.268	4.218	-1.162
0.600	7.830	7.673	-2.003	3.553	3.645	2.575	4.122	4.151	0.691
0.700	7.000	6.787	-3.043	3.452	3.514	1.792	4.004	4.078	1.836
0.750	6.780	6.577	-2.994	3.408	3.487	2.312	3.954	4.052	2.491
0.800		6.300		3.368	3.451	2.473	3.907	4.011	2.670

Table 4.4 Residual and wave resistance coefficients, and form factor of Wigley III S/L = 0.3

Fn	C_R (x 10^{-3})			C_W (x 10^{-3})			1+k (CFD)	Re
	Exp	CFD	Error (%)	Exp	CFD	Error (%)		
0.200	0.905	0.630	-30.387	0.197	0.286	45.178	1.076	1.31E+06
0.247	1.433	1.150	-19.759	0.755	0.779	3.135	1.086	1.62E+06
0.272	1.289	0.969	-24.791	0.625	0.596	-4.591	1.087	1.78E+06
0.300	2.431	2.140	-11.968	1.780	1.714	-3.670	1.102	1.96E+06
0.310	2.628	2.422	-7.807	1.981	1.974	-0.353	1.108	2.03E+06
0.350	1.435	1.112	-22.493	0.803	0.688	-14.432	1.104	2.29E+06
0.367	1.402	1.157	-17.435	0.776	0.668	-13.935	1.122	2.40E+06
0.400	3.048	2.790	-8.465	2.433	2.333	-4.116	1.116	2.62E+06
0.500	5.221	4.956	-5.072	4.632	4.506	-2.729	1.119	3.27E+06
0.600	4.277	4.028	-5.806	3.708	3.523	-4.997	1.139	3.93E+06
0.700	3.548	3.273	-7.747	2.996	2.709	-9.564	1.161	4.58E+06
0.750	3.372	3.090	-8.358	2.826	2.525	-10.667	1.162	4.91E+06
0.800		2.849			2.289		1.162	5.24E+06
						Average	1.119	

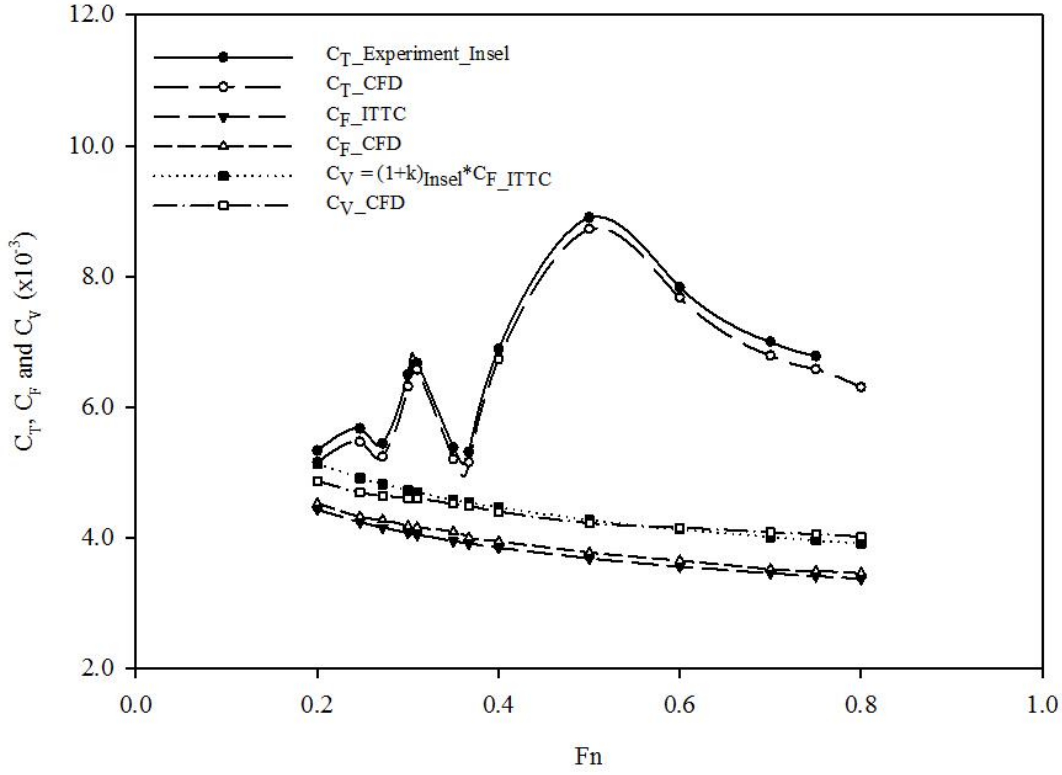

Figure 4.6 Total, frictional and viscous resistance coefficients of Wigley III S/L = 0.3

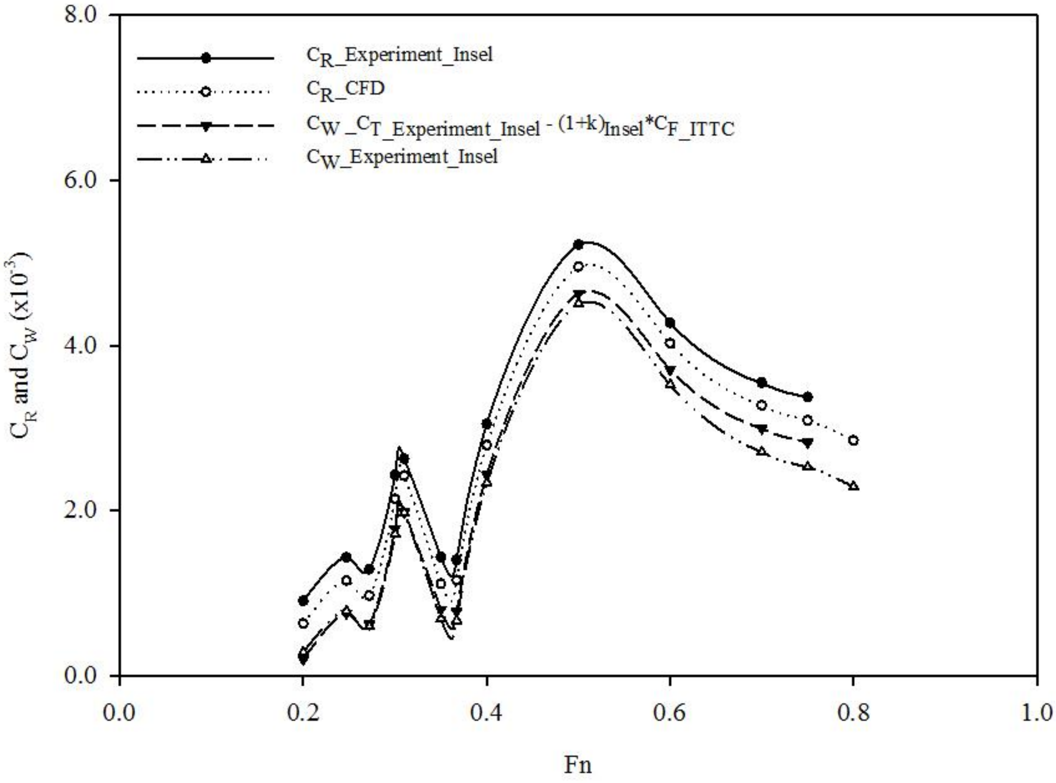

Figure 4.7 Residual and wave resistance coefficients of Wigley III S/L = 0.3

4.3 Form Factor (1+k), Viscous Resistance (β) and Wave Resistance Interference Factors (τ)

4.3.1 Monohull

The CFD form factor of the monohull is presented in figure 4.8 together with other hull configurations. The average CFD form factor for the monohull is about 1.041 while Insel's experimental form factor is 1.05. The results show that form factor seems to increase with Froude number with a small fluctuation. For 0.20 < Fn < 0.30, the CFD form factor shows a steady trend and then rise significantly for 0.30 < Fn < 0.50 and then show a small gradient for Fn > 0.40.

4.3.2 Catamaran S/L = 0.3

The comparison of the form factor for different hull configurations are shown in figure 4.8, the results for S/L = 0.2 and 0.4 can be seen in appendix A. The average form factor for catamaran S/L = 0.3 calculate using CFD code is 1.119 compared with the experimental form factor of 1.16, see figure 4.8. The similarity can be seen for S/L = 0.2, a CFD form factor is smaller than Insel’s experiment. A CFD f5orm factor seems to increase with speed (Fn). The trend line of the CFD form factor of S/L = 0.3 shows a linear trend, which is slightly different from other hull configurations. The CFD 1+k seems to be steady for the high-speed range where Fn > 0.6 for S/L = 0.3.

The viscous resistance interference factor (β), presented in figure 4.9 for S/L = 0.3, shows the same trend as the other hull separations and seems to increase with the decreasing hull separation. The highest viscous resistance interference factor occurs at Fn = 0.3, which is about 6.30. For Fn > 0.30 viscous resistance interference factor seems to decrease. Another two humps, which occur for all hull configurations can be seen at Fn = 0.60 and 0.75. The CFD wave resistance interference factor (τ) for S/L = 0.3, shown in figure 4.10, is validated against Insel’s experiment and shows a good agreement. The fluctuation of wave resistance interference factor of S/L = 0.3 is inverted where 0.35 < Fn < 0.50 compared with other hull configurations, see figure B.3. Both CFD and Insel’s experimental wave resistance interference factors decrease where Fn > 0.500.

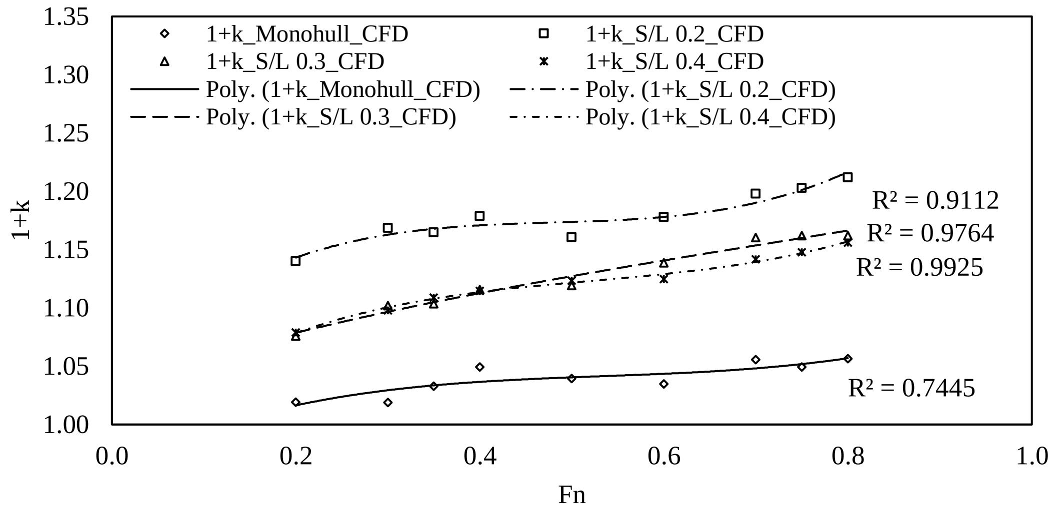

Figure 4.8 Comparison of form factor of Wigley hull

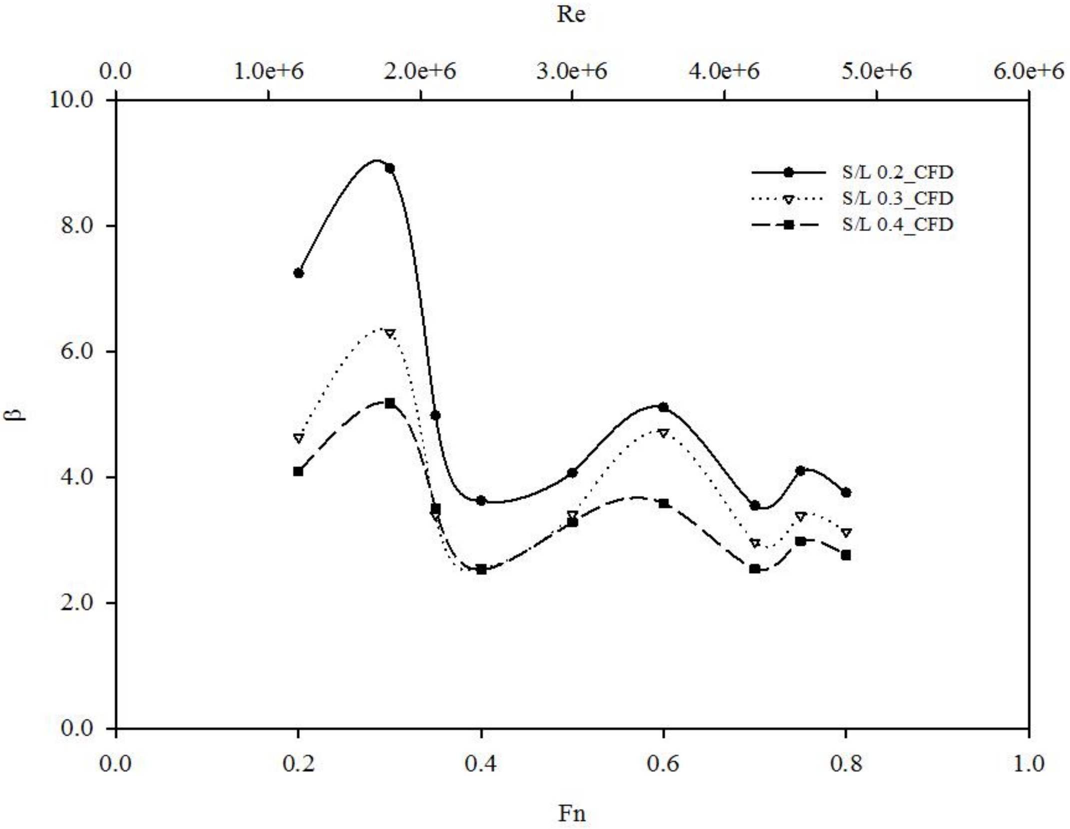

Figure 4.9 Comparison of viscous resistance interference factor of Wigley III

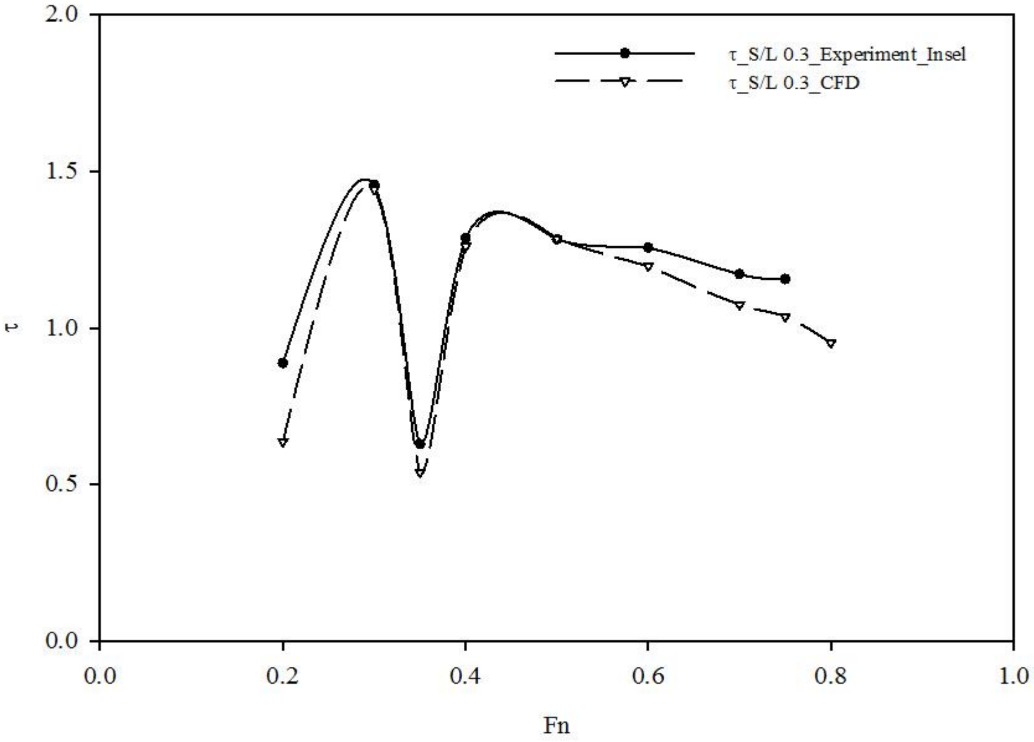

Figure 4.10 Wave resistance interference factor of Wigley III S/L = 0.3

4.4 Wave Elevation along the Hull

Wave cut along the hull is made for Fn = 0.35 and 0.50 and validated against Insel's experiment. For the catamaran configurations, wave elevation measurements are made on both sides of the demihulls. Wave elevations along the hull for the monohull are presented in figures 4.11 and 4.12 and for the catamaran S/L = 0.3 are in figures 4.13 to 4.16.

The measurement of wave elevation along the hull for catamaran S/L = 0.2 cannot be validated throughout the range of demihulls for Fn = 0.50. Insel expressed that the quality of data acquisition was too low due to the excessive wave height and spray in the separation space between demihulls and towing tank. At lower Froude number, the result from CFD shows a good agreement with experiment for all hull configurations while at Fn = 0.50 the results are not satisfied with the experimental data. (see appendix C)

As discussed in chapter 3 section 3.1, the number of cells per wave height plays an important role in affecting the accuracy of the free surface flow. Although the number of cells is applied correctly, the differences in the wave elevation along the hull between CFD and experiment are quite high for Fn = 0.50.

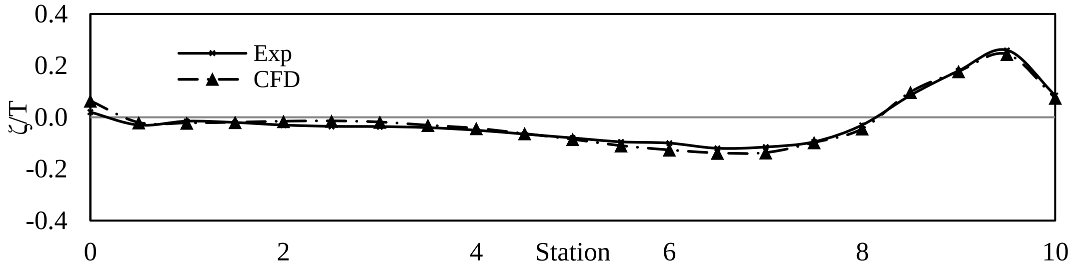

Figure 4.11 Wave elevation along the hull of Wigley III monohull at Fn = 0.35

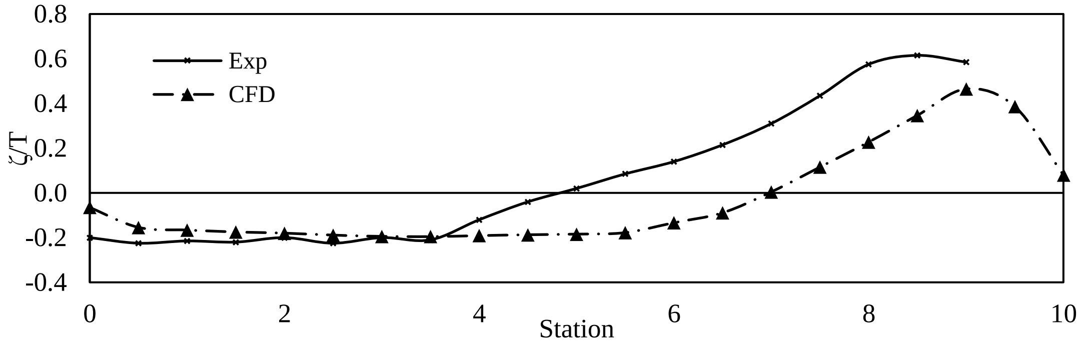

Figure 4.12 Wave elevation along the hull of Wigley III monohull at Fn = 0.50

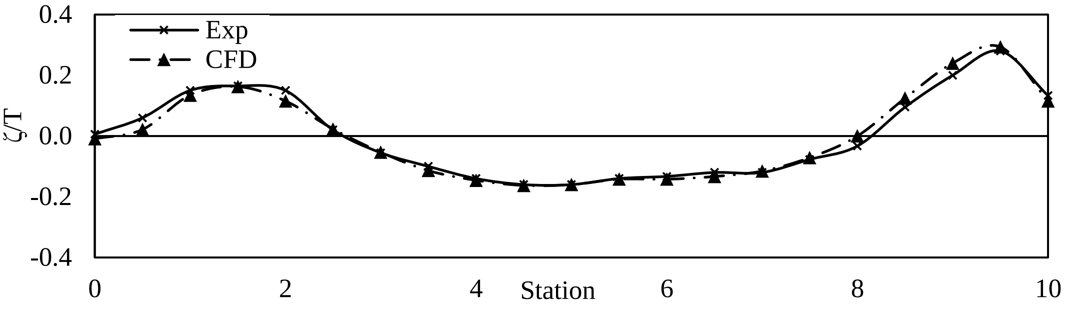

Figure 4.13 Wave elevation along the hull of Wigley III S/L = 0.3 (inboard) at Fn = 0.35

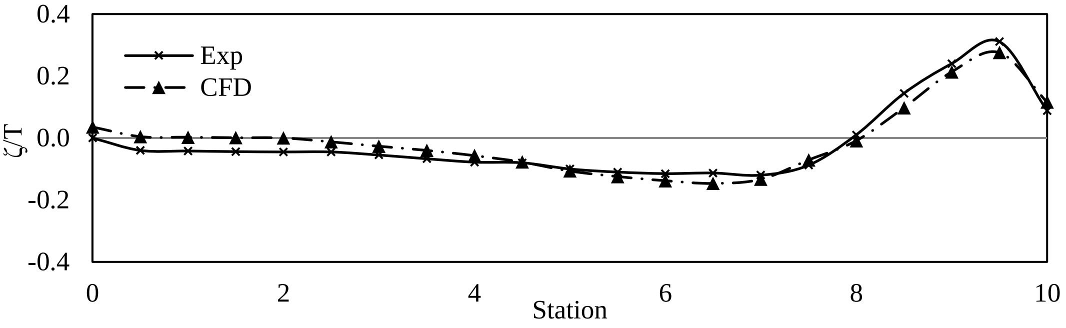

Figure 4.14 Wave elevation along the hull of Wigley III S/L = 0.3 (outboard) at Fn = 0.35

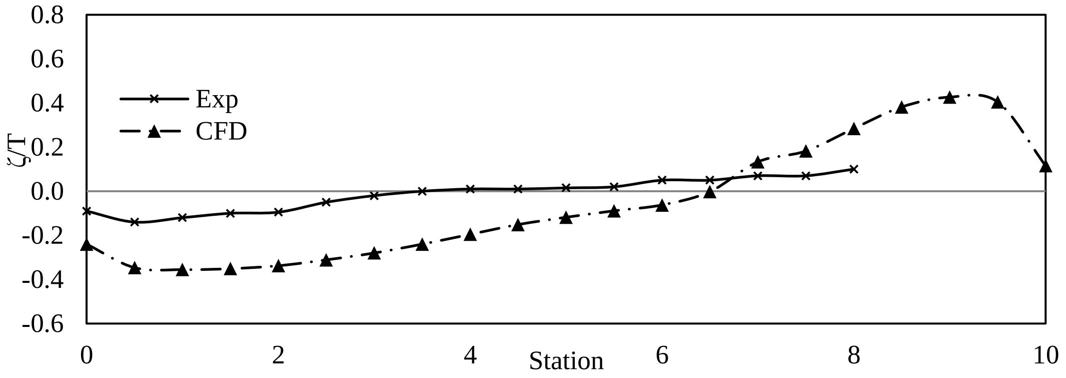

Figure 4.15 Wave elevation along the hull of Wigley III S/L = 0.3 (inboard) at Fn = 0.50

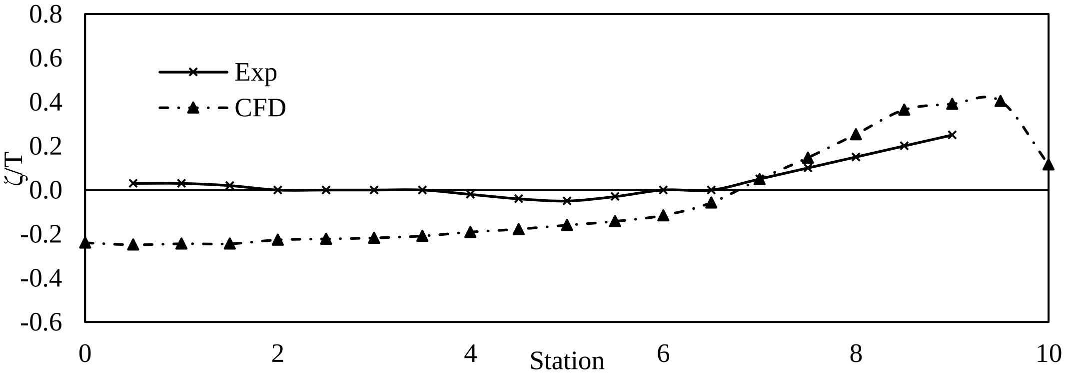

Figure 4.16 Wave elevation along the hull of Wigley III S/L = 0.3 (outboard) at Fn = 0.50

4.5 Wave Cut Error Discussion

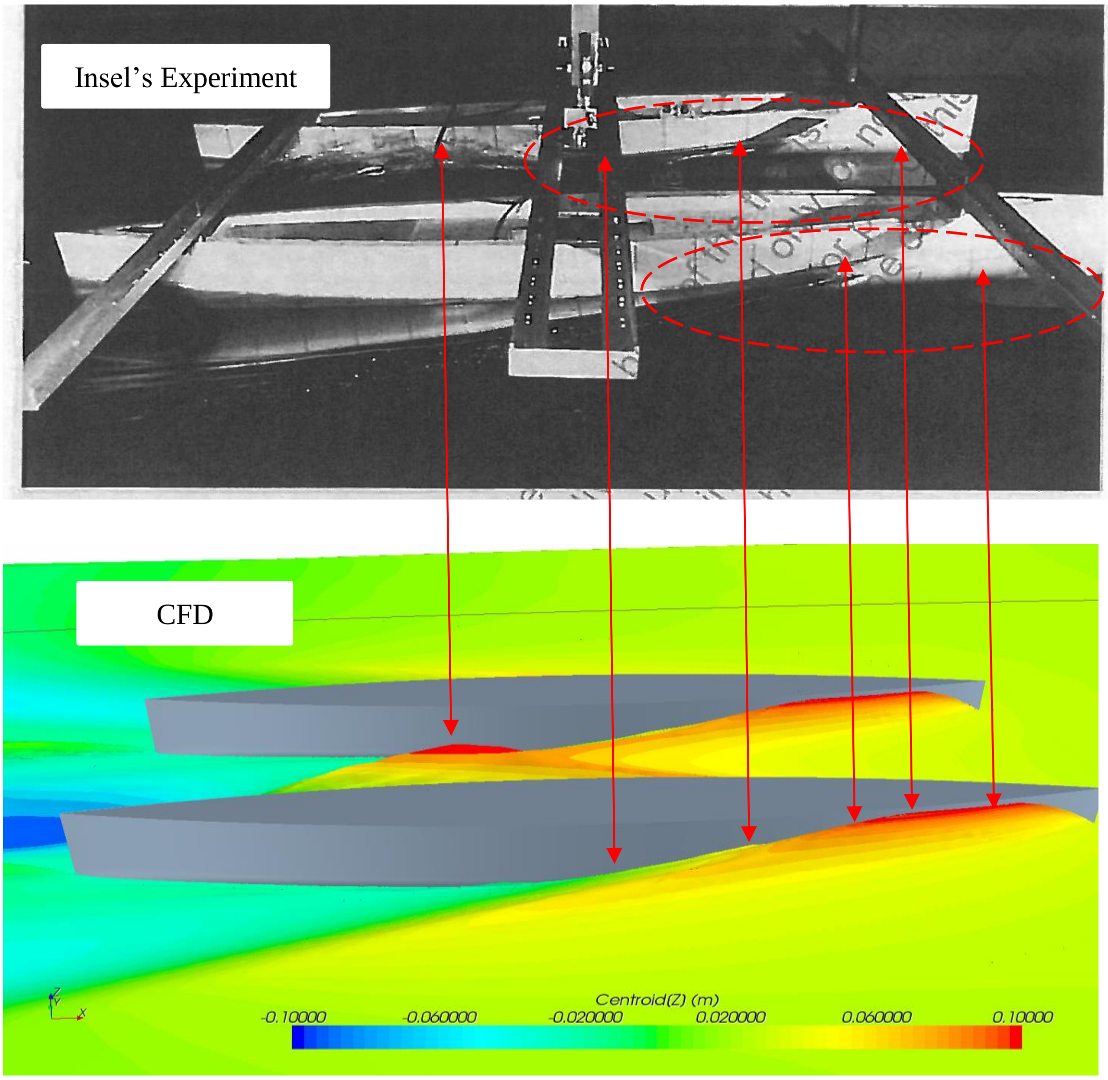

Figure 4.17 Wave elevation along the hull for Wigley III S/L = 0.3 at Fn = 0.75

Figure 4.17 presents the comparison between the photograph taken by Insel and the free surface created in CFD code using the same point of view. From the previous section for high Froude numbers, the CFD wave elevations appear to be lower than the experiment. It should be highlighted that the way Insel measured wave elevation is different from this study. In the experiment, a high-speed camera was used to capture the wave elevation and the hull was marked at bow and stern at every 5mm interval. The differences between the experiment and CFD might be from these data acquisition methods.

The experimental photograph showed that the highest free surface level was projected on the hull while the CFD wave elevation is measured by creating the intersection line between the hull and free surface, which is attached to the hull surface. The differences of the measurement techniques result in the significant errors between CFD and experiment. It can be seen that the highest wave elevation occurs slightly away from the hull surface as shown in figures 4.18 and 4.19.

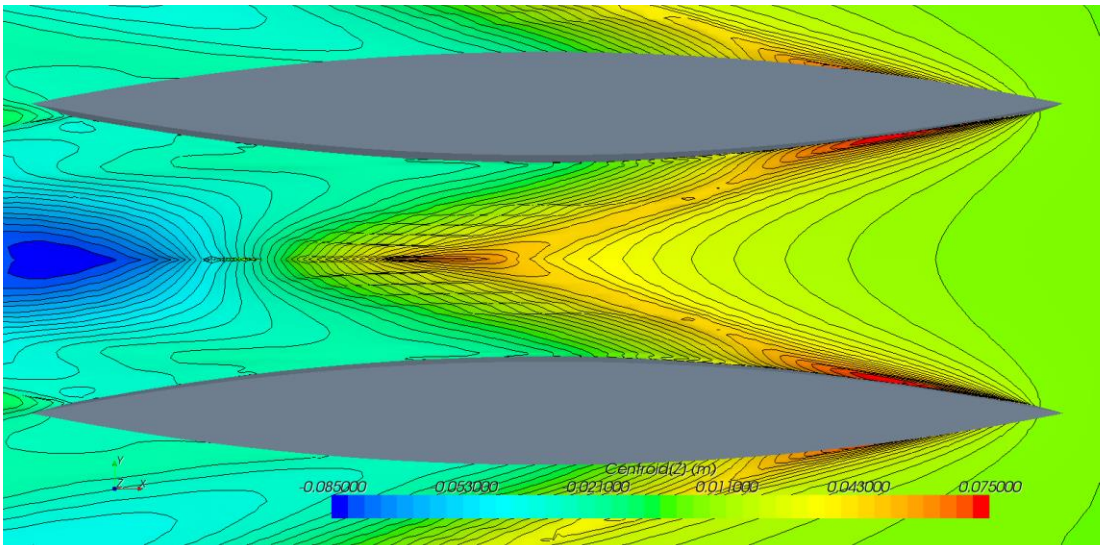

Figure 4.18 Top view of free surface around the hull for Wigley III S/L = 0.3 at Fn = 0.75

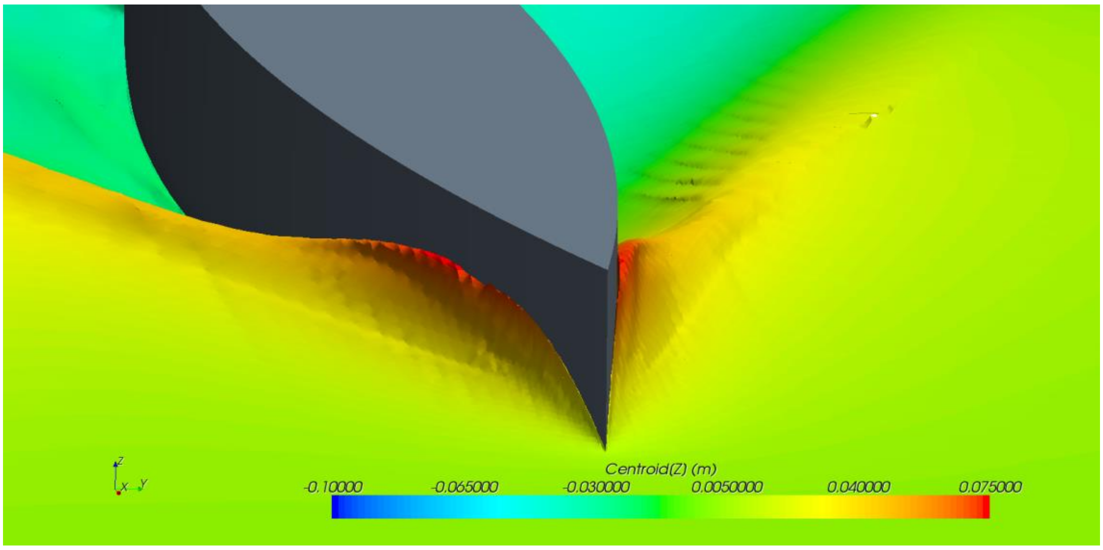

Figure 4.19 Front view of free surface around the hull for Wigley III S/L = 0.3 at Fn = 0.75

4.6 Chapter Summary

Four hull configurations of Wigley III are investigated in this chapter including monohull, catamaran S/L = 0.2, 0.3 and 0.4. Resistance components (C_T, C_F, C_V, C_R and C_W), form factors (1+k) and wave elevations along the hull are investigated for all hull configurations. Additional to those, the viscous and wave resistance interference factors (β and τ) are estimated for catamarans.

CFD resistance components show a good agreement with Insel's experiments. Mostly, CFD resistance components are lower than the experimental data except for frictional resistance coefficient (C_F), which is slightly over predicted. The CFD form factors (1+k) are slightly lower than the experimental form factor for all hull configurations. Form factor appears to increase with speed (Fn). The catamaran form factors are higher than monohull form factor and decrease with the increasing hull separation. Viscous resistance interference factor (β) also decreases with the increasing hull separation. Wave resistance interference factor (τ) also shows a good agreement with the experiment.

The wave elevation validations are made against the experiment for two Froude numbers, Fn = 0.35 and 0.50. At the low Froude number, Fn = 0.35, the CFD wave elevation shows a good agreement with experiment while the higher Froude number, Fn = 0.50, CFD results show an accepted validation with significant error as discussed in section 4.5.

Chapter 5: Scale Effects on Form Factor for Wigley III Catamarans

5.1 Numerical Domains and Mesh Techniques

5.1.1 Numerical Domain

The Wigley III with the separation to length ratio, S/L = 0.3 is selected for this study because the results from the previous chapter show that the interference effects between demihulls for the narrower hull separation are too strong, and there is a slight difference for the wider hull separation. Hence catamaran with S/L = 0.3 could be the most suitable for this investigation to represent the scale effects.

Two additional scales are investigated as seen in table 5.1. These scale ratios are selected because the sizes of the hull are not changed rapidly, which will result in large domain dimensions and mesh problems. The domain dimensions are set as the same ratio as the previous simulations to maintain the same flow characteristics and conditions. A symmetry plane is also used to reduced domain size and number of cells. Boundary conditions are set as the same with the model scale used in chapter 4. Resistance components are calculated and measured using the same techniques applied to the model size.

In order to increase model size, it is important to ensure that model dimension is scaled correctly. Due to the fact that hull dimensions are a function of L, B, T, WS and ∇, models extended three dimensionally need to consider the scale factor into these parameters. To this point, L, B and T are related to the first order of the scale while WS and ∇ are depended on the second and third order of scale respectively. Table 5.1 represents the results of model scaling for the different sizes.

Table 5.1 Wigley III model scale validation

Model	2L			4L		
	Calculation	CFD	% Error	Calculation	CFD	% Error
L, *m*	3.60	3.60	-	7.20	7.20	-
B, *m*	0.36	0.36	-	0.72	0.72	-
T, *m*	0.225	0.225	-	0.45	0.45	-
C_B	0.444	0.4438	-0.045	0.444	0.4438	-0.045
WS, m^2	1.928	1.922	-0.332	7.712	7.752	0.519
∇, m^3	0.129	0.128	-0.775	2.064	2.047	-0.823

5.1.2 Mesh Techniques

Grid generation is slightly different from the model due to the fact that although the hull geometry is larger, flow characteristics do not change. Boundary layer and first layer thickness are also the key factors for grid generation to maintain the same y^+. As a larger model, the boundary layer thickness is smaller with respect to the hull length, this leads to a huge difference in cell size between the boundary layer and core zones. To overcome this issue, more grid refinements are required which results in increasing number of cells from 5-6M cells to 7-9M and 12-15M cells for 2L and 4L respectively.

5.1.3 Resistance Validation Method

Because there are no experimental results available for validation for the scaled-up models, Froude and Hughes approaches are used to calculate the reference data from Insel's experiment. The details of the Froude approach used to calculate the experimental result for scaled-up model is derived as below:

$$C_{T\_Scale\_Exp} = C_{F\_ITTC\_Scale} + C_{R\_1L\_Eep} \qquad 5.1$$

From equation 5.1, the experimental total resistance of the scaled-up model is equated the sum of frictional resistance of the scaled model calculated using ITTC correlation line and the residual resistance of the model. In order to find the viscous and wave resistance components (C_V and C_W), Hughes approach together with a form factor are applied and derived as shown in equations 5.2 and 5.3.

$$C_{T\_Scale\_Exp} = C_{V\_Scale\_Exp} + C_{W\_Scale\_Exp} \qquad 5.2$$

$$C_{T\_Scale\_Exp} = (1+k)C_{F\_ITTC\_Scale} + C_{W\_scale\_Exp} \qquad 5.3$$

From equation 5.3, it can be seen that frictional resistance coefficient is known by using ITTC correlation line and form factor (1+k) from the experiment. By subtracting the frictional resistance coefficient on the right-hand side of equation 5.3 from total resistance coefficient calculated using equation 5.1, wave resistance coefficient of the scaled model is known.

5.2 Resistance Components

5.2.1 2L Catamaran

Resistance components of Wigley III for 2L presented in table 5.2 and figure 5.1 are total resistance (C_T), frictional resistance (C_F) and viscous resistance (C_V). The CFD total resistance is validated against the experimental results and show a good agreement with the range of the under prediction between 1.82 and 2.94 percent. The differences between CFD and experimental results are quite steady over the range of Froude number with a small fluctuation where $Fn < 0.40$.

Frictional resistance coefficient calculated using CFD code is validated against ITTC correlation line and shows a good agreement with the over prediction over the range of Froude number between 1.66 and 2.93 percent. The CFD frictional resistance coefficient of the 2L model shows the same characteristics as the 1L model. The largest error between CFD and ITTC correlation line C_F are seen for $Fn = 0.247$ and $0.310 < Fn < 0.75$.

The CFD viscous resistance coefficient validation is made against the experimental results calculated using $C_V = (1+k)*C_F$ as shown in equation 5.3. The results show a good agreement with the experimental data as seen in table 5.2. The CFD viscous resistance coefficient seems to be under predicted for the low-speed range, $Fn < 0.50$ and over predicted for $Fn > 0.50$. The plot of CFD C_V against experimental C_V is shown in figure 5.1. The differences between CFD and experimental C_V seem to decrease with speed (Fn). There is a small fluctuation of CFD C_V prediction at the $Fn < 0.40$, initially the CFD C_V below the experimental C_V then marginally larger than experimental C_V.

Residual resistance (C_R) and wave resistance (C_W) coefficients for the 2L model are shown in table 5.3 and figure 5.2. The CFD residual resistance coefficient shows a fair agreement with the experimental results with the range of the under prediction between 5.41 and 16.87 percent. The error is very high for low Froude numbers and then reduces gradually with speed (Fn).

The validation of wave resistance coefficient between CFD and experimental results is highlighted in table 5.3 and figure 5.2. The CFD wave resistance coefficient shows a fair agreement with the experiment. The CFD results show a mix of both over and under prediction. For Fn < 0.310, the CFD results are higher than the experiment, especially for the lowest Froude numbers where Fn = 0.20. The large difference between CFD and experimental results might be from the largest under prediction of the viscous resistance. The under prediction of CFD C_W is seen for Fn > 0.30. The under prediction seems to be small for 0.30 < Fn < 0.367. For the higher Froude number, Fn > 0.40, the over prediction of CFD C_W is found and increases with speed.

Table 5.2 Total, frictional and viscous resistance coefficients of Wigley III S/L = 0.3_2L

Fn	C_T (x 10^{-3})			C_F (x 10^{-3})			C_V (x 10^{-3})		
	Exp	CFD	Error (%)	ITTC	CFD	Error (%)	Exp	CFD	Error (%)
0.200	4.498	4.411	-1.943	3.593	3.659	1.817	4.168	3.929	-5.747
0.247	4.886	4.752	-2.743	3.453	3.554	2.912	4.006	3.834	-4.290
0.272	4.681	4.587	-2.008	3.392	3.451	1.734	3.935	3.827	-2.732
0.300	5.762	5.658	-1.817	3.332	3.387	1.662	3.865	3.712	-3.950
0.310	5.939	5.814	-2.109	3.312	3.375	1.911	3.842	3.726	-2.996
0.350	4.674	4.588	-1.849	3.240	3.326	2.669	3.758	3.685	-1.953
0.367	4.614	4.523	-1.966	3.212	3.284	2.242	3.726	3.693	-0.881
0.400	6.210	6.061	-2.404	3.163	3.224	1.933	3.669	3.650	-0.507
0.500	8.261	8.061	-2.423	3.041	3.123	2.709	3.527	3.557	0.847
0.600	7.222	7.010	-2.937	2.946	3.023	2.626	3.417	3.464	1.354
0.700	6.417	6.273	-2.243	2.869	2.928	2.046	3.328	3.386	1.737
0.750	6.208	6.071	-2.203	2.836	2.887	1.800	3.290	3.353	1.915
0.800		5.716		2.805	2.859	1.915	3.254	3.329	2.313

Table 5.3 Residual and wave resistance coefficients, and form factor of Wigley III S/L = 0.3_2L

Fn	C_R (x 10^{-3})			C_W (x 10^{-3})			1+k (CFD)	Re
	Exp	CFD	Error (%)	Exp	CFD	Error (%)		
0.200	0.905	0.752	-16.873	0.330	0.482	46.096	1.074	3.70E+06
0.247	1.433	1.198	-16.373	0.880	0.918	4.300	1.079	4.57E+06
0.272	1.289	1.136	-11.857	0.746	0.760	1.811	1.109	5.04E+06
0.300	2.431	2.271	-6.586	1.898	1.946	2.528	1.096	5.55E+06
0.310	2.628	2.439	-7.176	2.098	2.088	-0.485	1.104	5.74E+06
0.350	1.435	1.262	-12.051	0.916	0.903	-1.426	1.108	6.48E+06
0.367	1.402	1.239	-11.608	0.888	0.830	-6.521	1.125	6.79E+06
0.400	3.048	2.837	-6.906	2.542	2.411	-5.143	1.132	7.41E+06
0.500	5.221	4.938	-5.412	4.734	4.504	-4.859	1.139	9.26E+06
0.600	4.277	3.987	-6.769	3.805	3.547	-6.791	1.146	1.11E+07
0.700	3.548	3.345	-5.711	3.089	2.887	-6.531	1.156	1.30E+07
0.750	3.372	3.184	-5.569	2.918	2.718	-6.845	1.161	1.39E+07
0.800		2.857			2.387		1.165	1.48E+07
						Average	1.123	

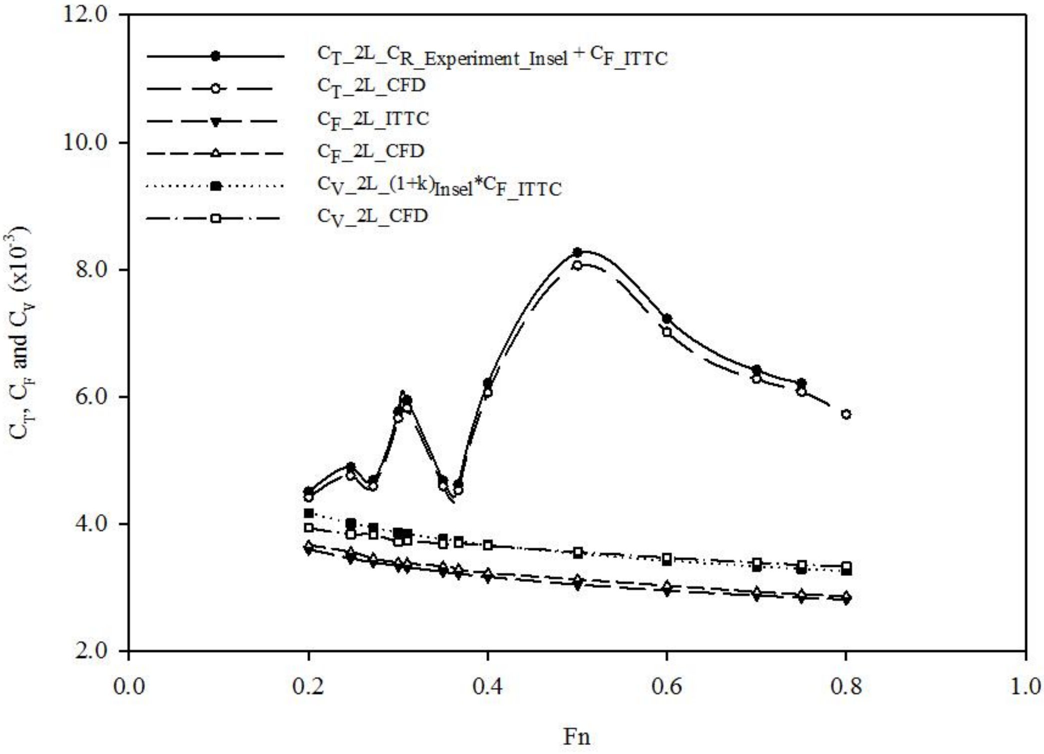

Figure 5.1 Total, frictional and viscous resistance coefficients of Wigley III S/L = 0.3_2L

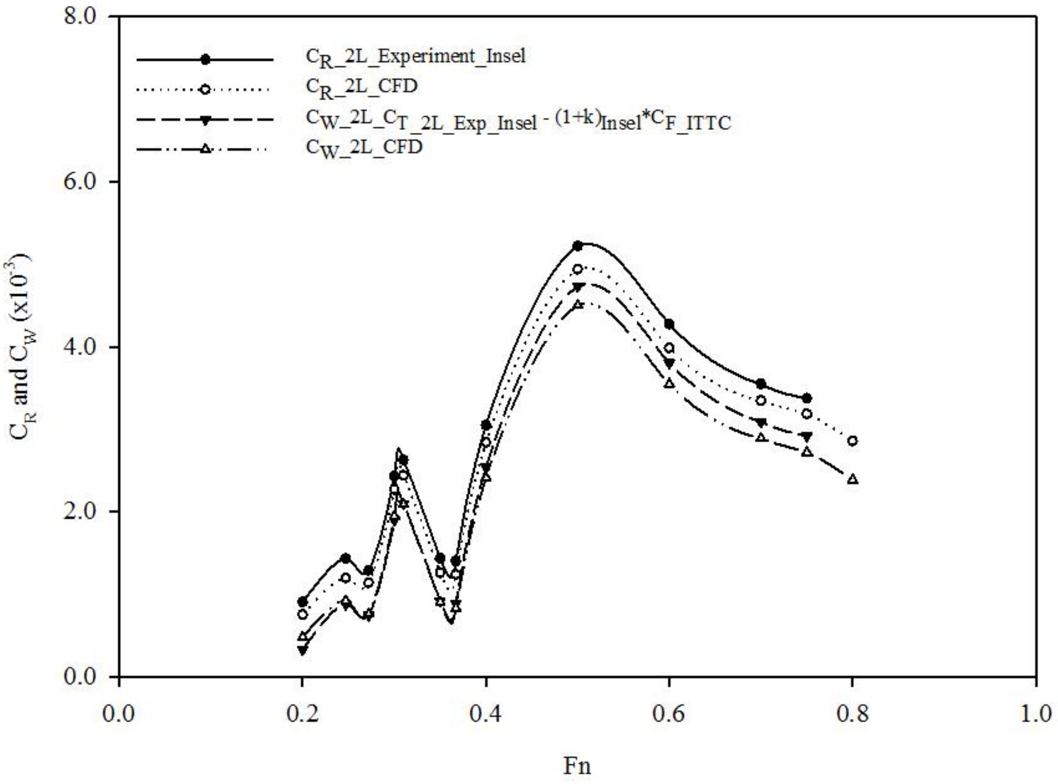

Figure 5.2 Residual and wave resistance coefficients of Wigley III S/L = 0.3_2L

5.2.2 4L Catamaran

Total (C_T), frictional (C_F) and viscous (C_V) resistance coefficients of the 4L catamaran are shown in table 5.4 and figure 5.3. The CFD total resistance coefficient shows a good agreement with the experimental results with a small error between 1.33 and 2.06 percent. The CFD C_T shows under prediction over the range of Froude numbers. The error seems to be steady for all speed (Fn) except for Fn = 0.272 where the error is higher than 2.0 percent and for 0.40 < Fn < 0.70 where the error is lower than 1.50 percent.

The CFD frictional coefficient shows a good agreement with the ITTC correlation line. The CFD C_F are over predicted over the range of Froude number, which is similar to other models. The errors are between 1.30 and 2.78 percent. A small fluctuation in CFD C_F prediction can be seen at Fn = 0.20, 0.367 and 0.40 where the CFD C_F error exceeds 2.0 percent.

The CFD viscous resistance coefficient validation shows a good agreement with the experimental results. Like the smaller models, the CFD C_V is under predicted for low Froude numbers (Fn < 0.40) and over prediction for high Froude numbers (Fn > 0.367).

Table 5.5 and figure 5.4 show the CFD residual and wave resistance coefficients against the experimental results. The CFD C_R shows a fair agreement with experimental results with the range of under prediction over Froude numbers between 2.543 and 14.771 percent. The differences between CFD and experimental results which exceed 10.0 percent can be seen for Fn = 0.20 and 0.267.

Wave resistance results are presented in table 5.5 and figure 5.4. The CFD wave resistance coefficient shows a mix of both over prediction and under prediction. The over prediction of CFD results is found for Fn < 0.30. The largest over prediction is off 23.74 percent for Fn = 0.20. The under prediction occurs for the Fn > 0.272 and seem to be increased with speed (Fn). There are three Froude numbers where the under prediction of CFD C_R exceeds 5.0 percent, which include Fn = 0.367, 0.70 and 0.75.

Table 5.4 Total, frictional and viscous resistance coefficients of Wigley III S/L = 0.3_4L

Fn	C_T (x 10^{-3})			C_F (x 10^{-3})			C_V (x 10^{-3})		
	Exp	CFD	Error (%)	ITTC	CFD	Error (%)	Exp	CFD	Error (%)
0.200	3.881	3.814	-1.727	2.976	3.043	2.240	3.452	3.283	-4.891
0.247	4.303	4.237	-1.535	2.870	2.914	1.524	3.329	3.201	-3.859
0.272	4.113	4.028	-2.057	2.824	2.867	1.530	3.276	3.176	-3.041
0.300	5.208	5.112	-1.846	2.778	2.814	1.305	3.222	3.154	-2.116
0.310	5.390	5.289	-1.876	2.763	2.810	1.708	3.205	3.146	-1.828
0.350	4.142	4.087	-1.333	2.708	2.756	1.790	3.141	3.087	-1.711
0.367	4.088	4.012	-1.863	2.686	2.761	2.782	3.116	3.107	-0.298
0.400	5.696	5.588	-1.903	2.649	2.704	2.083	3.073	3.088	0.500
0.500	7.776	7.691	-1.089	2.555	2.603	1.882	2.964	2.991	0.921
0.600	6.758	6.684	-1.100	2.482	2.526	1.779	2.879	2.912	1.148
0.700	5.970	5.871	-1.664	2.422	2.461	1.590	2.810	2.874	2.274
0.750	5.768	5.662	-1.845	2.397	2.442	1.894	2.780	2.851	2.552
0.800		5.453		2.373	2.416	1.514	2.752	2.830	2.822

Table 5.5 Residual and wave resistance coefficients, and form factor of Wigley III S/L = 0.3_4L

Fn	C_R (x 10^{-3})			C_W (x 10^{-3})			1+k (CFD)	Re
	Exp	CFD	Error (%)	Exp	CFD	Error (%)		
0.200	0.905	0.771	-14.771	0.429	0.531	23.740	1.079	1.05E+07
0.247	1.433	1.323	-7.663	0.974	1.036	6.414	1.098	1.29E+07
0.272	1.289	1.161	-9.917	0.837	0.852	1.792	1.108	1.42E+07
0.300	2.431	2.298	-5.447	1.986	1.958	-1.407	1.121	1.57E+07
0.310	2.628	2.479	-5.645	2.186	2.143	-1.947	1.120	1.62E+07
0.350	1.435	1.331	-7.228	1.001	1.000	-0.149	1.120	1.83E+07
0.367	1.402	1.251	-10.766	0.972	0.905	-6.882	1.125	1.92E+07
0.400	3.048	2.884	-5.368	2.624	2.500	-4.718	1.142	2.09E+07
0.500	5.221	5.088	-2.543	4.812	4.700	-2.327	1.149	2.62E+07
0.600	4.277	4.158	-2.771	3.879	3.772	-2.769	1.153	3.14E+07
0.700	3.548	3.410	-3.885	3.160	2.997	-5.166	1.168	3.67E+07
0.750	3.372	3.220	-4.502	2.988	2.811	-5.935	1.167	3.93E+07
0.800		3.037			2.623		1.171	4.19E+07
						Average	1.132	

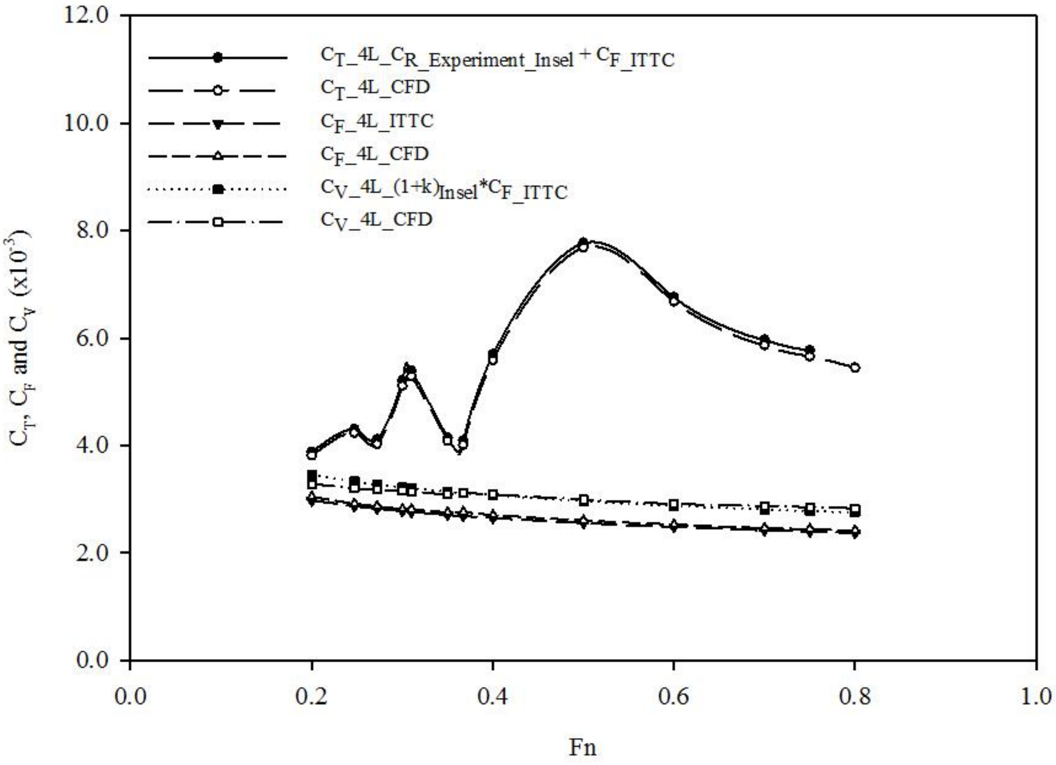

Figure 5.3 Total, frictional and viscous resistance coefficients of Wigley III S/L = 0.3_4L

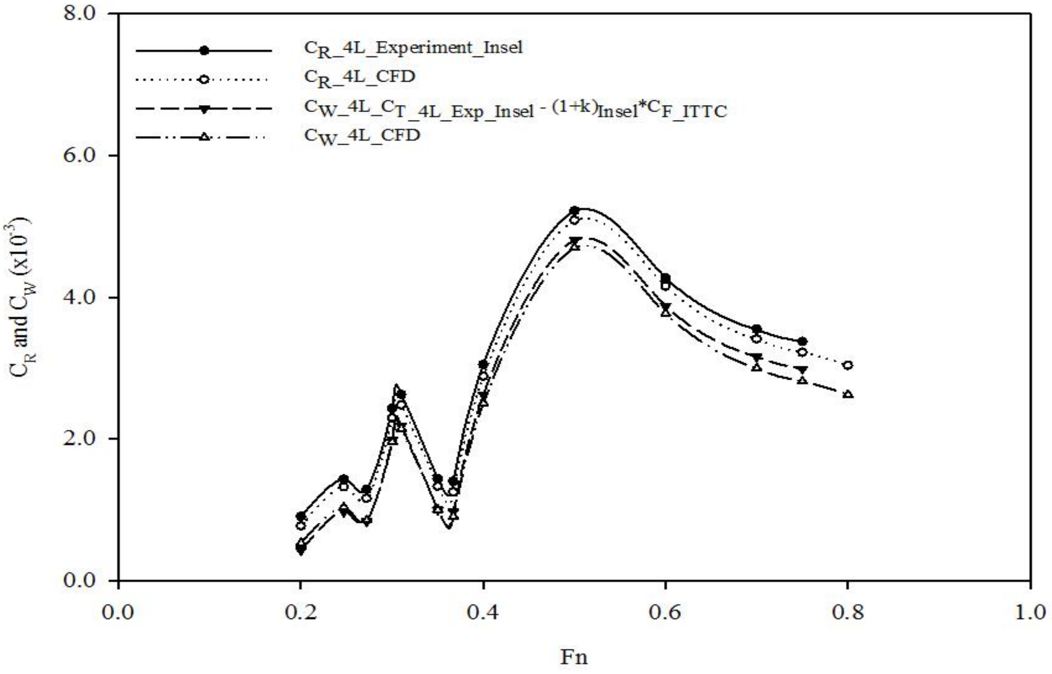

Figure 5.4 Residual and wave resistance coefficients of Wigley III S/L = 0.3_4L

5.2.3 Comparison of the Resistance Components

Figure 5.5 shows the comparison of the total (C_T), frictional (C_F) and viscous (C_V) resistance coefficients of Wigley III catamaran S/L = 0.3 for different model scales. The results show that the CFD C_T prediction is improved with the increasing model size as can be seen that the error decreases with model size. Hence, the bigger model shows the better results. The CFD C_T reduces with Reynolds' number, which agrees with the experimental results. All the CFD total resistance results show an under prediction for all model scales compared with the experiment.

The CFD frictional resistance coefficient reduces with Reynolds' number, which agrees with the ITTC correlation line. The differences between CFD and ITTC correlation line C_F are quite steady over the range of Froude numbers, which the CFD C_F is over predicted for all model scales.

Viscous resistance coefficient, C_V, estimated using CFD code shows that the bigger model has the better results. As shown in figure 5.5, the error of the smallest model, 1L, at the low-speed regime seems to be higher than the bigger models. The biggest model seems to have the lowest error. The CFD C_V slightly decreases with smaller gradient compared with the experiment.

The comparison of CFD residual resistance coefficient with experimental results for different model scales is shown in figure 5.6. Theoretically, residual resistance coefficient should be similar for all model scales. The CFD C_R shows a good agreement with this statement with a small error. From the CFD results, it can be seen that the differences between CFD and experimental C_R are highest for the smallest model, 1L. The CFD C_R accuracy improves with the increasing model size, which the largest model shows the most accurate results.

Wave resistance coefficient comparison for different model scales is shown in figure 5.7. The CFD results show good agreement with the experiment with a small error. The results show that the CFD wave resistance coefficient increases with the model size and shows an over prediction for the low Froude numbers and under prediction for the higher Froude numbers.

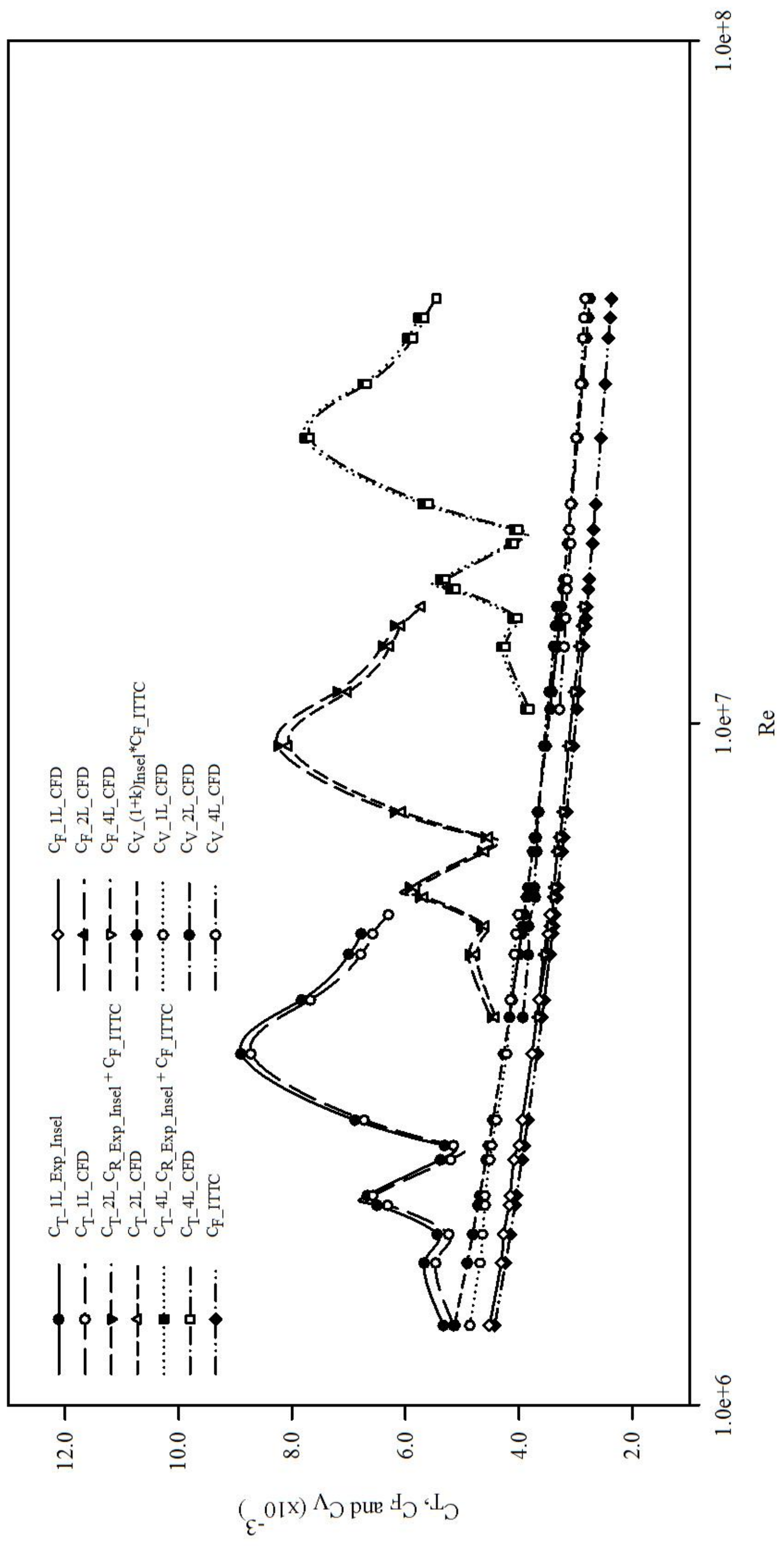

Figure 5.5 Comparison of Total, frictional and viscous resistance coefficients of Wigley III

S/L = 0.3

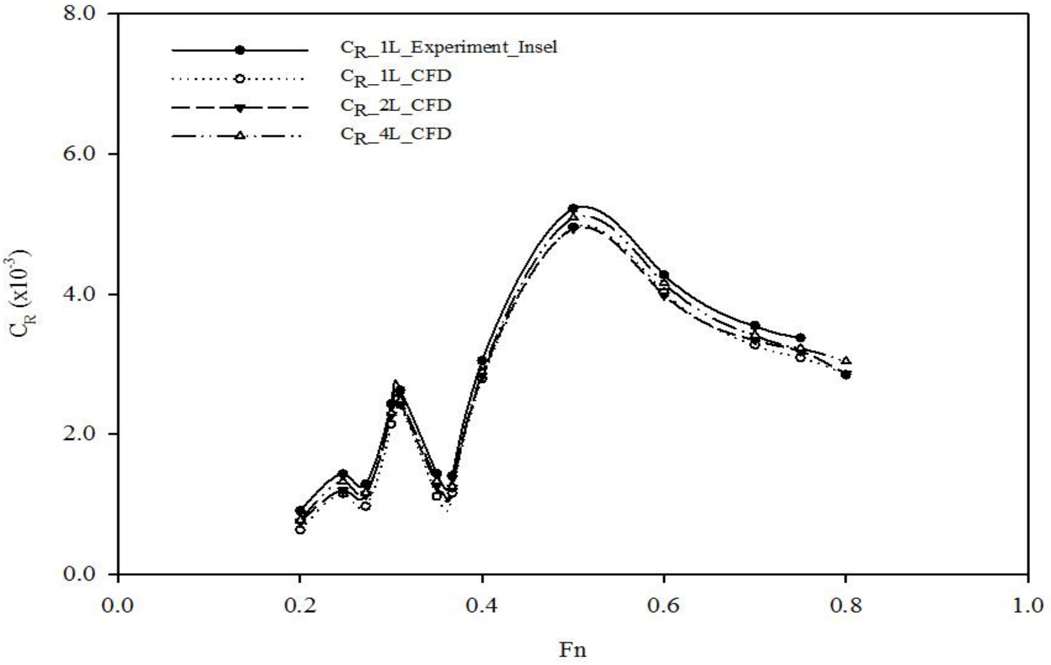

Figure 5.6 Comparison of residual resistance coefficients of Wigley III S/L = 0.3

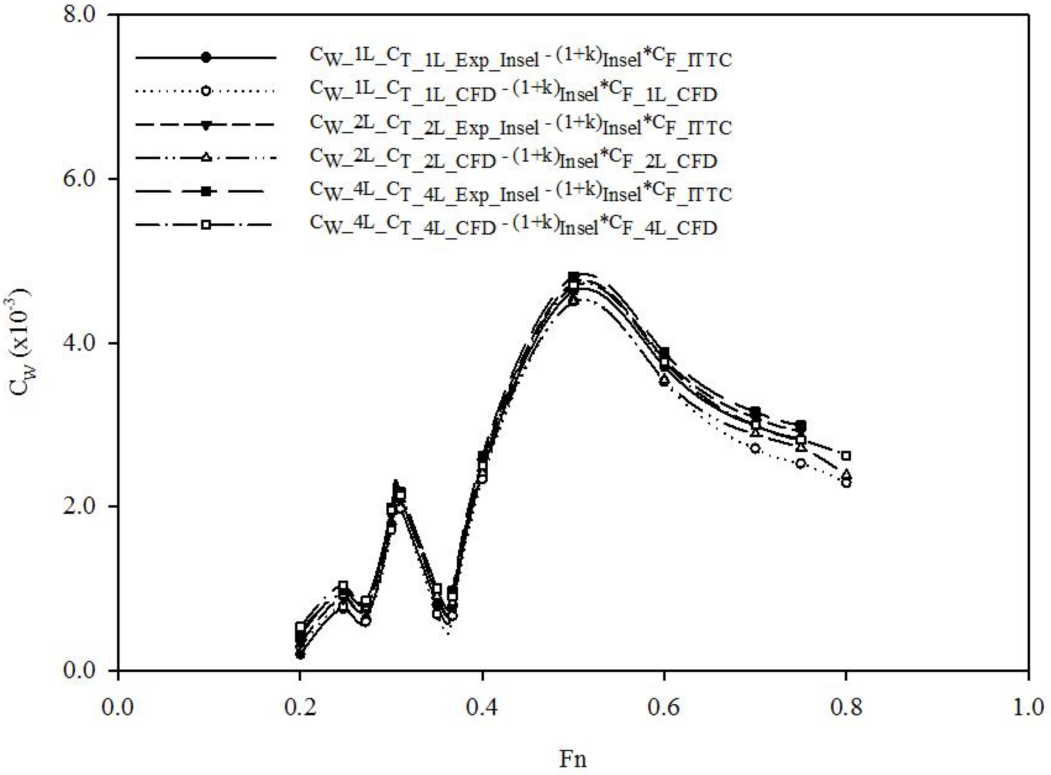

Figure 5.7 Comparison of wave resistance coefficients of Wigley III S/L = 0.3

5.3 Form Factor

Figure 5.8 shows the CFD form factors for the different model scales against Froude number. The results show that form factor increases with the increasing model size. The fitted curves of the form factor for all models show a similar trend. The increase of form factor seems to be very steep for Froude number, Fn < 0.40, and then the gradient seems to reduce for all models. However, the differences of the form factor for different model scales are very large for Fn = 0.40 and 0.50 where the increase of total resistance coefficient is very sharp. Moreover, there are some Froude numbers that form factor at 2L is smaller than 1L i.e. Fn < 0.35 and Fn = 0.70.

The dependence of form factor (1+k) on Reynolds' number (Re) is presented in figure 5.9. At the same Froude number for different model scales, form factor seems to increase. The gradient of the increase of form factor dependence on Reynolds' number for all Froude number is not linear. The gradient between 1L and 2L is steeper than 2L and 4L.

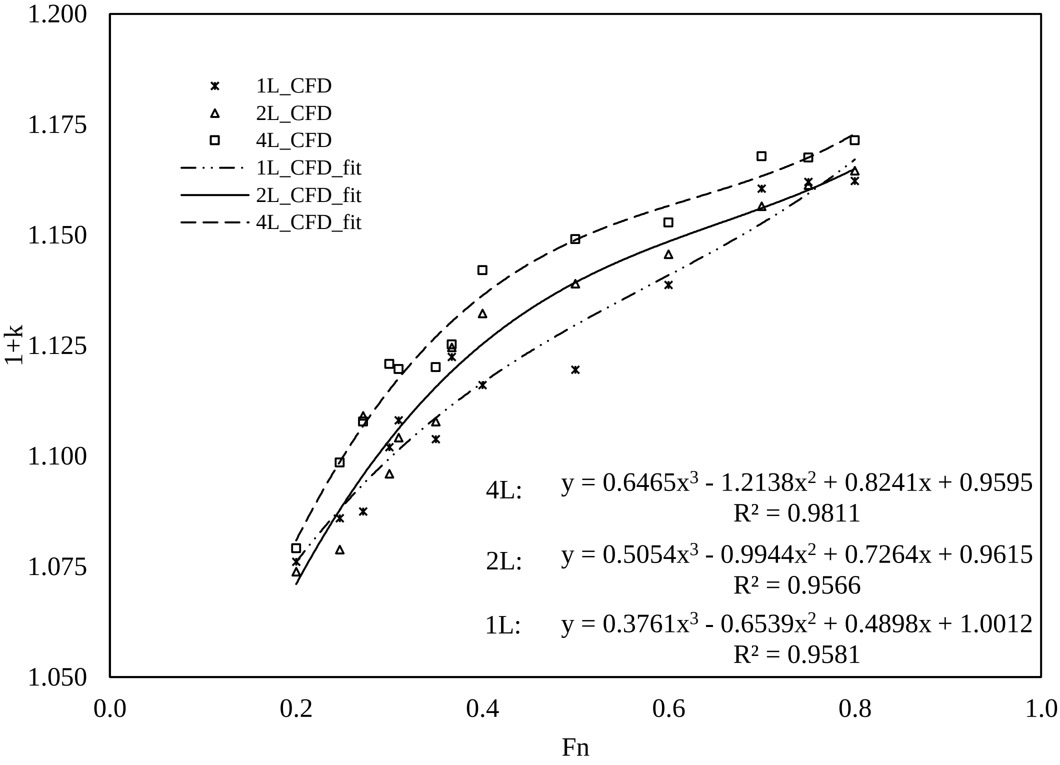

Figure 5.8 Comparison of form factor of Wigley III S/L = 0.3 at different model scales

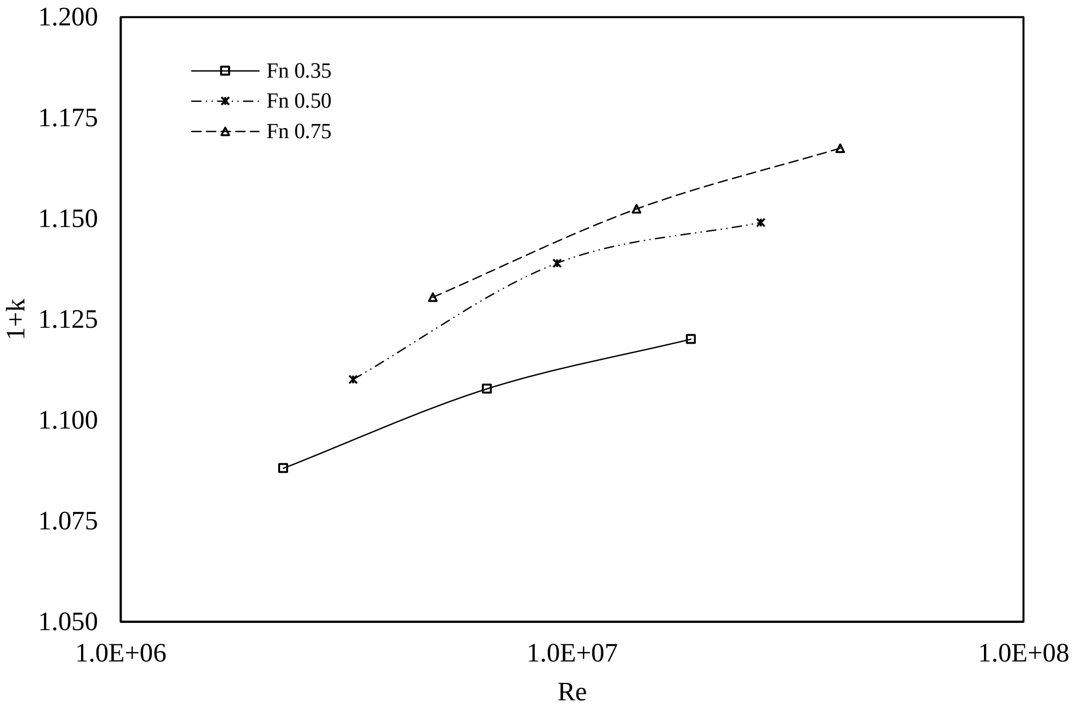

Figure 5.9 Comparison of form factor of Wigley III S/L = 0.3 at same Froude number

5.4 Chapter Summary

This chapter presents the scale effects on resistance component prediction and form factor for three different model scales of 1L, 2L and 4L. The model used in this study is Wigley III catamaran with S/L = 0.3. Because of the limitation of experimental validation data, the method in calculating resistance components for the experiment is introduced in section 5.1.3.

The CFD results show that some resistance components show a good agreement with the experimental results including total resistance (C_T), frictional resistance (C_F) and viscous resistance (C_V) coefficients. The CFD residual resistance (C_R) and wave resistance (C_W) coefficients show a fair agreement with the experimental results.

The scale effects on form factor show that form factor increases with Reynolds' number, which agrees with the literature. For the iso-Froude numbers, the increase of form factor is non-linear for all model scales. The increase in form factor between the smallest and intermediate models (1L and 2L) seems to be steeper than the intermediate and largest models (2L and 4L).

Chapter 6: Resistance and Form Factor for the Hull with a Transom Stern

6.1 Numerical Domain and Mesh Techniques

6.1.1 Hull Geometry

The simulation study duplicates Insel's experiment. The NPL 5b hull with transom stern is selected because it is one of the most particularly investigated as the representation of the hull with a transom stern. The NPL 5b hull particulars and bodyplan are shown in table 6.1 and figure 6.1. Froude Numbers investigated in this step are between 0.20 and 1.0 and increased with the 0.10 interval except for some areas that need more points i.e. 0.273 and 0.433.

The hull is fixed with dynamic sinkage and trim which were investigated and measured by Insel. This is to avoid extending the complexities of the flow problem to the studies and to reduce the simulation time. For the catamaran study, the separation to length ratio S/L = 0.3 is used. The S/L is chosen because the previous study on the hull without transom stern shows that the interference effects due to hull separation slightly change for larger separations. While the narrower hull separation, i.e. 0.2, shows a high influence of the hull separation on resistance components and flow characteristics as also discussed by Insel.

Table 6.1 NPL 5b hull particulars

Model	NPL 5b
L, m	1.60
L/B	11.00
B/T	2.00
$L/\nabla^{1/3}$	8.479
C_B	0.397
C_P	0.693
C_M	0.565
WS, m^2	0.276

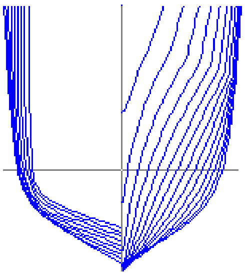

Figure 6.1 NPL 5b bodyplan (Molland et. al, 2003)

6.1.2 Monohull

Mesh techniques obtained from Wigley III are used in this study except for mesh at the transom stern need to be dealt with carefully. To overcome this, from previous studies and some literatures, the length of hollow is about six times the half transom breadth. Hence, this region is treated differently from other parts of numerical domain. To generate a mesh to capture flow separation around transom stern, the same technique as the numerical wave tank is applied (~30-40 cells per wave height). The refinement blocks added into the transom stern area are shown in figures 6.2 and 6.3. The mesh resolutions for the free surface are treated the same way as for the Wigley III as shown in figures 6.2 to 6.4.

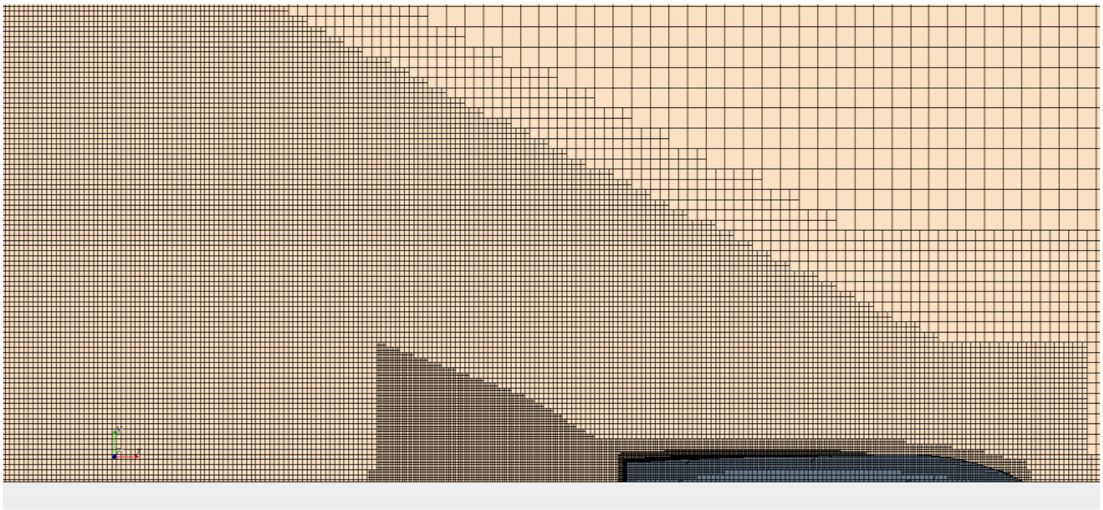

Figure 6.2 Top view mesh for NPL 5b monohull

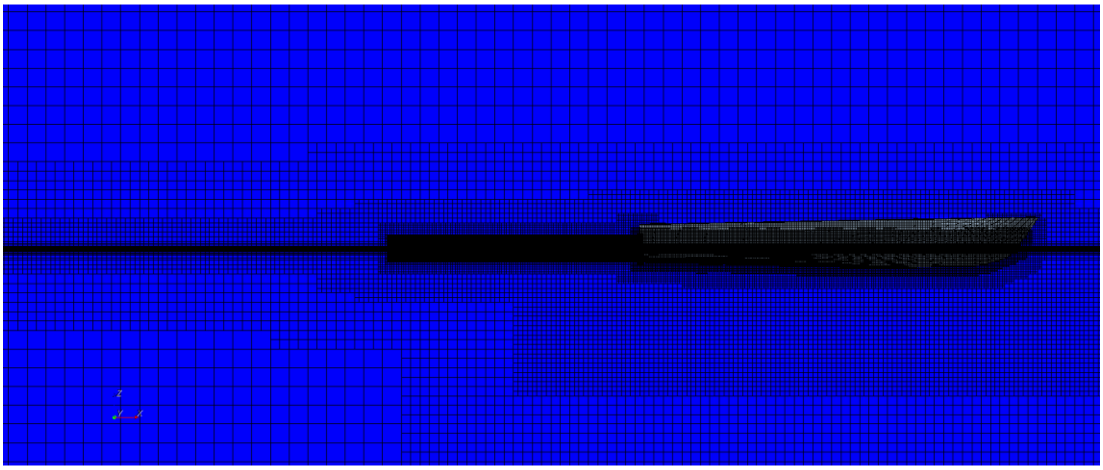

Figure 6.3 Side view mesh for NPL 5b monohull

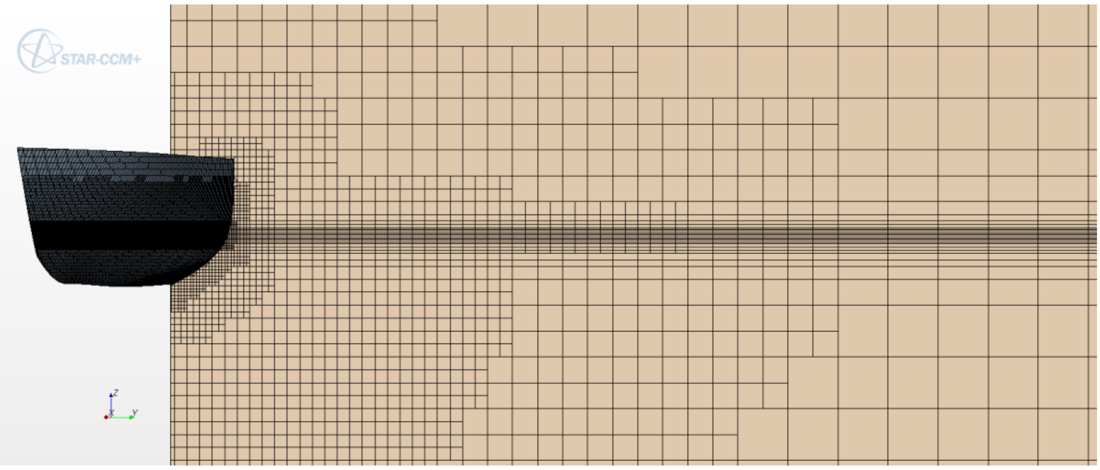

Figure 6.4 Free surface mesh for NPL 5b monohull

6.1.3 Catamaran S/L = 0.3

The mesh generations for the catamaran with a transom stern study are shown in figures 6.5, 6.6 and 6.7. Figure 6.5 shows the top view mesh for the free surface around catamaran. Four regions are treated with refinement blocks including around demihulls, wake system area, transom stern and the interference area between demihulls. The number of cells per wave height is applied following the numerical towing tank study.

The mesh density in the z-direction for the hollow behind transom stern is shown in figure 6.6. Due to the strength of the flow interference between demihulls, another refinement block is placed in between the demihulls as presented in figure 6.7.

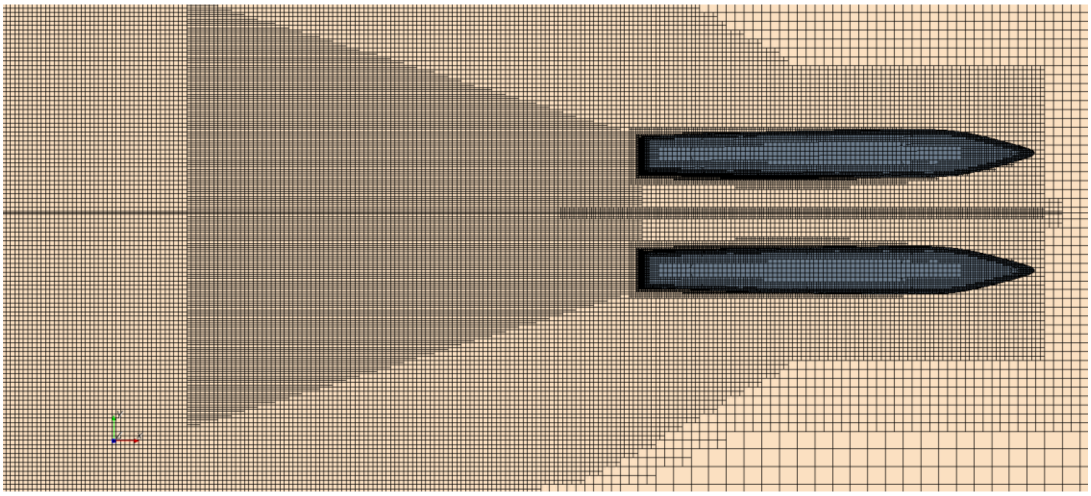

Figure 6.5 Top view mesh for NPL 5b catamaran

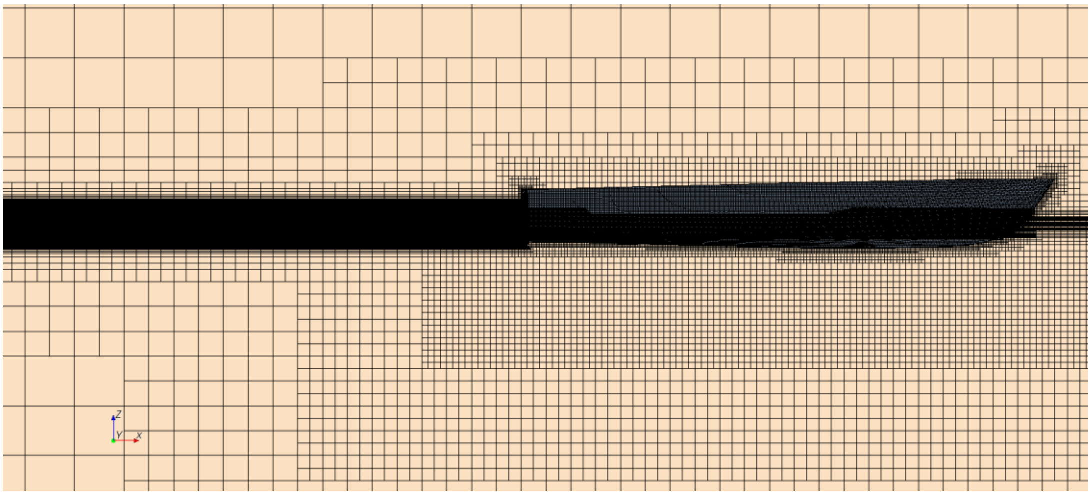

Figure 6.6 Side view mesh for NPL 5b catamaran

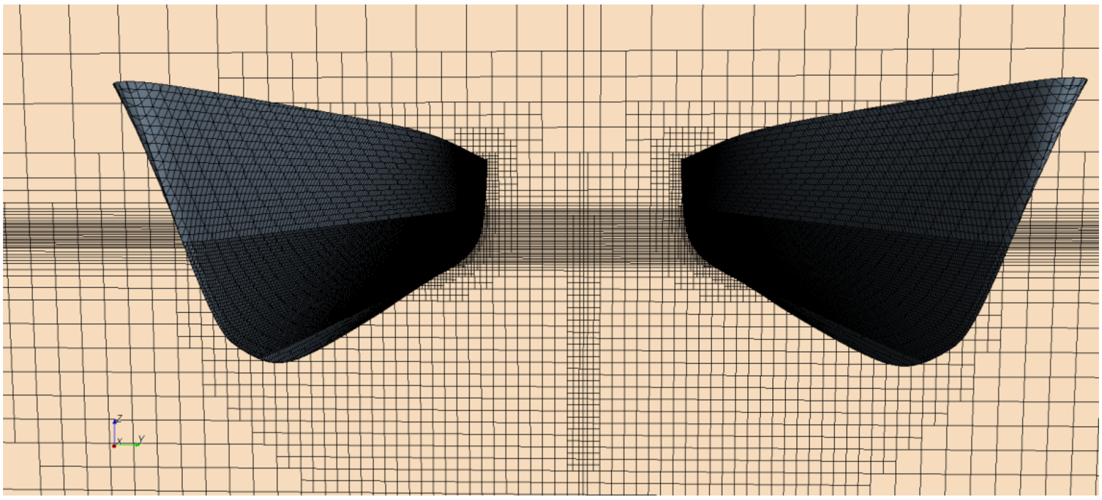

Figure 6.7 Free surface mesh for NPL 5b catamaran

6.2 Resistance Components

6.2.1 Monohull

The resistance components of the NPL 5b monohull are shown in tables 6.2 and 6.3 and figures 6.8 and 6.9. These resistance components consist of the total (C_T), frictional (C_F), viscous (C_V), residual (C_R) and wave (C_W) resistance.

Table 6.2 and figure 6.8 show the validation of total (C_T), frictional (C_F) and viscous (C_V) resistance coefficients. The total resistance coefficient is validated against Insel's experimental results. The CFD C_T shows a good agreement with the experiment with a small error between 0.275 and 2.133 percent over the range of Froude number. The CFD C_T is under predicted compared with the experiment. For Fn > 0.360, the difference between CFD and experimental C_T is larger than 1.0 percent except for Fn = 0.50, 0.70 and 1.0. Another point that shows the under prediction over 1.0 percent for the total resistance is the lowest Froude number, Fn = 0.20.

The CFD frictional resistance coefficient (C_F) is validated against the ITTC correlation line and shows a good agreement, which can be seen in table 6.2 and figure 6.8. The CFD C_F shows an over prediction over the range of Froude number with the range of error between 1.215 and 2.739 percent. The CFD results show a very good agreement with the ITTC correlation line on either ends of the Froude number range for Fn < 0.26 and Fn > 0.80, where the error is lower than 1.50 percent. For 0.20 < Fn < 0.90, the CFD C_F shows a good agreement with small fluctuations.

The CFD viscous resistance coefficient (C_V) validation against the experiment shows a good agreement as shown in table 6.2 and figure 6.8. The differences between CFD C_V and experimental results show a mix of both under and over predictions. For the low-speed range, Fn < 0.60, the CFD C_V is lower than the experimental results. The higher Froude numbers, for Fn > 0.50, the CFD C_V shows a slightly over prediction compared with the experiment. As can be seen, the gradient of the decrease of viscous resistance prediction for the experiment is steeper than the CFD, hence this results in the over prediction of CFD C_V for high Froude numbers.

The CFD prediction of residual resistance coefficient (C_R) is shown in table 6.3 and figure 6.9. The validation of CFD C_R against the experimental results shows a fair agreement with the range of error between 3.777 and 10.726 percent. Generally, the CFD C_R is under predicted. The differences between CFD and experimental C_R seem to be steady over the range of Froude number except for Fn = 0.20, 0.60 and 0.80, where the error exceeds 7.0 percent.

The prediction and validation against experimental results for CFD wave resistance coefficient (C_W) are shown in table 6.3 and figure 6.9. The CFD C_W shows a fair agreement with the experimental results with a combination of under and over predictions. The range of error is between 0.916 and 13.264 percent. For $0.20 < Fn < 0.80$, the CFD C_R shows a fair agreement with the experimental results, the error is smaller than 5.0 percent of both under and over predictions. On either ends of the Froude number ranges, $Fn < 0.26$ and $Fn > 0.70$, the error is higher than 5.0 percent.

Table 6.2 Total, frictional and viscous resistance coefficients of NPL 5b monohull

Fn	C_T (x10^{-3})			C_F (x10^{-3})			C_V (x10^{-3})		
	Exp	CFD	Error (%)	ITTC	CFD	Error (%)	Exp	CFD	Error (%)
0.200	6.556	6.428	-1.952	4.595	4.654	1.295	5.376	5.273	-1.908
0.260	6.667	6.612	-0.825	4.346	4.422	1.750	5.085	4.995	-1.765
0.273	6.611	6.587	-0.363	4.302	4.401	2.303	5.033	4.953	-1.595
0.300	6.778	6.713	-0.959	4.219	4.311	2.186	4.936	4.874	-1.255
0.327	6.778	6.716	-0.915	4.145	4.215	1.692	4.849	4.801	-1.000
0.360	6.722	6.688	-0.506	4.065	4.176	2.739	4.756	4.721	-0.729
0.400	7.056	6.923	-1.885	3.979	4.043	1.597	4.656	4.625	-0.664
0.433	7.222	7.102	-1.662	3.917	3.991	1.888	4.583	4.548	-0.763
0.500	6.944	6.915	-0.418	3.808	3.897	2.349	4.455	4.446	-0.198
0.600	6.111	6.020	-1.489	3.675	3.762	2.361	4.300	4.319	0.441
0.700	5.500	5.482	-0.327	3.569	3.654	2.391	4.175	4.216	0.974
0.800	5.111	5.002	-2.133	3.480	3.546	1.894	4.072	4.114	1.039
0.900	4.889	4.814	-1.534	3.405	3.446	1.215	3.983	4.021	0.949
1.000	4.722	4.709	-0.275	3.339	3.384	1.341	3.907	3.975	1.744

Table 6.3 Residual and wave resistance coefficients, and form factor of NPL 5b monohull

Fn	C_R (x10^{-3})			C_W (x10^{-3})			1+k (CFD)	Re
	Exp	CFD	Error (%)	Exp	CFD	Error (%)		
0.200	1.961	1.774	-9.558	1.223	1.155	-5.560	1.133	1.10E+06
0.260	2.321	2.190	-5.647	1.556	1.617	3.920	1.130	1.43E+06
0.273	2.309	2.186	-5.330	1.611	1.634	1.428	1.125	1.50E+06
0.300	2.559	2.402	-6.144	1.856	1.839	-0.916	1.131	1.65E+06
0.327	2.633	2.501	-5.019	1.889	1.915	1.376	1.139	1.79E+06
0.360	2.657	2.512	-5.469	1.944	1.967	1.183	1.131	1.97E+06
0.400	3.077	2.880	-6.389	2.389	2.298	-3.809	1.144	2.19E+06
0.433	3.305	3.111	-5.868	2.611	2.554	-2.183	1.140	2.38E+06
0.500	3.136	3.018	-3.777	2.500	2.469	-1.240	1.141	2.74E+06
0.600	2.436	2.258	-7.298	1.778	1.701	-4.331	1.148	3.29E+06
0.700	1.931	1.828	-5.350	1.306	1.266	-3.063	1.154	3.84E+06
0.800	1.631	1.456	-10.726	1.000	0.888	-11.200	1.160	4.39E+06
0.900	1.484	1.368	-7.840	0.914	0.793	-13.264	1.167	4.94E+06
1.000	1.383	1.325	-4.180	0.833	0.734	-11.885	1.175	5.49E+06
						Average	1.174	

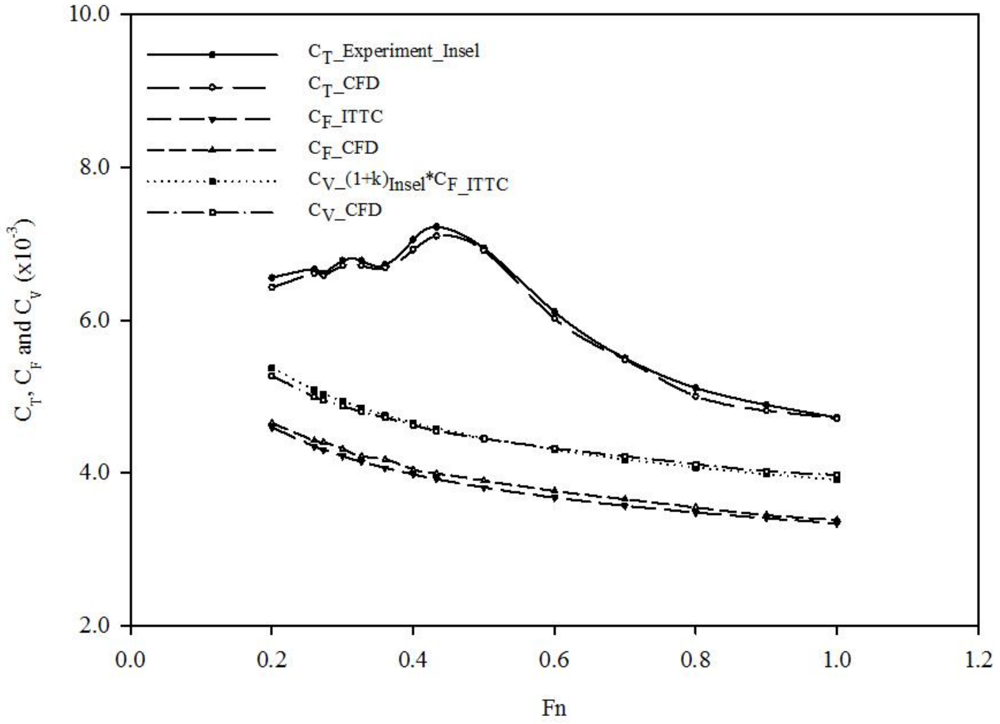

Figure 6.8 Total, frictional and viscous resistance coefficients of NPL 5b monohull

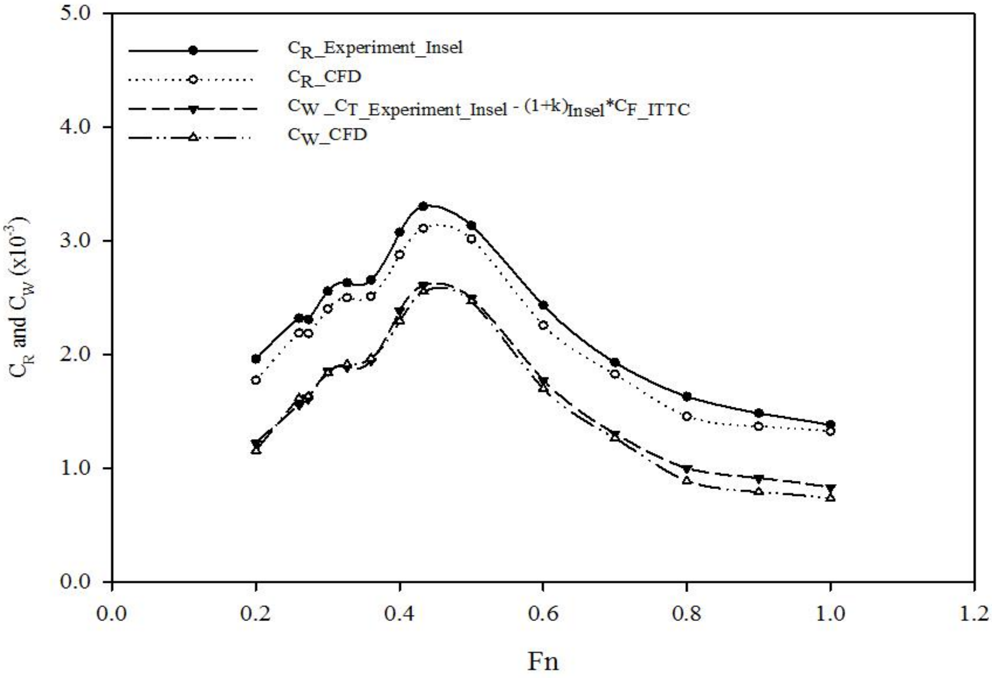

Figure 6.9 Residual and wave resistance coefficients of NPL 5b monohull

6.2.2 Catamaran S/L = 0.3

The CFD results and validations of the NPL 5b catamaran S/L = 0.3 are shown in tables 6.4 and 6.5 and figures 6.10 and 6.11. Table 6.4 and figure 6.10 show the validations of CFD results for total (C_T), frictional (C_F) and viscous (C_V) resistance coefficients whilst table 6.5 and figure 6.11 show the results and validations for residual (C_R) and wave (C_W) resistance coefficients.

The total resistance coefficient (C_T) calculated using CFD and validations show a good agreement with the experimental results with the errors smaller than 3.0 percent. All the CFD C_T prediction are under estimated compared with the experiment. The errors of CFD C_T prediction seems to be steady over the range of Froude number. However, there are some points where the errors in CFD C_T are higher than 1.50 percent including Fn < 0.273, Fn = 0.433 and Fn > 0.80. There is a single Froude number that shows the over prediction of CFD C_T, where Fn = 0.80.

The CFD frictional resistance coefficient (C_F) is validated against the ITTC correlation line and shows a good agreement with a range of error between 2.475 and

4.028 percent. The frictional resistance coefficient calculated using CFD code shows an over prediction compared with the ITTC correlation line. The differences between CFD and ITTC correlation line seem to be steady over the range of Froude numbers with small fluctuations. There are five Froude numbers that show the error higher than 3.50 percent, which are Fn = 0.26, 0.30, 0.36, 0.433 and 0.50.

The CFD viscous resistance coefficient (C_V) results show a fair agreement with experimental results. The range of the differences between CFD and experimental results is between 0.917 and 7.996 percent. Unlike the monohull configuration, the entire CFD C_V curve for catamaran are under predicted over the range of Froude numbers. The error in CFD C_V prediction seemingly decreases with speed (Fn). The differences between CFD and experimental viscous resistance are higher than 5.0 percent for Fn < 0.327 and lower than 3.0 percent for Fn > 0.40.

The residual resistance coefficient (C_R) results and validation for CFD are shown in table 6.5 and figure 6.11. The CFD C_R shows a fair agreement with the experimental results with the range of error between 3.816 and 11.194 percent. The differences between CFD and experimental results seem to be linear for 0.30 < Fn < 0.90, where the error is lower than 7.0 percent. The differences seem to exceed 7.0 percent for both ends of the CFD C_R curve where Fn < 0.327 and Fn > 0.80.

The wave resistance coefficient (C_W) calculated using CFD results and validation are shown in table 6.5 and figure 6.11. The CFD C_W shows a fair agreement with the experimental results. The largest and smallest error between CFD and experimental results are 0.048 and 38.954 percent respectively. The CFD C_W results show a combination of under and over prediction. Most of the CFD C_W are over predicted while for Fn > 0.80 the CFD C_W shows an under prediction compared with the experimental results. The smallest fluctuation in CFD C_W prediction can be seen for 0.30 < Fn < 90, which is lower than 8.0 percent. The differences between CFD and experimental results exceed 8.0 percent can be seen on either sides of the Froude number range, where Fn < 0.327 and Fn > 0.90.

Table 6.4 Total, frictional and viscous resistance coefficients of NPL 5b S/L = 0.3

Fn	C_T (x10^{-3})			C_F (x10^{-3})			C_V (x10^{-3})		
	Exp	CFD	Error (%)	ITTC	CFD	Error (%)	Exp	CFD	Error (%)
0.200	7.388	7.246	-1.922	4.595	4.753	3.449	6.432	5.918	-7.996
0.260	7.777	7.568	-2.687	4.346	4.521	4.028	6.084	5.722	-5.955
0.273	7.556	7.512	-0.582	4.302	4.416	2.652	6.023	5.631	-6.504
0.300	7.778	7.688	-1.157	4.219	4.387	3.988	5.906	5.586	-5.422
0.327	8.222	8.124	-1.192	4.145	4.255	2.658	5.803	5.532	-4.667
0.360	7.889	7.789	-1.268	4.065	4.219	3.797	5.691	5.447	-4.279
0.400	9.000	8.942	-0.644	3.979	4.113	3.357	5.571	5.385	-3.342
0.433	9.388	9.215	-1.843	3.917	4.061	3.675	5.484	5.309	-3.189
0.500	8.722	8.653	-0.791	3.808	3.952	3.794	5.331	5.193	-2.581
0.600	7.444	7.385	-0.793	3.675	3.789	3.095	5.145	5.017	-2.494
0.700	6.556	6.489	-1.022	3.569	3.657	2.475	4.996	4.896	-2.004
0.800	6.111	6.112	0.016	3.480	3.589	3.130	4.872	4.811	-1.254
0.900	5.889	5.771	-2.004	3.405	3.498	2.742	4.766	4.713	-1.122
1.000	5.722	5.575	-2.569	3.339	3.426	2.599	4.675	4.632	-0.917

Table 6.5 Residual and wave resistance coefficients, and form factor of NPL 5b S/L = 0.3

Fn	C_R (x10^{-3})			C_W (x10^{-3})			1+k (CFD)	Re
	Exp	CFD	Error (%)	Exp	CFD	Error (%)		
0.200	2.793	2.493	-10.757	0.956	1.328	38.958	1.245	1.10E+06
0.260	3.431	3.047	-11.194	1.693	1.846	9.057	1.266	1.43E+06
0.273	3.254	3.096	-4.858	1.533	1.881	22.677	1.275	1.50E+06
0.300	3.559	3.301	-7.256	1.872	2.102	12.302	1.273	1.65E+06
0.327	4.077	3.869	-5.105	2.419	2.592	7.142	1.300	1.79E+06
0.360	3.824	3.570	-6.651	2.198	2.342	6.528	1.291	1.97E+06
0.400	5.021	4.829	-3.816	3.429	3.557	3.739	1.309	2.19E+06
0.433	5.471	5.154	-5.793	3.904	3.906	0.048	1.307	2.38E+06
0.500	4.914	4.701	-4.343	3.391	3.460	2.022	1.314	2.74E+06
0.600	3.769	3.596	-4.584	2.299	2.368	3.016	1.324	3.29E+06
0.700	2.987	2.832	-5.199	1.560	1.593	2.125	1.339	3.84E+06
0.800	2.631	2.523	-4.102	1.239	1.301	5.013	1.340	4.39E+06
0.900	2.484	2.273	-8.508	1.123	1.058	-5.748	1.347	4.94E+06
1.000	2.383	2.149	-9.812	1.047	0.943	-9.943	1.352	5.49E+06
						Average	1.306	

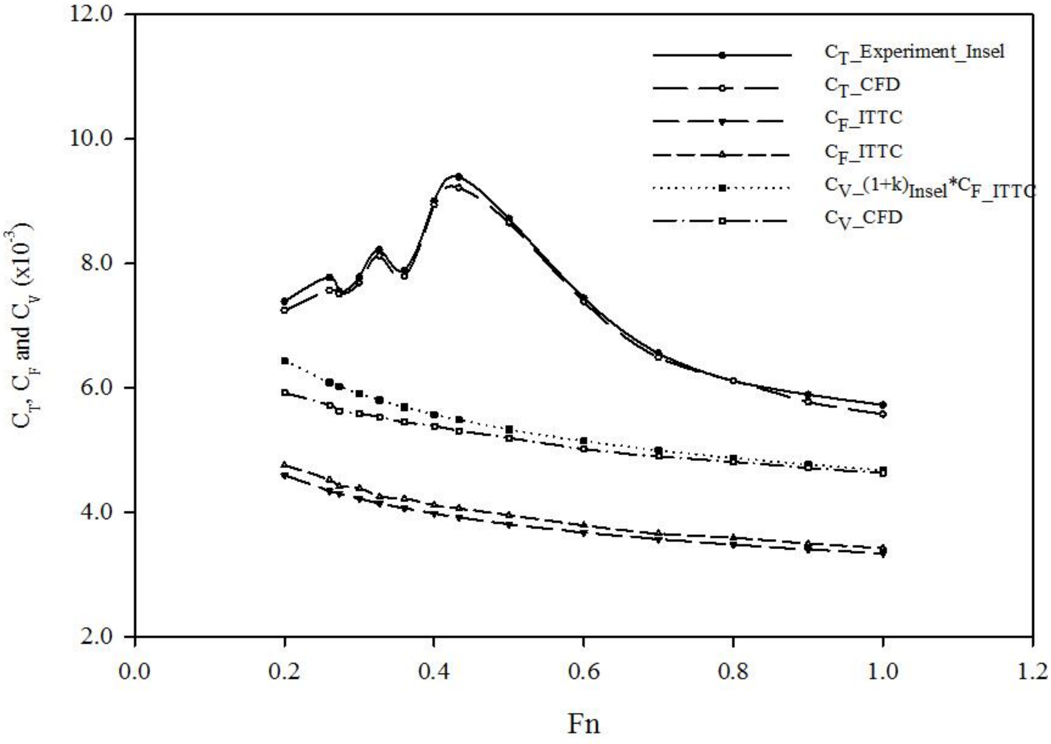

Figure 6.10 Total, frictional and viscous resistance coefficients of NPL 5b S/L = 0.3

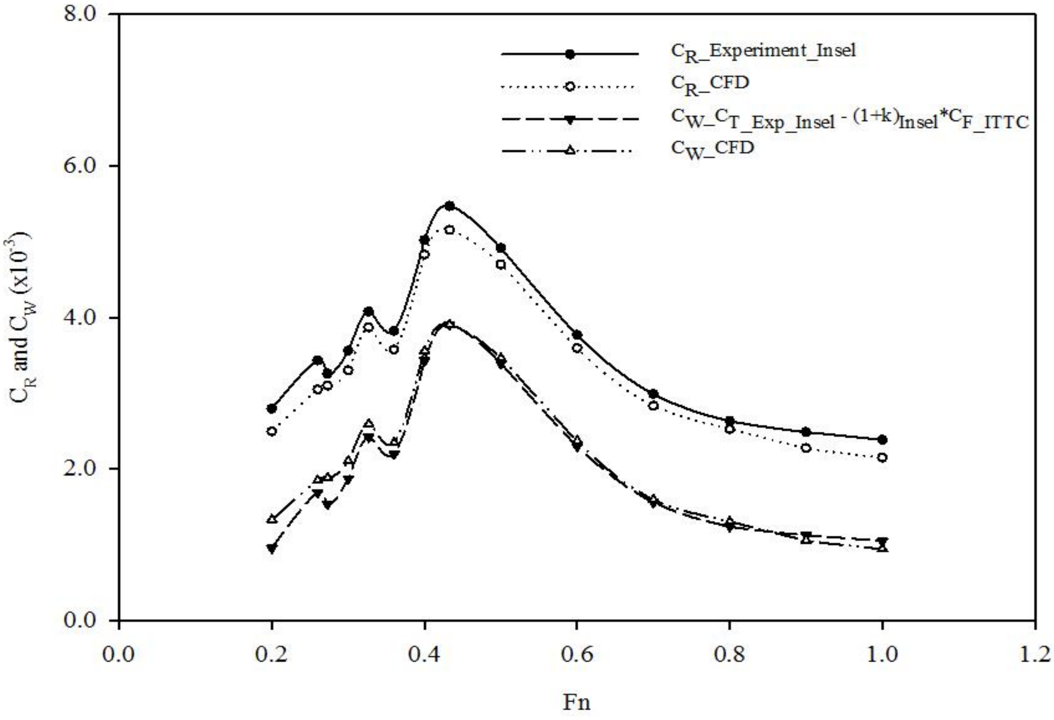

Figure 6.11 Residual and wave resistance coefficients of NPL 5b S/L = 0.3

6.3 Form Factor (1+k), Viscous Resistance (β) and Wave Resistance Interference Factors (τ)

6.3.1 Monohull

The form factor of NPL 5b monohull is shown in table 6.3 and figure 6.12. The form factor seems to increase linearly with a small gradient over the range of Froude numbers. The average CFD form factor (1+k) for the monohull is 1.174 while the experimental form factor is 1.17. The CFD (1+k) rises from the low magnitude of 1.133 at Fn = 0.20 to 1.175 at Fn = 1.0. Although the increase of form factor seems to be linear, there is a fluctuation at Fn < 0.50 as shown in figure 6.12. The fluctuation of CFD form factor at the low-speed range is from the fact that although the CFD C_V decreases linearly while the decrease of CFD C_F prediction is not smooth and linear as seen in table 6.2. The percentage error of CFD C_F is fluctuating and not uniform throughout this speed region (Fn < 0.50).

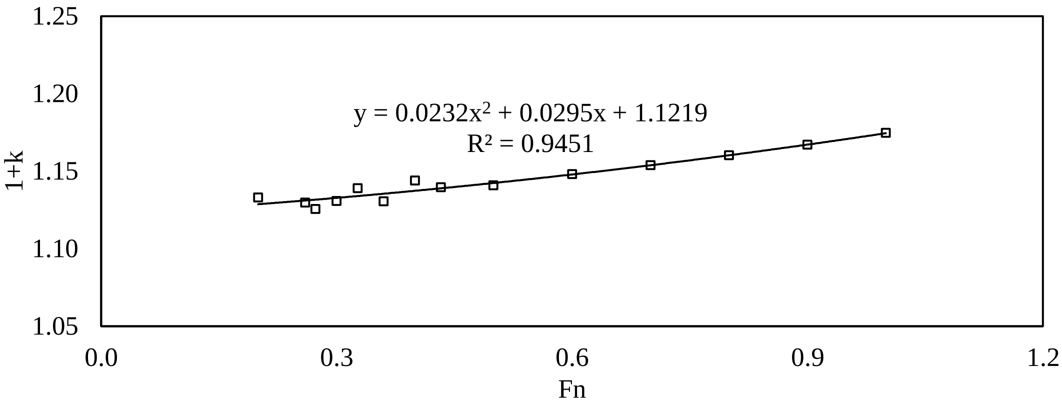

Figure 6.12 Form factor of NPL 5b monohull

6.3.2 Catamaran

The NPL 5b catamaran form factor (1+k) is presented in table 6.5 and figure 6.13. The average CFD form factor is 1.306 while the experimental (1+k) is around 1.40. Unlike the monohull, the increase of catamaran form factor calculated using CFD is non-linear over the range of Froude number. The gradient of (1+k) increment for Fn < 0.40 is significantly steeper than for Fn > 0.40. The higher gradient for the low Froude number is from the decrease of error in CFD C_V prediction. The rate of error declination for Fn < 0.40 is very high compared with the higher Froude number whilst the error in CFD C_F prediction for Fn < 0.40 seems to be higher than Fn > 0.40.

Moreover, the fluctuation in (1+k) prediction occurs over the range of Froude number as seen in figure 6.13. The fluctuation is directly affected by the CFD C_V and C_F predictions and mostly dominated by C_F since the fluctuation in frictional resistance prediction is higher than viscous resistance.

The viscous resistance interference factor (β) of NPL 5b S/L = 0.3 is presented in figure 6.14. The average viscous resistance factor is about 2.10. Most of the β are quite satisfied with the average value except for the lowest speed, Fn = 0.20, where the β is lowest at 1.84. This occurs because the difference between (1+k) of monohull and (1+ βk) of the catamaran is relatively small compared with other Froude numbers. The declination of viscous resistance interference factor is also found for Fn > 0.75.

Figure 6.15 shows the validation of CFD wave resistance interference factor (τ) against the experimental results. The CFD τ shows a good agreement with the experiment. As seen in the figure 6.15, all CFD wave resistance interference factors are over predicted. However, there are some points that the CFD values are much higher than the experimental results i.e. Fn = 0.20 and 0.80. For Fn < 0.35, CFD wave resistance interference factor seems to be linear with a very small deviation but the differences between CFD and experimental results are quite high. Another region that the differences between CFD and experimental τ are quite high is at Fn > 0.50, especially for Fn = 0.80.

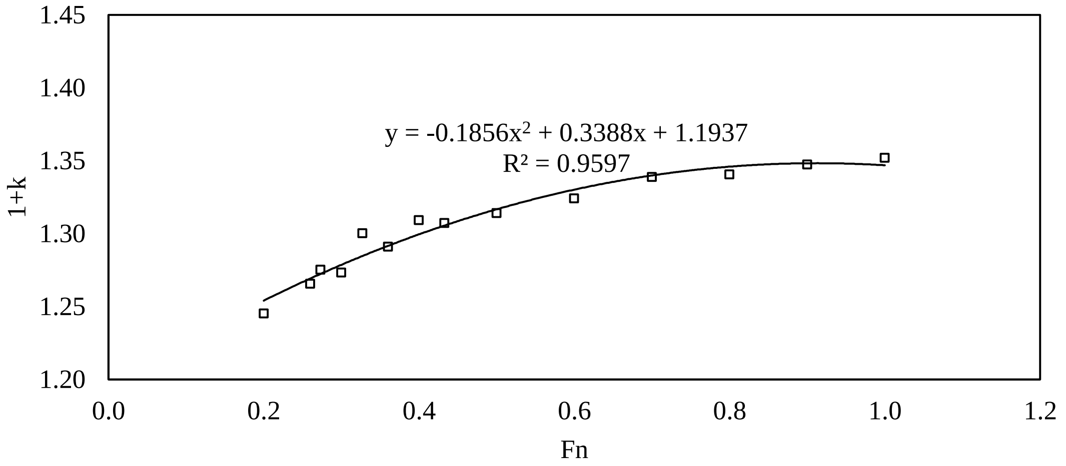

Figure 6.13 Form factor of NPL 5b S/L = 0.3

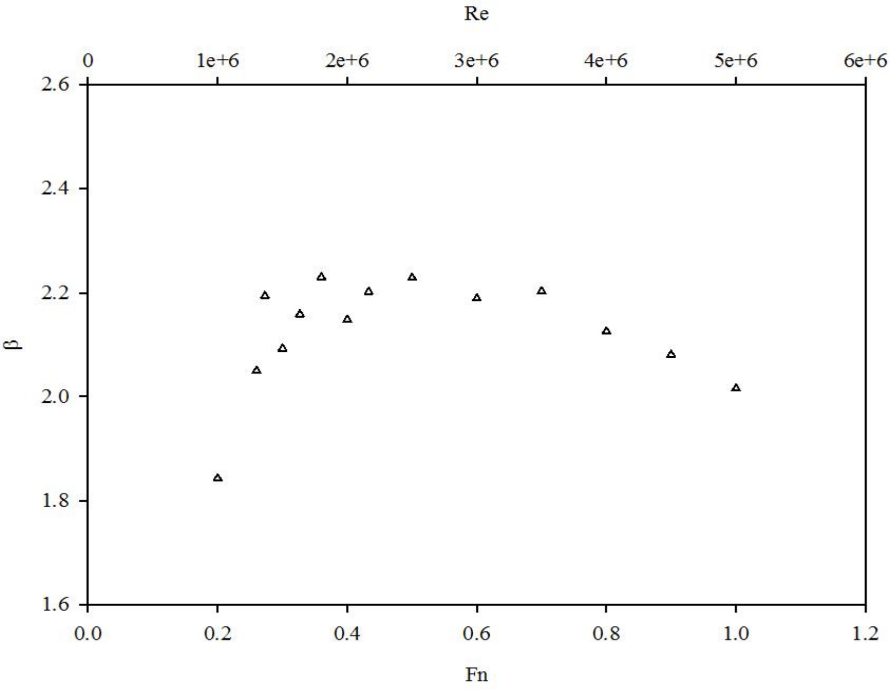

Figure 6.14 Viscous resistance interference factor of NPL 5b S/L = 0.3

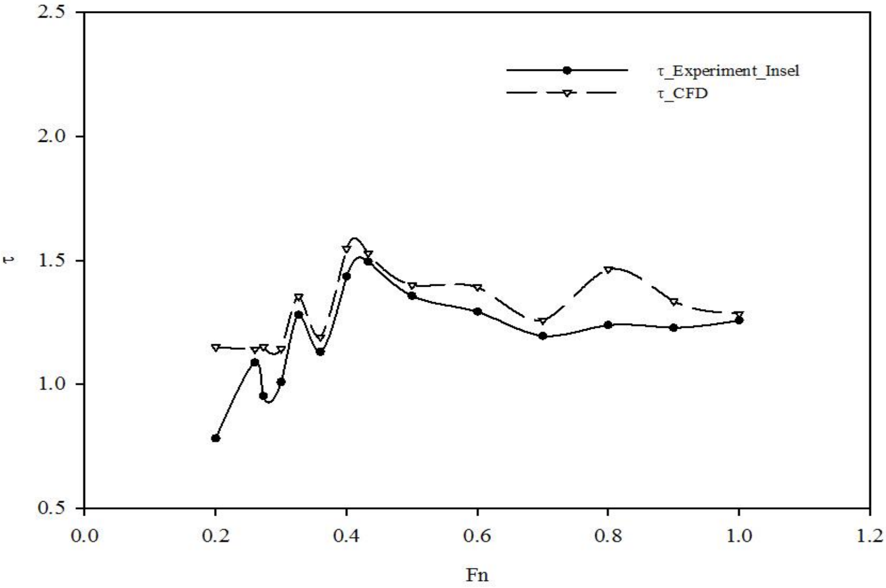

Figure 6.15 Wave resistance interference factor of NPL 5b S/L = 0.3

6.4 Chapter Summary

Two hull configurations of the hull with transom stern (NPL 5b) are investigated in this chapter to demonstrate the CFD methodology in estimating resistance components and form factor. This chapter starts by introducing the importance of the study and then follows by describing the considerations into numerical domains and meshing techniques as seen in section 6.1.

The resistance components and form factor of monohull calculated using CFD code are presented in section 6.2.1. All resistance components are validated against the reference data including Insel's experimental results and ITTC correlation line. Some of the resistance components show a good agreement with validated data with a small amount of error including total resistance (C_T), frictional resistance (C_F). Viscous resistance coefficient (C_V) show also a good agreement with the experimental results with a robust trend. However, residual resistance (C_R) and wave resistance (C_W) coefficients show a fair agreement with the experimental results with some large degree of error for the low-speed range. The CFD results also show that form factor (1+k) increases with speed (Fn) with a linear trend as discussed in section 6.3.1.

Section 6.2.2 shows the results of the catamaran with separation to length ratio (S/L) = 0.3. Similar to the monohull study, total resistance (C_T) and frictional resistance (C_F) coefficient shows a good agreement while viscous resistance coefficient (C_V) also show a stiff trend of declination. Residual resistance (C_R) and wave resistance (C_W) coefficients behave the same way with the monohull, which the differences between CFD and experimental results are very high for the low Froude numbers.

Section 6.3.2 shows form factor (1+k), viscous resistance interference factor (β) and wave resistance interference factor (τ) of the catamaran. Unlike the monohull, the catamaran form factor calculated using CFD shows a slightly different increasing trend. It is not uniform throughout the range of Froude numbers. The increase in form factor is seemingly high for the low Froude numbers and then the increasing gradient reduces. The viscous resistance interference factor (β) is also determined but it cannot be validated with the experiment because it is a constant value for the experiment. Wave resistance interference factor (τ) calculated and validated against the experimental results show a good agreement with the experimental results.

Chapter 7: Blockage Effects and Scale Effects on Form Factor of NPL 5b

7.1 Blockage Effects

The dimension of the towing tank is one of the crucial factors that affect the prediction of resistance components. To avoid blockage due to wall distance of breadth, length and depth of the towing tank some formulae are proposed. ITTC recommendation procedures and guideline 2011 pointed out that the key parameters, which consist of blockage parameter (*m*), Froude number (Fn) and the depth Froude number (Fn_h) need to be considered.

Three formulae are recommended by ITTC including Schuster, Scott and Tamura. These three formulae have different conditions in determining the blockage effects. The Schuster correction is normally recommended for finite water depth (Fn_h). The limitation to the Schuster correction is that it can provides good quality in determining blockage effects up to Fn = 0.30. Scott's correction is Froude number dependent and the best method available for general use. However, there are some limitations for Scott correction with the following conditions: tank breadth to water depth ratio is approximately 2:1, and $3.5 < L < 9.0$ metres and valid only for $0.08 < Fn < 0.40$. The Tamura correction formula is similar to Scott correction which finite depth (Fn_h) is also taken into account. The differences between those two correctors are that model length (L) and breadth (B) are included in the Tamura correction.

The model used in the blockage effect investigation is the NPL 5b, which is the same as the investigation of the hull with the transom stern. Two numerical domain sizes based on Southampton Solent and Southampton Boldrewood towing tank dimensions are evaluated. These numerical domains are selected due to Insel's experimental results, which are used as the validation data and the existence of the new facility at the University of Southampton. The details of Solent towing tank are mentioned in section 3.2.2. The dimensions of Boldrewood tank are as follow; 138.0 metres long, 6.0 metres wide and 3.50 metres deep. The comparisons of the model and numerical dimensions are seen in table 7.1.

Table 7.1 Comparison of blockage effect on total resistance of NPL 5b S/L = 0.3

Model	S/L	Tank	$0.5W_{Tank}/L$	Blockage %
1.6 m	0.3	Solent	1.156	0.100
1.6 m	0.3	Boldrewood	1.875	0.032

According to the conditions and limitations, the Schuster and Tamura corrections are used for this study due to the model size. The Schuster and Tamura correction formulae are as seen in equations 7.1 and 7.2.

- ***Schuster Blockage Correction***

$$\frac{\Delta V}{V} = \frac{m}{1 - m - Fn_h^2} + \frac{2}{3} * \left(1 - \frac{C_V}{C_T}\right) * Fn_h^{10} \qquad 7.1$$

Where $m = {}^{A_{model}}/_{A}$, A_{model} is model cross-section area and A is tank cross-section area.

C_V is viscous resistance coefficient and C_T is total resistance coefficient.

- ***Tamura Blockage Correction***

$$\frac{\Delta V}{V} = 0.67 * m * \left(\frac{L}{B}\right)^{0.75} * \frac{1}{(1 - Fn_h^2)} \qquad 7.2$$

Where $m = {}^{A_{model}}/_{A}$, A_{model} is model cross-section area and A is tank cross-section area.

L is the model length and B is the model breadth.

Mesh techniques obtained from NPL 5b are used. Due to the increase of numerical domain dimensions from Solent towing tank to Boldrewood tank, the number of cells rises from 5-6.5 million to 6-7 million cells. The mesh resolution for the free surface is kept the same for those two tanks; hence the increase of cells are from the fact that free surface of Boldrewood towing tank is larger than Solent towing tank.

Since there are two types of Froude number involved, the results are separated into two parts depending on Froude numbers used, either Fn or Fn_h. The aims of the presentation of the results for different Froude number dependants are to present the blockage effects on resistance for the same Fn_h following the Schuster and Tamura, and show how the blockage effects influence the prediction of resistance and flow characteristics for the same Froude number (Fn).

7.1.1 Blockage Effects

Four Froude depth numbers, shown in table 7.2, are investigated. The CFD results are validated against the experimental results. Table 7.2 and figures 7.1 and 7.2 show the blockage correction calculated using the Schuster correction. It can be seen that the CFD results agree very well with experiment for the same tank size. However, there are no experimental results to validate the Boldrewood tank.

The effects of the blockage seem to reduce with the increasing tank size. The average blockage correction of the experiment and CFD for Solent towing tank are 1.184 x 10^{-3} and 1.185 x 10^{-3} respectively whilst the average CFD blockage correction for Boldrewood towing tank is 0.393 x 10^{-3}. The comparison of the Schuster and Tamura correction are shown in table 7.3. The results show that the blockage effects calculated using the Tamura corrector are higher than the Schuster correction. The results also confirm that the bigger tank has less influence due to the blockage.

Table 7.2 The blockage effects calculated using the Schuster correction

Fn_h	C_T (x 10^{-3})			C_V (x 10^{-3})			$\Delta V/V$ (x 10^{-3})		
	Exp	Solent	Bold	Exp	Solent	Bold	Exp	Solent	Bold
0.189	7.388	7.246	7.543	6.432	5.918	5.979	1.038	1.038	0.332
0.283	7.778	7.688	9.110	5.906	5.586	5.392	1.089	1.089	0.349
0.377	9.000	8.942	8.422	5.571	5.385	5.105	1.182	1.183	0.388
0.471	8.722	8.653	6.512	5.331	5.193	4.852	1.428	1.432	0.504
Average							1.184	1.185	0.393

Table 7.3 Comparison of blockage effects for different corrections

Fn_h	$\Delta V/V$ (x 10^{-3})			
	Solent Tank		Boldrewood Tank	
	Schuster	Tamura	Schuster	Tamura
0.189	1.038	4.196	0.332	1.343
0.283	1.089	4.399	0.349	1.408
0.377	1.182	4.718	0.388	1.510
0.471	1.428	5.203	0.504	1.665

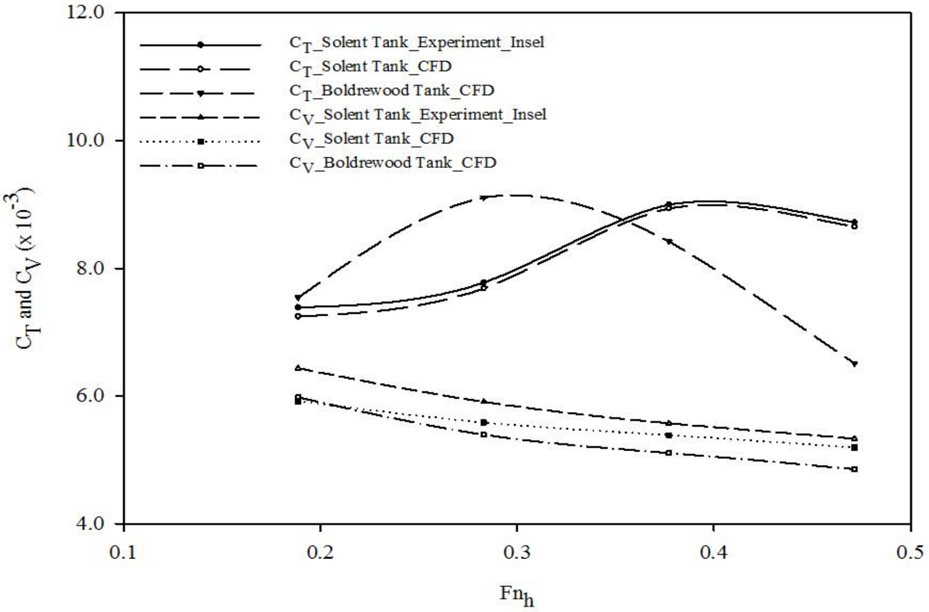

Figure 7.1 Resistance components for NPL 5b for different Froude depth number

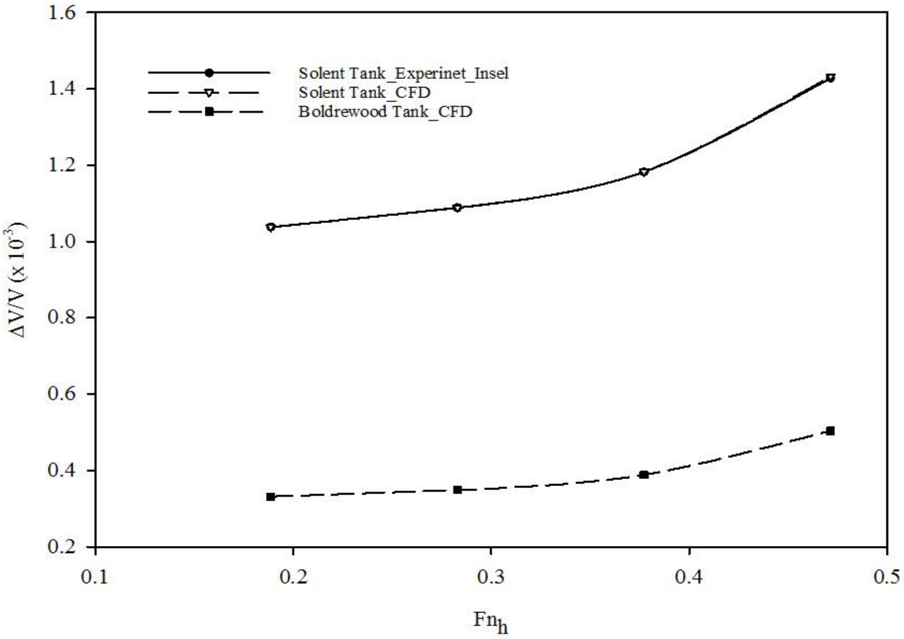

Figure 7.2 Comparison of blockage correction of NPL S/L 0.3

7.1.2 Resistance Components

To ensure that the CFD blockage corrections are valid, the models are run with the same Froude number. Four Froude numbers including Fn = 0.273, 0.433, 0.70 and 0.90. These Froude numbers are selected to represent the different speed regimes i.e. low, intermediate, high and very high. The CFD resistance components and validations include C_T, C_F, C_V, C_R and C_W are shown in tables 7.4 – 7.8 and figures 7.3 and 7.4.

The CFD results show that the resistance components of the NPL 5b measured in the Boldrewood towing tank is significantly higher than Solent towing tank. For example, the average error of the C_T under prediction for Boldrewood towing tank drops from 1.363 percent of Solent towing tank to 0.891 percent.

The CFD prediction of form factor (1+k) is also improved with the decreasing blockage effect as seen in table 7.9. The CFD form factor determined from Boldrewood tank is higher than Solent tank over the Froude number range. Figure 7.5 shows the comparison of free surface flow around demihulls for Solent and Boldrewood towing tank at different Froude numbers. Wave patterns of Solent and Boldrewood towing tank are similar before the reflections occur.

Table 7.4 Comparison of blockage effect on total resistance of NPL 5b S/L = 0.3

Fn	C_T (x 10^{-3})				
	Exp	Solent	Error (%)	Bold	Error (%)
0.273	7.556	7.512	-0.582	7.522	-0.450
0.433	9.388	9.215	-1.843	9.278	-1.172
0.700	6.556	6.489	-1.022	6.501	-0.839
0.900	5.889	5.771	-2.004	5.824	-1.104
Average			-1.363		-0.891

Table 7.5 Comparison of blockage effect on frictional resistance of NPL 5b S/L = 0.3

Fn	C_F (x 10^{-3})				
	Exp	Solent	Error (%)	Bold	Error (%)
0.273	4.302	4.416	2.652	4.398	2.233
0.433	3.917	4.061	3.675	4.053	3.471
0.700	3.569	3.657	2.475	3.641	2.027
0.900	3.405	3.498	2.742	3.491	2.537
Average			2.886		2.567

Table 7.6 Comparison of blockage effect on viscous resistance of NPL 5b S/L = 0.3

Fn	C_V (x 10^{-3})				
	Exp	Solent	Error (%)	Bold	Error (%)
0.273	6.023	5.577	-7.394	5.601	-7.002
0.433	5.484	5.381	-1.879	5.394	-1.639
0.700	4.996	4.904	-1.844	4.906	-1.804
0.900	4.766	4.572	-4.083	4.687	-1.668
Average			-3.800		-3.028

Table 7.7 Comparison of blockage effect on residual resistance of NPL 5b S/L = 0.3

Fn	C_R (x 10^{-3})				
	Exp	Solent	Error (%)	Bold	Error (%)
0.273	3.254	3.096	-4.858	3.124	-3.997
0.433	5.471	5.154	-5.793	5.225	-4.495
0.700	2.987	2.832	-5.199	2.844	-4.798
0.900	2.484	2.273	-8.508	2.333	-6.093
Average			-6.090		-4.846

Table 7.8 Comparison of blockage effect on wave resistance of NPL 5b S/L = 0.3

Fn	C_W (x 10^{-3})				
	Exp	Solent	Error (%)	Bold	Error (%)
0.273	1.556	1.935	24.331	1.921	23.458
0.433	3.944	3.834	-2.785	3.884	-1.521
0.700	1.556	1.585	1.861	1.595	2.506
0.900	1.111	1.199	7.931	1.137	2.340
Average			7.835		6.696

Table 7.9 Comparison of blockage effect on form factor of NPL 5b S/L = 0.3

Fn	1+k			
	Solent	Error(%)	Bold	Error(%)
0.273	1.263	-9.786	1.274	-9.033
0.433	1.325	-5.357	1.331	-4.938
0.700	1.341	-4.214	1.347	-3.755
0.900	1.307	-6.643	1.343	-4.100
Average	1.309	-6.500	1.324	-5.457

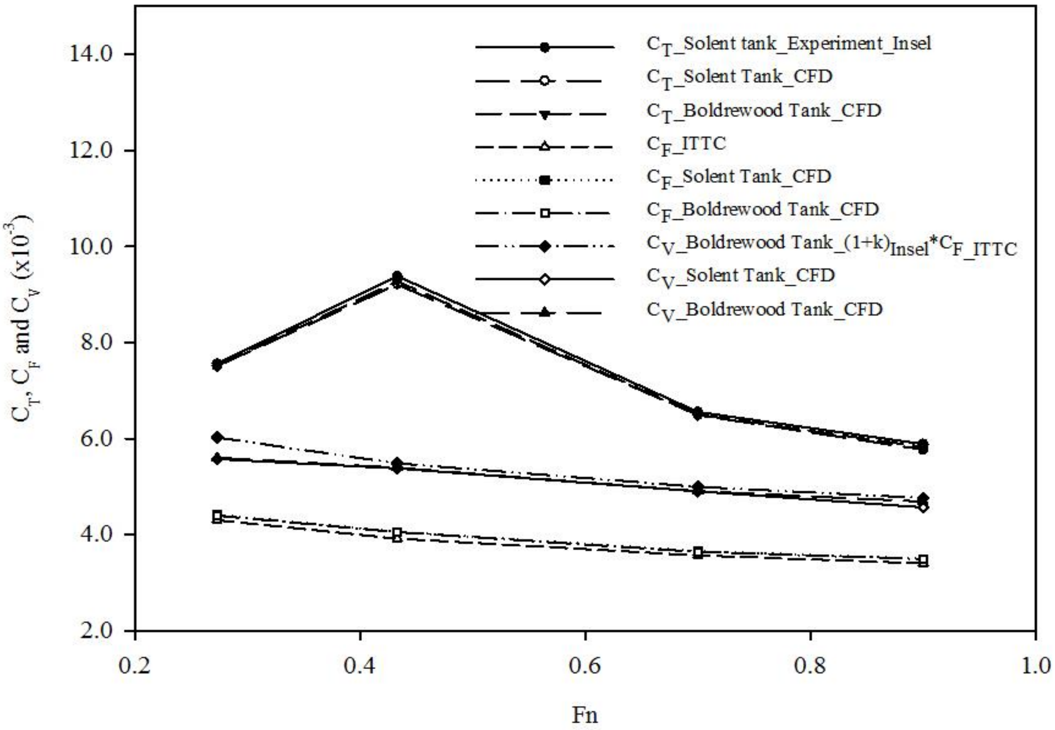

Figure 7.3 Comparison of blockage effect on C_T, C_F and C_V of NPL 5b S/L = 0.3

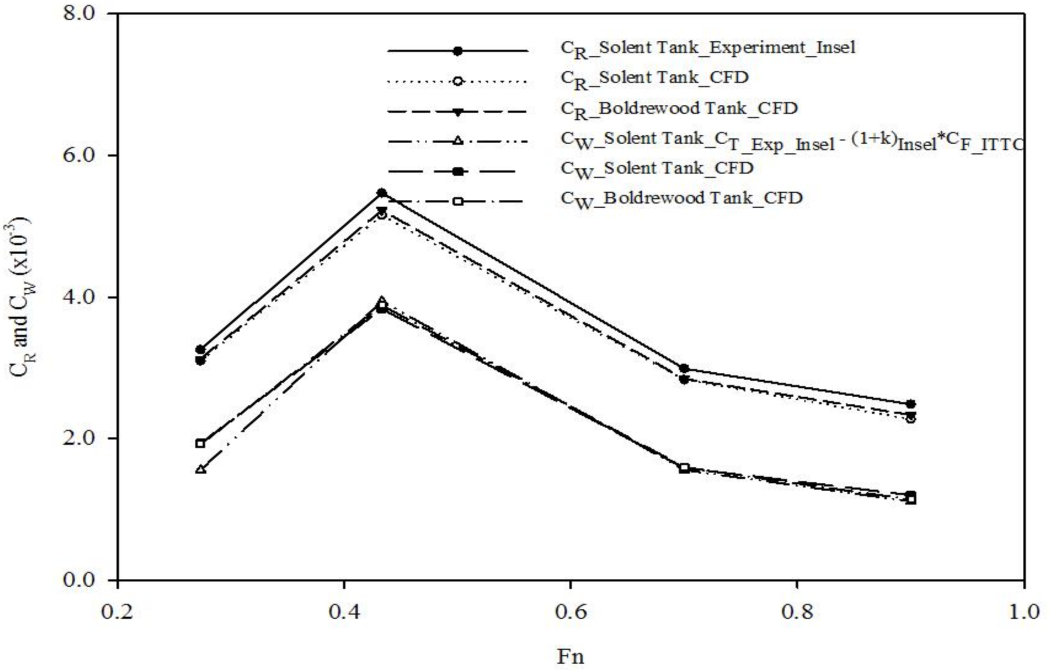

Figure 7.4 Comparison of blockage effect on C_R and C_W of NPL 5b S/L = 0.3

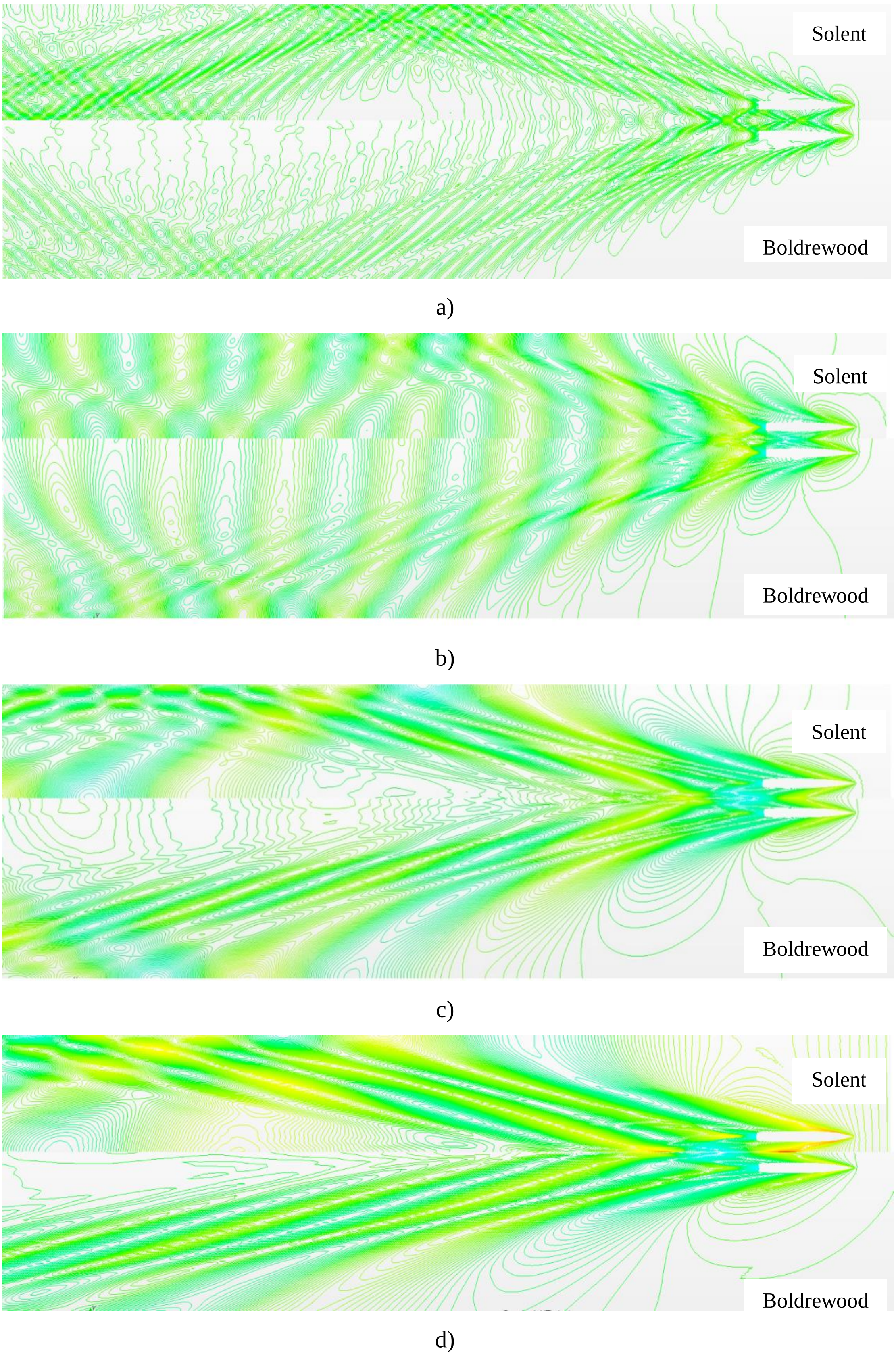

Figure 7.5 Free surface around demihulls of NPL 5b S/L = 0.3 at a) Fn = 0.273, b) Fn = 0.433, c) Fn = 0.70 and d) Fn =0.90

7.2 Scale Effects

7.2.1 Numerical Domains and Mesh Techniques

Three catamaran scales are investigated including 1L (model size), 2L and 10L. The original model (1L) is already described in chapter 6. Two larger models are investigated in this chapter. The double-size model 2L is taken into the considerations to ensure that the CFD is capable of predicting resistance and flow characteristics correctly for a bigger model. For this study, the 10L model is considered as the full-scale ship. Table 7.10 shows the comparison of the blockage for different model scales. It can be seen that 2L model running in Boldrewood towing tank has the highest blockage while the difference between 1L and 10L is not large compared with 2L. Model particulars and verifications are shown in table 7.11. The validation shows that the errors of the CFD-scaled models are less than 0.50 percent for all parameters.

Table 7.12 shows the numerical domain dimensions for different model scales. The distance from the inlet to the bow and from the outlet to the stern are kept constant for all models to avoid reflection from outlet and reversed flow. The numerical domain width and depth for 2L duplicated the Boldrewood towing tank. The biggest model is considered as unbounded representing open seaway. The depth of the numerical domain is 2 times of model length to ensure that it is deep enough to neglect the effect from the seafloor. The width of numerical domain for the 10L model is set as 4 times of the model length to avoid the reflection from the boundary. The top boundary is 10 meters from the water level to reduce air blockage.

The grid generations for the bigger model scales are treated slightly different from the 1L. Due to fact that fluid particle size is not changed, the mesh resolution and density around demihulls need more refinement. To overcome these problems, more refinement blocks are placed around the hulls to control cell size. Skewness is another problem when scaling up the hull geometry because the rapid change between mesh regions can cause the problems. The maximum skewness angle, which STAR CCM+ allows the simulations to run without error and result divergence is 87.0 degrees. Hence, a very slow progress trimmer mesh is used. This results in the increase in the total cells to 7-9M cells for model running Boldrewood tank, 10-12M cells for 2L and 15-18 million cells for 10L.

Table 7.10 Comparison of blockage for model scales

Model	S/L	Tank	$0.5W_{Tank}/L$	$0.5W_{Tank}/B$	Blockage %
1.6 m	0.3	Solent	1.156	12.758	0.101
1.6 m	0.3	Bold	1.875	20.690	0.032
3.2 m	0.3	Bold	0.938	10.345	0.127
16 m	0.3	Unbound	4.0	44.138	0.016

Table 7.11 Model particulars

Model	2L			10L		
	Calculation	CFD	% Error	Calculation	CFD	% Error
L, *m*	3.20	3.20	-	16.00	16.00	-
B, *m*	0.29	0.29	-	1.45	1.45	-
T, *m*	0.145	0.145	-	0.725	0.725	-
C_B	0.397	0.398	0.251	0.397	0.398	-0.251
WS, m^2	1.104	1.100	-0.363	27.60	27.57	-0.108
∇, m^3	0.0536	0.0534	-0.373	6.70	6.682	-0.268

Table 7.12 Domain dimensions

	Solent	Boldrewood	Unbounded
Inlet from bow, *m*	3L	3L	3L
Outlet from stern, *m*	8L	8L	8L
Side, *m* from	1.85	3.00	4L
Top, *m*	1.00	2.00	10.00
Bottom, *m*	1.80	3.50	2L

7.2.2 Resistance Components

The experimental results for C_T, C_V, C_R and C_W are calculated using equations 5.1, 5.2 and 5.3.

7.2.2.1 NPL 5b 2L model

The resistance components of the NPL 5b 2L model are shown in tables 7.13 and 7.14 and figures 7.6 and 7.7. Table 7.13 and figure 7.6 show total resistance (C_T), frictional resistance (C_F) and viscous resistance (C_V) coefficients respectively. Table 7.14 and figure 7.7 show residual resistance (C_R) and wave resistance (C_W) coefficients.

The validation of total resistance coefficient (C_T) shows that the CFD C_T shows a good agreement with experimental results with the error between 1.3886 and 2.529 percent. The under prediction of CFD C_T can be seen throughout the whole range of Froude numbers. The large differences between CFD and experimental results, which exceed 2.0 percent, can be seen for Fn = 0.30, 0.36 and 0.90.

The CFD frictional resistance coefficient is validated against the ITTC correlation line and shows a good agreement with an over prediction between 1.20 and 3.60 percent. The percentage error of CFD C_F seems to be steady over the range of Froude numbers between 2.0 - 3.0 percent. However, the high degree of error occurs for the lowest Froude number, Fn = 0.20 of 3.60 and Fn = 0.40 of 3.03 percent. Only a single Froude number that shows percentage error lower than 2.0 percent is at Fn = 0.433 of 1.20 percent.

The prediction of CFD C_V shows the same trend with the model size, which the error seems to decrease with speed. The CFD C_V validation against the experimental results shows a fair agreement with experimental results and shows a mix of under and over predictions with the percentage error between 0.36 and 7.45. The under prediction can be found for most of the Froude numbers, Fn < 0.90.

The CFD C_R shows under prediction compared with experimental results with a percentage error between 4.10 and 12.48 percent. The largest percentage error between CFD and experimental results, which exceed 10.0 percent is of 12.48 percent at Fn = 0.40.

The CFD C_W shows a fair agreement with the experimental results with a combination of under and over prediction. The range of over prediction percentage error is between 0.90 and 20.24 percent. This can be found in the low-speed regime for Fn < 0.50. The under prediction of the CFD C_W exists at Fn > 0.433 with the range of percentage error between 1.80 and 8.66. As shown in table 7.15 and figure 7.7 the differences between CFD and experimental C_W reduce with speed (Fn) and increase for Fn > 0.433.

Table 7.13 Total, frictional and viscous resistance coefficients of NPL 5b S/L = 0.3_2L

Fn	C_T (x10^{-3})			C_F (x10^{-3})			C_V (x10^{-3})		
	Exp	CFD	Error (%)	ITTC	CFD	Error (%)	Exp	CFD	Error (%)
0.200	6.511	6.412	-1.516	3.717	3.851	3.600	5.204	4.841	-6.980
0.260	6.967	6.835	-1.889	3.536	3.622	2.440	4.950	4.609	-6.880
0.273	6.757	6.654	-1.529	3.503	3.578	2.130	4.905	4.585	-7.450
0.300	7.001	6.826	-2.504	3.442	3.511	2.000	4.819	4.539	-6.600
0.327	7.465	7.389	-1.014	3.388	3.479	2.700	4.743	4.501	-6.080
0.360	7.153	6.988	-2.300	3.328	3.422	2.820	4.659	4.454	-5.480
0.400	8.285	8.152	-1.611	3.265	3.364	3.030	4.571	4.404	-2.260
0.433	8.689	8.569	-1.386	3.219	3.257	1.200	4.506	4.322	-1.580
0.500	8.051	7.891	-1.990	3.137	3.225	2.810	4.392	4.297	-2.150
0.600	6.806	6.671	-1.989	3.038	3.100	2.050	4.253	4.166	-2.040
0.700	5.945	5.834	-1.862	2.957	3.017	2.020	4.140	4.108	-0.780
0.800	5.521	5.423	-1.782	2.890	2.973	2.860	4.047	4.043	-0.090
0.900	5.318	5.208	-2.061	2.833	2.901	2.390	3.967	3.974	0.190
1.000	5.166	5.077	-1.729	2.784	2.841	2.060	3.897	3.911	0.360

Table 7.14 Residual and wave resistance coefficients, and form factor of NPL 5b S/L = 0.3_2L

Fn	C_R (x10^{-3})			C_W (x10^{-3})			1+k (CFD)	Re
	Exp	CFD	Error (%)	Exp	CFD	Error (%)		
0.200	2.793	2.561	-8.320	1.307	1.571	20.240	1.257	3.10E+06
0.260	3.431	3.213	-6.360	2.017	2.226	10.370	1.273	4.03E+06
0.273	3.254	3.076	-5.470	1.853	2.115	14.150	1.281	4.24E+06
0.300	3.559	3.315	-6.860	2.182	2.325	6.530	1.293	4.65E+06
0.327	4.077	3.910	-4.100	2.722	2.935	7.820	1.294	5.07E+06
0.360	3.824	3.566	-6.760	2.493	2.584	3.650	1.302	5.59E+06
0.400	5.021	4.788	-12.480	3.715	3.748	0.900	1.309	6.21E+06
0.433	5.471	5.312	-8.090	4.184	4.247	1.520	1.327	6.72E+06
0.500	4.914	4.666	-5.060	3.660	3.594	-1.800	1.332	7.76E+06
0.600	3.769	3.571	-5.250	2.554	2.505	-1.910	1.344	9.31E+06
0.700	2.987	2.817	-5.700	1.804	1.726	-4.340	1.362	1.09E+07
0.800	2.631	2.450	-6.880	1.475	1.380	-6.420	1.360	1.24E+07
0.900	2.484	2.307	-7.140	1.351	1.234	-8.660	1.370	1.40E+07
1.000	2.383	2.236	-6.160	1.269	1.166	-8.140	1.377	1.55E+07
						Average	1.320	

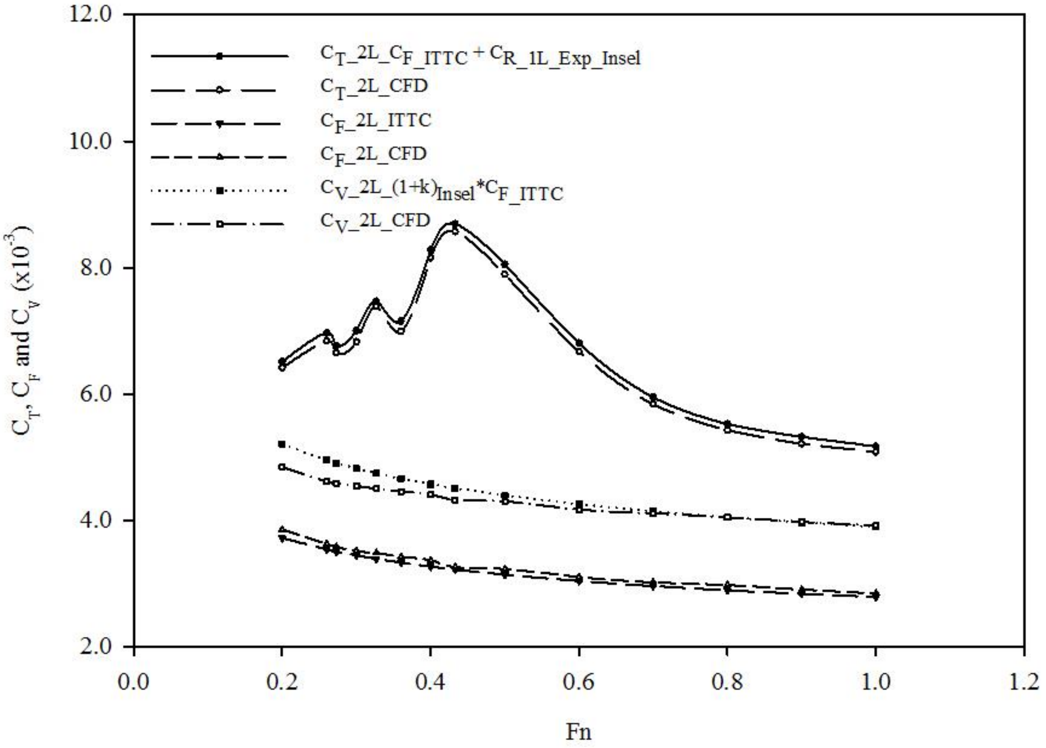

Figure 7.6 Total, frictional and viscous resistance coefficients of NPL 5b S/L = 0.3_2L

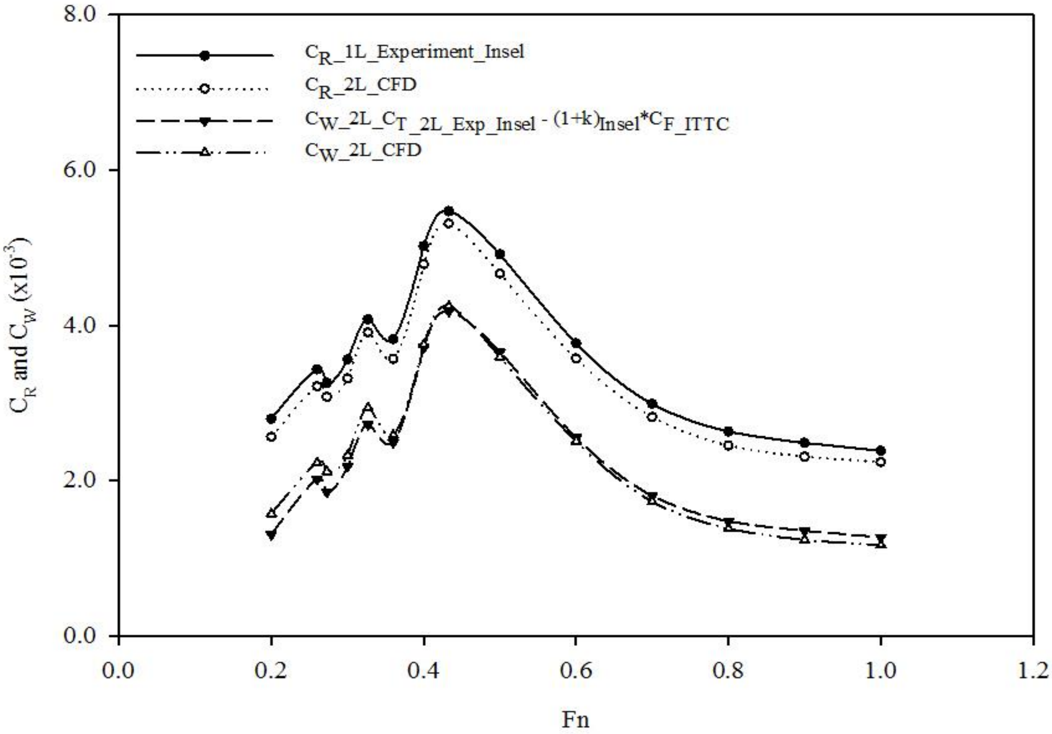

Figure 7.7 Residual and wave resistance coefficients of NPL 5b S/L = 0.3_2L

7.2.2.2 NPL 5b 10L model

The resistance components including total resistance (C_T), frictional resistance (C_F) and viscous resistance (C_V) coefficients are presented in tables 7.15 and 7.16 and figures 7.8 and 7.9. Tables 7.17 and 7.18 and figures 7.10 and 7.11 show residual resistance (C_R) and wave resistance (C_W) coefficients.

The CFD C_T shows a good agreement with the experimental results with the percentage error between 0.337 and 2.183. Most of the CFD C_T are under predicted compared with the experimental results. There are two points that the CFD C_T shows an over prediction including Fn = 0.40 and 0.433, where the total resistance changes rapidly.

The CFD C_F validated against ITTC correlation line shows a good agreement with the percentage error between 1.635 and 3.877. The CFD C_F is generally over predicted over the range of Froude numbers. For Fn < 0.60, the percentage error of CFD C_F is lower than 3.0 percent except at Fn = 0.30 and 0.40 where the error is less than 2.0 percent. The differences between the CFD C_F and ITTC correlation line rises and exceeds 3.0 percent for Fn > 0.50.

The CFD C_V shows a fair agreement with the experimental results with the range of error between -6.981 and 3.920 percent. The combination of the under prediction for lower Froude numbers and the over prediction for higher Froude numbers also occurs for the largest model size. The under prediction can be seen for Fn < 0.60, where the error reduces from -6.981 to -0.661 at Fn = 0.50. For Fn > 0.50, the CFD C_V is over prediction from 1.006 percent at Fn = 0.60 to 3.92 percent at Fn = 1.0.

The residual resistance coefficient (C_R) is validated against experimental data and shows a fair agreement with the range of error 2.43 and 12.93 percent. The majority of the CFD C_R are under predicted except for Fn = 0.433, where CFD C_R is over predicted by 12.93 percent. There are two Froude number ranges that the differences between CFD and experimental results are higher than 5 percent, which include 0.327 < Fn < 0.50 and Fn > 0.70.

The CFD C_W shows a fair agreement with the experiment with the combination of the over and under predictions. The percentage error of CFD C_W is between 0.484

and 10.40 percent. The under prediction of CFD C_W is found at Fn = 0.36 and Fn > 0.433 whilst the over prediction exists at Fn < 0.50.

Table 7.15 Total, frictional and viscous resistance coefficients of NPL 5b S/L = 0.3_10L

Fn	C_T (x 10^{-3})			C_F (x 10^{-3})			C_V (x 10^{-3})		
	Exp	CFD	Error (%)	ITTC	CFD	Error (%)	Exp	CFD	Error (%)
0.200	5.237	5.187	-0.953	2.443	2.503	2.438	3.421	3.182	-6.981
0.260	5.777	5.672	-1.818	2.346	2.411	2.773	3.284	3.085	-6.069
0.273	5.583	5.494	-1.586	2.328	2.388	2.566	3.260	3.075	-5.670
0.300	5.854	5.745	-1.869	2.295	2.341	1.995	3.213	3.052	-5.019
0.327	6.343	6.298	-0.703	2.265	2.331	2.894	3.172	3.055	-3.677
0.360	6.057	5.925	-2.183	2.233	2.297	2.870	3.126	3.033	-2.978
0.400	7.219	7.243	0.337	2.198	2.234	1.635	3.077	3.008	-2.252
0.433	7.643	7.778	1.762	2.172	2.228	2.560	3.041	2.986	-1.820
0.500	7.041	6.970	-1.014	2.127	2.175	2.261	2.978	2.958	-0.661
0.600	5.840	5.781	-1.011	2.071	2.146	3.606	2.900	2.929	1.006
0.700	5.013	4.928	-1.701	2.026	2.089	3.111	2.836	2.895	2.067
0.800	4.619	4.544	-1.620	1.988	2.057	3.476	2.783	2.859	2.729
0.900	4.440	4.369	-1.590	1.955	2.031	3.877	2.737	2.831	3.424
1.000	4.309	4.251	-1.356	1.927	2.001	3.860	2.697	2.803	3.920

Table 7.16 Residual and wave resistance coefficients, and form factor of NPL 5b S/L = 0.3_10L

Fn	C_R (x 10^{-3})			C_W (x 10^{-3})			1+k (CFD)	Re
	Exp	CFD	Error (%)	Exp	CFD	Error (%)		
0.200	2.793	2.684	-3.920	1.816	2.005	10.400	1.271	3.47E+07
0.260	3.431	3.261	-4.960	2.493	2.587	3.783	1.280	4.51E+07
0.273	3.254	3.106	-4.560	2.323	2.442	5.137	1.288	4.74E+07
0.300	3.559	3.404	-4.360	2.641	2.690	1.849	1.304	5.20E+07
0.327	4.077	3.967	-2.702	3.171	3.265	2.965	1.311	5.67E+07
0.360	3.824	3.628	-5.130	2.931	2.917	-0.484	1.320	6.25E+07
0.400	5.021	5.009	-8.440	4.141	4.235	2.262	1.346	6.94E+07
0.433	5.471	5.550	12.930	4.602	4.792	4.129	1.340	7.51E+07
0.500	4.914	4.795	-2.430	4.064	4.012	-1.272	1.360	8.67E+07
0.600	3.769	3.635	-3.550	2.940	2.852	-3.001	1.365	1.04E+08
0.700	2.987	2.839	-4.970	2.177	2.033	-6.612	1.386	1.21E+08
0.800	2.631	2.487	-5.470	1.836	1.685	-8.213	1.390	1.39E+08
0.900	2.484	2.338	-5.890	1.702	1.538	-9.651	1.394	1.56E+08
1.000	2.383	2.250	-5.570	1.612	1.448	-10.182	1.401	1.73E+08
						Average	1.340	

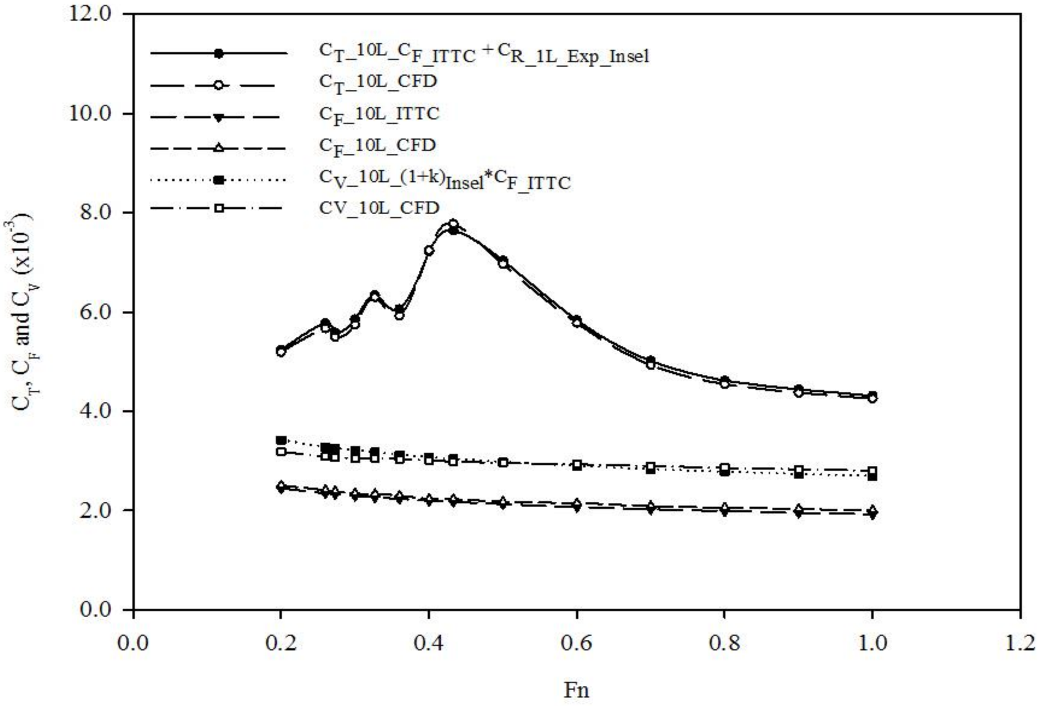

Figure 7.8 Total, frictional and viscous resistance coefficients of NPL 5b S/L = 0.3_10L

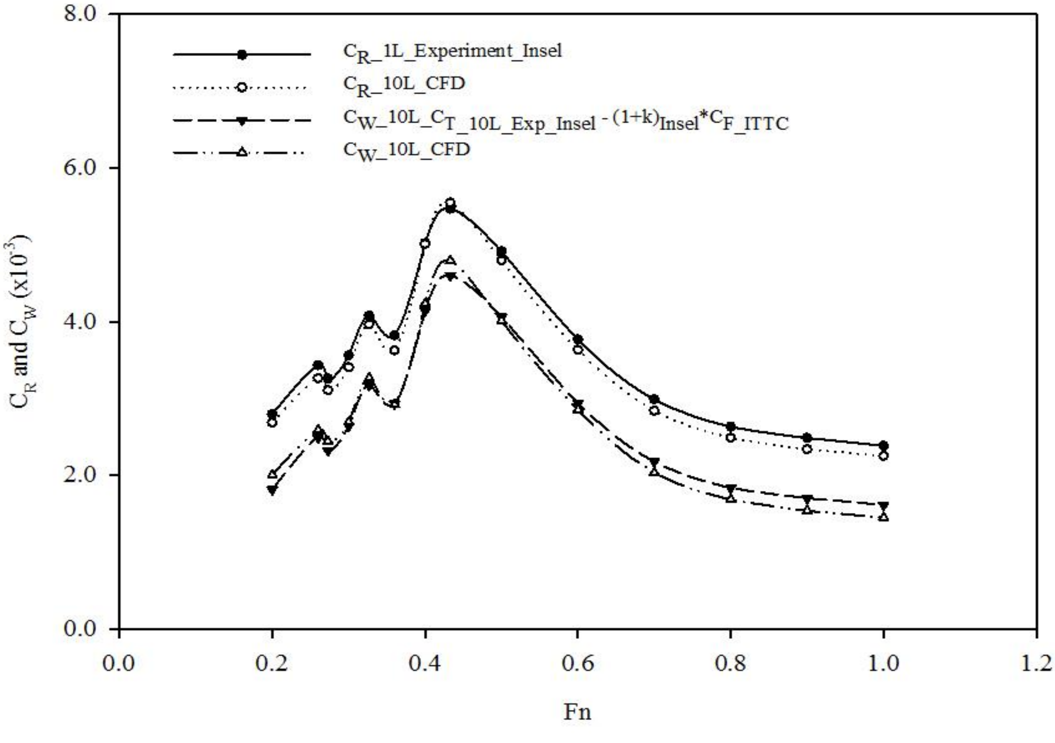

Figure 7.9 Residual and wave resistance coefficients of NPL 5b S/L = 0.3_10L

7.2.2.3 Comparison of the Resistance Components

Figure 7.10 shows the comparison of total resistance (C_T), frictional resistance (C_F) and viscous resistance (C_V) coefficients for different model scales. The CFD C_T shows good agreement with the experimental results for all model scales with the percentage error less than 5.0 percent. The under prediction of CFD C_T can be seen for all model scales. The CFD frictional resistance coefficient is validated against the ITTC correlation line. The CFD C_F shows an over prediction for all models, which seems to be steady with the increasing model sizes. The CFD C_V shows a fair agreement with the experimental results. The under and over prediction is found for all models. The under prediction reduces with the increasing model sizes. The range of CFD C_V over prediction seems to increase with the increasing model sizes.

The comparison of residual resistance coefficient (C_R) is presented in figure 7.11. The CFD C_R for different model scales is validated against the experimental results in the basis of the $C_{RM} = C_{RS}$. It is found that the CFD C_R for all model scales are under prediction except for the biggest model, 10L, where Fn = 0.433 over prediction exists. It can also be seen that the CFD C_R increases with increasing model sizes.

Figure 7.12 shows the comparison of wave resistance coefficient and validations against the experimental results for the different model scales. The wave resistance increases with the increasing model scales. For all model scales, the CFD C_W shows a mix of both the under and over predictions compared with the experimental results. The largest under prediction of CFD C_W is very high for the lowest Froude number, which is found in all models. The CFD C_W over prediction occurs at the low and intermediate Froude numbers where $0.20 < Fn < 0.5.0$ for all models.

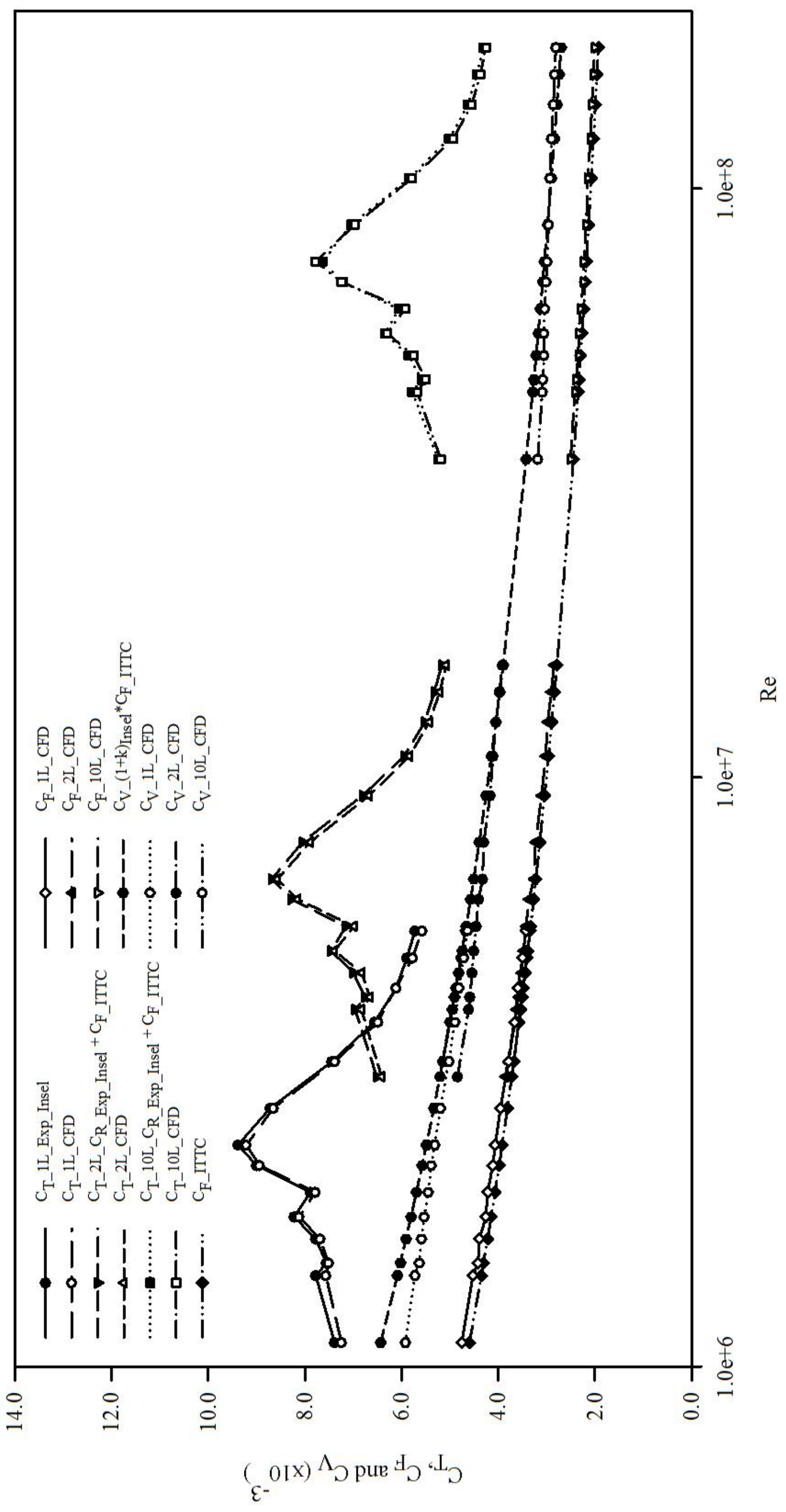

Figure 7.10 Comparison of total, frictional and viscous resistance coefficients of NPL 5b S/L = 0.3

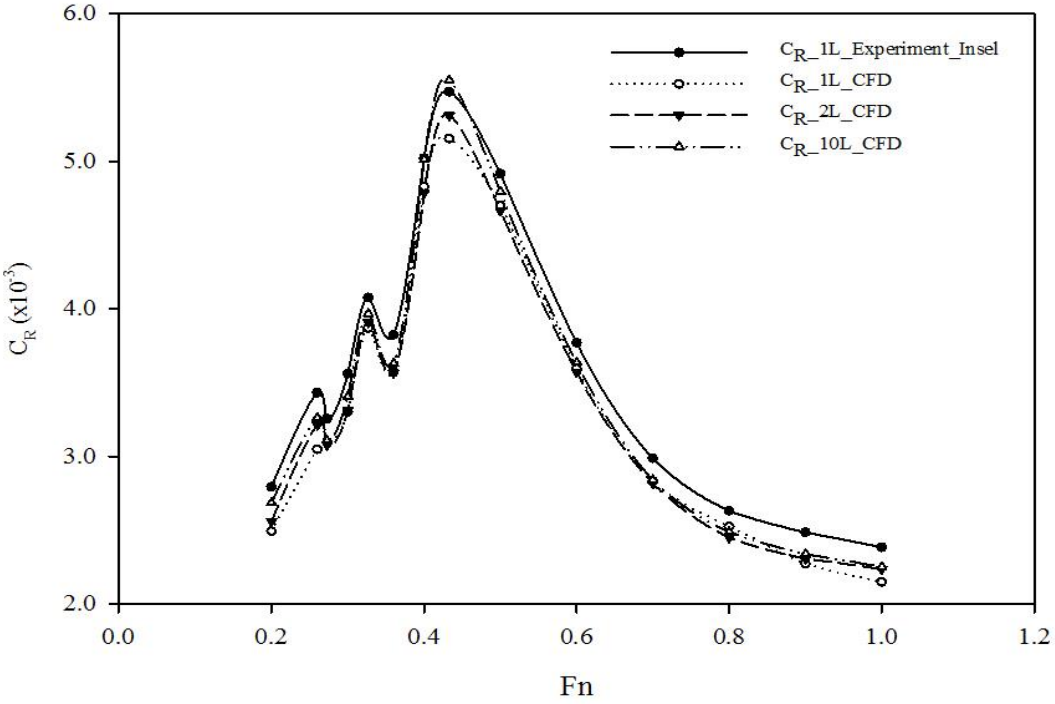

Figure 7.11 Comparison of residual resistance coefficients of NPL 5b S/L = 0.3

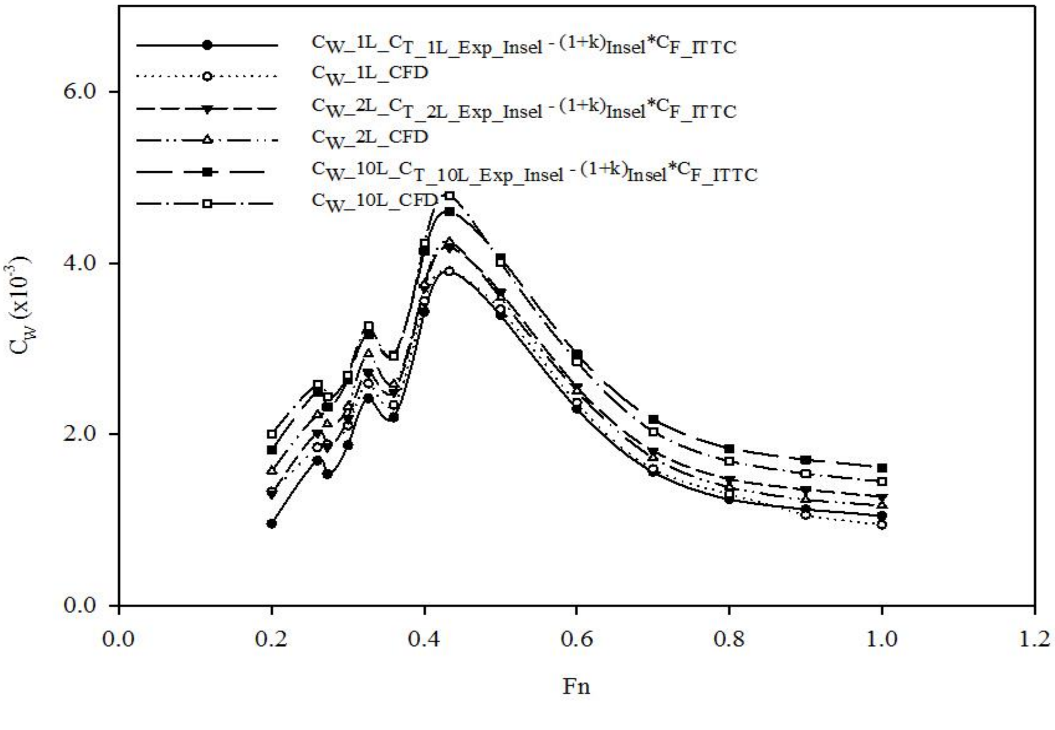

Figure 7.12 Comparison of wave resistance coefficients of NPL 5b S/L = 0.3

7.2.3 Form Factor

Figures 7.13 and 7.14 show the form factor (1+k) of 2L and 10L models. Both models show the same trend of increasing form factor. The increase of form factor for the Froude number Fn < 0.50 has the higher gradient than the higher Froude number range.

The comparison of 1+k for different model scales is shown in figure 7.15. The form factors for all models show the same trend, which increases with speed (Fn). The gradient of the form factor is steeper for low Froude numbers i.e. Fn < 0.50. The differences of the form factor are not linear over the range of Froude numbers. The form factors for different model scales increase slightly with the increasing model sizes over the Froude number range i.e. at low Froude number range i.e. for Fn < 0.40, the increase of 1+k is less than for Fn > 0.40

The dependence of 1+k on Reynolds' number (Re) is shown in figure 7.16. There are four Froude numbers that are presented including Fn = 0.273, 0.433, 0.70 and 0.90. The comparison shows that the form factor of the NPL 5b catamaran slightly increases with model size (Re). For the same speed (Fn), the gradient of 1+k shows that the difference between 1L and 2L model seems to be steeper than for 2L and 10L.

The 1+k tends to converge into a single value for bigger models for low speed i.e. Fn = 0.273 and 0.433. For the high-speed regime, Fn = 0.70 and 0.90, the gradient of 1+k between 2L and 10L models is higher than the lower speeds. Hence, the form factor calculated using CFD code for geosim series seems to increase and converge to a single value for a much larger model compared with the lower Froude numbers.

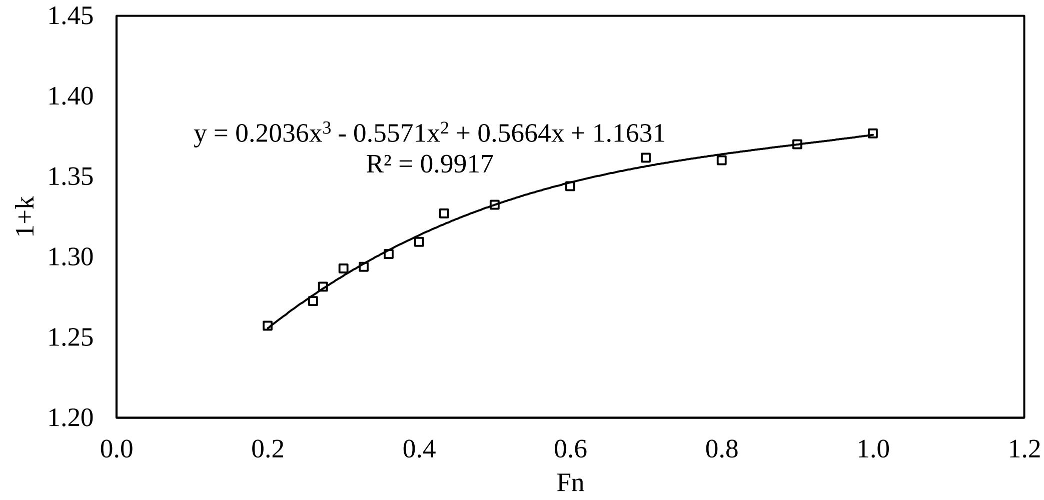

Figure 7.13 Form factor of NPL 5b S/L = 0.3_2L

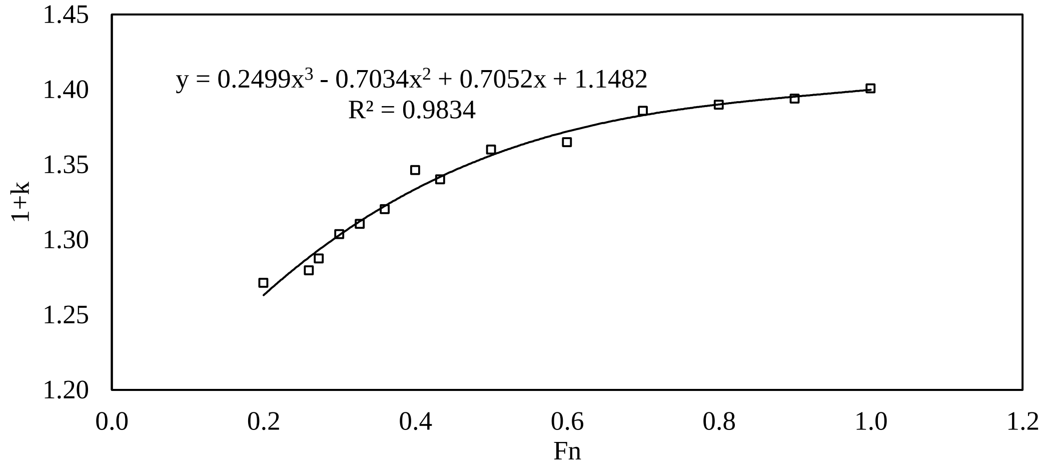

Figure 7.14 Form factor of NPL 5b S/L = 0.3_10L

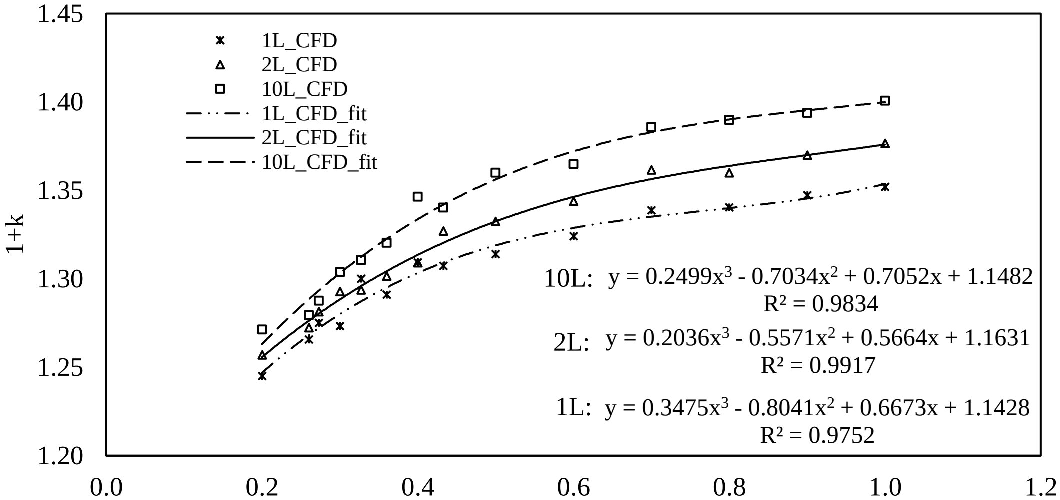

Figure 7.15 Comparison of form factor of NPL 5b S/L = 0.3

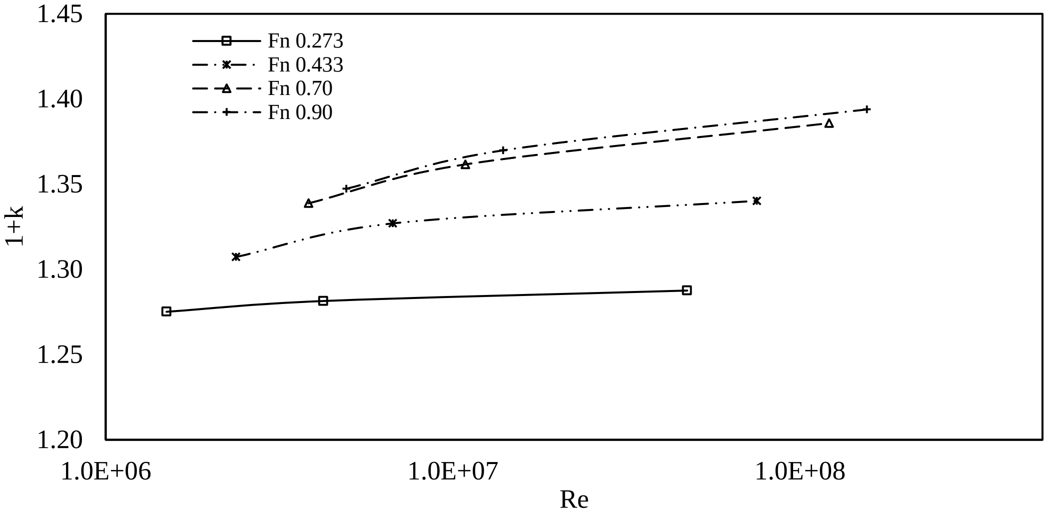

Figure 7.16 Comparison of form factor of NPL 5b S/L = 0.3 for different Reynolds' number

7.3 Wave Elevation

Wave elevation is measured at the different positions of the numerical domain including wave elevation along the hull, behind transom stern, at the centre between demihulls and at y/L = 0.5. These four positions of the wave elevation are considered to represent the flow field for the different model scales.

The notation "Model" used in the figures for this section indicates 1L model.

7.3.1 Free Surface Flow

Figures 7.17, 7.18, 7.19 and 7.20 show the free surface of the NPL 5b for different model scales at Fn = 0.273, 0.433, 0.70 and 0.90 respectively. The results show that the flow field at the free surface for all models are similar before the reflection occurs. The flow field contours show that the wave elevation for the 2L model is highest compared with other models, especially for the highest Froude number.

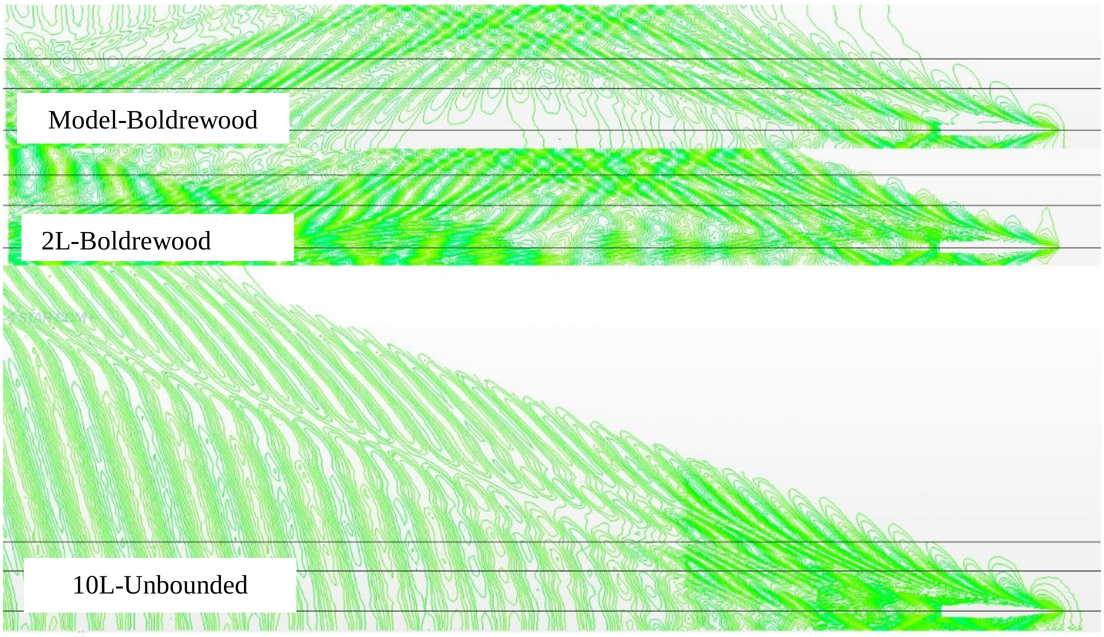

Figure 7.17 Wave pattern of NPL 5b S/L = 0.3 at Fn = 0.273

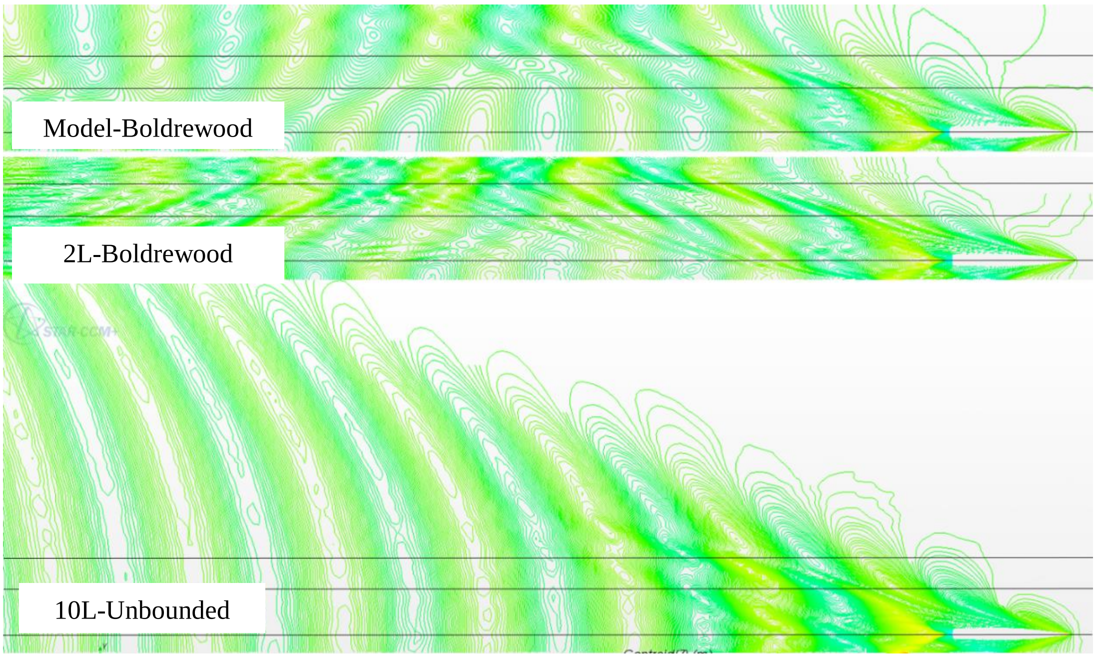

Figure 7.18 Wave pattern of NPL 5b S/L = 0.3 at Fn = 0.433

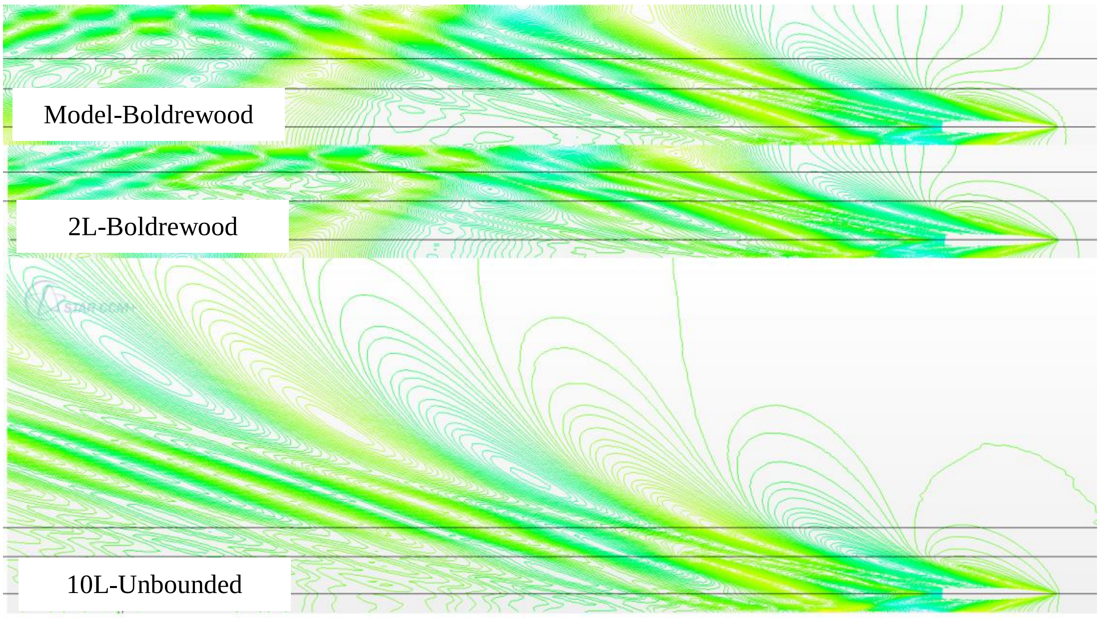

Figure 7.19 Wave pattern of NPL 5b S/L = 0.3 at Fn = 0.70

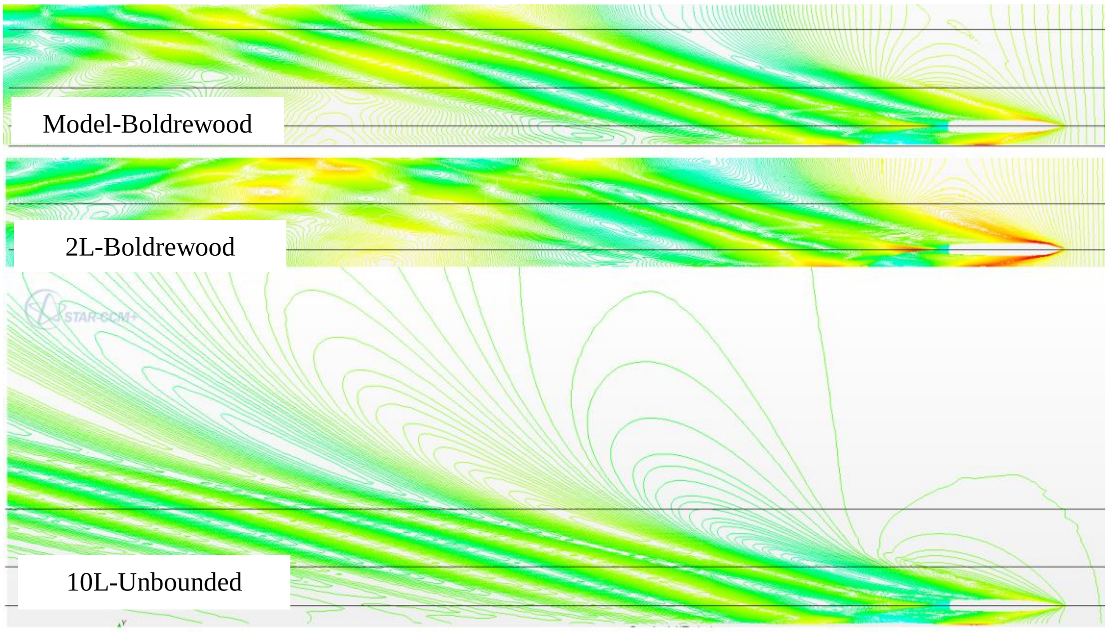

Figure 7.20 Wave pattern of NPL 5b S/L = 0.3 at Fn = 0.90

7.3.2 Wave Elevation along the Hull

The CFD wave elevation measurements along the hull are made on both sides of the demihulls and shown from figures 7.21 to 28 for Fn = 0.273, 0.433, 0.70 and 0.90. For Fn < 0.90, the wave elevation along the hull on both sides on the demihulls shows the similar pattern for all models with only small differences. It can be seen that the model and the 10L catamaran give similar results while the 2L catamaran shows the highest elevation for Fn = 0.273. However, for Fn = 0.433 wave elevation along the hull of the biggest model, 10L, shows the highest level at the bow area where x/L is between 0.7 and 1.0.

For the high Froude number, Fn = 0.70, the wave elevation along the hull shows that the model running in Boldrewood towing tank agrees very well with the 10L model. The 2L model shows the highest elevation compared with other models. The model running in Solent towing tank shows that the wave height is slightly higher than the model running Boldrewood tank and slightly lower than 2L.

The differences between the models are very high for the highest Froude number, Fn = 0.90. The 2L catamaran shows a very high wave elevation on both sides of the demihulls compared with other models. The differences of the wave elevation at the bow area between the 2L and models are almost double. The model catamaran running in the Boldrewood towing tank shows the similar wave elevation with the 10L catamaran while the model running in Solent towing tank gives the values between the 2L and 10L catamarans.

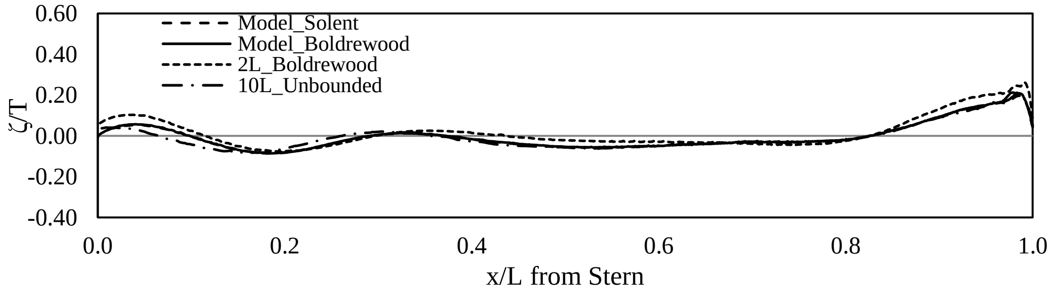

Figure 7.21 Wave elevation along the hull of NPL 5b S/L = 0.3 (inboard) at Fn = 0.273

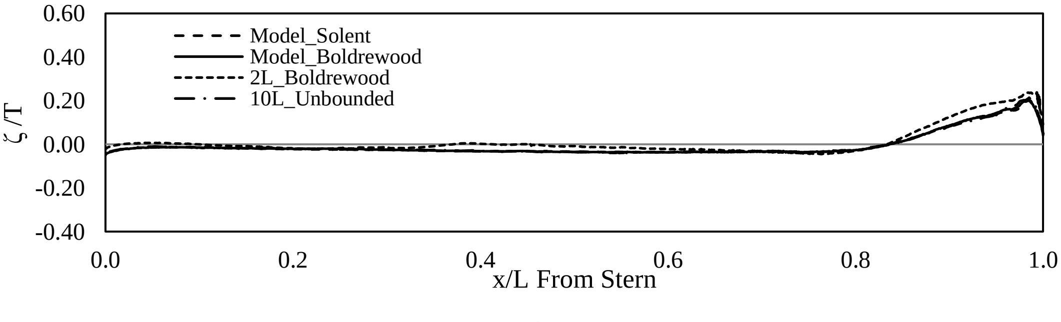

Figure 7.22 Wave elevation along the hull of NPL 5b S/L = 0.3 (outboard) at Fn = 0.273

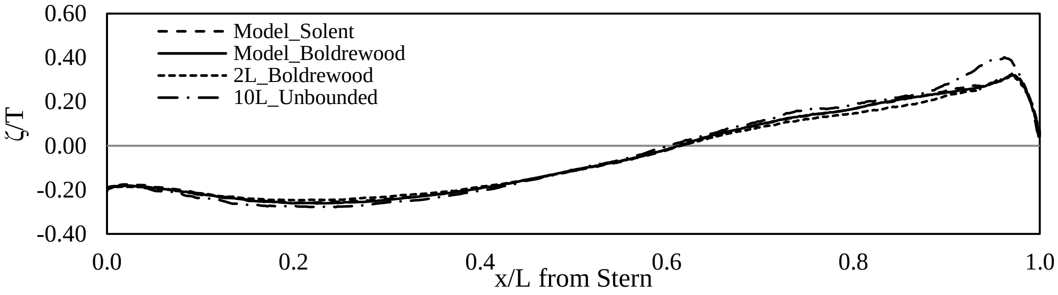

Figure 7.23 Wave elevation along the hull of NPL 5b S/L = 0.3 (inboard) at Fn = 0.433

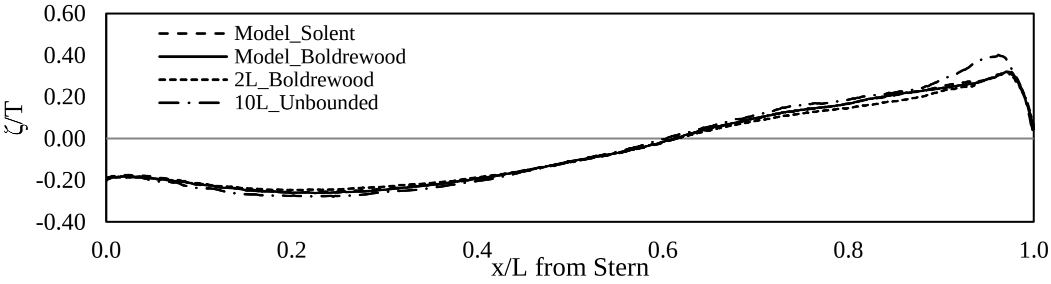

Figure 7.24 Wave elevation along the hull of NPL 5b S/L 0.3 (outboard) at Fn 0.433

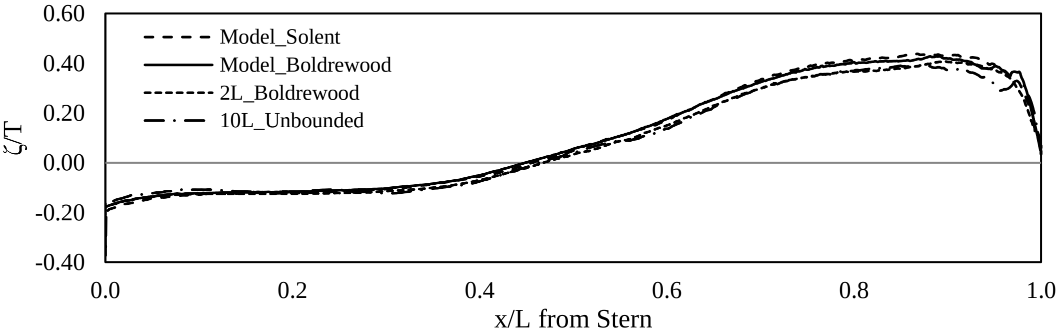

Figure 7.25 Wave elevation along the hull of NPL 5b S/L = 0.3 (inboard) at Fn = 0.70

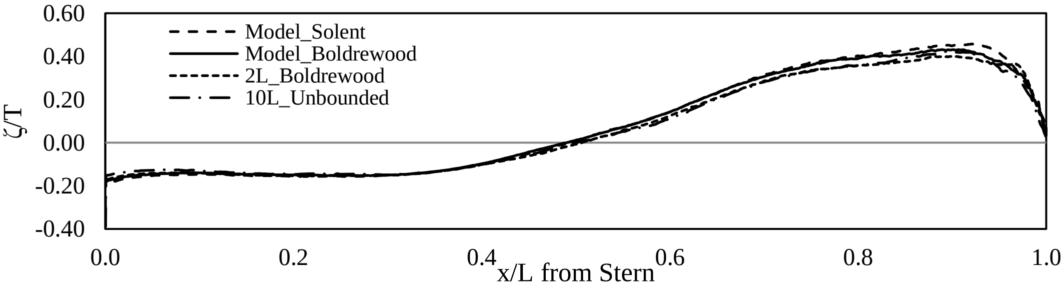

Figure 7.26 Wave elevation along the hull of NPL 5b S/L = 0.3 (outboard) at Fn = 0.70

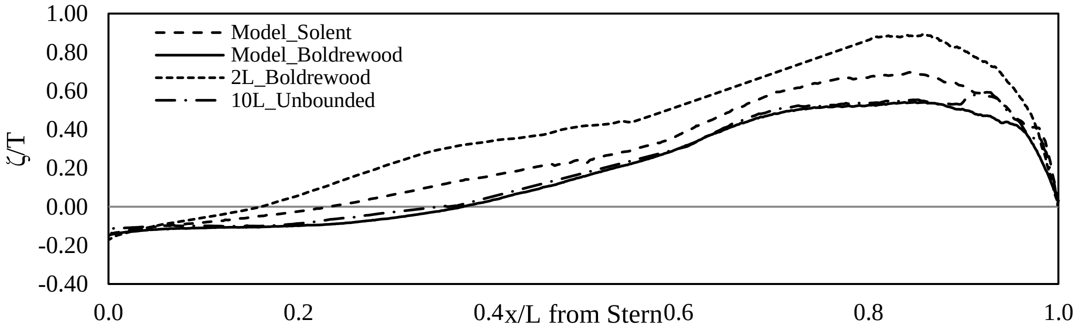

Figure 7.27 Wave elevation along the hull of NPL 5b S/L = 0.3 (inboard) at Fn = 0.90

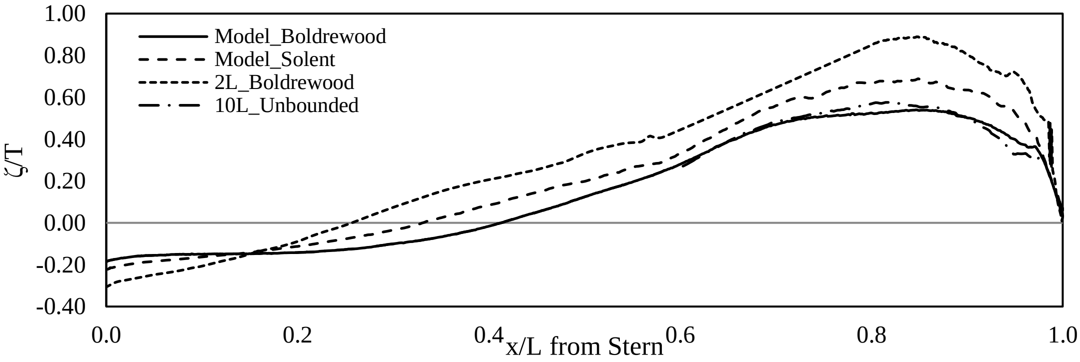

Figure 7.28 Wave elevation along the hull of NPL 5b S/L = 0.3 (outboard) at Fn = 0.90

7.3.3 Wave Cut behind Transom Stern

The wave elevation behind transom stern of all models is shown in figures 7.29 to 7.32 for Fn = 0.273, 0.433, 0.70 and 0.90. The lowest Froude number shows that the wave elevation behind transom stern for all model scales has the same pattern as for x/L < 2.0. For x/L > 2.0, the wave pattern behind transom stern for the model and 10L catamarans show the similarity while the 2L catamaran shows a higher wave amplitude and shorter wavelength. The large differences seem to be from the blockage of the tank which the 2L has the smallest $0.5B_{Tank}/L$. The reflection for 2L catamaran occurs around x/L = 2.0, which causes a high wave amplitude.

The measurement of wave elevation behind transom stern for Fn = 0.433 is shown in figure 7.30. It can be seen that the similarity of wave pattern for all catamarans occurs at x/L < 3.0. Although the wave patterns are similar, the amplitude is different. For the model and 2L catamarans, the wave amplitudes are not much different while the 10L catamaran shows higher wave amplitude. Due to the $0.5W_{Tank}/L$ effects, the reflection of the 2L catamaran occurs around x/L = 2.0 which results in the high measurement of wave elevation behind transom stern compared with the wider $0.5B_{Tank}/L$.

The wave cut behind transom stern for Fn = 0.70 is shown in figure 7.31. The wave pattern is similar for all catamarans for $x/L < 3.0$. For $x/L > 3.0$, the wave pattern for model running in Boldrewood towing tank and the 10L catamaran is quite similar while the pattern and amplitude for the model running in Solent tank and the 2L catamaran are higher due to the reflection. The reflection of the tank side for the 2L catamaran occurs at $x/L = 3.0$ while the reflection happens at $x/L = 4.0$ for the model running in Solent towing tank.

The highest Froude number shows that the wave pattern behind transom stern for all catamarans is similar up to $x/L < 3.0$. Wave amplitude increases with decreasing $0.5B_{Tank}/L$, which can be seen that the 2L catamaran has the highest wave elevation. The wave pattern for the model running in Boldrewood tank and 10L catamaran is similar throughout the numerical domain, which the 10L catamaran has slightly higher wave amplitude.

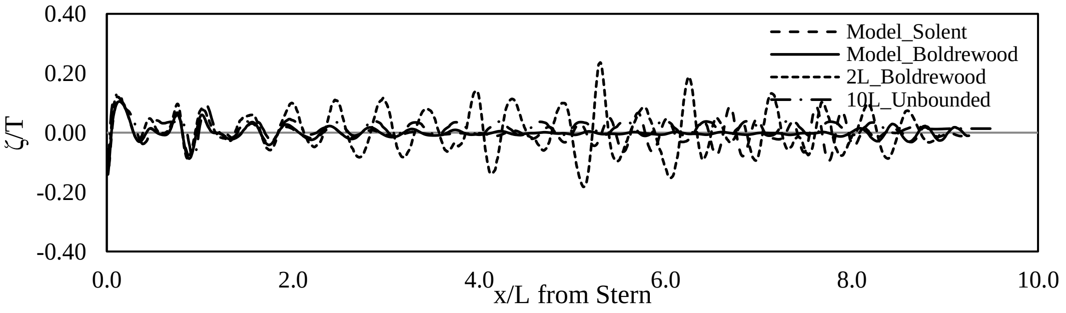

Figure 7.29 Wave cut behind transom stern of NPL 5b S/L = 0.3 at Fn = 0.273

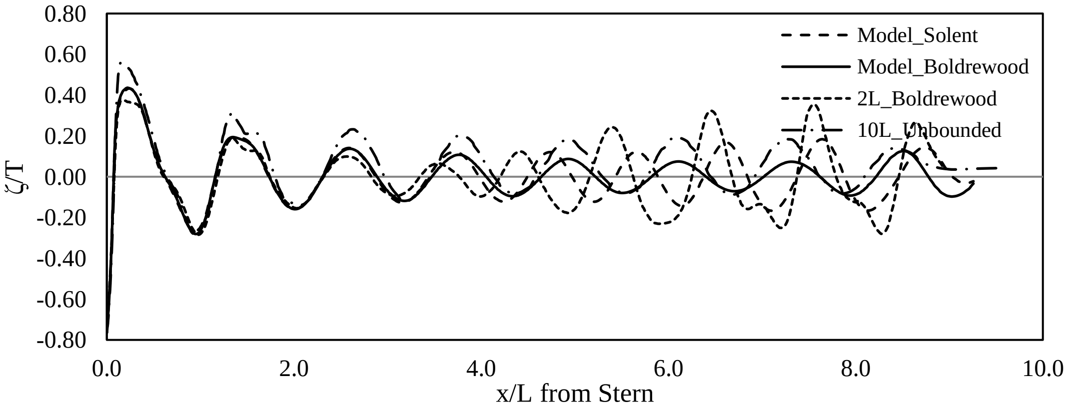

Figure 7.30 Wave cut behind transom stern of NPL 5b S/L = 0.3 at Fn = 0.433

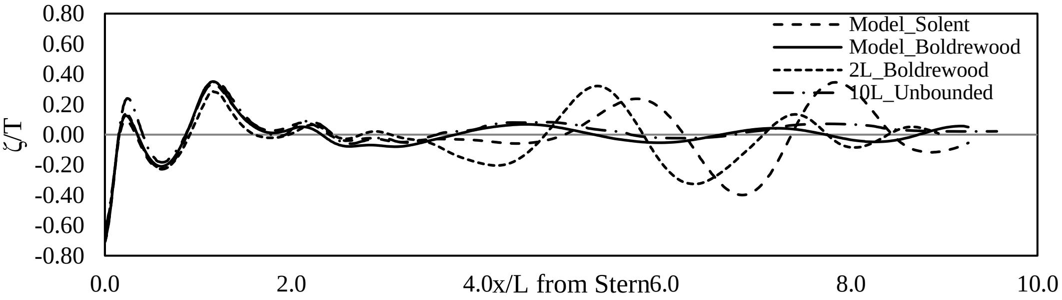

Figure 7.31 Wave cut behind transom stern of NPL 5b S/L = 0.3 at Fn = 0.70

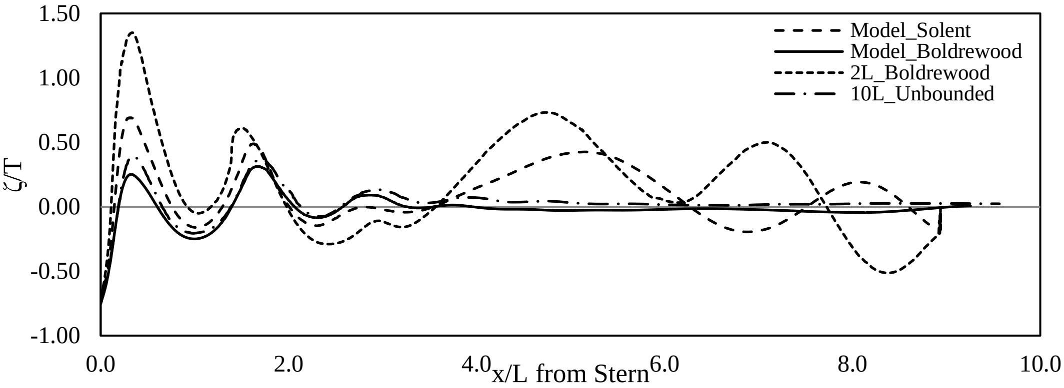

Figure 7.32 Wave cut behind transom stern of NPL 5b S/L = 0.3 at Fn = 0.90

7.3.4 Wave Cut between Demihulls

The comparisons of wave elevation between demihulls for different model scales are shown in figures 7.33 to 7.36. The x/L origin point is placed parallel to the forward perpendicular of the catamaran and at the middle between demihulls. The wave pattern for Fn = 0.273 shows that all catamarans have similar wave pattern for x/L < 3.0. The wave pattern seems to maintain the similarity for models running in both Solent and Boldrewood towing tank and 10L catamaran throughout the numerical domain. The 2L catamaran has the higher wave elevation due to the wall reflection.

For Fn = 0.433 shown in figure 7.34, the wave elevation for all catamarans shows the same pattern for x/L < 4.0. At this x/L region, the wave elevation of the 10L catamaran shows the highest amplitude with a small difference from other catamarans. For the x/L > 4.0, the 2L catamaran shows the shortest wavelength with the highest wave height. The similar flow pattern can be found for the model running in Boldrewood towing tank and 10L catamaran.

The wave cut between demihulls for Fn = 0.70 is shown in figure 7.35. The results show that the wave pattern for all catamarans shows similarity for x/L < 3.0. The wave amplitude of the10L catamaran is higher than other models, which is similar to lower speeds. At the region where x/L > 3.0, the wave pattern is not similar for all catamarans. Wavelength decreases with decreasing wall distance, which results in shorter wavelength for the 2L catamaran and the model running in the Solent towing tank.

Like other Froude numbers, the wave pattern for Fn = 0.90 is similar for all catamarans at x/L < 3.0. However, the highest Froude number shows that the highest wave elevation in this region is from the 2L catamaran for the first two wave crests. For x/L > 3.0, the 2L catamaran has the highest amplitude with the shortest wavelength. The model running in the Solent tank also shows the similar result with the 2L catamaran due to the reflection of the tank side. However, for x/L > 3.0 the wave pattern for the model running in the Boldrewood towing tank is similar to the 10L catamaran.

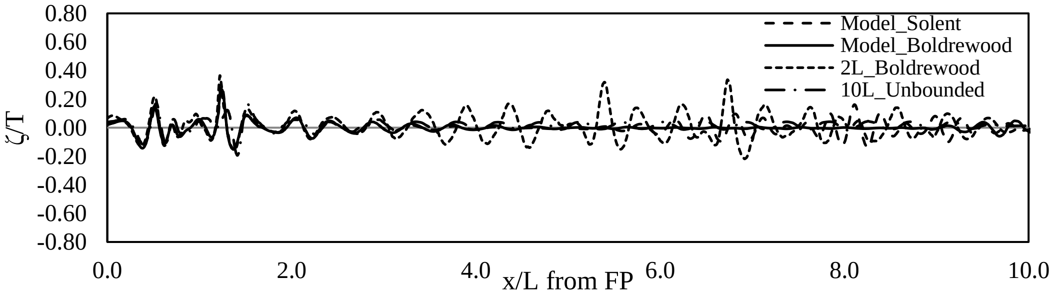

Figure 7.33 Wave cut between demihulls at centreline of NPL 5b S/L = 0.3 at Fn = 0.273

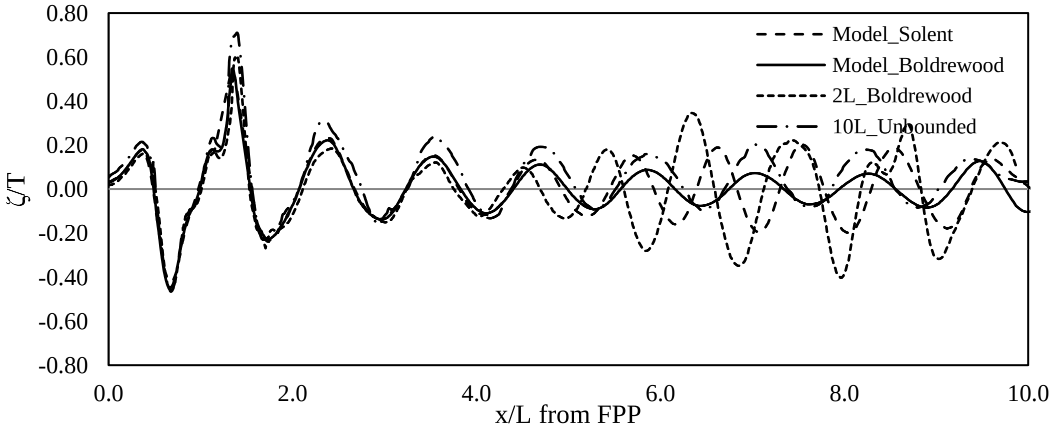

Figure 7.34 Wave cut between demihulls at centreline of NPL 5b S/L = 0.3 at Fn = 0.433

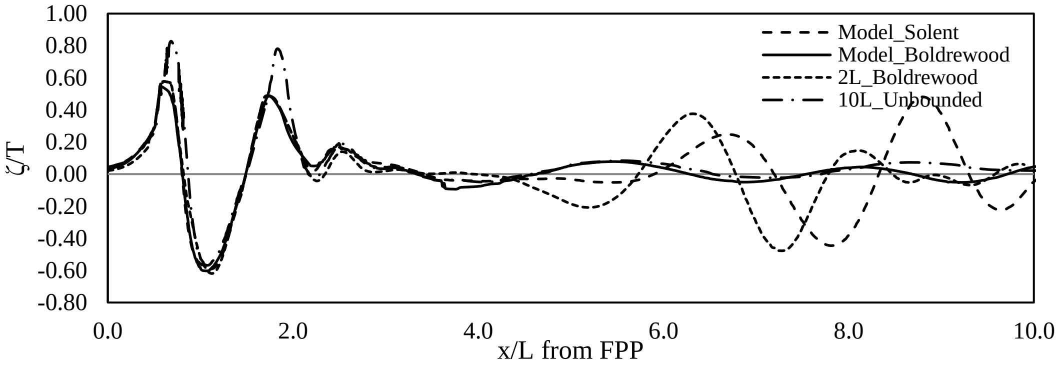

Figure 7.35 Wave cut between demihulls at centreline of NPL 5b S/L = 0.3 at Fn = 0.70

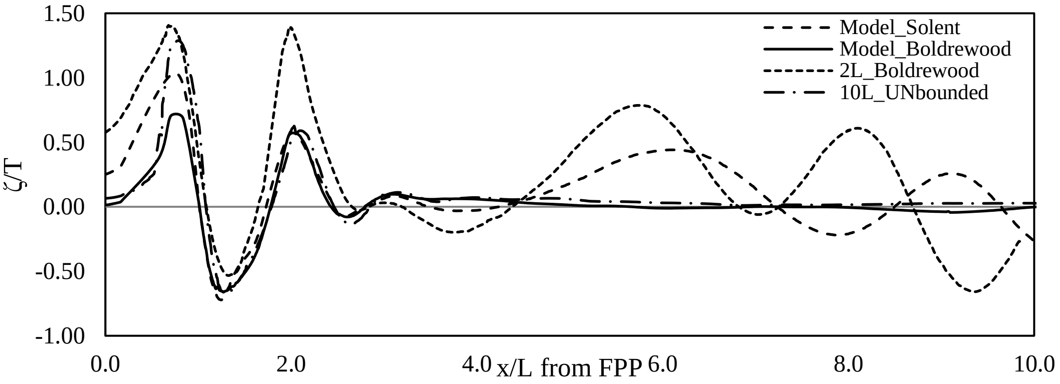

Figure 7.36 Wave cut between demihulls at centreline of NPL 5b S/L = 0.3 at Fn = 0.90

7.3.5 Wave Cut at y/L = 0.5

Figures 7.37 to 7.40 show the wave cut at the y/L = 0.5. The wave elevation is presented against the x/L, which x originates parallel to the forward perpendicular in y-direction. The lowest Froude number shows that the wave pattern is similar for all catamarans for the region where x/L < 3.0. The wave pattern for x/L > 3.0 is quite similar for the model running in both the Solent and the Boldrewood towing tanks, and 10L catamaran. For x/L > 3.0, the wavelength for the 2L catamaran is shorter than other catamarans and the wave height also shows the highest amplitude due to the reflection off the wall.

Wave pattern for Fn = 0.433 is similar for all models up to x/L < 3.0 for both wavelength and wave height. For x/L > 3.0, the model running in the Boldrewood towing tank and the 10L catamaran still maintain the similarity of wave pattern whilst the model running in the Solent tank shows slightly shorter wavelength. At this region, the 2L catamaran has the highest wave elevation and shortest wavelength.

The similarity in wave pattern is found at x/L < 3.0 for all catamarans for Fn = 0.70 due to the reflection off the wall, which results in the differences for wave pattern occurs at x/L > 4.0. The 2L catamaran has a shorter wavelength following by the model running in the Solent towing tank. Like the lower Froude numbers, wave pattern for the model running in the Boldrewood towing tank and the 10L catamarans show the similarity.

For the highest Froude number, the wave pattern is also similar for x/L < 3.0; however, the amplitude of the first wave crest increases with the decreasing wall reflection distance, which can be seen in figure 7.40. Due to the disturbance of the wall distance, the 2L catamaran seems to have the highest wave height throughout the numerical domain. The model catamaran running in the Solent towing tank is also affected by the wall reflection, which results in high wave elevation. For the model catamaran running in the Boldrewood towing tank and the 10L catamaran, the wave pattern is quite similar over the x/L range.

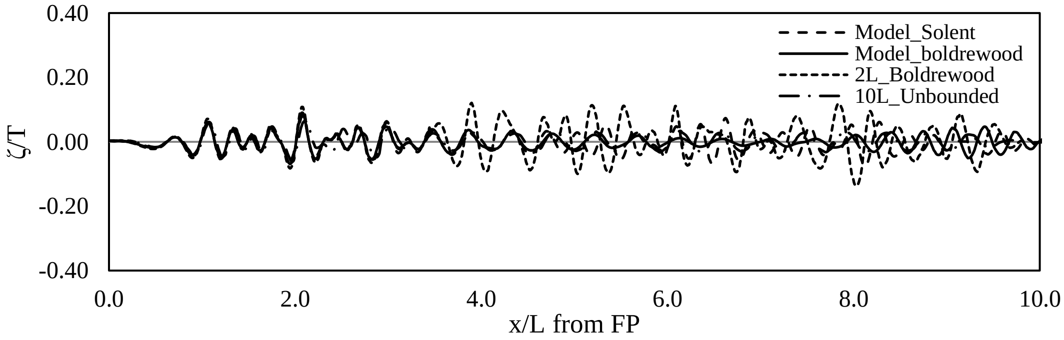

Figure 7.37 Wave cut at y/L 0.5 of NPL 5b S/L = 0.3 at Fn = 0.273

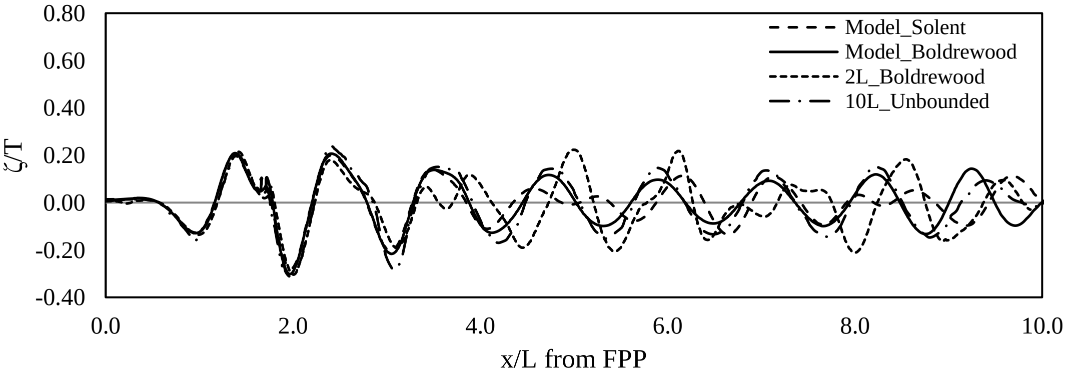

Figure 7.38 Wave cut at y/L 0.5 of NPL 5b S/L = 0.3 at Fn = 0.433

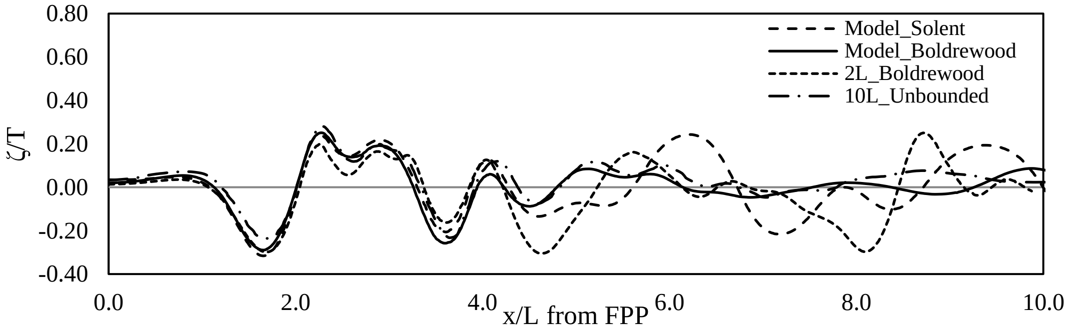

Figure 7.39 Wave cut at y/L 0.5 of NPL 5b S/L = 0.3 at Fn = 0.70

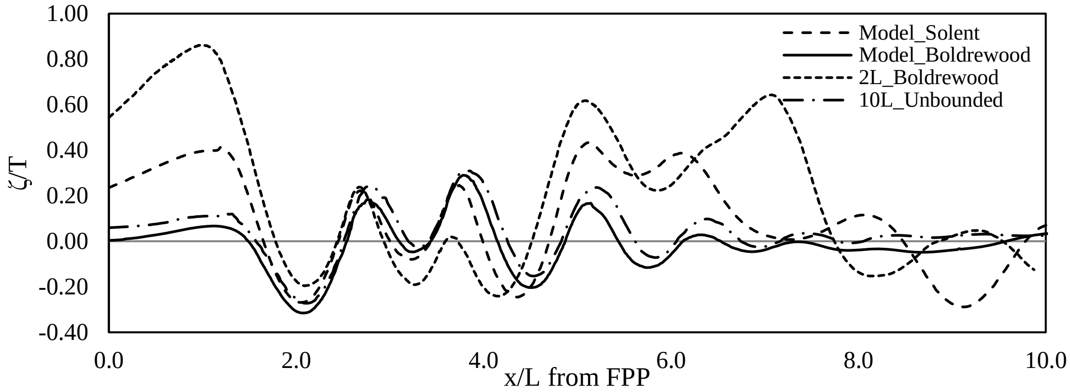

Figure 7.40 Wave cut at y/L 0.5 of NPL 5b S/L = 0.3 at Fn = 0.90

7.4 Chapter Summary

In this chapter, three main objectives are achieved including the blockage effect due to the tank dimension, Scale effects on resistance and form factor for the catamaran with transom stern-NPL 5b, and the wave cuts at different positions.

The Schuster and Tamura correctors are used to validate the CFD results. Two numerical domains duplicating the Solent and Boldrewood towing tank are investigated. The results show that the percentage blockage directly influences resistance prediction as can see in dropping of the model true speed (ΔV/V) which directly results in under prediction of resistance components. The validations show that the CFD results show a good agreement with the experimental results.

Three different model scales are investigated including model (1L), 2L and 10L catamarans. The CFD results are validated against Insel's experimental and scaled results. The results show good agreement for some resistance coefficients i.e. C_T and

C_F. The CFD results show that form factor (1+k) increases with the model size (Re) and seems to converge to a single value for large models for low Froude numbers.

Wave elevations are measured at different positions; along the hull, behind transom stern, between demihulls and at y/L = 0.5. Three different catamaran sizes are investigated following the resistance and form factor studies. The results show that the model (1L) running the Boldrewood towing tank and 10L (unbounded) catamarans share similarities in some wave cut positions for all Froude numbers. The model (1L) running in the Solent towing tank and 2L catamarans seem to receive the strong blockage effects from the tank side which result in showing shorter wavelength and higher wave amplitude.

Chapter 8: Overall Discussions

8.1 General

As the resistance of a catamaran is treated slightly different from a monohull due to the interference effects, both monohull and catamaran for the model scale (1L) are estimated at Froude numbers between 0.2-1.0, Reynolds' numbers up to 5.24x10^6. In the early stages, hull without transom stern is used to minimize the modelling complexity. Wigley III is used because of its high slenderness. Afterwards, NPL 5b is investigated to demonstrate the further understanding of a more realistic hull, which is used commercially. Three hull configurations which are S/L = 0.2, 0.3 and 0.4 are investigated for Wigley III while only one separation to length ratio (S/L = 0.3) is investigated for NPL 5b.

Three model scales are investigated including model (1L), 2L and 4L for the Wigley hull at separation to length ratio 0.3. Whilst, the NPL 5b is treated slightly different by investigating a larger hull size (10L instead of 4L). The range of speeds is varied in the same way with model scale, with corresponding to Reynolds' numbers between 1.31x10^6 – 5.24x10^7 and 1.10x10^6 – 1.73x10^8 for the Wigley III and the NPL 5b respectively.

Regarding the experimental data and towing tank facilities in the University of Southampton, two numerical domain sizes are considered consisting of the Solent towing tank where Insel conducted the experiment in 1990 and the Boldrewood towing tank. Four Froude numbers are investigated include 0.273, 0.433, 0.70 and 0.90 to demonstrate the blockage effects.

These numerical studies are carried out using the commercial CFD code STAR CCM+ v8.04. This software is chosen under the consideration that it allows users to run the cases up to millions of cells with accurate results, good supports from CD-adapco in consulting the problems. The early investigations done by many researchers, as discussed in literature review section, indicate that commercial CFD code STAR CCM+ v8.04 is capable of accurately estimating resistance components.

8.1.1 Hull Geometries

Two hull geometries including Wigley III and NPL 5b are investigated. The Wigley III is chosen as the beginning studies to minimise the complexities and due to the highest hull slenderness in the series. The NPL 5b is selected to represent a hull with the transom stern.

Three different model scales are investigated for the Wigley III, which are 1L (model), 2L and 4L. The model size is doubling to avoid the rapid change in flow physics and number of cells. Three different model scales are also investigated for the NPL 5b which include 1L (model), 2L and 10L. The largest scale for the NPL 5b is increased to 10 times of the model size to represent the full-scale ship.

8.1.2 Hull Configurations

Since the investigation follows Insel’s experiment, three hull separation to length ratios including S/L = 0.2, 0.3 and 0.4 are investigated for Wigley III. Only S/L = 0.3 was investigated for the scale effects for Wigley III. This hull separation is chosen because the literature and results in this study show that the influences on resistance prediction and flow characteristics are very strong for the narrowest hull separation whilst only slightly changed for S/L > 0.3. Only one hull separation is chosen for the NPL 5b which is S/L = 0.3. The cases investigated for both hull geometries are summarised in table 8.1.

Table 8.1 Hull configurations for models

Hull Configurations	Wigley III	NPL 5b
S/L = 0.2	√	
S/L = 0.3	√	√
S/L = 0.4	√	
1L for S/L = 0.3	√	√
2L for S/L = 0.3	√	√
4L for S/L = 0.3	√	
10L for S/L = 0.3		√

8.2 Grid Dependency

The grid dependency study is done for both the numerical towing tank and the resistance component prediction. The numerical study is the process used to find the most suitable number of cells per wave height for capturing the wave elevation to validate against the experimental data. The results and validation of the numerical towing tank are shown in chapter 3 and it is found that the number of cells per wave height between 30 and 40 cells should give the desirable results, which agrees with the literature. This number of cells per wave height is used throughout the investigations in this study.

The grid dependency is also applied to the resistance component prediction to find the total number of cells to calculate the most accurate result. The literature suggested that the total number of cells should be at least million cells. The total resistance coefficient (C_T) is calculated for 5 different grids. The results show that the CFD C_T converged to Insel's experimental result and it is found that total number of cells between 5 and 6 million cells are the optimum range to calculate the resistance coefficients.

8.3 Resistance Components

8.3.1 Total Resistance Coefficient, C_T

The total resistance coefficient for different hull configurations shows that the CFD C_T agrees very well with the Insel's experimental data. The majority of the CFD C_T values are under predicted compared with the experimental data. Due to the influence of the interference between the demihulls, the total resistance coefficient for the catamarans are higher than the monohull for both Wigley III and NPL 5b. The total resistance coefficient decreases with the increasing hull separation, which can be seen for the Wigley III.

The CFD C_T shows that the differences between the CFD and experimental data decrease with the increase of the model size. It also shows that for the highest C_T, the difference between CFD and experimental appears to be higher. This might be from the rapid change in residual and wave resistance for the intermediate Froude numbers.

The percentage error of the CFD C_T for Wigley III shows quite similar results for the monohull and catamaran S/L = 0.4, see table 8.2 while the results for catamaran S/L 0.2 and 0.3 are quite similar. The NPL 5b shows that the range of percentage error of the CFD C_T for catamaran S/L = 0.3 is slightly higher than the monohull. The investigation into model scales shows that the percentage error of CFD C_T for Wigley III reduces with the increasing model size as shown in table 8.3. The NPL 5b also shows the improvement in C_T prediction for increasing model size.

Table 8.2 The range of the percentage error of total resistance (C_T)

	Wigley III		NPL 5b	
	Under	Over prediction	Under	Over prediction
Mono	0.510 – 1.327		0.275 – 2.133	
S/L =	0.563 – 3.633			
S/L =	1.447 – 3.722		0.582 – 2.687	0.016
S/L =	0.563 – 1.677			

Table 8.3 The range of the percentage error of C_T for different scales

Model	Wigley III		NPL 5b	
	Under	Over prediction	Under	Over prediction
1L	1.447 – 3.722		0.582 – 2.687	0.016
2L	1.817 – 2.937		1.014 – 2.504	
4L	1.100 – 2.057			
10L			0.703 – 2.183	0.337 – 1.762

8.3.2 Frictional Resistance Coefficient, C_F

The CFD frictional resistance coefficient (C_F) is calculated from the shear force tangential to the hull and is validated against the ITTC correlation line. The CFD C_F results for all hull geometries and configurations are significantly over predicted. The differences between the CFD and the ITTC correlation line might be the fact that the ITTC correlation considers the 2D skin friction while CFD integrates the 3D shear force around the hull.

Table 8.4 shows the range of the percentage error of the CFD C_F compared with the ITTC correlation line. The range of percentage error of C_F for Wigley III shows a similar trend for all hull configurations. However, the error of the NPL 5b increases for the catamaran configuration, which is almost doubling in magnitude.

The percentage error of the CFD C_F for different model scales is shown in table 8.5. The change in percentage error of C_F for Wigley III model scales shows a slight declination with increasing model size. The NPL 5b shows that the percentage error of C_F is highest for the 1L model and decreases with the increasing model size.

Table 8.4 The range of the percentage error of frictional resistance coefficient (C_F)

	Wigley III		NPL 5b	
	Under	Over prediction	Under	Over prediction
Mono		1.369 – 3.307		1.215 – 2.739
S/L =		0.975 – 3.663		
S/L =		1.792 – 3.617		2.475 – 4.028
S/L =		1.386 – 2.519		

Table 8.5 The range of the percentage error of C_F for different scales

	Wigley III		NPL 5b	
	Under	Over prediction	Under	Over prediction
1L		1.792 – 3.617		2.475 – 4.028
2L		1.662 – 2.709		1.200 – 3.600
4L		1.305 – 2.872		
10L				1.635 – 3.877

8.3.3 Viscous Resistance Coefficient, C_V

The CFD C_V is calculated using the double-model method described in chapter 3. For all hull configurations, the characteristics of the CFD C_V are quite similar, which slightly decreases and shows very large differences from the experimental data for the low Froude numbers. The CFD C_V prediction for the larger model scales i.e. 4L for Wigley III and 10L for NPL 5b is seemingly over predicted for the higher Froude numbers. The large differences for the lower Froude numbers could be caused by the way C_V is calculated for the experimental data, which assumes that the form factor (1+k) is constant over the range of Froude numbers.

The range of the percentage error of C_V for all hull configurations is shown in table 8.6. For the Wigley III, the CFD results show a slight increase of percentage error with increasing hull separation. The highest error magnitude is found for the catamaran S/L = 0.3 for both under and over predictions. NPL 5b results also show the similar trend with the Wigley III, which the percentage error increases for catamaran. The range of the percentage error of C_V is quite similar for all Wigley III model scales as shown in table 8.7. The NPL 5b shows the slight increase in C_V over prediction for the bigger models.

Table 8.6 The range of the percentage error of viscous resistance (C_V)

	Wigley III		NPL 5b	
	Under	Over prediction	Under	Over prediction
Mono	0.159 – 3.052		0.198 – 1.908	0.441 – 1.744
S/L =	0.253 – 3.123	0.145 – 2.327		
S/L =	1.162 – 5.241	0.691 – 2.670	0.917 – 7.996	
S/L =	0.445 – 4.087	0.139 – 2.169		

Table 8.7 The range of the percentage error of C_V for different scales

	Wigley III		NPL 5b	
	Under	Over prediction	Under	Over prediction
1L	1.162 – 5.241	0.691 – 2.670	0.917 – 7.996	
2L	0.507 – 5.747	0.847 – 2.313	0.090 – 6.980	0.190 – 0.360
4L	0.298 – 4.891	0.500 – 2.822		
10L			0.661 – 6.981	1.006 – 3.920

8.3.4 Residual Resistance Coefficient, C_R

The CFD C_R for all models and hull configurations show the combination of under and over prediction compared with Insel's experimental data. For the lowest Froude number, the largest under prediction of CFD C_R appears. At the lowest Froude number, Insel's experimental C_T and C_V are very close to each other while CFD values show a larger gap. The under prediction of CFD C_R at the lower Froude numbers is caused by the under prediction of the CFD C_T and over prediction of the CFD C_F.

The CFD results show that C_R decreases with increasing hull separation. Theoretically, the residual resistance is constant for all model scales; however, the CFD results show a slight increase of C_R corresponding to the increasing model size.

The range of the percentage error of the CFD C_R for different hull geometries and configurations is shown in table 8.8. The comparison shows that the qualities of CFD C_R for Wigley III slightly change between hull configurations, which the S/L = 0.4 give the most accurate results. The results for NPL 5b are quite similar for the monohull and catamaran S/L = 0.3.

The scale effect study shows that the CFD results improve with the increasing model size for both the Wigley III and NPL 5b. The maximum value of percentage error for all model scales decreases with the increasing model size as shown in table 8.9. However, the over prediction of CFD C_R is found as a single value for NPL 5b of 12.093%.

Table 8.8 The range of the percentage error of residual resistance (C_R)

	Wigley III		NPL 5b	
	Under	Over prediction	Under	Over prediction
Mono	3.809 – 29.633		3.777 – 10.726	
S/L =	4.340 – 12.663			
S/L =	5.072 – 30.387		3.816 – 11.194	
S/L =	0.475 – 14.487			

Table 8.9 The range of the percentage error of C_R for catamarans S/L = 0.3

Model	Wigley III		NPL 5b	
	Under	Over prediction	Under	Over prediction
1L	5.072 – 30.387		3.816 – 11.194	
2L	5.412 – 16.873		4.100 – 12.480	
4L	2.543 – 14.771			
10L			2.430 – 8.440	12.093

8.3.5 Wave Resistance Coefficient, C_W

The combination of the over and under prediction of CFD C_W are found for all hull geometries. The CFD results show that wave resistance coefficient increases with the decreasing hull separation and the increasing model scale.

Table 8.10 shows the range of the percentage error of the wave resistance for all hull geometries and configurations. The range of percentage error for the Wigley III shows that the error for the monohull is similar to those of the catamaran S/L = 0.4, which is slightly affected by the interference effect. For the Wigley III catamaran S/L = 0.2 and 0.3 the range of error is quite similar for the under prediction. The range of error of the over prediction shows the similar trend for monohull and catamaran S/L = 0.3 and 0.4 while the catamaran S/L = 0.2 shows a narrow range of large error. The percentage error of the NPL 5b seems to be high for the catamaran S/L = 0.3 compared with the monohull, which can be seen for both the over prediction. The scale models show that the percentage error of both under and over prediction for Wigley III decrease corresponding to the increasing model scale as shown in table 8.11. The NPL 5b scaled models show that the under prediction is quite similar for 2L and 10L with the wider range compared with the 1L. The range of over prediction of CFD C_W for NPL 5b seems to decrease corresponding to the increasing model size.

Table 8.10 The range of the percentage error of wave resistance (C_W)

	Wigley III		NPL 5b	
	Under prediction	Over prediction	Under prediction	Over prediction
Mono	0.614 – 3.682	0.576 – 58.513	0.916 – 13.264	1.183 – 3.920
S/L = 0.2	0.399 – 11.019	20.644 – 60.903		
S/L = 0.3	0.353 – 14.432	3.135 – 45.178	5.748 – 9.943	0.048 – 38.958
S/L = 0.4	1.638 – 5.259	1.254 – 73.557		

Table 8.11 The range of the percentage error of C_W for catamarans S/L = 0.3

	Wigley III		NPL 5b	
	Under prediction	Over prediction	Under prediction	Over prediction
1L	0.353 – 14.432	3.135 – 45.178	5.748 – 9.943	0.048 – 38.958
2L	0.485 – 6.845	1.811 – 46.096	1.800 – 8.660	0.900 – 20.240
4L	0.149 – 6.882	1.792 – 23.740		
10L			0.484 – 10.182	1.272 – 10.400

8.3.6 Computational Effort

All CFD simulations are run in the University of Southampton super computer "Iridis 4". There are four ranges of the grid generation are created in this investigation as shown in table 8.12. The Iridis 4 allows the simulation to run with the 16 core processors and maximum wall time of 60 hours. The maximum number of iterations for the stopping criteria in the simulation is set to be 50000 to ensure the convergence of the results and flow field. It can be seen that the number of iterations per wall time limit for different grids are varied and corresponded to number of cells. The smallest domain containing smallest number of cells of 5-6M cells has the largest iterations per wall time limit while the largest domain containing 15-18M cells can run only 5000 iterations per wall time limit. The overall time to complete the simulation is about 200 hours for the smallest model and 600 hours for the largest model.

Table 8.12 Comparison of computational usage for difference grids

Model	1L	2L	4L	10L
Cells (millions)	5-6	7-9	10-12	15-18
No. of Processors	16	16	16	16
Total No. of Iterations	5 x 10^4	5 x 10^4	5 x 10^4	5 x 10^4
Iterations / Wall time limit	~ 15000	~ 10000	~ 7500	~ 5000
Total time (hrs)	~ 200	~ 300	~ 400	~ 600
Total time (days)	~ 8.33	~ 12.50	~ 16.67	~ 25

8.4 Form Factor

The comparison of the CFD form factor (1+k) and the experimental form factors for Wigley III and NPL 5b is shown in table 8.13. The CFD 1+k for the Wigley III is lower than the experimental 1+k for all hull configurations. The percentage differences are 1.79, 2.25, 3.53 and 2.69 for monohull, catamaran S/L = 0.2, 0.3 and 0.4 respectively. It can be seen that the experimental 1+k for catamaran S/L = 0.3 and 0.4 are slightly different while the CFD 1+k are similar. The similar 1+k for these hull configurations indicates that the influence of the interference effect has less contribution to the 1+k prediction for wider hull separations. The NPL 5b monohull shows a slightly higher CFD 1+k compared with the experiment by 0.34% while the catamaran S/L = 0.2 shows a lower 1+k by 6.71%.

The Wigley III catamaran S/L = 0.3 is scaled up for another two model sizes including 2L and 4L, which are run in the range of Reynolds' number between 3.70 – 1.48 x 10^6 and 1.05 – 4.19 x 10^7 respectively, see section 5.2. The NPL 5b is also scaled to create two models including 2L and 10L which are run in the range of

Reynolds' number between 3.10 x 10^6 – 1.55 x 10^7 and 3.47 x 10^6 – 1.73 x 10^8 as seen in section 7.2.

The reference 1+k is fixed for all model scales as calculated by Insel as shown in table 8.13. The CFD 1+k for the Wigley III is significantly lower than the experimental 1+k for all model scales. The results show that the CFD 1+k increases with the increasing model size. The CFD 1+k for the NPL 5b are also lower than the experimental 1+k for all models as shown in table 8.13. It can be seen that the CFD 1+k also increases corresponding to the increasing model size. However, the percentage differences between CFD and experimental 1+k for Wigley III are lower than the NPL 5b for all model sizes.

Table 8.13 Form factor comparison for different hull geometries and configurations

	Wigley			NPL 5b		
	Exp	CFD	% Diff	Exp	CFD	% Diff
Mono	1.06	1.041	- 1.79	1.17	1.174	0.34
S/L = 0.2	1.20	1.173	- 2.25			
S/L = 0.3	1.16	1.119	- 3.53	1.40	1.306	- 6.71
S/L = 0.4	1.15	1.119	- 2.69			

Table 8.14 The comparison of form factor for different model scales

	Wigley III S/L = 0.3			NPL 5b S/L = 0.3		
	Exp	CFD	% Diff	Exp	CFD	% Diff
1L	1.16	1.119	- 3.53	1.40	1.306	- 6.71
2L		1.123	- 3.19		1.32	- 5.71
4L		1.132	- 2.41			
10L					1.34	- 4.29

8.5 Blockage Effects

The blockage effects on resistance prediction are discussed in section 7.1. Two towing tanks; Southampton Solent and Boldrewood are investigated. The NPL 5b catamaran S/L = 0.3 model is used in this investigation. The percentage blockage of these tanks are 0.10 and 0.032 percent respectively. The Schuster and Tamura corrections are used to validate the CFD results. It is found that the blockage effects due to the tank dimensions can affect the prediction of the resistance of the ship model.

The CFD results show that the resistance components of the NPL 5b catamaran are higher for the bigger tank and close to the experimental results.

8.6 Wave Elevation Measurement

Four positions of wave elevation are measured, which include wave elevation along the hull, behind transom stern, at the centreline between demihulls and at y/L = 0.5. Wave elevation along the hull is measured on both sides of the hull. For the Wigley III, the CFD results show a good agreement with the experiment for the low speed i.e. 0.273 and 0.433. The differences are very high for the higher speed, Fn > 0.433. From the discussion on the possible sources of differences presented in section 4.5, it is concluded that the errors might be from the data acquisition method. The experimental data were determined from photographs taken by a high-speed camera while the CFD results are determined by creating the intersection line between the free surface and the hull surface.

Wave elevation behind transom stern, the centreline between demihulls and at y/L = 0.5 are measured for the scale effects on resistance component prediction and form factor for NPL 5b catamaran. The results show that the wave elevation for the 2L model running in the Boldrewood towing tank is highest compared with other models due to the reflection from the tank side while wave elevation at all positions for 1L and 10L models shows quite similar results.

Chapter 9: Conclusions and Recommendations

9.1 General Conclusions

- The literature shows that the total resistance of displacement catamarans is equated to the summation of resistance components in a similar manner to the monohull, which includes frictional resistance, viscous resistance and wave resistance, for example. However, due to the interference effects between demihulls, form or viscous interference resistance and wave interference resistance are needed to be taken into account, especially in the high-speed regime. The current investigation focuses on addressing how the model scale influences form factor and demonstrating how the blockage affects the prediction of resistance components and form factor. The work is divided into three main parts including the resistance of high-speed catamaran, scales and blockage effects.

9.2 Grid Dependence

- The numerical wave tank investigation indicates that the suitable number of cells per wave height to capture wave elevation and wave pattern is at least 20 – 30 cells and 30 – 40 cells for the short wave, which agrees with the literature. The validation shows good agreement with theory, experimental and Wood's numerical results.
- The number of cells per wave height is then used to capture wave elevation along the hull both inboard and outboard for catamarans. The results are validated against experimental data retrieved from Insel. The results show that at a low speed (Fn = 0.35), numerical results show a good agreement with experiment, while at high-speed regime i.e. Fn = 0.50 and 0.70 the differences increase significantly.
- A grid dependence study, which focuses on finding the acceptable total cells to estimate the accurate resistance components, indicates that the number of cells

should be between 5M and 6M to provide an acceptable result for determining resistance for Wigley III with 1.8m long model. The SST k-ω turbulence model is used as it gives more accurate results compared with k-ε.

9.3 Resistance components

- The resistance components for Wigley III estimated using the CFD code are validated against Insel's experimental results and show a good agreement. For the monohull, total and frictional resistance coefficients show that the difference is ~1.0 – 4.0%. Residual resistance coefficient is underestimated over the whole Froude number range, and very high at the low Froude numbers ($0.20 < Fn < 0.367$). Viscous resistance coefficient is significantly underestimated at the low Froude numbers then rises constantly and slightly over predicted for higher Froude numbers i.e. at $Fn > 0.6$. Wave resistance coefficient is mostly underestimated with smallest difference ~14.0% at $Fn = 0.35$ while the largest difference is ~45.0% at the lowest Froude number.

- Three separations to length ratios (S/L) are investigated including 0.2, 0.3 and 0.4. Results demonstrate that resistance component prediction shows the same trend with monohull in term of differences between the CFD and experimental results.

- The investigation into the hull with transom stern, NPL 5b, indicates that total resistance is slightly under predicted while frictional resistance is higher than the ITTC correlation line. Viscous resistance also behaves the same way as the Wigley III, which is under predicted at the low speeds (Fn) and increases for the higher speeds and then is over predicted.

- Only one separation to length ratio (S/L = 0.3) is determined for the NPL 5b. This hull configuration was chosen because it represents a realistic example and the influence of hull interaction. Total resistance, frictional and residual resistance shows the similar characteristics as for the single hull while viscous resistance is lower than the experimental results over the range of Froude numbers.

- In term of computational efficiency, the 10L model is still significantly computationally expensive compared with the smaller models (1L and 2L) running in the smaller numerical domain. The total number of cells for the 1L running in the Boldrewood tank is about 7-9M cells while the 10L model is 15-18M cells, which requires 200 and 600 hours on high performance computing cluster respectively. As the results show the improvement for resistance prediction for bigger model, i.e. 2L, the length of the model between 3.0 – 4.0m for Wigley III and NPL 5b together with the $0.5W_{Tank}/L > 2.0$ are recommended for the numerical investigation.

9.4 Form Factor

- The Wigley III monohull form factor increases with speed (Fn), and is lower than the average form factor from Insel's experiment at low speeds ($Fn < 0.50$). The CFD average form factor is lower than from the experiments, with the experimental $(1+k) = 1.15$ and CFD $(1+k) = 1.119$ respectively. The CFD form factor is lowest for the single hull and increases with decreasing hull separation for catamarans. The difference between $S/L = 0.3$ and 0.4 is very small because these hull configurations are relatively wide; hence the hull interaction creates less interference effects.

- The single hull NPL 5b shows that form factor linearly increases with speed (Fn). Although there is a fluctuation at the low Froude numbers, for the higher Froude numbers i.e. $Fn > 0.50$, form factor increases linearly. The NPL 5b catamaran form factor also increases over the range of Froude numbers. However, at the lower Froude numbers, $Fn < 0.5$, form factor increases with a higher gradient. Unlike the monohull, the CFD average form factor for catamaran is slightly lower compared with the experiment.

9.4.1 Influence of Scale

- By adding two larger model sizes, 2L and 4L for the Wigley III, to investigate how form factor is affected, the results show that form factor increases corresponding to the increasing model size. The increase of the form factor seems to be non-uniform at the iso-Froude number when increases the model size. At the lower Froude numbers, Fn < 0.50, the gradient of the form factor is significantly steeper than the higher Froude numbers for all model sizes.

- The similar investigation is done for NPL 5b; however, the biggest model is set to be 10 times of model scale instead of 4L. The simulation results also suggest that the form factor increases with increasing model size. The increase of form factor is not steady for NPL 5b, the gradient increases corresponding to the model scale.

- This investigation into the scale effects on the form factor suggests that form factor increases with scale (Re) for the iso-Froude number, with higher gradient for low speed i.e. Fn < 0.50. The NPL 5b hull shows a slightly different form factor characteristic compared with the Wigley III because the gradient of the form factor for the NPL 5b increases with the increasing model size.

9.4.2 Influence of Tank Blockage on Form Factor

- The investigation into tank blockage effects is made for two existing towing tanks; Southampton Solent tank and University of Southampton Boldrewood tank. The results are validated against experimental data done by Insel in the Southampton Solent Tank and the blockage corrections suggested by ITTC recommended procedures. The CFD results agree well with the theoretical and experimental results and emphasis that the bigger tank provides the better results.

- Three numerical domains are investigated for the NPL 5b catamaran S/L = 0.3 including the Southampton Solent tank, University of Southampton Boldrewood tank and the unbounded condition to find a suitable model scale and numerical domain dimensions. Flow field is focused for four Froude numbers including Fn = 0.273, 0.433, 0.7 and 0.9. It is found that the half of the numerical domain width to the model length ratio ($0.5W_{Tank}/L$) between 1.875 and 4.0 together with the blockage less than 0.033% for the NPL 5b catamaran S/L = 0.3 shows the similar results and better than other domain dimensions.

9.4.3 Recommendations for Tank Blockage Effects and Scale

- One of the objectives of this research is to use the CFD code to enhance the results and understanding obtained from towing tank experiments. Although the ITTC recommendations suggested that the restricted flow caused by the boundaries is necessary if tank breadth is larger than model breadth about 10 – 15 times, the CFD results show that the resistance predictions are slightly different corresponding to tank dimensions but the flow is significantly affected.
- Form factor should be estimated at the operating speed rather than at either low or high speeds. It is found that the form factor for the catamarans increases with speed, especially at the low Froude numbers, the gradient of the form factor is steeper than the higher Froude numbers and increases with the increasing model size (Re). The increase of the form factor corresponding to scale (Re) seems to smaller than corresponding to speed, hence it is recommended that the form factor of catamaran should be determined for the operating speed with the suitable model scale as concluded in previous sections.

9.5 Recommendations for Future Works

Some aspects related to this research project have not been fulfilled. Those interesting points and recommendations are listed below:

- All the numerical investigation in this research project are run using fixed trim and sinkage retrieved from Insel's experiment. To minimize the cases studies, steady state simulation is used so models are not free to move when running in water. For example, this is quite interesting with the blockage effects because the distance between the model centerline and the tank wall might affect sinkage and trim. This phenomenon is seen in the scale effect investigation, which model 2L running in a small tank, i.e. Boldrewood towing tank, the free surface level seems to rise higher than the wider domain. This results in significantly higher measurement for wave elevations and wave patterns. Hence, if the model is free to sink and trim the measurement data of sinkage, trim, wave elevation, wave pattern and resistance components might be worth to investigate.

- Due to the lack of the experiment data for model scales, the experimental investigations with bigger model in new bigger tank, i.e. Boldrewood tank is highly recommended.

As aims and objectives of this project are to focus on scaling up catamarans, only model size, 1L, is investigated on both monohull and catamaran. This means that viscous interference resistance factor (β) and wave resistance interference factor (τ) has been not investigated. These factors can provide more understanding of how the form factor changes between monohull and catamarans.

- Only one hull separation to length ratio is investigated ($S/L = 0.3$). The interference effects from the demihulls is not fully investigated.
- Flow separation behind transom stern is another aspect that should be looked at as seen in many literatures that transom drag also significantly affects total resistance.
- Influence of water depth is also necessary to investigate because some of catamarans are operated in shallow water.
- The full-scale catamaran is not investigated in this project due to the very high computational cost.

List of References

Aktar, S., Saha, G. K., and Alim, M. A. (2013*). Drag analysis of different ship models using Computational Fluid Dynamics tools*. A Journal of Momentum, Vol.10.

Anderson, J. D., (1995). *Computational fluid dynamics: the basics with applications*. International Editions. McGraw-Hill, Inc.

Bertram, V., and Schneekluth, H. (1998). *Ship design for efficiency and economy 2nd Edition*: Butterworth-Heinemann, A Division of Reed Educational and Professional Publishing Limited, Oxford, UK.

Broglia, R., Zaghi, S., and Di Mascio, A. (2011). *Numerical simulation of interference effects for a high-speed catamaran*. Journal of marine science and technology, Vol. 16(3), pp. 254 – 269.

Broglia, R., Jacob, B., Zaghi, S., Stern, F., and Olivieri, A. (2014). *Experimental investigation of interference effects for high-speed catamarans.* Ocean Engineering, Vol. 76, pp. 75 – 85.

Bruzzone, D., Cassella, P., Miranda, S., Pensa, C., and Zotti, I. (1997). *The form factor by means of multiple geosim model tests.* the Proceedings of NAV and HSMV.

Chandraprabha, S., (2003). *An investigation into wave wash and wave resistance of high-speed displacement ships*. PhD Thesis, University of Southampton.

Clements, R. (1959). *An Analysis of Ship Model Correlation Data Using the 1957 ITTC Line*. Transactions of the Royal Institution of Naval Architects, Vol. 101, pp. 373.

Demirel, Y. K., Khorasanchi, M., Turan, O., Incecik, A., and Schultz, M. P. (2014). *A CFD model for the frictional resistance prediction of antifouling coatings*. Ocean Engineering, Vol. 89, pp. 21 – 31.

Denchfield, S., Wood, C., Hudson, D., Tan, M., and Temarel, P. (2010). *Comparisons between CFD predictions and experiments for rogue wave-ship interactions.*

At PRADS 2010: 11th International Symposium on Practical Design of Ships and Other Floating Structures, Brazil. 19 – 24 Sep 2010. pp. 7.

Doctors, L. J. (2003). *The influence of viscosity on the wave making of a model catamaran.* Paper presented at the Proceeding of the Eighteenth International Workshop on Water Waves and Floating Bodies, Le Croisic, France, April 2003.

Doctors, L. J. (2007). *A Numerical Study of the Resistance of Transom-Stern Monohulls*. Ship Technology Research, Vol. 54(3), pp. 134 – 144.

García-Gómez, A. (2000*). On the form factor scale effect*. Ocean Engineering, Vol. 27(1), pp. 97 – 109.

Garofallidis, D. A., (1996). *Experimental and numerical investigation of the flow around a ship model at various Froude numbers.* Part II: uncertainty analysis for measurements. PhD Thesis, Department of Naval Architecture and Marine Engineering, National Technical University of Athens.

Grigson, C. W. B. (1993). *An accurate smooth friction line for use in performance prediction*. Transactions of the Royal Institution of Naval Architects, Vol. 135, pp. 149 – 162.

Hino, T. (2005*). CFD workshop Tokyo 2005*. National Maritime Research Institute, Japan.

Hughes, G. (1954). *Friction and form resistance in turbulence flow and a proposed formulation for use in model and ship correlation*. Transaction of the Royal Institution of Naval Architects, Vol. 96, pp. 314 – 376.

Insel, M. (1990). *An investigation into the resistance components of high-speed displacement catamarans.* PhD Thesis, University of Southampton

Insel, M. and Molland, A. F. (1992), *An Investigation into Resistance Components of High-Speed Displacement Catamarans.* Transaction of Royal Institute of Naval Architects, Vol.134, pp 1 – 20.

Iqbal, M., and Trimulyono, A. (2014). *Optimisation of catamaran demihulls form in early stage of the design process*. KAPAL : Jurnal Ilmu Pengetahuan & Teknologi Kelauatan, Vol. 11(3), pp. 126 – 131.

ITTC. (1981). *Report of Performance Committee*. Proceedings of 16th ITTC

ITTC. (1983). *Report of Performance Committee.* Proceedings of 17th ITTC

ITTC. (1993). *Report of Performance Committee*. Proceedings of 20th ITTC

ITTC. (1996). *Report of Performance Committee.* Proceedings of 21th ITTC

ITTC. (2002). *Report of the Resistance Committee*. Proceedings of 23rd ITTC

ITTC. (2011). *Recommended Procedure, Resistance Test*. Proceedings of 25th ITTC

Jones, B. M. (1929). *The streamline aeroplane*. The Journal of the Royal Aeronautical Society. Vol. 33. pp. 357 – 385.

Journée, J. (1992). *Experiments and calculations on 4 Wigley hull forms in head waves.* Delft University of Technology, Report (0909).

Jupp, M., Sime, R., and Dudson, E. (2014). *XSS–A Next Generation Windfarm Support Vessel.* Paper presented at the International Conference, Design & Operation of Wind Farm Support Vessels. London.

Kasahara, M., and Masuda, S. (1998). *Verification of simulation flow field around ships by using CFD code.* Paper presented at the Proceedings of the Third Osaka Colloquium Advanced CFD Applications to Ship Flow and Hull Form Design, Osaka, Japan.

Kouh, J. S., Chen, Y. J., and Chau, S. W. (2009). *Numerical study on scale effect of form factor*. Ocean Engineering, Vol.36 (5), pp. 403 – 413.

Lackenby, H. (1955). *BSRA Resistance Experiments on the Lucy Ashton Part III-The Ship-Model Correlation for Shaft-Appendage Conditions.* Transaction of the Royal Institute of Architects. Vol. 95. pp. 350 – 436.

Larsson, L., Stern, F., and Bertram, V. (2002). *Gothenburg 2000: A Workshop on Numerical Ship Hydrodynamics.* Proceedings of the Chalmers University of Technology.

Larsson, L., Stern, F., and Visonneau, M. (2010). *Gothenburg 2010, A Workshop on Numerical Ship Hydrodynamics*. Gothenburg, Sweden.

Lo´pez-Acevedo, M. (1955). *Viscous resistance and the correlation between model and ship according with new criteria in the case of a larger tanker*. 5th Congress of Naval Architects.

Menter, F. R. and Kuntz, M. (2002). *Adaptation of Eddy Viscosity Turbulence Models to Unsteady Separated Flows Behind Vehicles*. The Aerodynamics of Heavy Vehicles: Trucks, Buses and Trains, Springer, Asilomar, CA, USA.

Molland, A. F., Wellicome, J. F., and Couser, P. R. (1994). *Resistance experiment on a systematic series of high speed displacement catamaran forms: Varian of length-displacement ratio and breadth-draught ratio*. Ship Science Report, Vol. 71.

Molland, A. F., Turnock, S. R., and Hudson, D. A., (2011), *Ship Resistance and Propulsion.* Cambridge University Press, New York, USA.

Moraes, H., Vasconcellos, J., and Latorre, R. (2004). *Wave resistance for high-speed catamarans*. Ocean Engineering, Vol. 31(17), pp. 2253 – 2282.

Patel, V. C., Nakayama, A., and Damian, R. (1973). *An experimental study of the thick turbulent boundary layer near the tail of a body of revolution.* Iowa Institute of Hydraulic Research, Iowa City, USA.

Pranzitelli, A., Nicola, C., and Miranda, S. (2011). *Steady-state calculations of free surface flow around ship hulls and resistance predictions*. High Speed Marine Vehicles (IX HSMV), Naples, Italy.

Prohaska, C. W. (1996*). A Simple Method for Evaluation of Form Factor and the Low Speed Wave Resistance.* Proceeding of 11th ITTC, pp. 65 – 66.

Raven, H. C., Van der Ploeg, A., Starke, A., and Eça, L. (2008). *Towards a CFD-based prediction of ship performance progress in predicting full-scale resistance and scale effects*. Proceedings of Royal Institute of Naval Architectures, Part A: International Journal of Maritime Engineering. London, UK.

Samuel, M., Iqbal, M. and Utama, I. (2015). *An Investigation into the Resistance Components of Converting a Traditional Monohull Fishing Vessel into Catamaran Form*. International Journal of Technology, Vol. 3.

Schoenherr, K. E. (1932). *Resistance of flat surfaces moving through a fluid*. Transactions of the Society of Naval Architects and Marine Engineers. Vol. 40.

Srinakaew ,S., Taunton, D. J. and Hudson, D. A. (2016). *A Study of Resistance of High-Speed Catamarans and Scale Effects on Form Factor*. Proceeding of the 19th Numerical Towing Tank Symposium (NUTTS'16), St Pierre d'Oleron, France, pp. 144 – 149.

Telfer, E. V. *Ship resistance similar*ity. Transactions of the Royal Institution of Naval Architects, Vol. 69, 1927, pp. 174 – 190.

Tzabiras, G. (1992). *A numerical investigation of the Reynolds scale effect on the resistance of bodies of revolution.* Journal of the National Academies of Science, British Maritime Technology

Tzabiras, G., and Garofallidis, D. (2006). *Computation of the resistance of a Series-60, C_B= 0.6 model under a measured free-surface*. Maritime Transportation of Ocean and Coastal Resources, pp. 295.

Utama, I. (1999). *Investigation of the viscous resistance components of catamaran forms*. PhD Thesis, University of Southampton.

van Lammeren, W., Van Manen, J., and Lap, A. (1960). *Scale Effect Experiments on Victory Ships and Models*. Netherlands Ship Model Basin.

van't Veer, R. (1998). *Experimental results of motions and structural loads on the 372 catamaran model in head and oblique waves*. Delft University of Technology, Faculty of Mechanical Engineering and Marine Technology, Ship Hydromechanics Laboratory.

Voxakis, P. (2012). *Ship hull resistance calculations using cfd methods*. Department of Mechanical Engineering, Massachusetts Institute of Technology.

Wackers, J., Koren, B., Raven, H. C., Van der Ploeg, A., Starke, A., Deng, G., and Ohashi, K. (2011). *Free-surface viscous flow solution methods for ship hydrodynamics*. Archives of Computational Methods in Engineering, Vol. 18(1), pp. 1 – 41.

Wellicome, J., Molland, A., Cic, J., and Taunton, D. J. (1999). *Resistance experiments on a high-speed displacement catamaran of series 64 form*. Ship Science Report No. 127.

Wilcox, D. C. (1998). *Turbulence Modeling for CFD*. 2nd edition, DCW Industries, Canada.

Windén, B., Turnock, S. R., and Hudson, D. A. (2012). *Validating force calculations using OpenFOAM on a fixed Wigley hull in waves*. 15th Numerical Towing Tank Symposium, Cortona, Italy.

Wood, C. (2013*). Compartment Flooding and Motions of Damaged Ship*. PhD Thesis. University of Southampton.

Zha, R., Ye, H., Shen, Z., and Wan, D. (2015). *Numerical computations of resistance of high speed catamaran in calm water.* Journal of Hydrodynamics, Ser. B, Vol.26(6), pp. 930 - 938.

Appendices

Appendix A Resistance Components for Wigley III Catamarans

A.1 S/L = 0.2

Resistance components of the narrowest hull separation are shown in figures A.1 and A.2, and tables A.1 and A.2. Total resistance coefficient, C_T, shows a good agreement with the experimental results over the range of Froude numbers. Most of the CFD C_T values are slightly lower than the experiment. The differences are linear over the range of Froude number except for Fn = 0.20 and 0.28, which the error is less than 1.0 percent. The validation of total resistance can be done for Fn < 0.70 because of the availability of experimental data. Insel commented that the excessive wave height and water spray in the tunnel between the demihulls caused the uncertainty of data acquisition and lack of safety.

The frictional resistance coefficient (C_F) estimated using CFD shows a good agreement with the ITTC correlation line. The CFD C_F is found over predicted over the range of Froude numbers with the range between 0.975 and 3.663 percent. The CFD viscous resistance is under predicted for Fn < 0.373, and over predicted for higher Froude numbers, which is similar to monohull.

CFD residual resistance coefficient (C_R) indicates a fair agreement validated against Insel's experiment, which can be seen in figure A.2 and table A.2. Generally, CFD C_R is under predicted and the error is steady except for Fn = 0.323 and Fn > 0.40, where the difference between CFD and experimental data is lower than 10.0 percent. The under prediction of residual resistance is from the fact that the CFD C_F is slightly higher than ITTC correlation line and the under prediction of the CFD C_T.

CFD wave resistance coefficient (C_W), presented in figure A.2 and table A.2, shows the combination of under and over prediction with the range of error between -0.399 and 60.903 percent. The CFD C_W is over prediction compared with the experiment for Fn = 0.20 and 0.28 due to the large under prediction of viscous resistance from CFD and small under prediction of the CFD C_T.

Table A.1 Total, frictional and viscous resistance coefficients of Wigley III S/L = 0.2

Fn	C_T (x 10^{-3})			C_F (x 10^{-3})			C_V (x 10^{-3})		
	Exp	CFD	Error (%)	1957	CFD	Error (%)	Exp	CFD	Error (%)
0.200	5.500	5.450	-0.909	4.425	4.511	1.947	5.310	5.144	-3.123
0.255	6.000	5.875	-2.083	4.206	4.274	1.617	5.047	4.926	-2.401
0.280	5.330	5.300	-0.563	4.126	4.221	2.302	4.951	4.843	-2.185
0.300	6.330	6.100	-3.633	4.069	4.109	0.975	4.883	4.802	-1.662
0.323	7.220	7.100	-1.662	4.009	4.075	1.646	4.811	4.786	-0.516
0.350	6.500	6.350	-2.308	3.945	4.054	2.763	4.734	4.722	-0.253
0.373	5.800	5.700	-1.724	3.895	3.988	2.388	4.674	4.681	0.145
0.400	6.440	6.250	-2.950	3.842	3.921	2.056	4.610	4.622	0.252
0.500	9.780	9.650	-1.329	3.679	3.814	3.663	4.415	4.427	0.270
0.600	9.000	8.750	-2.778	3.553	3.632	2.209	4.264	4.279	0.347
0.700		7.600		3.452	3.516	1.850	4.143	4.212	1.676
0.750		7.200		3.408	3.479	2.078	4.090	4.185	2.327
0.800		7.000		3.368	3.405	1.104	4.041	4.127	2.118

Table A.2 Residual and wave resistance coefficients, and form factor of Wigley III S/L = 0.2

Fn	C_R (x 10^{-3})			C_W (x 10^{-3})			1+k (CFD)	Re
	Exp	CFD	Error (%)	Exp	CFD	Error (%)		
0.200	1.075	0.939	-12.663	0.190	0.306	60.903	1.140	1.31E+06
0.255	1.794	1.601	-10.758	0.953	0.949	-0.399	1.153	1.67E+06
0.280	1.204	1.079	-10.382	0.379	0.457	20.644	1.147	1.83E+06
0.300	2.261	1.991	-11.930	1.447	1.298	-10.287	1.169	1.96E+06
0.323	3.211	3.025	-5.793	2.409	2.314	-3.952	1.174	2.11E+06
0.350	2.555	2.296	-10.137	1.766	1.628	-7.814	1.165	2.29E+06
0.373	1.905	1.712	-10.131	1.126	1.019	-9.485	1.174	2.44E+06
0.400	2.598	2.329	-10.354	1.830	1.628	-11.019	1.179	2.62E+06
0.500	6.101	5.836	-4.340	5.365	5.223	-2.645	1.161	3.27E+06
0.600	5.447	5.118	-6.031	4.736	4.471	-5.592	1.178	3.93E+06
0.700		4.084			3.388		1.198	4.58E+06
0.750		3.721			3.015		1.203	4.91E+06
0.800		3.595			2.873		1.212	5.24E+06
						Average	1.173	

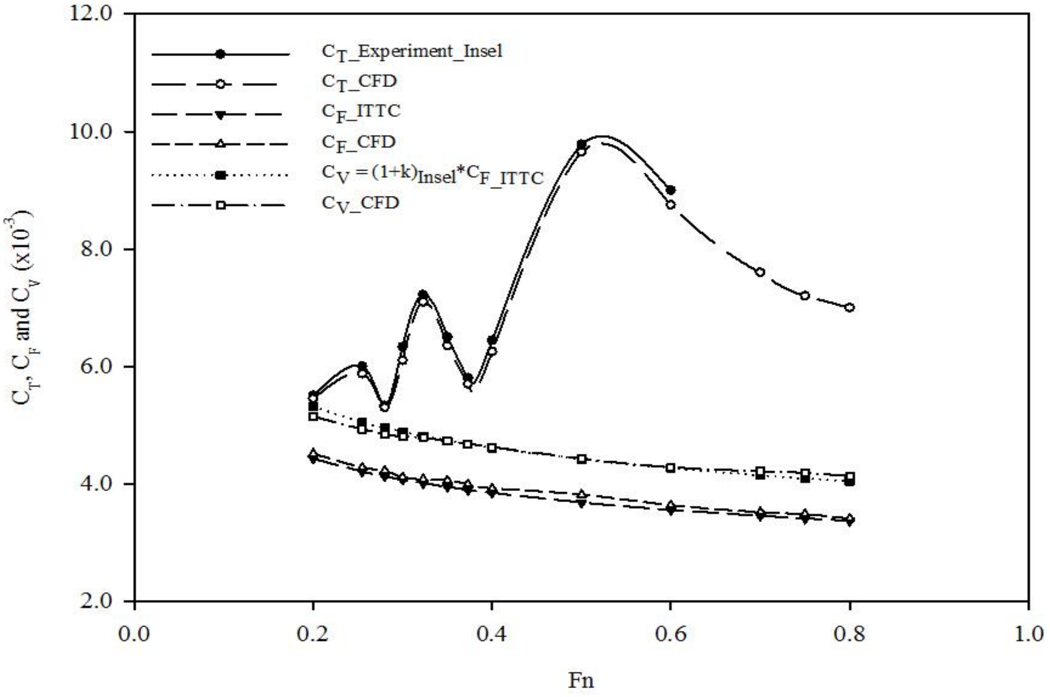

Figure A.1 Total, frictional and viscous resistance coefficients of Wigley III S/L = 0.2

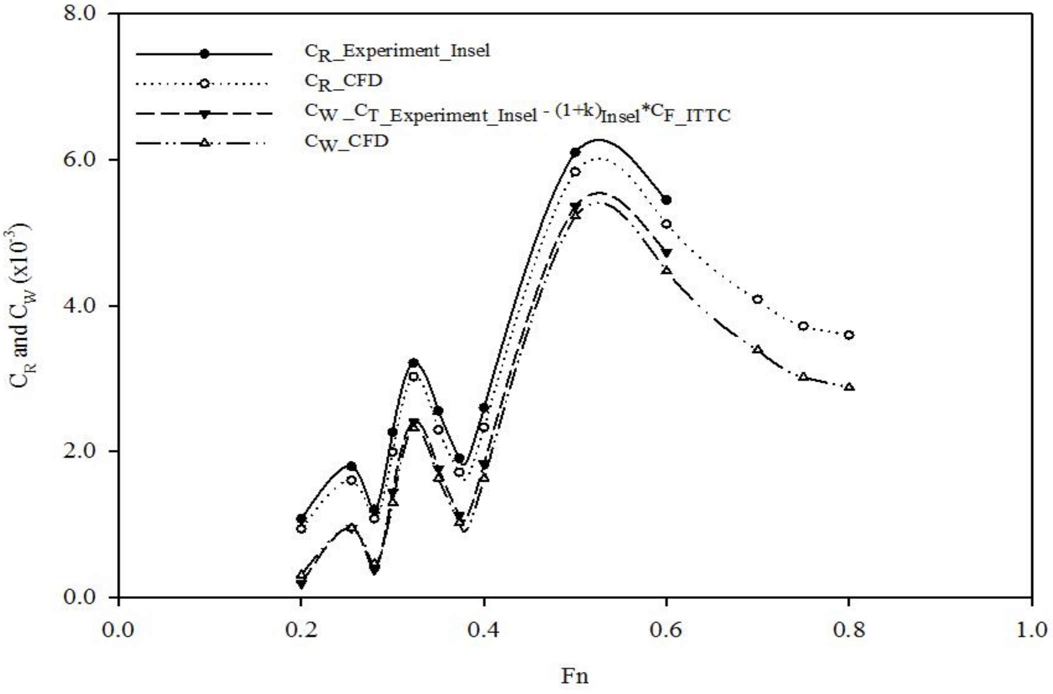

Figure A.2 Residual and wave resistance coefficients of Wigley III S/L = 0.2

A.2 S/L = 0.4

Resistance components of the largest separation to length ratio (S/L = 0.4) are presented in figures A.3 and A.4 and tables A.3 and A.4. The CFD total resistance coefficient (C_T) agrees very well with experimental results over the range of Froude number with the range of under prediction between -0.563 and -1.677 percent for Fn < 0.80 and over prediction of 0.61 percent for Fn = 0.80.

The CFD fictional resistance coefficient (C_F) shows a good agreement with ITTC correlation line with the range of error between 1.386 and 2.519 percent. However, the CFD C_F is higher than C_F ITTC correlation line all over Froude number range. The differences between CFD C_F and ITTC correlation line seem to be linear over the Froude numbers except for Fn = 0.20, 0.264, 0.30 and 0.60 where the over prediction exceeds 2.0 percent. Viscous resistance coefficient shows a fair agreement with experiment; however, the under prediction is found for the low Froude number, Fn < 0.50, and slightly over predicted for Fn > 0.45, which shows a similar trend with other hull configurations. The viscous resistance component agrees very with experimental data at 0.40 < Fn < 0.60, then seems to increase and are slightly higher than experiment for Fn > 0.70.

The CFD C_R is under predicted over the range of Froude numbers with percentage error between -0.475 and 14.487. The error seems to be very high and exceeds 6.0 percent for the low Froude numbers, Fn < 0.40. The CFD C_W show a mix of under and over prediction with range of error between -1.638 and 73.557 percent. The under prediction is found for Fn > 0.35 while the over prediction is found very high for lower Froude numbers, Fn < 0.40, which exceeds 10.0 percent. The differences of wave resistance between CFD and experiment are very small at the intermediate Froude numbers 0.25 < Fn < 0.50. The error seems to increase for the high Froude numbers for Fn > 0.40 and then agrees very well with experiment for the highest Froude number.

Table A.3 Total, frictional and viscous resistance coefficients of Wigley III S/L = 0.4

Fn	C_T (x 10^{-3})			C_F (x 10^{-3})			C_V (x 10^{-3})		
	Exp	CFD	Error (%)	ITTC	CFD	Error (%)	Exp	CFD	Error (%)
0.200	5.330	5.300	-0.563	4.425	4.523	2.221	5.089	4.881	-4.087
0.238	5.670	5.611	-1.041	4.266	4.335	1.607	4.906	4.722	-3.759
0.264	5.330	5.250	-1.501	4.177	4.264	2.084	4.803	4.657	-3.050
0.300	6.330	6.246	-1.327	4.069	4.167	2.401	4.680	4.575	-2.237
0.350	5.560	5.512	-0.863	3.945	4.000	1.386	4.537	4.463	-1.633
0.400	7.560	7.450	-1.455	3.842	3.901	1.525	4.419	4.388	-0.696
0.450	8.330	8.200	-1.561	3.755	3.825	1.865	4.318	4.299	-0.445
0.500	8.440	8.320	-1.422	3.679	3.751	1.951	4.231	4.237	0.139
0.600	7.560	7.463	-1.283	3.553	3.643	2.519	4.087	4.098	0.281
0.700	6.975	6.858	-1.677	3.452	3.513	1.763	3.970	4.011	1.033
0.750	6.722	6.650	-1.071	3.408	3.469	1.784	3.919	3.982	1.597
0.800	6.560	6.600	0.610	3.368	3.423	1.638	3.873	3.957	2.169

Table A.4 Residual and wave resistance coefficients, and form factor of Wigley III S/L = 0.4

Fn	C_R (x 10^{-3})			C_W (x 10^{-3})			1+k (CFD)	Re
	Exp	CFD	Error (%)	Exp	CFD	Error (%)		
0.200	0.905	0.777	-14.16	0.241	0.419	73.557	1.079	1.31E+06
0.238	1.404	1.276	-9.088	0.764	0.889	16.425	1.089	1.56E+06
0.264	1.153	0.986	-14.487	0.527	0.593	12.630	1.092	1.73E+06
0.300	2.261	2.079	-8.037	1.650	1.671	1.254	1.098	1.96E+06
0.350	1.615	1.512	-6.360	1.023	1.049	2.551	1.116	2.29E+06
0.400	3.718	3.450	-4.535	3.141	3.062	-2.522	1.125	2.62E+06
0.450	4.575	4.375	-4.373	4.012	3.901	-2.762	1.124	2.95E+06
0.500	4.761	4.569	-4.028	4.209	4.083	-2.991	1.130	3.27E+06
0.600	4.007	3.820	-4.655	3.473	3.365	-3.123	1.125	3.93E+06
0.700	3.523	3.345	-5.048	3.005	2.847	-5.259	1.142	4.58E+06
0.750	3.314	3.181	-4.008	2.803	2.668	-4.802	1.148	4.91E+06
0.800	3.192	3.177	-0.475	2.687	2.643	-1.638	1.156	5.24E+06
						Average	1.119	

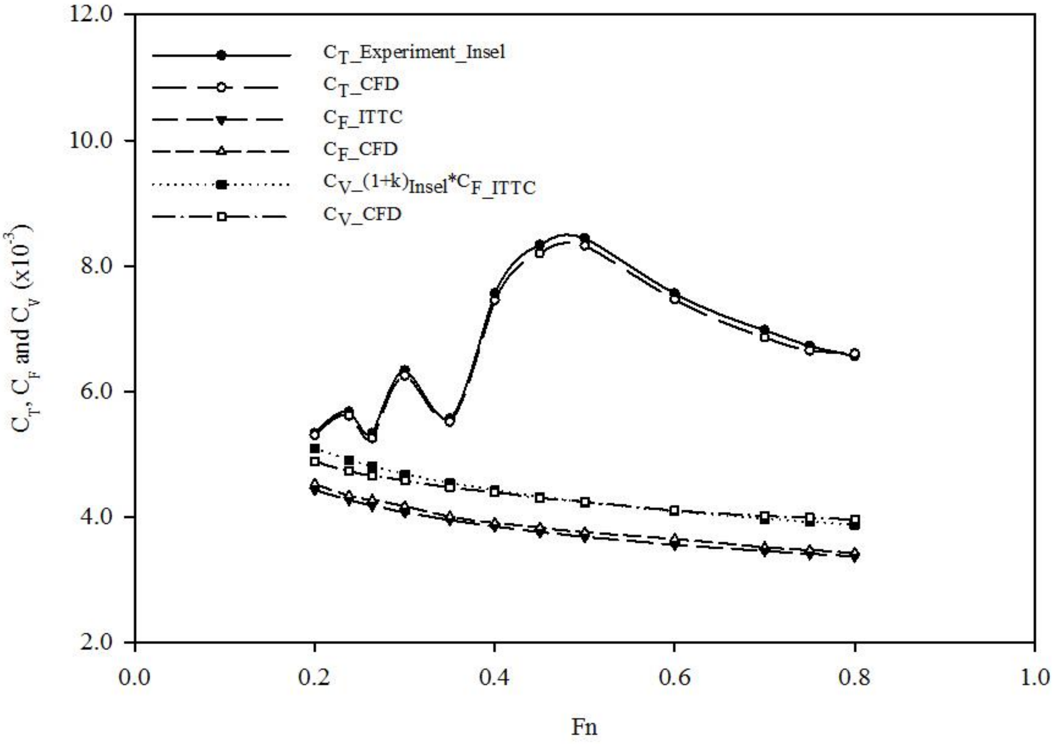

Figure A.3 Total, frictional and viscous resistance coefficients of Wigley III S/L = 0.4

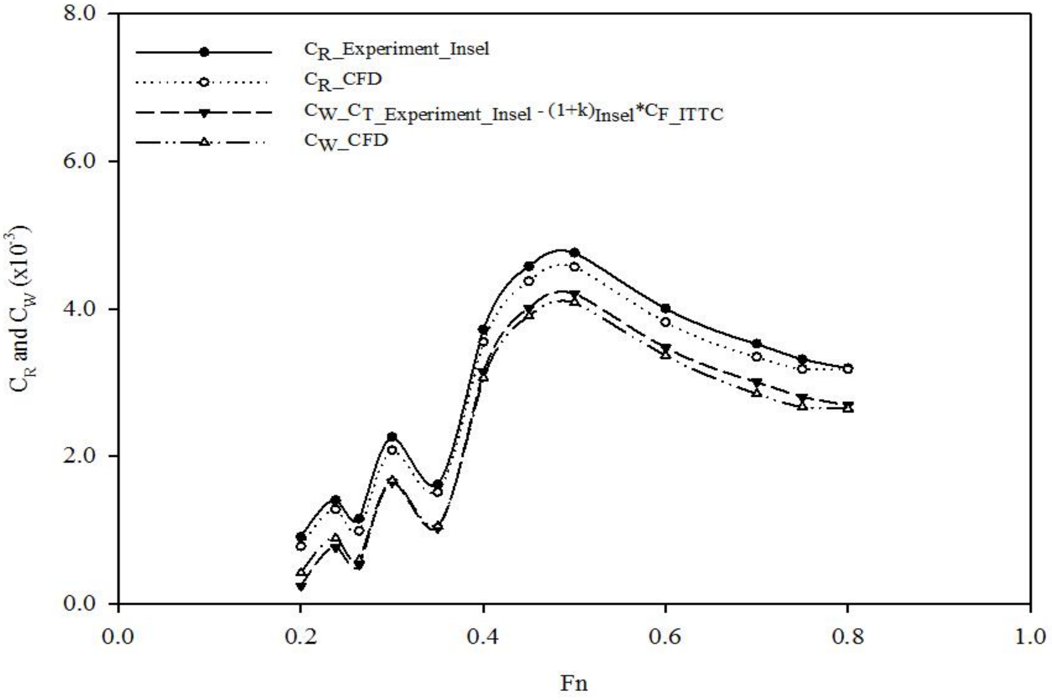

Figure A.4 Residual and wave resistance coefficients of Wigley III S/L = 0.4

A.3 Comparison of Resistance Coefficients for Wigley III Catamarans

Figure A.5 shows the comparison of CFD residual resistance coefficient (C_R) for Wigley III with different hull configurations. It can be seen that a single hull gives the lowest C_R because there is no disturbance between demihulls. In case of catamarans, residual resistance coefficient seems to decrease with the increasing hull separation, which agrees with Insel's experiment. For the low speed regime, Fn < 0.40, residual resistance has less contribution to total resistance. The highest residual resistance contributed to the total resistance is at Fn ~ 0.50, which can be found for all hull configurations. At the high-speed range, Fn > 0.60, residual resistance seems to decrease significantly.

The comparison of wave resistance coefficient (C_W) for Wigley III is shown in figure A.6. Wave resistance characteristic also behaves in the same way with residual resistance, as both are Froude number dependence. Wave resistance for the monohull has less influence on the total resistance compared with the catamarans. Due to the effects of flow interference between demihulls, wave resistance decreases with the increasing hull separation. Wave resistance shows the largest effect on total resistance at Fn ~ 0.50.

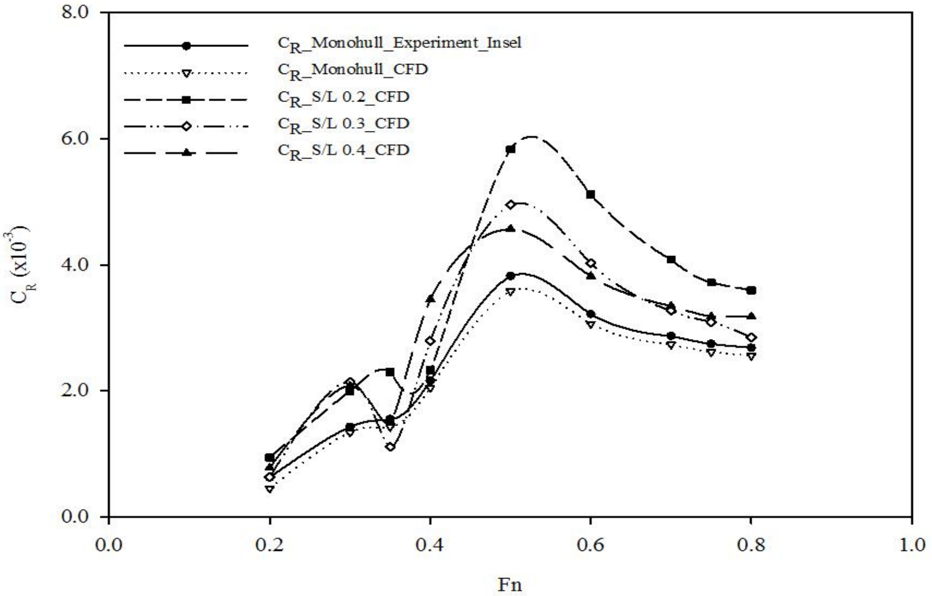

Figure A.5 Comparison of residual resistance coefficient of Wigley III

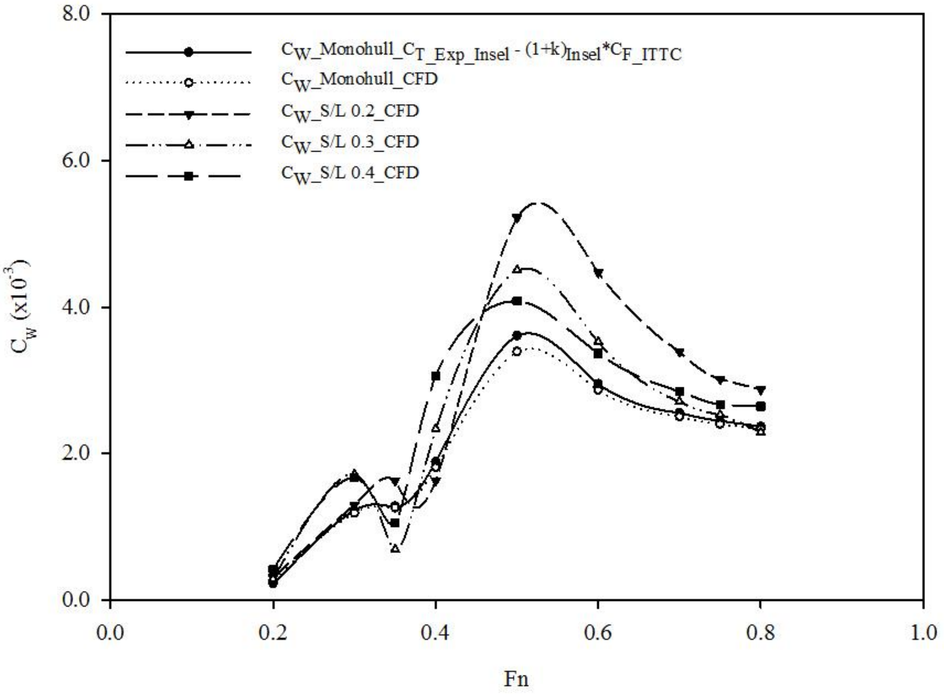

Figure A.6 Comparison of wave resistance coefficient of Wigley III

Appendix B Wave Resistance (τ) Interference Factors for Wigley III Catamarans

B.1 S/L = 0.2

The viscous resistance interference factor (β) is also estimated and shown in figure 4.9. CFD results are very high for the Froude number, Fn < 0.35 with the highest at Fn = 0.30 of about 8.70. For the higher Froude number, Fn > 0.35, the average viscous resistance interference factor is around 4.0. Generally, it can be seen that viscous resistance interference factor seems to decrease with Froude number. Compared with other hull configurations, the narrowest separation shows the highest viscous resistance interference factor.

The wave resistance interference factor (τ) for catamaran S/L = 0.2 shown in figure B.1, shows a good agreement with experiment with a fluctuation between 0.30 < Fn < 0.50. For Fn > 0.50 wave resistance interference factor seems to decrease steadily. The validation can be made up to Fn = 0.60 due to the reasons discussed in the resistance section, section 4.2.2. The comparison made against other hull configurations presented in figure B.3 shows that for Fn > 0.40 the narrowest hull separation gives higher wave resistance interference factor. The fluctuation of wave resistance interference factor of S/L = 0.2 seems to be inverted for the intermediate Froude numbers, 0.30 < Fn < 0.50 compared with other hull configurations.

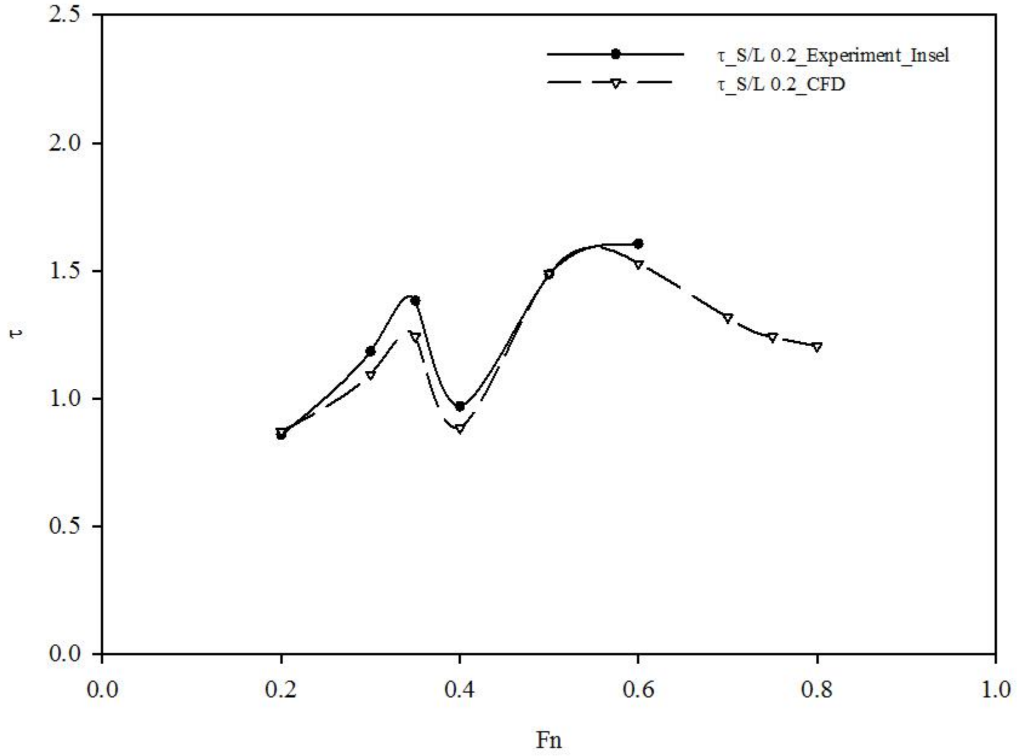

Figure B.1 Wave resistance interference factor of Wigley III S/L = 0.2

B.2 S/L = 0.4

The CFD viscous resistance interference factor (β) for S/L = 0.4, presented in figure 4.9, shows the same trend as other hull configurations and the values are close to those from S/L = 0.3. The small differences between S/L = 0.3 and 0.4 might be the fact that the differences of form factor of these two hulls are very small. Wave resistance interference factor (τ) for S/L = 0.4 also shows a good agreement with experiment with a fluctuation at Fn > 0.30 and Fn = 0.50, see figure B.2. For Fn > 0.50, wave resistance interference factor seems to be steady with small declination.

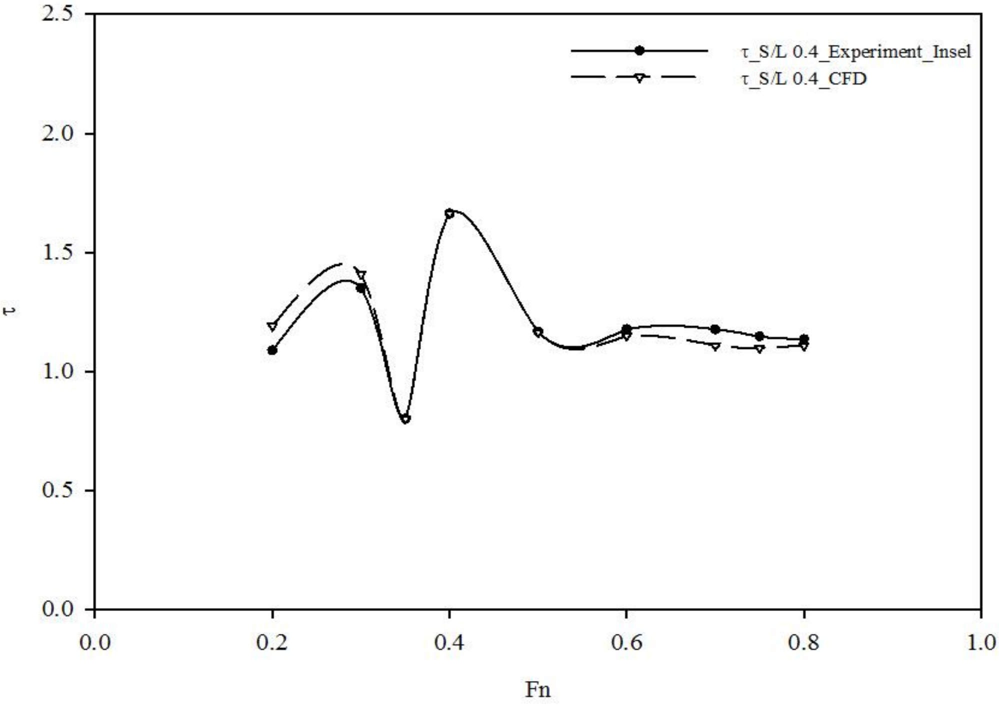

Figure B.2 Wave resistance interference factor of Wigley III S/L = 0.4

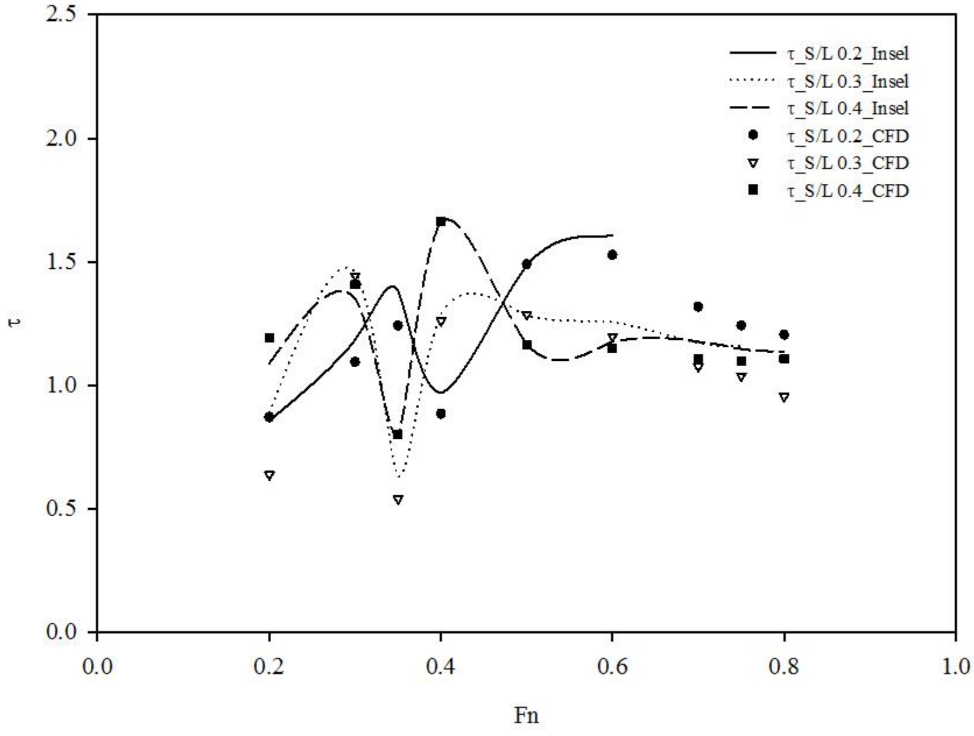

Figure B.3 Comparison of wave resistance interference factor for Wigley III

Appendix C Wave Elevation along the Hulls for Wigley III Catamarans

C.1 S/L = 0.2

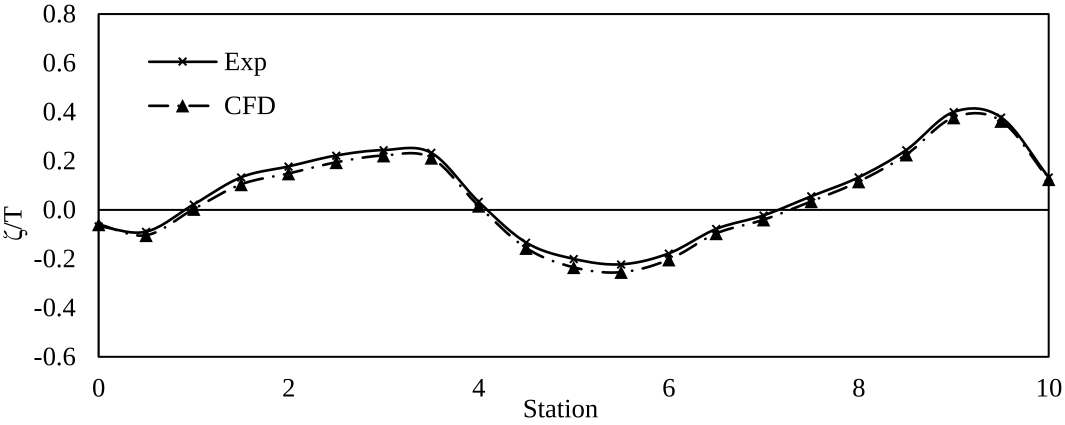

Figure C.1 Wave elevation along the hull of Wigley III S/L = 0.2 (inboard) at Fn = 0.35

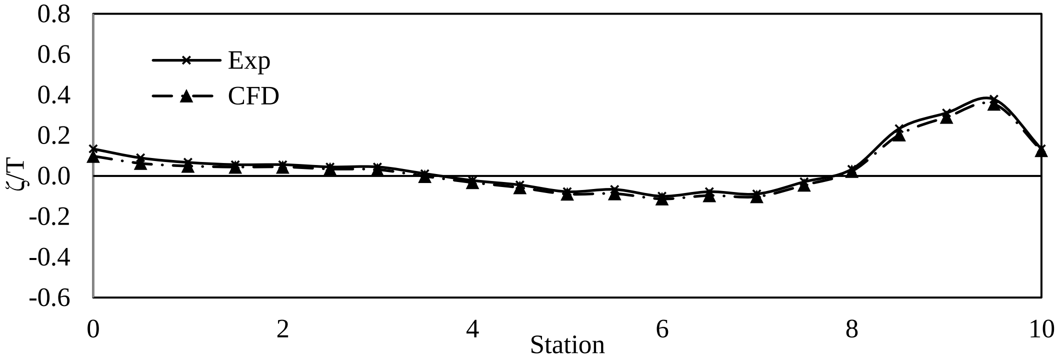

Figure C.2 Wave elevation along the hull of Wigley III S/L = 0.2 (outboard) at Fn = 0.35

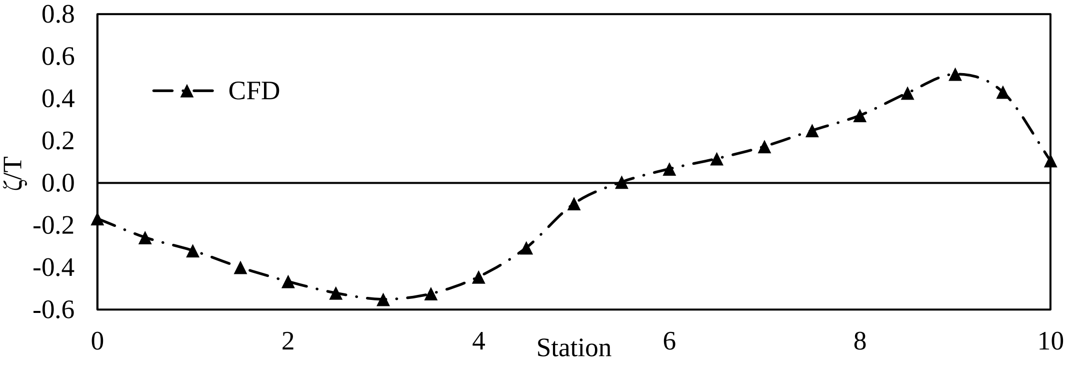

Figure C.3 Wave elevation along the hull of Wigley III S/L = 0.2 (inboard) at Fn = 0.50

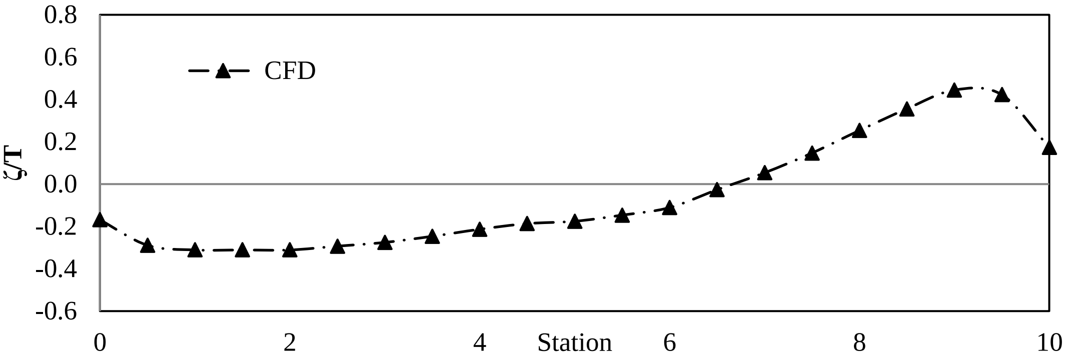

Figure C.4 Wave elevation along the hull of Wigley III S/L = 0.2 (outboard) at Fn 0.50

C.2 S/L = 0.4

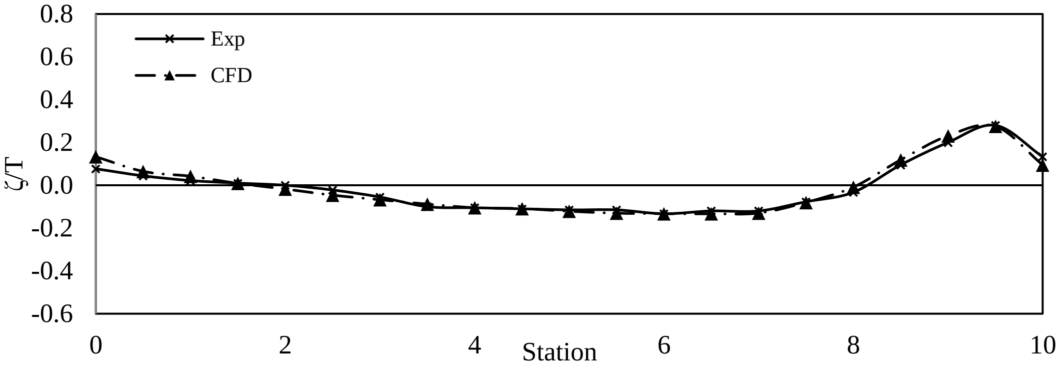

Figure C.5 Wave elevation along the hull of Wigley III S/L = 0.4 (inboard) at Fn = 0.35

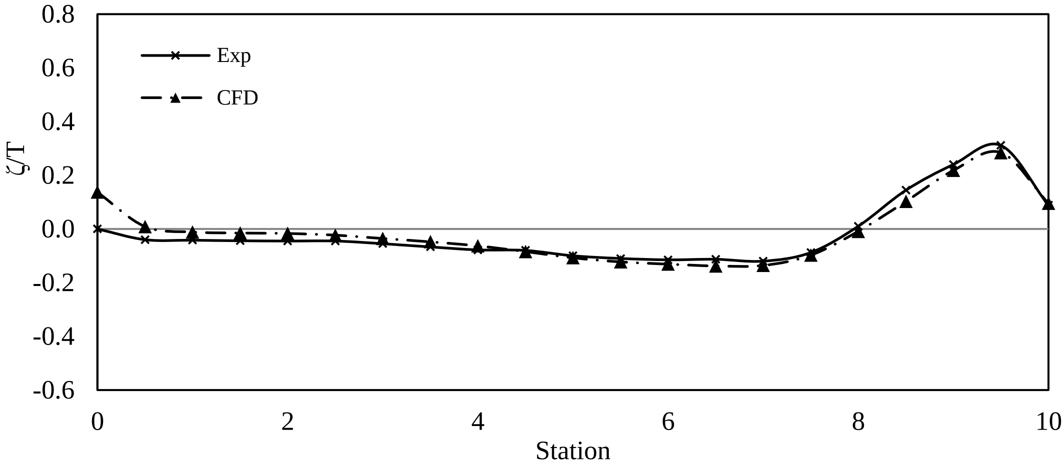

Figure C.6 Wave elevation along the hull of Wigley III S/L = 0.4 (outboard) at Fn = 0.35

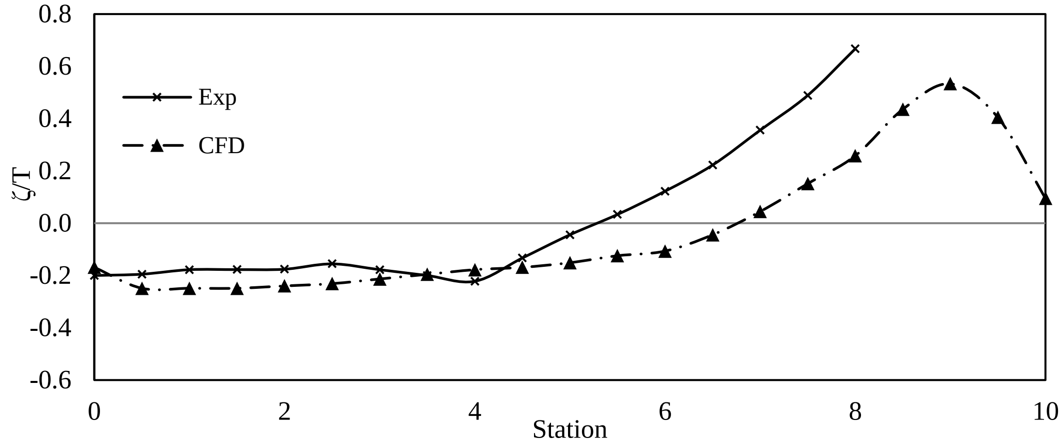

Figure C.7 Wave elevation along the hull of Wigley III S/L = 0.4 (inboard) at Fn = 0.50

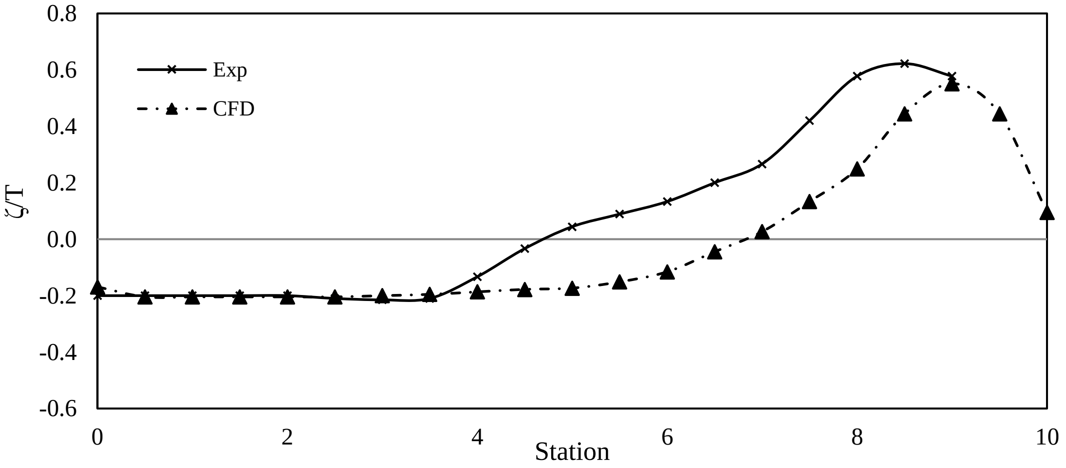

Figure C.8 Wave elevation along the hull of Wigley III S/L = 0.4 (outboard) at Fn = 0.50